

University of Southampton Research Repository

Copyright © and Moral Rights for this thesis and, where applicable, any accompanying data are retained by the author and/or other copyright owners. A copy can be downloaded for personal non-commercial research or study, without prior permission or charge. This thesis and the accompanying data cannot be reproduced or quoted extensively from without first obtaining permission in writing from the copyright holder/s. The content of the thesis and accompanying research data (where applicable) must not be changed in any way or sold commercially in any format or medium without the formal permission of the copyright holder/s.

When referring to this thesis and any accompanying data, full bibliographic details must be given, e.g.

Thesis: Yifan Jiang (2020) "Modelling and performance evaluation of an electromagnetic regenerative shock absorber with mechanical motion rectifier", University of Southampton, Faculty of Engineering Physical Science, PhD Thesis, pagination.

University of Southampton

Faculty of Engineering and Physical Science

Mechatronic Research Group

Modelling and Performance Evaluation of an Electromagnetic
Regenerative shock absorber with Mechanical Motion Rectifier

By

Yifan Jiang

Thesis for the degree of Doctor of Philosophy

September 2020

University of Southampton

ABSTRACT

FACULTY OF ENGINEERING AND PHYSICAL SCIENCE

Mechatronic Research Group

Doctor of Philosophy

Modelling and performance evaluation of an electromagnetic regenerative shock absorber with mechanical motion rectifier

By Yifan Jiang

This thesis is mainly concerned with the modelling of an electromagnetic regenerative shock absorber with mechanical motion rectifier (MMR), and its performance evaluation when it is implemented in the suspension of a road vehicle. Unlike a conventional regenerative shock absorber, the inclusion of a sprag-clutch within the MMR module enables the conversion of bi-directional rotational motion into unidirectional rotary input to the coupled electromagnetic generator. Previous studies have shown that the dynamics of a regenerative shock absorber with MMR can be modelled as a piecewise linear system produced by the engagement and disengagement of sprag-clutches within the MMR. It is seen that the MMR based system potentially works as a switchable *inert*er in parallel with a switchable damper. To characterise the proposed energy harvesting technique, the system is initially discussed when one terminal of the design is blocked, which allows further validations through experiments. In order to comprehensively study dynamics of MMR system, its energy harvesting as well as mechanical power flow performance are evaluated. Additionally, an analogy between the electrical and mechanical active and reactive power flow, using force-current analogy is carried out. This allows better understanding of the power transmission between sub-systems. Moreover, the output of a conventional regenerative shock absorber is generally coupled with an electrical rectifier to convert the AC voltage signal to DC signal for either energy storage or charging electronic devices. In this work, to justify the usage of each rectifier, the electrical rectifier-based regenerative shock absorber is studied in both electrical and mechanical systems. The discussion is further extended to compare performances between electrical rectifiers and MMR in different scenarios. It is shown that MMR is able to offer much superior performance than electrical rectifiers, typically for lower power application. To validate theoretical predictions, the MMR based regenerative shock absorber is tested in a hydraulic Instron machine. A dynamic model of the proposed design is implemented, and its parameters are estimated from the measured data.

In order to establish whether MMR allows acceptable energy harvesting performance when incorporated into the suspension of road vehicles, the first step is to investigate the characteristics of the vibration environment. By using the concept of mechanical impedance and mobility, dynamics of the vibration source is studied when the regenerative shock absorber is incorporated into a road vehicle. According to the vibration source characteristic results, the implementation of the MMR based regenerative shock absorber in the suspension system of road vehicles is discussed. The result shows that MMR enables better performance under certain conditions, but it results in a high jerk motion (excessive change of acceleration) as a trade-off. Finally, the procedure for the design of a mechanical motion rectified regenerative shock absorber for a road vehicle suspension system is presented. The proposed design guidelines enable a designer to select desirable parameters for the regenerative shock absorber based on the system constraints and the application environment.

Table of Contents

Table of Contents	<i>i</i>
Table of Tables	<i>v</i>
Table of Figures	<i>vii</i>
Research Thesis: Declaration of Authorship	<i>xv</i>
Acknowledgements	<i>xvii</i>
Definitions and Abbreviations	<i>xix</i>
Symbols.....	<i>xx</i>
Chapter 1 <i>Introduction</i>	<i>1</i>
1.1 <i>Background</i>	<i>1</i>
1.2 <i>Thesis motivation and objectives</i>	<i>4</i>
1.3 <i>Novel contributions</i>	<i>6</i>
1.4 <i>Structure of the thesis</i>	<i>7</i>
Chapter 2 <i>Literature Review</i>.....	<i>9</i>
2.1 <i>Electromagnetic regenerative shock absorber for vehicle suspension system</i>	<i>9</i>
2.1.1 <i>Linear electromagnetic regenerative shock absorber</i>	<i>10</i>
2.1.2 <i>Rotational electromagnetic regenerative shock absorber</i>	<i>11</i>
2.2 <i>Mechanical motion rectifier</i>	<i>13</i>
2.3 <i>Model of electromagnetic vibration regenerative shock absorber</i>	<i>15</i>
2.3.1 <i>Conventional ideal model</i>	<i>16</i>
2.3.2 <i>Inerter based ideal model</i>	<i>17</i>
2.3.3 <i>Nonlinear model</i>	<i>21</i>
2.4 <i>Mobility and impedance methods in vibration analyses</i>	<i>23</i>
2.4.1 <i>Simple lumped elements</i>	<i>23</i>
2.4.2 <i>Connection to a vibration source</i>	<i>24</i>
2.5 <i>Mechanical power flow</i>	<i>26</i>
2.6 <i>Summary</i>	<i>27</i>
Chapter 3 <i>Regenerative shock absorber with MMR</i>.....	<i>29</i>
3.1 <i>Linear model of regenerative shock absorber</i>	<i>30</i>
3.2 <i>Piecewise linear model of MMR regenerative shock absorber</i>	<i>32</i>
3.2.1 <i>Dynamics of piecewise linear systems</i>	<i>33</i>
3.2.2 <i>Dynamics of velocity source</i>	<i>38</i>

3.2.3	Dynamics of Torque/Force source	43
3.3	<i>Performance evaluation of MMR based regenerative shock absorber</i>	<i>47</i>
3.3.1	Linear system	48
3.3.2	Piecewise linear system (Velocity input)	51
3.3.3	Piecewise linear system of MMR (Torque/Force input)	58
3.4	<i>Multiple harmonics input.....</i>	<i>67</i>
3.5	<i>Summary.....</i>	<i>70</i>
Chapter 4	<i>Regenerative shock absorber with electrical rectifier.....</i>	<i>73</i>
4.1	<i>Dynamics of electrical rectification</i>	<i>73</i>
4.2	<i>Regenerative shock absorber with electrical rectifier.....</i>	<i>75</i>
4.2.1	Electrical system analysis.....	76
4.2.2	Mechanical system analysis.....	79
4.3	<i>Theoretical comparison between electrical rectifier and MMR</i>	<i>81</i>
4.4	<i>Summary.....</i>	<i>84</i>
Chapter 5	<i>Experimental characteristic of regenerative shock absorber with MMR</i>	<i>87</i>
5.1	<i>Mechanism of the design.....</i>	<i>88</i>
5.2	<i>Experimental set up</i>	<i>90</i>
5.3	<i>Testing results and discussion</i>	<i>91</i>
5.3.1	Characteristics of MMR based regenerative shock absorber	92
5.3.2	Characteristics of electrical rectified regenerative shock absorber	96
5.4	<i>Summary.....</i>	<i>101</i>
Chapter 6	<i>Analysis of regenerative shock absorber in quarter car model.....</i>	<i>103</i>
6.1	<i>Vehicle suspension model</i>	<i>104</i>
6.2	<i>Mobility/Impedance model of quarter car system</i>	<i>105</i>
6.2.1	Source characteristic of suspension system	106
6.2.2	Vibration isolation.....	111
6.2.3	Energy harvesting analysis.....	116
6.3	<i>Application of MMR in Vehicle suspension system.....</i>	<i>118</i>
6.4	<i>Performance evaluation of MMR based regenerative shock absorber in quarter car model</i>	<i>123</i>
6.4.1	Energy harvesting performance quantification	123
6.4.2	Ride comfort evaluation	133

6.5	<i>Summary</i>	<i>137</i>
 Chapter 7 <i>Design procedure of MMR based regenerative shock absorber for road vehicle</i> 139		
7.1	<i>Design requirements</i>	<i>140</i>
7.2	<i>Design process</i>	<i>140</i>
7.2.1	Vibration source characteristics.....	142
7.2.2	Selection of maximum stroke length.....	142
7.2.3	Selection of the lead-screw.....	142
7.2.4	Selection of MMR gear module.....	145
7.2.5	Selection of generator, electrical load and flywheel	146
7.3	<i>Numerical Study.....</i>	<i>148</i>
7.4	<i>Summary</i>	<i>152</i>
 Chapter 8 <i>Conclusions and future work.....</i>153		
8.1	<i>Conclusions</i>	<i>153</i>
8.2	<i>Future Work.....</i>	<i>157</i>
8.2.1	Model extensions.....	157
8.2.2	Experimental validation and physical implementation	157
<i>Bibliography.....</i>		<i>163</i>
<i>Appendix A....</i>		<i>171</i>
<i>Appendix B.....</i>		<i>181</i>
<i>Appendix C.....</i>		<i>187</i>

Table of Tables

Table 3-1: System parameters of mechanical motion rectified regenerative shock absorber	48
Table 3-2: Force-current analogy between electrical and mechanical networks [86]	50
Table 3-3: Harvestable Power with different electrical damping coefficient (MMR versus Linear system)	55
Table 3-4: Harvestable Power with different generator inertia (MMR versus Linear system)	56
Table 3-5: Average harvestable electrical power and mechanical power loss with different electrical damping coefficient (MMR versus Linear system)	63
Table 3-6: Harvestable Power with different generator inertia (MMR versus Linear system)	65
Table 4-1: System parameters within the electrical domain	78
Table 4-2: Performance quantification of electrical rectifier-based regenerative shock absorber	78
Table 6-1: Road vehicle parameters [135, 136]	108
Table 6-2: Quarter car parameters	123
Table 6-3: Energy harvesting performance comparison between MMR and Linear system with different ce	130
Table 6-4: Energy Harvesting Performance comparison between MMR and Linear system with different generator inertance b_2	132
Table 7-1: Parameters for PMDC generators [152]	148
Table 7-2: Estimation of inertia and mass of each module	149
Table 7-3: Proposed regenerative shock absorber with six PMDC generator modules	149
Table 7-4: Performance quantification for each generator module (switching & non switching case)	150
Table 7-5: Suggested parameters of regenerative shock absorber design with model f	151

Table of Figures

Figure 1-1: Potential harvestable power for different types of vehicles [1]	2
Figure 1-2: Fuel efficiency potential improvement employing regenerative shock absorber [17]	2
Figure 2-1: Linear electromagnetic regenerative shock absorber (a) Diagram of the prototype (b) Cross section of the magnetic assembly [63]	10
Figure 2-2: Schematic configuration of rack-pinion regenerative shock absorber [72]	11
Figure 2-3: Schematic structure of ball-screw electromagnetic regenerative shock absorber [75]	12
Figure 2-4: Hydraulic transmission regenerative damper [79]	13
Figure 2-5: Mechanical motion rectifier gear module prototype [83]	14
Figure 2-6: Dual one-way clutch transmission system [22]	15
Figure 2-7: Schematic of a single degree of freedom electromagnetic vibration regenerative shock absorber connected to the electrical load resistance [72]	16
Figure 2-8: A mechanical-electrical Force-Current analogy [94]	18
Figure 2-9: Schematic structure of rack-pinion inerter [98]	19
Figure 2-10: Schematic structure of ball-screw inerter [95]	19
Figure 2-11: The working principle of the hydraulic inerter [99]	19
Figure 2-12: Inerter based vibration isolator	20
Figure 2-13: Schematic diagram of spring damper model of backlash effect [98]	22
Figure 2-14: A linear mechanical system with two forces applied	24
Figure 2-15: Vibration source of internal impedance Z_I connected to a load impedance Z_L	25
Figure 2-16: Schematic diagram of a vibration system	26
Figure 3-1: Schematic diagram of regenerative shock absorber (one terminal is clamped) excited under force input	30
Figure 3-2: Schematic diagram of motion rectifier gear module (a) Clockwise direction (b) Anti- clockwise direction	32
Figure 3-3: Equivalent diagram of the electrical load	35
Figure 3-4: Schematic of dynamics of switching inside MMR	36
Figure 3-5: Mass clamped SDOF system with on-off switchable inerter and damper (a) Engaged state (b) Disengaged state	38
Figure 3-6: Engaged state of MMR based regenerative shock absorber (Velocity Input)	39
Figure 3-7: Disengaged state of MMR based regenerative shock absorber (Velocity Input) (a) Primary unswitchable system (b) Secondary switchable system	40

Figure 3-8: The dynamic of switching between engagement and disengagement inside MMR (Velocity Input)	42
Figure 3-9: Engaged state of MMR based regenerative shock absorber (Torque/Force Input)	43
Figure 3-10: Disengaged state of MMR based regenerative shock absorber (Torque/Force Input) (a)Primary unswitchable system (b)Secondary switchable system.....	44
Figure 3-11: The dynamic of switching between engagement and disengagement inside MMR (Force/Torque Input)	46
Figure 3-12: System dynamics at its natural frequency ($f = 1Hz$) (a) Excitation velocity (b) Total input power	49
Figure 3-13: Dynamic of system subjected to its off-resonance frequency.....	50
Figure 3-14: Electrical/Mechanical equivalent circuit (a)Electrical power flow system (b) Mechanical Power flow system.....	51
Figure 3-15: Harvested power comparison between Linear case (without spring) and MMR case under velocity vibration source excitation.....	52
Figure 3-16: Simulated system Dynamics of MMR based regenerative shock absorber(a) Rotational velocity of each part (b) Input torque (c) Input mechanical power	53
Figure 3-17: Dynamics of generator speed with different electrical damping ce ($f = 1Hz$)	54
Figure 3-18: Dynamics of generator speed with different generator inertia Jg ($f = 1Hz$) ..	55
Figure 3-19: Dynamics of generator speed with different displacement amplitudes X	57
Figure 3-20: Dynamics of generator speed with different excitation frequencies f (a) $f = 1Hz$ (b) $f = 2Hz$ (c) $f = 4Hz$	57
Figure 3-21: Harvested electrical power comparison between Linear (without spring) and MMR case under force input excitation ($T=1Nm$, $f=10Hz$).....	58
Figure 3-22: Mechanical Power loss comparison between Linear (without spring) and MMR system under torque input excitation($T=1Nm$, $f=10Hz$)	59
Figure 3-23: Simulated System Dynamics (a) Rotational speed of each part (b) Total input Power & Reactive Power Flow (c) Total input torque & torque acting on the generator	60
Figure 3-24: Dynamics of generator speed with different electrical damping ce	62
Figure 3-25: Harvested electrical power of MMR vs linear system (without spring) with different electrical damping ce ($f=10Hz$) (a) $ce = 1Nms/rad$ (b) $ce = 5Nms/rad$ (c) $ce = 10Nms/rad$	62
Figure 3-26: Dynamics of generator speed with different generator inertia Jg ($f=10Hz$)	64

Figure 3-27: Instantaneous harvested electrical power with different generator inertia Jg ($f=10\text{Hz}$) (a) $Jg = 2.21\text{kgm}^2$ (b) $Jg = 1.21\text{kgm}^2$ (c) $Jg = 0.221\text{kgm}^2$...	65
Figure 3-28: Dynamics of generator speed with different amplitudes of applied torque T_0 ..	66
Figure 3-29: Instantaneous harvested electrical power under different frequency excitations (MMR versus Linear system (without spring)) (a) $f=1\text{Hz}$ (b) $f=5\text{Hz}$ (c) $f=10\text{Hz}$..	66
Figure 3-30: Time instant of switching on/off in different frequencies ($1\text{Hz} \leq f \leq 5\text{Hz}$)	68
Figure 3-31: Consequences of switching on system dynamics (1&2Hz excitation) (a) 1Hz, $\text{Max}(\theta_{in}) = 1.1\text{rad/s}$ (b) 2Hz, $\text{Max}(\theta_{in}) = 1.1\text{rad/s}$ (c) 1&2Hz, $\text{Max}(\theta_{in}) = 2.2\text{rad/s}$	69
Figure 3-32: Power dissipation/flow of MMR based regenerative shock absorber under 1&2Hz excitation (a) Electrical power dissipation (b) Mechanical reactive power flow	70
Figure 4-1: AC/DC circuit with electrical rectification	74
Figure 4-2: Diode voltage drop characteristic.....	74
Figure 4-3: Schematic representation of full-wave electrical rectifier circuit	76
Figure 4-4: Theoretical output voltage of the electrical rectifier.....	77
Figure 4-5: Schematic of regenerative shock absorber with electrical rectifier (a) Electrical circuit (b) mechanical schematic diagram.....	79
Figure 4-6: Energy harvesting performance comparison between electrical rectifier and mechanical rectifier with different input displacement ($f = 1\text{Hz}$, $c_e = 10\text{Ns/m}$) (a) $X = \pm 10\text{mm}$ (b) $X = \pm 50\text{mm}$ (c) $X = \pm 200\text{mm}$	82
Figure 4-7: Energy harvesting performance comparison between electrical rectifier and mechanical rectifier with different c_e ($f = 1\text{Hz}$, $X = \pm 50\text{mm}$) (a) $c_e = 1\text{Ns/rad}$ (b) $c_e = 10\text{Ns/rad}$ (c) $c_e = 500\text{Ns/rad}$	83
Figure 4-8: Energy harvesting performance comparison between electrical rectifier and mechanical rectifier in different excitation frequency ($X = \pm 50\text{mm}$, $c_e = 10\text{Ns/rad}$) (a) $f = 1\text{Hz}$ (b) $f = 2\text{Hz}$ (c) $f = 5\text{Hz}$	84
Figure 5-1: Final design of prototype	88
Figure 5-2: Motion rectifier module layout of principle components	88
Figure 5-3: Counter-clockwise torque transmission path	89
Figure 5-4: Clockwise torque transmission path.....	89
Figure 5-5: Schematic of the experimental set up of MMR based regenerative shock absorber	90
Figure 5-6: Experimental setup of electrical rectifier based regenerative shock absorber (a) Test rig setup (b) Electrical circuit configuration	91
Figure 5-7: Force-displacement curves for 0.1-2Hz excitation frequencies, $\pm 5\text{mm}$	92

Figure 5-8: Measured and simulated blocked force of MMR based regenerative shock absorber at 2Hz, $\pm 5\text{mm}$ sinusoidal excitation	94
Figure 5-9: Power spectral density of the output voltage under 1.0Hz $\pm 10\text{mm}$ and 2.0Hz, $\pm 5\text{mm}$ excitation.....	94
Figure 5-10: Measured and simulated voltage under 1Hz, $\pm 10\text{mm}$ excitation ($R_{Load} = 10\Omega, 100\Omega$)	95
Figure 5-11: Open circuit voltage(a) Time domain results (b) Power Spectral Density.....	98
Figure 5-12: Measured and simulated blocked force of regenerative shock absorber without any rectifier at 1Hz, $\pm 10\text{mm}$ sinusoidal excitation	98
Figure 5-13: Simulink model of the full-wave electrical rectifier	100
Figure 5-14: Simulated output voltage across the load resistance ($RL = 10\Omega$).....	100
Figure 6-1: Schematic diagram of isolator (one terminal is clamped) excited by a velocity input	104
Figure 6-2: Quarter car suspension model.....	104
Figure 6-3: Quarter-car equivalent diagrams (a) Norton equivalent system (b) Thévenin equivalent system.....	106
Figure 6-4: Isolator layout	108
Figure 6-5: Source Characteristic (a) $(Y_R + Y_I)/Y_s$ (b) V_{us}/V_{free} (c) FI/Fb	109
Figure 6-6: Two equivalent representations of vibration source (a) Force source (b) Velocity source.....	110
Figure 6-7: Characteristic of transmissibility T	112
Figure 6-8: (a) Mobility ratio amplitude $(Y_s + Y_I/Y_R)$ (b) Transmissibility between sprung mass and road (V_r/V_o)	113
Figure 6-9: Relative mobility Y_s/Y_R	114
Figure 6-10: Characteristics of $Y_s + Y_I + Y_R$	115
Figure 6-11: Average harvestable electrical power generation in different excitation frequencies.....	116
Figure 6-12: Schematic diagram of applying MMR in quarter car model during engaged state (Velocity Source).....	119
Figure 6-13: Schematic of disengaged state of the system (a) Primary unswitchable system (b) Secondary switchable system	121
Figure 6-14: Vehicle dynamics with MMR (a) Relative rotational speed across the electrical damper (b) Relative displacement between the sprung mass and road ..	122
Figure 6-15: Power extraction and dissipation comparison between MMR and Linear system (a) Electrical harvestable power (b) Mechanical Power loss	124
Figure 6-16: Mechanical active/reactive power flow of quarter car system with MMR	126

Figure 6-17: Electrical power extraction between linear and MMR system ($m_s \rightarrow \infty$)	128
Figure 6-18: Power extraction and dissipation comparison between MMR and Linear system ($c_e = 200Ns/m$) (a) Electrical harvestable power (b) Mechanical power loss	129
Figure 6-19: Power extraction and dissipation comparison between MMR and Linear system ($c_e = 50Ns/m$) (a) Electrical harvestable power (b) Mechanical power loss	129
Figure 6-20: Power extraction and dissipation comparison between MMR and Linear system ($b_2 = 200kg$) (a) Electrical harvestable power (b) Mechanical power loss	131
Figure 6-21: Power extraction and dissipation comparison between MMR and Linear system ($b_2 = 100kg$) (a) Electrical harvestable power (b) Mechanical power loss	131
Figure 6-22: Power extraction and dissipation comparison between MMR and Linear system ($b_2 = 10kg$) (a) Electrical harvestable power (b) Mechanical power loss	132
Figure 6-23: Sprung mass absolute acceleration x_r ($10kg \leq b_2 \leq 200kg$)	135
Figure 6-24: Sprung mass acceleration x_r by varying electrical damping ($50Ns/m \leq c_e \leq$ $400Ns/m$)	137
Figure 7-1: Design procedure of MMR based regenerative shock absorber	141
Figure 7-2: Lead-screw helix angle	143
Figure 7-3: Relative displacement between sprung mass and the road for broadband frequency	151

Research Thesis: Declaration of Authorship

Print name: Yifan Jiang

Title of thesis: Modelling and performance evaluation of an electromagnetic regenerative shock absorber with mechanical motion rectifier

I declare that this thesis and the work presented in it are my own and has been generated by me as the result of my own original research.

I confirm that:

1. This work was done wholly or mainly while in candidature for a research degree at this University;
2. Where any part of this thesis has previously been submitted for a degree or any other qualification at this University or any other institution, this has been clearly stated;
3. Where I have consulted the published work of others, this is always clearly attributed;
4. Where I have quoted from the work of others, the source is always given. With the exception of such quotations, this thesis is entirely my own work;
5. I have acknowledged all main sources of help;
6. Where the thesis is based on work done by myself jointly with others, I have made clear exactly what was done by others and what I have contributed myself;
7. None of this work has been published before submission.

Signature:.....

.....Date:

Acknowledgements

I wish to take the opportunity to thank all the people who have helped and supported me immensely, to make me feel blessed during the PhD journey.

First and foremost, I would like to express my sincere gratitude to my supervisor, Dr. Mohamed Moshrefi-Torbati and Dr. Timothy Waters, for their consistent guidance, support and encouragement throughout my studies. These works will not be possible to come this far without their kindness and willingness. They are always grateful to share their experience and I have learned insights on how to be a researcher.

My special thanks to Dr. Mehdi Hendijanzadeh for his invaluable advice and inspiration on developing analytical model.

I would like to thanks to Mr Yann Glauser for his great support in designing, assembling and manufacturing the prototype. And also, many thanks to Kevin Smith and John Young at EDMC workshop for their help in improving the design of regenerative shock absorber.

I would like to express my appreciation to Dr. Andrew Robinson for his great advice in designing rig and testing the regenerative shock absorber in TSRL lab.

I want to thanks to all the technicians at Electronics workshop for helping me building electrical circuit and debugging the oscilloscope.

Many thanks to all students and staff at Mechatronic research group who have contributed with their friendship and company through this journey.

Last, but by no means least, my unmeasurable thanks to my parents who always trust and encourage me for my entire life. I would also like to thank to my girlfriend, Xuejiao, for her love, support and understanding to me.

Definitions and Abbreviations

AC	Alternating Current
DC	Direct Current
DOF	Degree of freedom
EMF	Electromotive force
MMR	Mechanical motion rectifier
SDOF	Single degree of freedom
2DOF	Two degree of freedom
PMEM	Permanent magnet electric machinery

Symbols

a	Acceleration
A	Area of piston
a_{rms}	Root mean square value of acceleration
b	Inertance
b_1	Primary system inertance
b_2	Secondary system inertance
b_{eq}	Equivalent inertance
B	Flux density
C	Capacitor
c	Damping coefficient
c_{eq}	Equivalent damper
c_v	Viscous damping
c_{e_t}	Translational electrical damping
c_{e_r}	Rotary electrical damping
c_{m_t}	Translational mechanical damping
c_{m_r}	Rotary mechanical damping
c_r	Bearing limiting factor
d_m	Diameter
D	Displacement of hydraulic motor
D_m	Centre to centre diameter of ball bearing
E_d	Energy dissipation
E_e	Harvested electrical energy
E_m	Mechanical energy dissipation
E_{in}	Input energy
E_{in_v}	Input energy (velocity source)
E_{in_f}	Input energy (force source)
E_{out_v}	Output energy (velocity source)
E_{out_f}	Output energy (force source)
F_{in}	Input force
F_{eq}	Equivalent force
F_e	Electrical damping force
F_{em}	Back emf force
f_c	Coulomb friction force

F_b	Blocked force
F_s	Load disturbance force
F_r	Tyre stiffness force
G_r	Road roughness
I	Electrical current
J	Moment of inertia
J_f	Flywheel moment of inertia
J_{MMR}	MMR gear module moment of inertia
J_{eq}	Equivalent moment of inertia
J_g	Moment of inertia of generator
J_{ls}	Moment of inertia of lead-screw
J_{lg}	Moment of inertia of large gear
J_{sg}	Moment of inertia of small gear
k	Spring stiffness
k_t	Tyre stiffness
k_s	Suspension stiffness
k_e	Voltage coefficient
l	pitch of the screw
L	Length
m	Mass
m_s	Sprung mass
m_{us}	Unsprung mass
N_1	Lead-screw critical speed
N_2	Maximum allowable speed of bearing
p_{in}	Input power
p_d	Power dissipation
p_{dc_l}	DC load power
p_{ac}	AC power
$P_{average}$	Average power
p_{r_e}	Mechanical reactive power during engagement
p_{r_d}	Mechanical reactive power during disengagement
p_{int}	Internal power loss
p_m	Mechanical power dissipation
$p_{conduct}$	Diode conduction power loss
r	Radius of the gyration of flywheel
r_1	Radius of the pinion

r_2	Radius of the gear wheel
r_3	Radius of the flywheel
r_N	Gearhead ratio
r_g	Bevel gear ratio
R_{load}	Load resistance
S_v	Power spectral density
t	Time
t_1	Time instant of disengagement
t_2	Time instant of re-engagement
t_{upper}	Time instant of diode starts conducting voltage
t_2	Time instant of diode finishes conducting voltage
T	Torque
T_{free}	Free velocity transmissibility
T_o	Amplitude of applied torque
T_{ls}	Torque on lead-screw
T_{lg}	Torque on large bevel gear
T_{sg}	Torque on small pinion gear
$T_{friction}$	Static friction torque
T_{emf}	Electromagnetic torque
V_{free}	Free velocity
V	Voltage
V_d	Diode conducting voltage
V_{dc}	DC voltage
V_{max}	Maximum voltage
V_{output}	Output voltage
V_0	Reference spatial frequency
x_o	Road input displacement
x_r	Receiver displacement
x_{us}	Unsprung mass displacement
x_s	Sprung mass displacement
x_{in}	Input translational displacement
\dot{x}_{in_e}	Primary system translational velocity during engagement
\dot{x}_{in_d}	Primary system translational velocity during disengagement
Y	Displacement amplitude
Y_s	Source mobility
Y_R	Receiver mobility

Y_L	Load mobility
Z_s	Source Impedance
Z_I	Isolator Impedance
Z_R	Receiver Impedance
z_s	Displacement of sprung mass
z_{us}	Displacement of unsprung mass
z_r	Receiver displacement
z_e	Relative displacement between MMR and sprung mass during engagement
z_d	Relative displacement between MMR and sprung mass during disengagement
ω	Excitation frequency
ω_n	Natural frequency
ν	Spatial frequency
$\dot{\theta}$	Angular velocity
$\dot{\theta}_g$	Generator angular velocity
$\dot{\theta}_{in_e}$	Primary system angular velocity during engagement
$\dot{\theta}_{in_d}$	Primary system angular velocity during disengagement
\emptyset	Flux linkage
ΔK	Changing rate of kinetic energy
ΔU	Changing rate of potential energy
η_e	Energy harvesting efficiency
ζ	Damping ratio
α	Helix angle
β	Inertance to mass ratio

Chapter 1 Introduction

1.1 Background

It is well recognised that large vibration causes discomfort of vehicle occupants and deteriorate vehicle's road handling. In the past decades, the incorporation of various devices such as isolator, damper has been considered by numerous researchers and applied in practice to passively control the vibration motion to maintain its amplitude below certain thresholds. A conventional vehicle suspension is simply a spring-damper system which isolates vehicle body from road random disturbances. However, a large amount of vibration energy is converted into waste heat in the suspensions, which decreases the fuel efficiency of the vehicle. Decreasing vehicle energy losses becomes necessary to reduce the reliance on finite power sources such as batteries or super capacitors to provide power for the off-grid system. The concept of harvesting energy wasted in vehicles including the recovery of heat loss [1-3], braking energy [4-6], and shock absorbers [7, 8] has been proposed to improve engine efficiency.

Shock absorber is a key component of vehicle suspension system to reduce the vibration transmitted to the passenger when driving on a rough road. Typically, the vibration energy is dissipated through hydraulic friction and heat in a conventional shock absorber.[9] The energy wasted in shock absorbers has been estimated by several researchers. [10-12] The study presented by Segel and Lu [13] discuss how energy wasted in a vehicle shock absorber at different driving speed and road roughness. In 1986, Browne [14] investigated the energy dissipation in automotive shock absorbers of a road vehicle. It is found that each hydraulic shock absorber dissipates 40-60 watts when the vehicle is driving on urban road. According to ISO 8608, when the vehicle speed is 30 km/h at the Class A, B, C, D and E roads, the recoverable power is 2.08 W, 8.33 W, 33.35 W, 133.37 W, and 533.21 W, respectively. [15] Khoshnoud et al. [16] estimated the power dissipated in a 2DOF vehicle suspension model, the result indicates that the potential regeneration per damper is approximately 280 W. Consequently, 3% fuel efficiency improvement can be achieved in typical passenger cars for a 75% electrical energy conversion efficiency. Figure 1-1 and Figure 1-2 summarise the potential energy harvesting and fuel efficiency improvements for different vehicles. [1, 17]

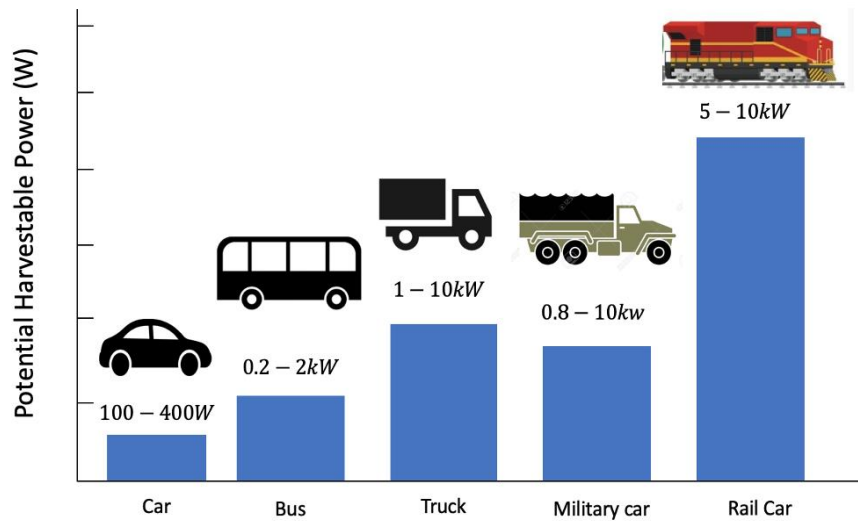


Figure 1-1: Potential harvestable power for different types of vehicles [1]

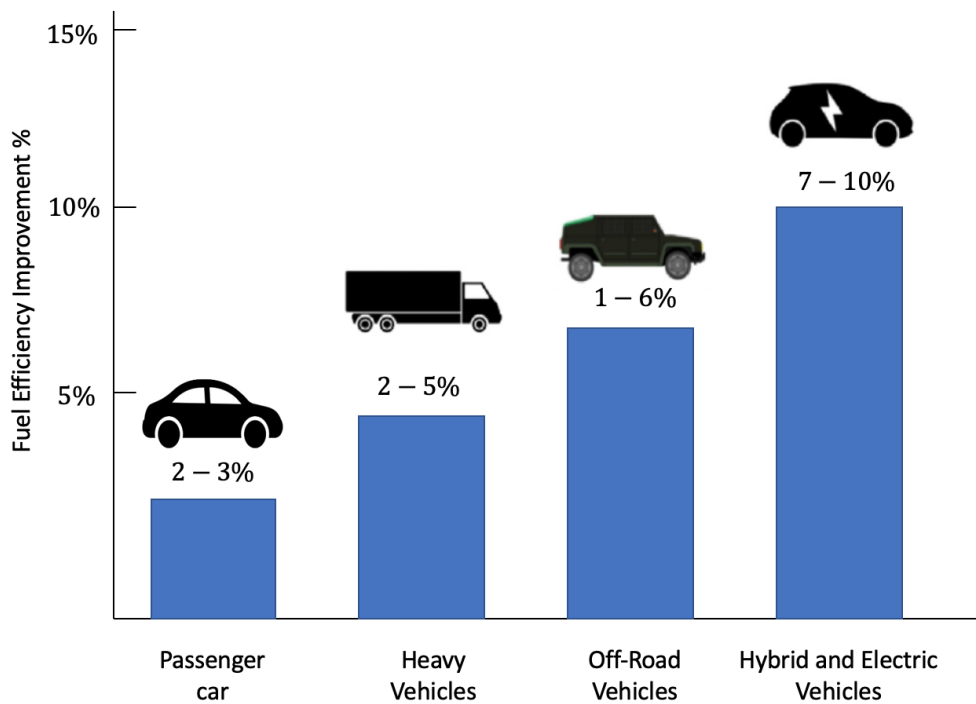


Figure 1-2: Fuel efficiency potential improvement employing regenerative shock absorber [17]

Energy harvesting is known as the process of capturing energy from the ambient environment and converting into useful off-grid electricity [18]. Implementing energy harvesting device in regenerative suspensions has attracted much interests in recent years due to the launch of electric vehicles. Several strategies for the implementation of a regenerative suspension system have been studied and proposed to recover the wasted mechanical energy. Primary intentions of developing regenerative shock absorber in a vehicle

suspension is to reduce costs and increase lifetimes of batteries for electrical and hybrid vehicle, improve the fuel efficiency and reduce exhaust emissions [19-21]. The harvested energy from the suspension vibration can be used for charging the batteries or supercapacitor that provide motive energy to the electric traction motors. [22, 23]. In the meantime, it is feasible to provide the power demand for the active or semi-active suspensions by employing a self-powered damper to achieve better ride quality and road handling [24-26]. The design of an energy harvesting technique can be classified depending on the mechanism through which the vibration energy is converted into electricity. Among various energy harvesting structures, electromagnetic regenerative shock absorbers have gained much attractions in vehicle suspension systems due to its high energy conversion efficiency, quick response, strong controllability and capability in energy recovery [27-29].

An electromagnetic regenerative shock absorber is generally developed based on Faraday's law. When the coil is moved relative to the magnetic field, an electromotive force is produced. If the coil is connected to an electrical load, current will flow through the circuit and thus the electrical power is generated. Electromagnetic regenerative shock absorbers can be divided into two main categories; linear [30-32] and rotary [33-35]. The linear type electromagnetic regenerative shock absorber directly converts the translational vibration motion into electrical power due to the relative movement between coil and magnetic. In contrast, the rotational type converts the translational motion into rotational input of an electromagnetic generator. It is generally recognized that the rotary electromagnetic regenerative shock absorber is more compact and has greater energy density as well as efficiency compared to linear type [36, 37].

For rotary electromagnetic regenerative shock absorbers, there are two general mechanisms of converting translational motion into rotational motion; mechanical and hydraulic transmissions. The mechanical motion conversion mechanism has been widely developed for regenerative shock absorbers due its simple construction. The most popular design prototypes include ball-screw [38, 39] and rack-pinion [40, 41] but other types have also been developed [42, 43]. For example, a hydraulic regenerative shock absorber mechanism was manufactured and its performance in vehicle suspension was investigated [44, 45]. From the mechanism property, the above rotary regenerative shock absorber converts translational vibration motion into a bi-directional oscillation of electrical generation and thus producing AC electrical power. However, it has been examined that the bi-directional irregular motion leads to a low mechanical reliability and bad vibration performance in practice [46-48]. It was claimed in [49], the rack teeth of conventional rack-pinion regenerative shock absorber were

worn out and broken quickly due to large impact force. In 2011, Li [29] proposed a mechanical motion rectifier gear module based regenerative shock absorber to convert bidirectional rotational motion to unidirectional rotary motion which offered smaller impact force caused by backlash effect to improve the energy conversion efficiency. In the meantime, the continuous unidirectional motion enables the generator to be driven unidirectionally and the produced current does not necessarily need to go through an electrical rectifier. Wang [50] realised a similar effect by applying two overrunning clutches and a planetary gearbox to a ball-screw regenerative shock absorber. Zhang [22] developed a regenerative shock absorber based on dual-overrunning clutches and applied in an electrical vehicle. Fang [51] proposed a hydroelectric shock absorber with four check valves to rectify the bidirectional flow into unidirectional flow to drive a hydraulic pump that could subsequently drive an electrical generator.

1.2 Thesis motivation and objectives

As stated earlier, conventional rotary regenerative shock absorbers convert translational vibration motion into a bi-directional rotation of coupled electromagnetic generator. In order to charge batteries or provide power for electronic devices, the oscillating motion/voltage needs to be coupled with either mechanical or electrical rectification to convert the AC input signal to DC signal. The literature so far has not made any recommendation on which rectification is more desirable for various applications. One cannot claim that advantages of MMR are always beyond an electrical rectifier, unless it is properly justified.

The dynamic model of an MMR-based regenerative shock absorber has already been developed for the lab-test case where one terminal of the design is clamped by the fixture [52, 53]. It is observed that the MMR-based regenerative shock absorber potentially works as a switchable inerter and damper system according to the switching between the engaged and disengaged states of the sprag-clutch inside the MMR. This work focused on the dynamics of an MMR-based system when it is subjected to a velocity excitation. In this case, the vibration source will actively vary the applied force and power during the disengagement period in order to maintain the prescribed velocity input. However, in some cases, the vibration input may behave as a prescribed force source. Therefore, the influence of switching on system dynamics when subjected to a force input needs to be discussed as well. Moreover, it has been demonstrated in the literature [53] that the switching within the MMR gear module allows the coupled generator to work more continuously and the regenerated voltage potentially never fall down to zero. However, it still remains unclear whether the

MMR-based system can enhance the system performance comparing to conventional linear energy harvesting system without MMR besides practical factors (less backlash and friction effect) as it has not been well concerned. Previous research focused on discussing the energy harvesting performance, while the consequence of switching on mechanical power flow needs to be addressed as well. This gives a deeper understanding of vibration power transmission between sub-systems by implementing MMR in regenerative shock absorber. Numerical study is needed to determine the impact of each element on system dynamics.

The first step of designing a regenerative shock absorber is to study characteristics of vibration environment. So far, much work has been conducted to improve the understanding of the isolator itself, but the fundamentals of vibration source characteristics of suspension system have not been well studied in previous investigations. It is initially unclear whether to assume the system is excited by a force or velocity source, as all parameters are frequency dependent which potentially affect the vibration source dynamics. Based on the vibration source characteristics of a road vehicle, it is necessary to discuss the implementation of MMR-based energy harvesting shock absorber in vehicle suspension systems. Guo and Zuo [40] conducted a performance evaluation of MMR on different vehicles in order to understand the consequence of employing an MMR-based regenerative shock absorber on system dynamics. However, their frequency domain conclusions are questionable since the switching between the engage and disengage states of sprag-clutch corresponds to a transient vibration which should generally be discussed in the time domain.

Furthermore, in the case of designing a regenerative shock absorber for vehicle suspension system, the maximum displacement of the sprung mass from its equilibrium is defined by the available space. In the meantime, the system damping ratio of vehicle suspension is generally fixed for vibration suppression purposes. By taking these physical constraints into considerations, a set of reliable guidelines for the design of an MMR based energy harvesting shock absorber can be developed to provide important references for its applications in vehicle suspension systems.

Motivated by above illustrations, the primary intention of this thesis is to develop a study to understand the implementation of mechanical motion rectified regenerative shock absorber in road vehicle suspension system. The research objectives are listed as follows:

- To study the characteristics of a linear regenerative shock absorber (i.e., without MMR) including mechanical power flow and dissipation.
- To predict and analyse the dynamic behaviour of the proposed MMR energy harvesting technique based on a laboratory-test case, where on terminal of the design

is clamped. Numerical studies will be conducted to identify the effect of each element on system dynamics.

- To demonstrate the characteristics of an electrical rectifier coupled regenerative shock absorber in both electrical and mechanical systems when one terminal of is clamped and compare its performance with MMR.
- To design and manufacture a testing rig and simultaneously improve the design of the existing prototype.
- To conduct experiments on the design prototype and obtain its response over a range of frequencies.
- To study the characteristics of the vibration source when the regenerative shock absorber is incorporated in a road vehicle suspension by using concepts of mechanical impedance and mobility.
- To identify the role of each mechanical element in energy harvesting and vibration isolation performance.
- To evaluate the performance of MMR-based regenerative shock absorber in a vehicle suspension system with respect to energy harvesting and ride comfort.
- To establish a procedure for designing an MMR-based regenerative shock absorber for vehicle suspension systems by considering physical constraints.

1.3 Novel contributions

The main original contributions of this research are listed as follows:

- Influences of switching between engaged and disengaged state of MMR gear module on the mechanical power flow, energy harvesting and ride comfort performance are investigated. Additionally, an analogy between the electrical and mechanical active & reactive power flow based on force-current analogy is carried out. This has enabled a deeper understanding of the consequence of employing MMR for both general applications and, in particular, for vehicle suspension systems.
- Characteristics of vibration source are studied when the regenerative shock absorber is installed in a road vehicle. By using the concept of mechanical impedance/mobility, a clear illustration of the dynamics of the vibration source over a range of frequencies can be established. The concept is further used to identify the role of inerter in both energy harvesting and vibration isolation performances. This study provides

important references for demonstrating the implementation of MMR-based energy harvesting shock absorber on the performance of vehicle suspension systems.

- Comparison between electrical rectifier and MMR is conducted. The study helps to understand the characteristics of regenerative shock absorbers by employing either an electrical rectifier or an MMR in both electrical and mechanical domains. The comparison provides criteria for the usage of each rectification module in different scenarios and applications.
- A set of guidelines for the design of an MMR-based regenerative shock absorber is developed. The proposed flow chart considers physical constraints of designing a regenerative shock absorber in a road vehicle suspension, including maximum allowable displacement of the mass and fixed damping ratio. The developed techniques provide reliable references for selecting desirable system parameters for its physical applications.
- Characteristics of the proposed MMR based regenerative shock absorber prototype are experimentally studied. This has enabled the construction of a more realistic and representative dynamic model by estimating the parameters of the proposed device.

1.4 Structure of the thesis

In Chapter 2, a brief review of different techniques for energy harvesting in vehicle suspension system including their design, model, implementation and analysis approach are presented. In particular, a review of the MMR-based electromagnetic regenerative shock absorber is given. In Chapter 3, dynamics of a linear regenerative shock absorber is studied and an active and reactive power analogy between electrical and mechanical systems (using force-current analogy) is carried out. The primary intention of this analogy is to understand the power flow characteristics of a linear system (i.e., a regenerative shock absorber without an MMR) which can then be extended to study the case when MMR module is incorporated. Next, dynamic models of MMR-based regenerative shock absorber excited by different vibration sources (prescribed force & velocity) are developed and analysed when one terminal of the design is clamped. Numerical studies are also conducted to improve the understand of dynamics of regenerative shock absorber with MMR which can be further validated through experimental tests. Moreover, the performance of MMR based regenerative shock absorber will be evaluated when it is subjected to multiple harmonics input. The result can answer whether the switching time instant will be dominated by single frequency. In Chapter 4, the performance of a regenerative shock absorber with electrical

rectifier is analysed in both electrical and mechanical domains. The main aim of this study is to determine which technique (i.e., electrical rectification or MMR) is more suitable for extracting power in different scenarios. Chapter 5 presents an experimental study of the regenerative shock absorber with a mechanical motion rectifier prototype. The measured results help to characterise the performance of the proposed design and the equivalent system parameters can be estimated based on the recorded data. Moreover, the measured generator's output voltage is used to quantify the energy harvesting of the proposed design as well as validating the dynamic model developed in Chapter 3. This was followed by an experimental comparison between electrical and mechanical rectification in order to investigate the performance and relevance of each technique. Chapter 6 investigates the implementation of MMR-based regenerative shock absorber in the suspension of a road vehicle. In order to address the problem properly, dynamics of the vibration source was initially studied by using the concept of mechanical impedance and mobility. Based on the results of the vehicle vibration source characteristics, influences of switching within MMR on vehicle dynamics with respect to energy harvesting as well as ride comfort can then be identified. In Chapter 7, a design flowchart is presented in order to provide guidance for selecting desirable system parameters of MMR-based regenerative shock absorber. The proposed methodology considers physical constraints such as maximum allowable displacement of the sprung mass and a fixed damping ratio. Finally, concluding remarks and the recommended future work are listed in Chapter 8.

Chapter 2 Literature Review

As discussed in Chapter 1, considerable energy can potentially be harvested from the vehicle suspension systems, previous research efforts have been made on developing regenerative shock absorber techniques in suspension systems. In this chapter, the current technologies of electromagnetic regenerative shock absorber are categorized and evaluated. Based on the mechanism of transferring mechanical vibration energy into useful electrical energy, two different types of electromagnetic regenerative shock absorbers (translational and rotational) are reviewed. Several attempts to model the dynamic behaviour of an energy harvesting device including linear and nonlinear properties are discussed. Subsequently, brief descriptions of implementing impedance/mobility in mechanical system and its usage of illustrating vibration source characteristics are presented. Additionally, an introduction of the concept of vibration power flow for linear system as well as its analysis approach is given. Finally, research gaps for the current study for modelling an electromagnetic regenerative shock absorber especially incorporating with MMR and its implementation in vehicle suspension system are identified, meanwhile the corresponding research questions have been proposed as well.

2.1 Electromagnetic regenerative shock absorber

By replacing a conventional spring-damper shock absorber with an electromagnetic regenerative shock absorber, the vertical oscillation of the suspension can be converted into useful electrical power. Incorporating an electromagnetic transducer (or a generator) into an isolator is one of the most popular harvesting technologies that is implemented in automotive suspension systems [17]. The main reason is according to its high energy conversion efficiency, simplicity design, quick response, strong controllability and energy recovery capability. [54, 55] The fundamental principle of electromagnetic technology is based on Faraday's law of electromagnetic induction [56]. It has been examined that both rotational and translational electromagnetic generators are able to harvest milli to tens watt levels of power. A number of research works [35, 57, 58] have shown that the implementation of electromagnetic regenerative shock absorbers in vehicle suspensions is a feasible way of achieving self-powered capabilities. The following sections present a review of different types of regenerative shock absorbers including their basic working principle and mechanisms.

2.1.1 Linear electromagnetic regenerative shock absorber

The linear electromagnetic regenerative shock absorber converts the kinetic energy of a reciprocating vertical oscillations directly into electrical power by electromagnetic induction [59]. In contrast to the rotary type that relies on a motion conversion mechanism transferring the translational input into rotational motion for the output generator, the linear module does not need such motion transmission. The vibration input from the ambient environment causes a relative displacement of the magnet in relation to the coil. This relative motion leads to a variation in the magnetic flux inside the coil where the induced emf voltage can be obtained according to the principle of Faraday's law [60]

$$V = -\frac{d\phi}{dt} \quad \text{eq (2-1)}$$

Where V is the generated voltage and ϕ is the magnetic flux.

Based on the working principle of a linear electromagnetic transducer, Suda and Shiiba [61] developed a hybrid control system with an active suspension control and energy recovery. Both simulation and bench test results show that the proposed hybrid system, employing linear electromagnetic transducer is able to achieve a fairly good performance of vibration suppression with less energy consumption. Karnopp [62] presents a study of moving coil system with high energy permanent magnets. The result shows that it is feasible to implement an electrodynamic variable shock absorber in road vehicle suspensions. Zuo [63] proposed a retrofit regenerative shock absorber prototype, shown in Figure 2-1, for vehicle suspension by using a linear electromagnetic transducer is able to achieve greater vibration energy recovery efficiency.

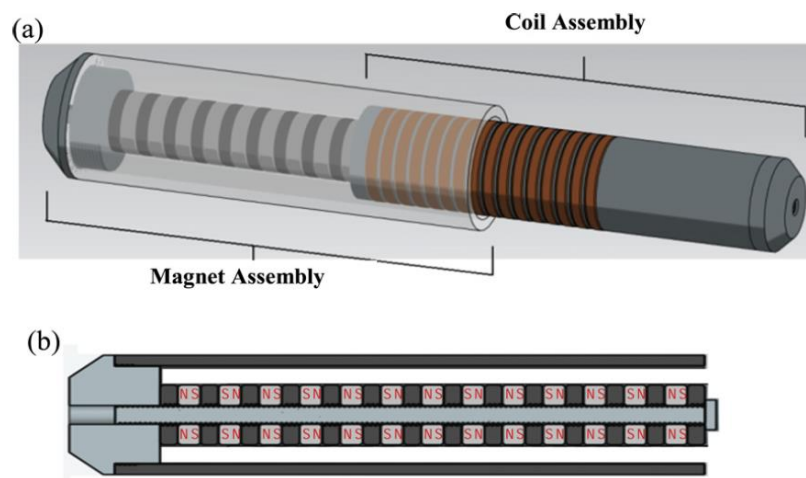


Figure 2-1: Linear electromagnetic regenerative shock absorber (a) Diagram of the prototype (b) Cross section of the magnetic assembly [63]

As stated earlier, one key advantage of the linear electromagnetic regenerative shock absorber is its ability to directly convert mechanical kinetic energy into electricity without using motion translation mechanism. Furthermore, it is beneficial for implementation in active and semi-active suspensions. [26, 41] However, the size of a linear type is usually too bulky, and the manufacturing cost can be very expensive.

2.1.2 Rotational electromagnetic regenerative shock absorber

Unlike the linear type electromagnetic regenerative shock absorber which directly transfers vibration energy into electrical power, for a rotational type to drive a rotary generator, the translational oscillation needs to be converted into rotational motion through a motion conversion mechanism. Based on the motion conversion mechanism, the rotary electromagnetic regenerative shock absorber can be classified into two main types, namely, mechanical and hydraulic.

Mechanical rotary electromagnetic regenerative shock absorber

Employing a mechanical motion conversion mechanism in a rotational electromagnetic regenerative shock absorber is one of the most popular designs due to its simple construction and great energy conversion efficiency. A number of rotational electromagnetic regenerative shock absorber including ball-screw [64-66], rack-pinion [67, 68], algebraic screw mechanism [69] and helical gears [70] have already been prototyped and studied. Graves [71] presented a study of comparing the design of rotating and linear electromagnetic dampers. Results show that the rotating electromagnetic dampers have the advantage of mechanical motion amplification compared to the linear type. The implementation of the design allows the use of smaller and cheaper regenerative shock absorbers in vehicle suspension systems.

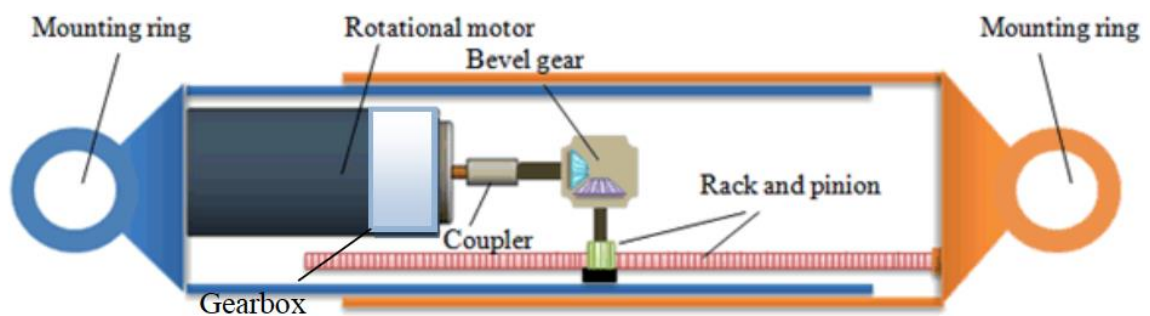


Figure 2-2: Schematic configuration of rack-pinion regenerative shock absorber [72]

One of the common mechanisms of converting linear to rotary motion is rack-and-pinion. Figure 2-2 shows the schematic configuration of rotary regenerative shock absorber employing a rack and pinion mechanism [72]. The vertical oscillation, produced by the vehicle rolling on an uneven road, is translated into a rotational motion through the rack and pinion. Similarly, Suda [73] studied a regenerative active suspension combining rack-and-pinion and a rotary generator. Beno [74] developed electronically controlled active suspension system which adopted the rack-and-pinion mechanism. The experimental results quantify increases in rolling resistance from flat to rough terrain and demonstrate that active suspension systems can limit this increase to 50% comparing to passive suspension systems.

Another motion conversion mechanism which has been widely used in rotary regenerative shock absorber is ball-screw. Figure 2-3 shows the schematic structure of the ball-screw electromagnetic regenerative shock absorber, where the applied torque to drive the generator is created by the ball-screw and the assembled nut. In 2011, Wang [75] developed a novel mechatronic suspension structure design, which is composed of a ball-screw coupled with a permanent magnet electric machinery (PMEM). It was found that the implementation of the proposed mechatronic strut can improve the performance of vehicle suspensions. Song [46, 47] proposed a regenerative shock absorber prototype based on the ball-screw mechanism which achieved a considerable power conversion efficiency. Murty [76] also proposed a ball screw electromagnetic regenerative shock absorber whose applied force can be adjusted by changing the shunt electrical resistance. Xie [77, 78] developed an energy harvesting absorber with ball-screw motion mechanism and multiple controlled generators to recover the kinetic energy loss from the suspension vibration and changes the damping coefficient during operation according to road conditions.

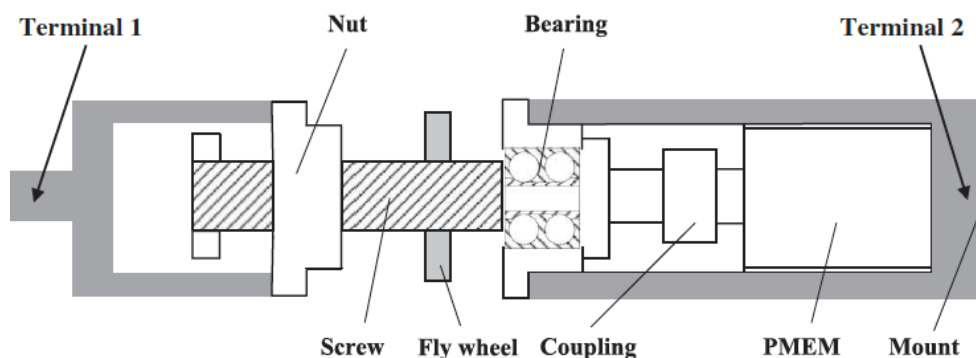


Figure 2-3: Schematic structure of ball-screw electromagnetic regenerative shock absorber [75]

Hydraulic rotary electromagnetic regenerative shock absorber

Another type of rotary electromagnetic regenerative shock absorber is to employ a hydraulic mechanism. The fundamental working principle of a hydraulic regenerative shock absorber is to transfer the up and down oscillation of the cylinder to a hydraulic pump/motor that is attached to an electrical circuit in order to harvest energy from the ambient environment. Based on this hydraulic mechanism, Levant Power Corp [79] proposed a regenerative damper called 'GenShock'.



Figure 2-4: Hydraulic transmission regenerative damper [79]

The developed prototype combines hydraulic transmission with the electrical generator shown in Figure 2-4. It was found that the GenShock improves fuel economy as well as the ride quality. Fang [51, 80] developed a compact hydraulic electromagnetic regenerative shock absorber prototype with an energy harvesting efficiency of 16%. Xu [81] proposed a hydraulic electromagnetic regenerative suspension and revealed that its overall performance is superior to that of a passive suspension.

2.2 Mechanical motion rectifier

In vehicle suspension systems, shock absorbers are installed between the chassis and wheels to suppress vibration resulting from road roughness. Conventional rotary regenerative shock absorbers convert suspension vibration into bidirectional rotation by using mechanical mechanism such as a ball-screw or a rack and pinion. However, the irregular bidirectional oscillation has caused numerous problems, such as low mechanical reliability and poor

vibration performance due to backlash and friction in the transmission system. [82] It was claimed in [49], the rack teeth were worn out and broken quickly due to large impact forces in their early prototype. Furthermore, the bidirectional motion will produce an irregular AC voltage. In order to charge batteries or power electronic devices, the produced voltage of conventional regenerative shock absorber needs to be commutated with an electrical rectifier to produce DC output, in which the forward voltage of diodes unavoidably reduces the circuit's efficiency especially for lower power application. In order to sort out the problem, Li [82] proposed a mechanical motion rectifier coupled with a rack-pinion regenerative shock absorber to convert the bi-directional oscillation into unidirectional rotational motion. The developed module, which shown in Figure 2-5, is able to reduce the impact forces and friction. Due to the one-way clutch inside the gear module, this design can provide a unidirectional rotary motion to the generator and hence the output voltage signal does not necessarily need to go through an electrical rectifier. Both bench and on road tests were also conducted to verify the concept and advantages of MMR. The MMR based regenerative shock absorber can achieve mechanical efficiency over 60% and the backlash impact was significantly reduced. The average harvested power is around 40.4 and 25.6 watts on 30 and 93.4 Ω external resistance under 0.047 m/s vibration input. The prototype was also installed in a rod vehicle to show its feasibility, in which 15.4 watts is obtained at 15 mph when the vehicle is travelled on a smooth paved road.

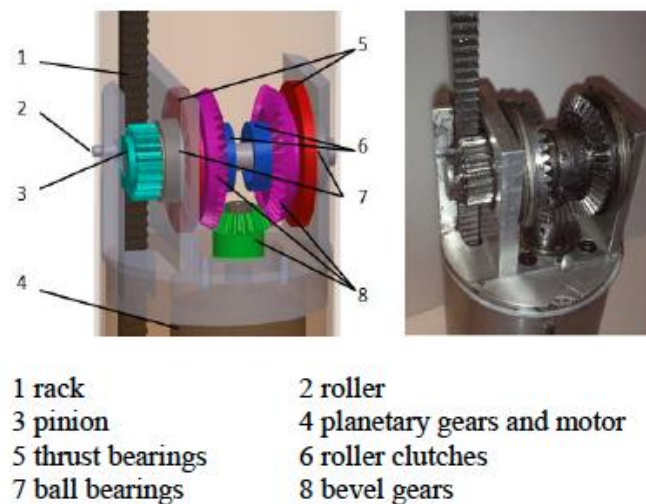


Figure 2-5: Mechanical motion rectifier gear module prototype [83]

Inspired by the this, Zhang [22] developed a similar design of rack-pinion regenerative shock absorber with two one-way clutches. The prototype of their motion rectification module was shown in Figure 2-6. The manufactured prototype is able to generate electrical power around 4.302 watts at 2.5 Hz, 7.5 mm harmonic input.

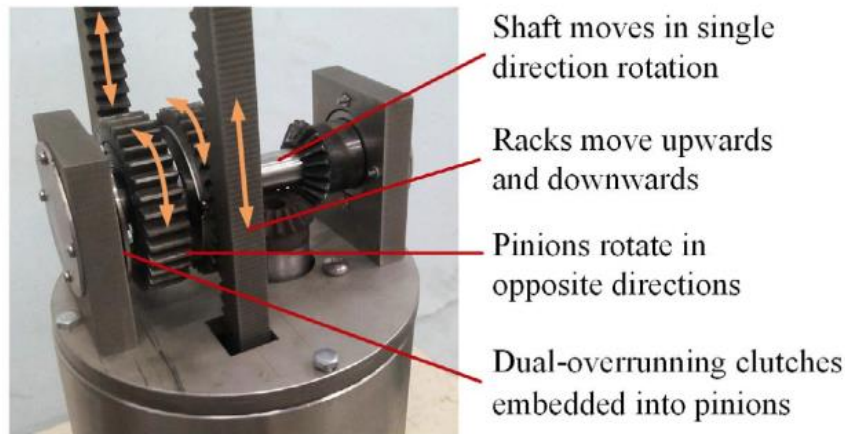


Figure 2-6: Dual one-way clutch transmission system [22]

Similarly, Liu [84] adopted the MMR gear module with the ball-screw regenerative shock absorber to further reduce the backlash effect and the energy harvesting efficiency can go up to 51.9% when the prototype was excited by 4 Hz, 2mm vibration input. Field test was also conducted in [52] to show the feasibility of the proposed energy harvesting technique. The result shows that the average electrical power extraction is 13.3 watts in 8 seconds which proves the design is able to continuously extract a significant amount of energy from vehicle suspension systems. Salman [70] employed helical gears and one-way clutches to convert bidirectional shaft motion into unidirectional motion. With this mechanism, low-wattage electrical device of an electric vehicle was powered and a maximum efficiency of up to 52% under a 1Hz harmonic vibration input was achieved. Wang [85] applied two one-way clutches and a planetary gearbox on regenerative shock absorber by using ball-screw mechanism. Fang [51] proposed a hydroelectric shock absorber with four check valves to rectify the bidirectional flow into unidirectional flow in order to drive a hydraulic pump which could subsequently drive an electrical generator.

2.3 Model of electromagnetic vibration regenerative shock absorber

As stated earlier, electromagnetic regenerative shock absorber can be realized as an interface between mechanical and electrical system which converts vibration energy into harvestable electrical energy. In this section, a review of an electromagnetic regenerative shock absorber model including its linear and nonlinear properties will be presented. This helps to develop a better understanding of the regenerative shock absorber characteristics in physics and predict its behaviour over the frequency ranges of interest.

2.3.1 Conventional ideal model

Generally, an ideal electromagnetic vibration energy harvesting system can be modelled as a spring-mass-damper system coupled to a generator. [72] For a SDOF electromagnetic regenerative shock absorber with external vibration excitation shown in Figure 2-7, the governing equation of motion can be given by

$$M\ddot{z} + c\dot{z} + kz = -M\ddot{y} - Bil \quad \text{eq (2-2)}$$

Where y is the excitation displacement, M is the mass; c is the mechanical damping coefficient; k is the spring stiffness; z is the relative displacement between the mass and base; i is the current through the circuit; B is the magnetic field flux density; l is the length of the wire which constitutes the coil. Assuming the electromagnetic harvester has a voltage source, the governing equation of the electrical system is given by

$$V = Bl \frac{dz}{dt} - (R + R_e)i - L_e \frac{di}{dt} \quad \text{eq (2-3)}$$

Where V is the produced voltage; R, R_e and L_e are the electrical internal, load resistance and coil inductance respectively.

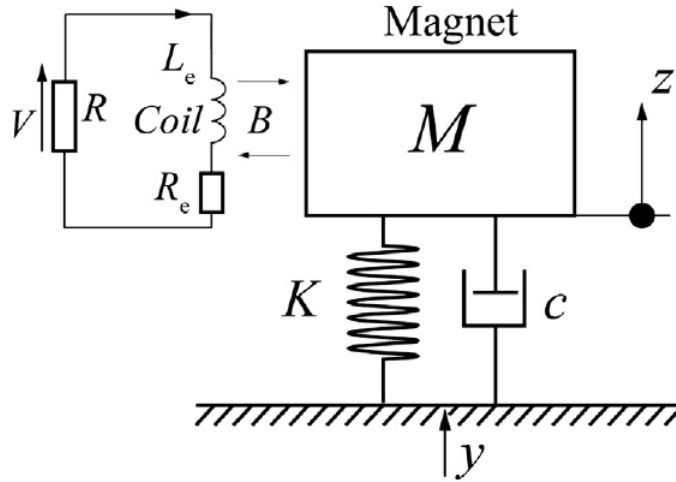


Figure 2-7: Schematic of a single degree of freedom electromagnetic vibration regenerative shock absorber connected to the electrical load resistance [72]

The model in Figure 2-7 is generally used to understand the conversion from mechanical vibration energy into electricity and is only valid for linear electromagnetic regenerative shock absorbers.

2.3.2 Inerter based ideal model

Inerter is a newly developed mechanical element that was first introduced by Smith [86]. In the past few years, significant advantages of employing passive inerter-based isolators as well as energy harvesters have been identified for engineering applications [87-89]. Inerter can be used to change the dynamic property of a vibration system, and it has been employed in the design of vehicle suspension systems, aircraft landing gear shimmy suppression and building vibration control systems are examples of its many applications [90-92]. Among these applications, inerter always appears in some mechanical vibration isolation systems which result in a more complex structure than a conventional system consisting only springs and dampers. In this section, the concept, physical realization and the ideal model of an inerter based regenerative shock absorber are reviewed.

Concept of Inerter

The generally used force-current analogy between mechanical and electrical systems introduced by Firestone [93], sets the mechanical force F analogues to electrical current i , and the relative velocity Δv to electrical voltage V . With the force-current analogy, the electrical inductor and resistor can be mapped to the mechanical spring and damper respectively. According to the Newton's second law, the applied force to the mechanical mass is proportional to its absolute acceleration, where one terminal of the mass is grounded [93]. However, its analogy to the capacitor with one terminal grounded is obviously incomplete, where the capacitor works based on the voltage difference between two terminals. The concept of Inerter was first proposed by Smith [86] to give a complete analogy between mechanical and electrical systems. Equivalent to the capacitor, inerter is a two-terminal device in which the applied force is proportional to the relative acceleration

$$F = b(\dot{v}_1 - \dot{v}_2) \quad \text{eq (2-4)}$$

where \dot{v}_1 and \dot{v}_2 are the accelerations of the two terminals of the inerter. The constant b is called inertance which has the same unit as mass.

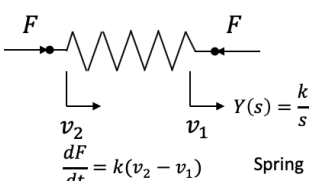
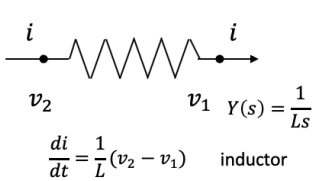
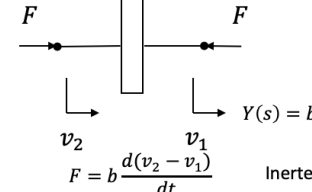
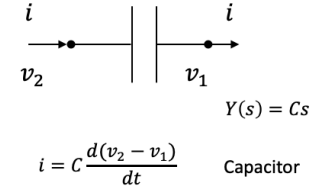
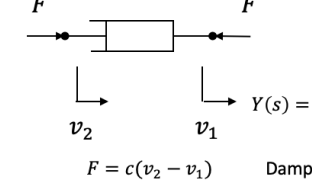
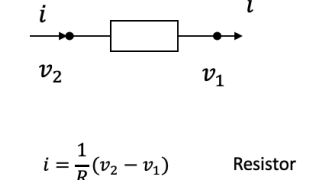
Mechanical	Electrical
 <p> F v_2 v_1 F $Y(s) = \frac{k}{s}$ $\frac{dF}{dt} = k(v_2 - v_1)$ Spring </p>	 <p> i v_2 v_1 i $Y(s) = \frac{1}{Ls}$ $\frac{di}{dt} = \frac{1}{L}(v_2 - v_1)$ inductor </p>
 <p> F v_2 v_1 F $Y(s) = bs$ $F = b \frac{d(v_2 - v_1)}{dt}$ Inerter </p>	 <p> i v_2 v_1 i $Y(s) = Cs$ $i = C \frac{d(v_2 - v_1)}{dt}$ Capacitor </p>
 <p> F v_2 v_1 F $Y(s) = c$ $F = c(v_2 - v_1)$ Damper </p>	 <p> i v_2 v_1 i $Y(s) = \frac{1}{R}$ $i = \frac{1}{R}(v_2 - v_1)$ Resistor </p>

Figure 2-8: A mechanical-electrical Force-Current analogy [94]

As shown in Figure 2-8, with this representation of an inerter, an electrical circuit (consisting of a resistor, a capacitor and an inductor) can be made analogous to a mechanical system, which has a spring, a damper and an inerter.

Physical realisations

Physical realisations of an inerter can be classified into three categories: rack-pinion, ball-screw and hydraulic based mechanisms. The rack-pinion inerter is constructed by meshing a flywheel with a rack-pinion gear [95, 96], while the screw based inerter can be designed as a flywheel mounted on a ball-screw [97]. The schematics of these two mechanisms are respectively shown in Figure 2-9 and Figure 2-10 [98]. A hydraulic inerter, shown in Figure 2-11 [99], works based on the pressure difference on either sides of the cylinder's piston that pushes the fluid through the pipes in order to drive the hydraulic motor. Based on above illustrations, inerter is essentially a two-port inertia device that works on the acceleration difference between two terminals. Note that, when one terminal of the inerter is grounded, it behaves as a mass that is equal to the inerter's inertance. The value of inertance can be simply tuned by adjusting the moment of inertia of flywheel, so it is possible to tune its apparent mass much bigger than its actual mass.

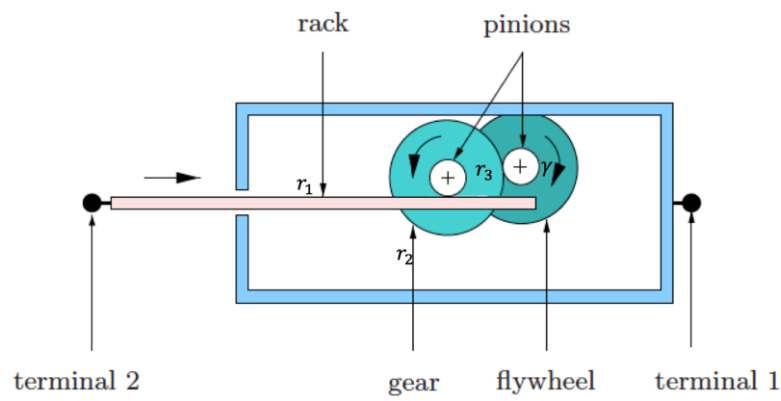


Figure 2-9: Schematic structure of rack-pinion inerter [98]

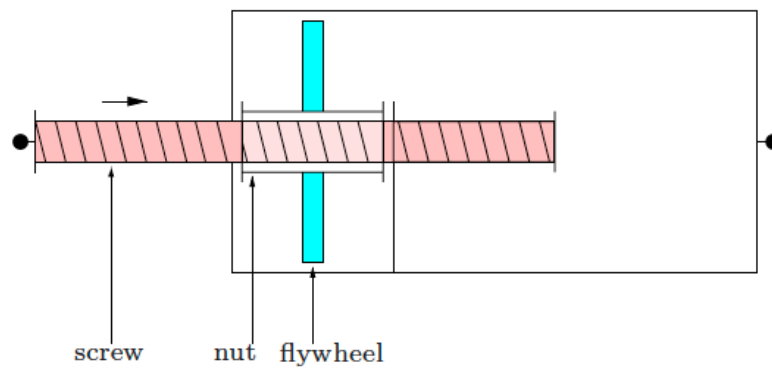


Figure 2-10: Schematic structure of ball-screw inerter [95]

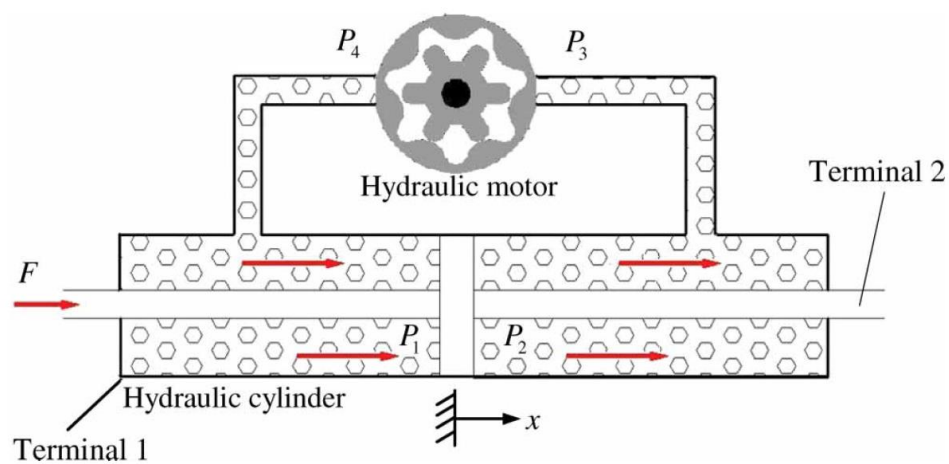


Figure 2-11: The working principle of the hydraulic inerter [99]

Application of inerter in isolator and regenerative shock absorber

In [86], Smith introduced initial ideas for applications of the inerter to enhance the performance of a vibration absorber and subsequently helped to design a new suspension

structure by replacing the mass element. The inerter, known as a 'J-damper' was firstly applied for the suspension of a Formula one racing car, manufactured by McLaren in 2005 [100], where a parallel spring-damper-inerter isolator layout was introduced, see Figure 2-12, to achieve a better handling and grip [101].

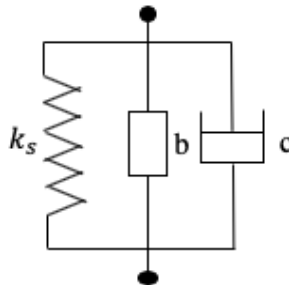


Figure 2-12: Inerter based vibration isolator

Studies the inerter-based suspension for road vehicles have been developed in the literature. Smith and Wang [91] demonstrated eight inerter based suspension layouts in both quarter car and full car models through that, compared with a conventional spring damper isolator, 10% improvement in ride comfort, tyre grip and dynamic load carrying can be achieved. In [86] it is shown that by allowing higher mechanical impedance for the vibration isolator, better vehicle dynamic performance can be achieved [102].

Furthermore, the concept of inerter has been expanded to model of an energy harvesting device. In [75], an inerter-based mechatronic system has been applied to vehicle suspension control which achieves significant performance improvement. Nakano and Suda [103] developed a self-powered active regenerative shock absorber based on the ball-screw mechanism and their numerical solutions showed that it can obtain better suppression performance than a passive or a semi-active control systems without consuming external energy. Nakamura [104] proposed a novel electromagnetic inertial mass damper (EMID) consisting of an inerter and an electromagnetic (EM) damper, in which the former provides inertance and the latter provides EM damping. The design shows a great potential to evolve to be self-powered semi-active damper or even serves as the power source for structural monitoring system. Zuo [82] developed a rack-pinion based regenerative shock absorber which can be realized as a spring-damper-inerter system. Besides theoretical analysis, road tests were conducted to physically demonstrate its damping characteristics and energy recovery performance in a passenger vehicle.

2.3.3 Nonlinear model

In analytical models, an ideal regenerative shock absorber is usually assumed with negligible mass and other typical device features (i.e. friction, backlash, elastic effect etc.) are not considered. Some nonlinear properties of the existing models of a ball-screw based electromagnetic regenerative shock absorber are discussed in [105]. Moreover, nonlinearities including friction, backlash effects and their influences on vehicle suspension performance were investigated in [98]. The parameters are then adjusted by comparing the time response of the theoretical model and the regenerative shock absorber's experimental results. Therefore, lab-tests need to be undertaken to compare the physical characteristics of devices with the ideal models. It is important to have a general understanding of how to build a realistic model by observing experimental results, that can provide accurate predictions of a regenerative shock absorbers' behaviour.

Coulomb Friction

Coulomb friction is a type of constant mechanical damping in which energy is dissipated via sliding friction. According to the coulomb damping model [106], the restoring force due to the friction can be expressed as

$$F = F_c \text{sgn}(\dot{z}) \quad \text{eq (2-5)}$$

Where F_c is the coulomb damping coefficient which can be identified when the applied velocity changes the sign function of velocity \dot{z}

$$\text{sgn}(\dot{z}) = \begin{cases} 1, \dot{z} > 0 \\ 0, \dot{z} = 0 \\ -1, \dot{z} < 0 \end{cases} \quad \text{eq (2-6)}$$

In [98], it is clearly defined that for an inerter based regenerative shock absorber/isolator, the friction of the device dominates the low frequency range of the force response, while the effect of viscous damper, inertance is negligible compared with coulomb friction.

Backlash model

The backlash effect can be defined as the lost motion in a mechanism caused by gaps between the parts. The impact of backlash can be stated as a mechanical element which reaches the maximum distance or angle, continuously moving in one direction without applying any force to the next part in a mechanical sequence [107].

Hunt and Crossley [108] developed a method to obtain the backlash effect by using a spring-damper model. Wang [109] realized that Hunt's model can be used to apply to similar rotary designs. In Figure 2-12, considering a displacement x in the axial direction, the corresponding deformation may be shown as $x_s = x_1 - x_3$, the backlash displacement as $x_b = x_3 - x_2$ and linear displacement between two terminals as $x_d = x_1 - x_2$. Therefore, the corresponding force F according to Figure 2-13 can be expressed by

$$F(t) = k_s x_s + c_s \dot{x}_s = k_s (x_d - x_b) + c_s (\dot{x}_d - \dot{x}_b) \quad \text{eq (2-7)}$$

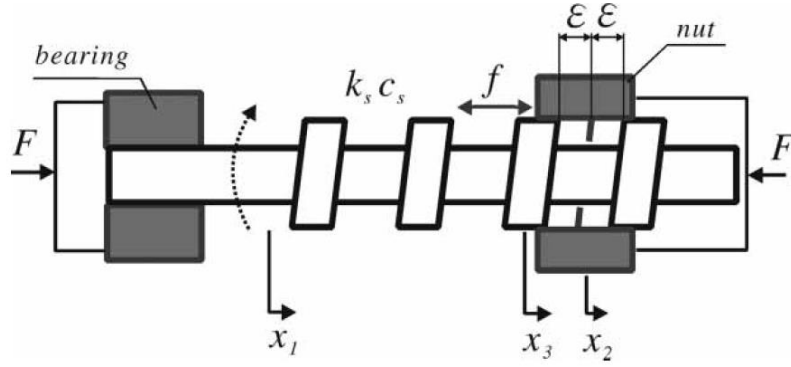


Figure 2-13: Schematic diagram of spring damper model of backlash effect [98]

Where k_s is the elasticity effect and c_s is the viscous damper.

It is shown in [98] that the backlash model can be expressed as a nonlinear dynamic system described by the following equation

$$x_b = \begin{cases} \max\left(0, \dot{x}_d + \left(\frac{k_s}{c_s}\right)(\dot{x}_d - \dot{x}_b)\right), & x_3 - x_2 = -\varepsilon, F \leq 0 \\ \dot{x}_d + \left(\frac{k_s}{c_s}\right)(\dot{x}_d - \dot{x}_b), & |x_3 - x_2| < \varepsilon, F = 0 \\ \min\left(0, \dot{x}_d + \left(\frac{k_s}{c_s}\right)(\dot{x}_d - \dot{x}_b)\right), & x_3 - x_2 = \varepsilon, F \geq 0 \end{cases} \quad \text{eq (2-8)}$$

Where ε is the deformation of the teeth.

The main purpose of tuning the model with backlash effect is to match the analytical model as closely as possible to the experimental behaviour of the proposed regenerative shock absorber prototype. In 2009, an experimental study of mechanical devices was presented to approximate the dynamics of an ideal inerter based regenerative shock absorber [95]. It was observed that force signals were not sinusoidal due to a high-frequency spiking characteristic in the experimental results. Attempting to reproduce and explain the spiking characteristic in simulations, a model of a spring-damper-inerter with backlash effect was established. In [97], nonlinear properties of inerter based regenerative shock absorbers were discussed in both quarter car and full car models. Analytical results illustrated that the performance

benefits were slightly degraded by the manufactured nonlinearities. It should be noted that the backlash effect is unavoidable for nearly all reversing mechanical couplings, even though this effect can be compensated.

2.4 Mobility and impedance methods in vibration analyses

Concepts of mechanical impedance and mobility are very useful in describing dynamics of structural vibration. The possibility of using the electrical impedance concept in a vibration system was first realised by Arthur G. Webster [110]. It has been widely used to study linear electrical-mechanical or purely mechanical vibration systems. [111] In this section, fundamental principles of impedance and mobility methods is presented, and it will be used later in this thesis to describe the dynamics of a vibration source. A more detailed analysis and discussion of impedance and mobility can be found in [112].

2.4.1 Simple lumped elements

Figure 2-14 shows a linear mechanical system with two connections. [112] If the mechanical element is considered as spring, damper or mass, the relationship between the force and displacement can be obtained respectively by following equations

$$f_1 = -f_2 = k(x_1 - x_2) \quad \text{eq (2-9)}$$

$$f_1 = -f_2 = c(\dot{x}_1 - \dot{x}_2) \quad \text{eq (2-10)}$$

$$f_1 + f_2 = m\ddot{x}_1 \quad \text{eq (2-11)}$$

Where k is the spring stiffness, c is the damping coefficient and m is the mass. Assume a harmonic force excitation to the proposed mechanical elements in a form of $f = Fe^{j\omega t}$ with displacement $x = Xe^{j\omega t}$, where ω is the angular frequency. By fixing one point of the spring and damper and set one of the forces on the mass to zero. According to the literature [113, 114], the mechanical impedance is a measure of how much a structure resisting motion when subjected to a harmonic force. The mechanical impedance is defined by the ratio of the applied force at a single point to the produced velocity [112]. Therefore, the mechanical impedance for each element can be expressed by

$$Z_k(\omega) = \frac{F_1}{\dot{x}_1} = \frac{k}{j\omega} \quad \text{eq (2-12)}$$

$$Z_c(\omega) = \frac{F_1}{\dot{x}_1} = c \quad \text{eq (2-13)}$$

$$Z_m(\omega) = \frac{F_1}{\dot{x}_1} = j\omega m \quad \text{eq (2-14)}$$

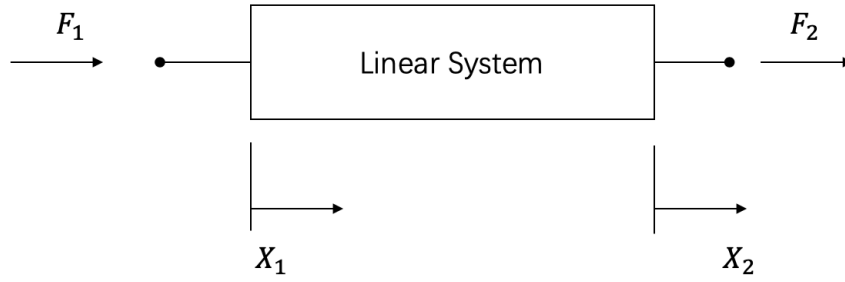


Figure 2-14: A linear mechanical system with two forces applied

The mobility of a mechanical element can simply be expressed by the reciprocals of eq (2-12) to eq (2-14), which are given by

$$Y_k(\omega) = \frac{\dot{X}_1}{F_1} = \frac{j\omega}{k} \quad \text{eq (2-15)}$$

$$Y_c(\omega) = \frac{\dot{X}_1}{F_1} = \frac{1}{c} \quad \text{eq (2-16)}$$

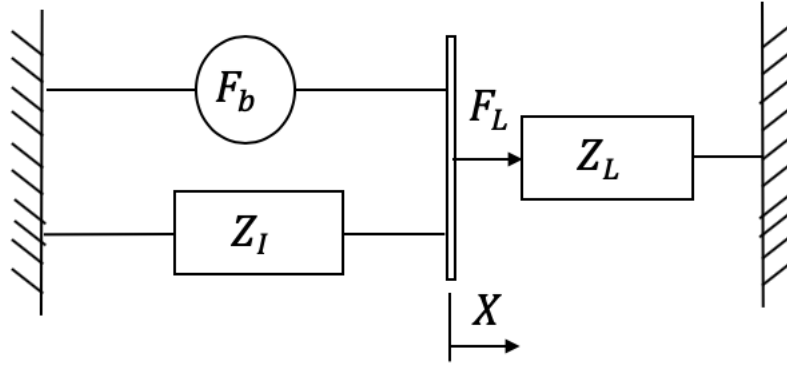
$$Y_m(\omega) = \frac{\dot{X}_1}{F_1} = \frac{1}{j\omega m} \quad \text{eq (2-17)}$$

As discussed in [111], one advantage of the mechanical impedance/mobility is to provide a relative easy method to combine mass, spring and damper at a single point without forming complex algebra equations. In the meantime, the concept is quite useful to help interpreting the dynamic behaviour of the system.

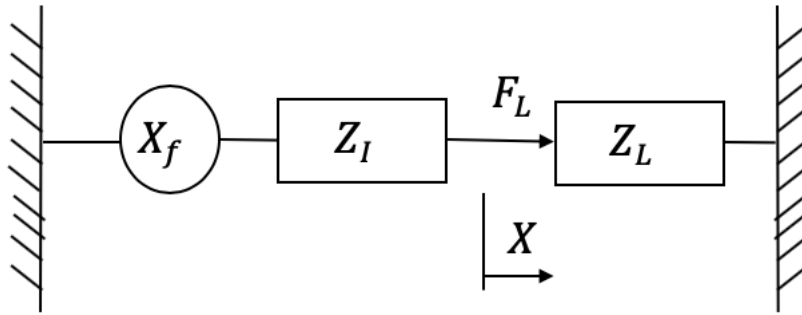
2.4.2 Connection to a vibration source

The impedance/mobility approach provides a convenient way to illustrate characteristics of a vibration source as discussed in [115]. Generally, a vibration source can either be represented as a blocked force F_b in parallel with an internal impedance Z_I (i.e., Thévenin equivalent system), or a free velocity \dot{X}_f in series with an internal impedance (i.e., Norton equivalent system). These equivalent systems are shown in Figure 2-15 [112] where they are connected to the load impedance Z_L . For a Thévenin equivalent system, the relationship between the blocked force F_b , free velocity \dot{X}_f and the source internal impedance Z_I can be expressed by

$$F_b = Z_I \dot{X}_f \quad \text{eq (2-18)}$$



(a) Thévenin equivalent system



(b) Norton equivalent system

Figure 2-15: Vibration source of internal impedance Z_I connected to a load impedance Z_L

Either Thévenin or Norton equivalent system can be used to describe the vibration source by using the relationship in eq (2-18). Referring to Figure 2-15(a), the force applied to the load impedance is related to the blocked force of the source impedance as

$$F_L = \frac{F_b}{1 + \frac{Z_I}{Z_L}} \quad \text{eq (2-19)}$$

It can be observed from eq (2-19) that if the load impedance is much greater than the source impedance ($|Z_L| \gg |Z_I|$), the applied force to the load tends to be equal to the blocked force (*i. e.*, $F_L \approx F_b$). In this case, the vibration source behaves as a force source. This means that the force applied to the load is insensitive to the dynamic of the load. [115]

Now, consider Figure 2-15(b), where the velocity of the load is related to the free velocity of the source by:

$$\dot{X}_L = \frac{\dot{X}_f}{1 + \frac{Z_L}{Z_I}} \quad \text{eq (2-20)}$$

In contrast to the previous case, if the load impedance is much less than the source impedance ($|Z_L| \ll |Z_I|$), then $\dot{X}_L \approx \dot{X}_f$. In this case, the source behaves as a velocity source, which means that the velocity input to the load is insensitive to the dynamic behaviour of the load [115].

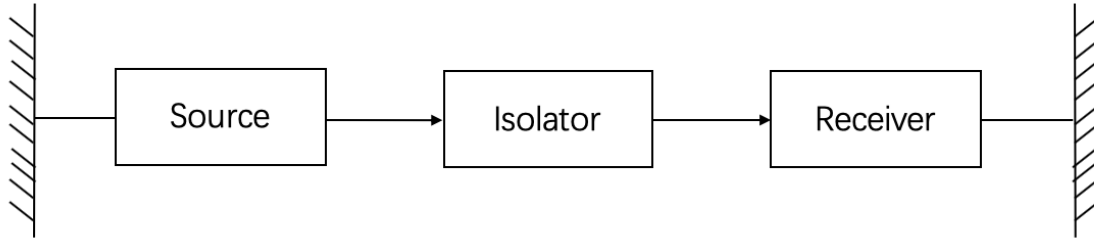


Figure 2-16: Schematic diagram of a vibration system

The general vibration isolation problem involves a source and a receiver with an isolator placed between them, see in Figure 2-16. The concept of mobility/impedance has been widely used to illustrate the dynamics of sources [111, 116], vibration isolation [117, 118], isolation effectiveness [115, 119] and vibration damping [120, 121]. The approach provides a convenient way to describe the vibration source-receiver characteristics and can further be expanded to discuss more complex vibration structures.

2.5 Mechanical power flow

The fundamental concept of vibration power flow was initially developed by Goyder and White [119, 122, 123]. In this study, the rate of change of mechanical energy is employed to characterise the dynamics of a vibration system. Different analytical approaches have been developed to understand the power flow characteristics of passive and active vibration control systems [124, 125]. Consequently, the concept has been further used to study the power flow in nonlinear energy harvesting systems [126, 127]. The implementation of power flow is useful as it combines characteristics of both force and velocity parameters. Moreover, it can be employed for a more in-depth analyses, reflecting vibration transmission between sub-structures within an integrated system [128].

To present the approach, let us start with the general governing equation of a single degree of freedom system that can be written as

$$m\ddot{x} + c\dot{x} + kx = f(t) \quad \text{eq (2-21)}$$

where $f(t)$ is the external force, \dot{x} denotes the corresponding velocity and m , c and k denote mass, damping and stiffness, respectively. Power flow in a vibration system is generally defined as the rate of change of mechanical energy, i.e.,

$$p(t) = f(t)v(t) \quad \text{eq (2-22)}$$

By multiplying the equation of motion eq (2-21) by the velocity $\dot{x}(t)$, the power balance equation is obtained as

$$m\ddot{x}\dot{x} + c\dot{x}\dot{x} + kx\dot{x} = f(t)\dot{x} \quad \text{eq (2-23)}$$

Where $kx\dot{x}$ and $m\ddot{x}\dot{x}$ are changing rates of the system's kinetic and potential energies respectively; while $c\dot{x}\dot{x}$ and $f(t)\dot{x}$ represent instantaneous power dissipation and input power respectively. The time average of power dissipation and input power can be obtained by

$$p_d = \frac{E_d}{t} = \frac{1}{t} \int_0^t c\dot{x}\dot{x} dt \quad \text{eq (2-24)}$$

$$p_{in} = \frac{E_{in}}{t} = \frac{1}{t} \int_0^t f(t)\dot{x} dt \quad \text{eq (2-25)}$$

According to [128], for a harmonically excited linear system, the change in mechanical energy eventually become zero over a full cycle, while the input energy always equals to the power dissipation. However, these conclusions might not hold for a nonlinear or piecewise linear system as the motion or force becomes nonharmonic. To obtain the power flow behaviour of a nonlinear or piecewise linear system, it is necessary to solve power balance equation in eq (2-23). The harmonic balance approach can be further used to understand the power input, transmission and dissipation relationships for both linear and nonlinear harmonic excitation systems.

2.6 Summary

Previous studies on modelling of linear regenerative shock absorbers, including power flow and dissipation, have provided sufficient theoretical foundation to predict their behaviours. However, the concept of mechanical power flow is rarely studied for a piecewise linear energy harvesting system. In [52], an MMR-based regenerative shock absorber is modelled as a piecewise linear system which is due to the switching between engagement and disengagement actions of one-way clutches. The mechanical power flow approach is helpful to interpret the power transmission between the primary mechanical and secondary electromechanical systems. More precisely, the approach can then be used to have deeper understand on the consequence of switching within MMR on system dynamics. Moreover, conventional regenerative shock absorbers need to commutate with electrical rectifiers in

order to regulate the produced voltage. The literature so far has not made any recommendations on when either an MMR or electrical rectification may be more beneficial and hence the desirable conditions for their usage have not been determined yet. Therefore, it is necessary to conduct a numerical study to compare the performance of these rectification options. As stated in Section 2.4, the concept of mechanical impedance/mobility is very useful to describe the vibration source characteristics [115]. This analysis approach has not previously been used to describe the dynamics of the vibration source in the case of a road vehicle suspension. It is generally unclear as what assumptions should be made on the vibration source characteristics (i.e., force or velocity) as it is potentially being affected by the relative mobility between the source, the isolator and the receiver. Moreover, the literature review [40] has revealed that it is necessary to conduct further investigation on the implementation of an MMR-based regenerative shock absorber in a vehicle suspension system. This should be done by considering the effect of switching within the MMR on power flow, energy harvesting and ride comfort. Additionally, in order to provide reliable guidance for implementing the MMR-based regenerative shock absorbers in road vehicles, it is necessary to develop a practical design process for selecting system parameters. The proposed technique is required to take into account all physical constraints including maximum allowable displacement of the sprung mass from its equilibrium point, maximum speed, acceptable generator size and the overall damping of the suspension. For example, the damping ratio of a vehicle suspension is generally fixed for vibration suppression purposes and this limiting factor must be addressed in the design process. Despite theoretical study, it is necessary to conduct a laboratory test of the developed prototype. The experimental study is able to give a physical identification of design prototype and study their departures from ideal behaviour. System parameters can be estimated from the measured data, which allows to build a more accurate model. The newly developed experimental model can provide important references for its actual application.

Chapter 3 Regenerative shock absorber with MMR

Previous researchers have shown that adopting the concept of mechanical motion rectifier gear module (MMR) in regenerative shock absorber, dynamics of whole structure tend to behave as a piecewise linear system. [53] It has been demonstrated that the switching between engagement and disengagement of the one-way clutch allows the coupled generator to work more continuously and the regenerated voltage potentially never falls to zero. However, it remains unclear whether MMR based system can enhance the energy harvesting performance over conventional regenerative shock absorber without MMR besides technical factors as it has not been well addressed in the literature. [36, 82, 83]

In this chapter, the performance of MMR based regenerative shock absorber corresponding to the lab-test case (one terminal of the design is clamped) will be evaluated. In order to comprehensively study dynamics of MMR system, its energy harvesting as well as mechanical power flow performance are evaluated. Additionally, an analogy of active and reactive power between electrical and mechanical systems is proposed based on force-current analogy, which can be expanded to have a deeper understand on power transmission between sub-systems of regenerative shock absorber with MMR. Moreover, the dynamic model developed in [53] is to assume the system is subjected to a prescribed velocity input, the actuator actively varies the applied force and power during the disengagement period in order to consistent the velocity input. While in some cases, the vibration source behaves as a prescribed force source, it is necessary to investigate system dynamics and consider whether MMR is beneficial when the vibration source behaves the other way around. After discussing the dynamics of MMR based regenerative shock absorber when it is subjected to a single frequency input, it is necessary to look at its response when the vibration input is considered as multiple harmonics. The result will demonstrate whether the time instant of disengagement and re-engagement will be dominated by one single frequency. In the meantime, the energy harvesting and power flow performance will be evaluated as well. The approach presented in this chapter is based on a piecewise compound model comprised of a primary system which is the lead-screw with MMR gear module and a secondary switchable system including generator and coupled electrical load. The secondary system can be engaged and disengaged from the primary system according to the mechanism of sprag-clutch inside the MMR module.

3.1 Linear model of regenerative shock absorber

First of all, the performance of linear regenerative shock absorber when one terminal of the design is clamped is evaluated in this section. The model is intended to demonstrate the dynamics of linear system including power flow and dissipation, while the result can be further used to compare with the MMR based piecewise linear system. As shown in Figure 3-1, an inerter based regenerative shock absorber consists of mechanical damping coefficient c_m, c_e ; a translational spring k and an inerter b . The regenerative shock absorber is subjected to a harmonic force excitation $f(t)$ with the corresponding steady-state response $x = X\sin(\omega t)$. The dynamic governing equation of motion in Figure 3-1 can be written in a form as

$$b\ddot{x} + (c_e + c_m)\dot{x} + kx = f(t) \quad \text{eq (3-1)}$$

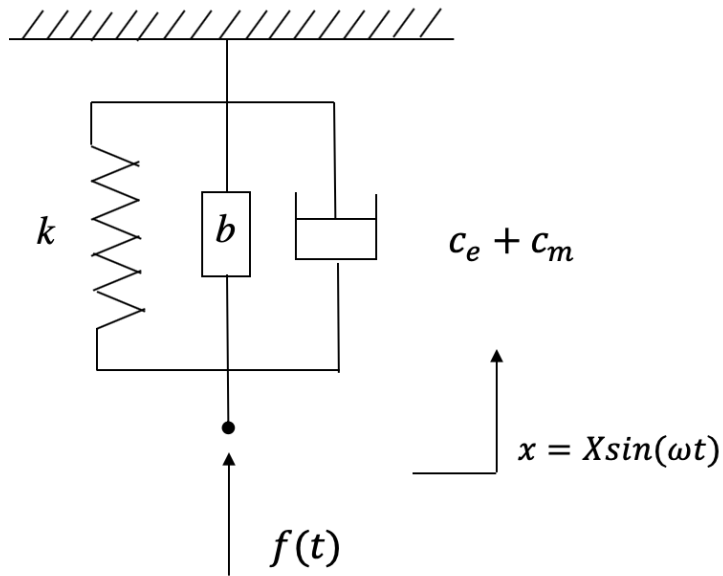


Figure 3-1: Schematic diagram of regenerative shock absorber (one terminal is clamped) excited under force input

Multiplying the governing eq (3-1) by the velocity \dot{x} , the power balance equation of the system then becomes

$$b\ddot{x}\dot{x} + (c_e + c_m)\dot{x}^2 + kx\dot{x} = f(t)\dot{x} \quad \text{eq (3-2)}$$

Alternatively, it can be rewritten in the form by

$$\dot{K} + p_d + \dot{U} = p_{in}(t) \quad \text{eq (3-3)}$$

Where $\dot{K} = b\dot{x}\dot{x}$ and $\dot{U} = kx\dot{x}$ are the changing rates of system kinetic and potential energies respectively; p_d and p_{in} are instantaneous dissipated and input power respectively. eq (3-3) illustrates that the instantaneous mechanical power into the system equals to the power absorbed by the damper plus the sum of changing rates of kinetic and potential energies. When the system is excited under its natural frequency $\omega_n = \sqrt{\frac{k}{b}}$, the sum of instantaneous changing rates of mechanical energy always equals to zero. In this case, the instantaneous input power p_{in} is equal to the corresponded power dissipation p_d .

When the system is excited under off-resonance frequency (i.e. $\omega \neq \omega_n$), an integration of the power balance eq (3-3) with respect to time t , which leads to

$$\Delta K + E_d + \Delta U = E_{in} \quad \text{eq (3-4)}$$

Where ΔK and ΔU are net changes of kinetic and potential energy; E_d and E_{in} are total dissipated and input energy respectively in the time domain. The change of system mechanical energy is obtained by summing ΔK and ΔU over a cycle. For a steady-state response $x = X\sin(\omega t)$, which leads to

$$\Delta K = \int_0^{2\pi/\omega} b\dot{x}\dot{x}dt = 0 \quad \text{eq (3-5)}$$

$$\Delta U = \int_0^{2\pi/\omega} kx\dot{x}dt = 0 \quad \text{eq (3-6)}$$

The sum of mechanical energy dissipation and extraction over a cycle is

$$E_d = \int_0^{2\pi/\omega} (c_e + c_m)\dot{x}^2 dt = \pi(c_e + c_m)\omega X^2 \quad \text{eq (3-7)}$$

From the expression eq (3-5) and eq (3-6), it is clearly that spring and inerter do not consume any energy by integrating the corresponding change of mechanical energy over a cycle. The mechanical power delivered to them flows back and forth between the vibration source and elements themselves. This can be illustrated in the same way as electrical reactive power, the reactive power exists when the voltage and current are not in phase, it flows to the load as much as it flows back. Ideally, it does not consume any real power, but it requires more current drawn through the transmission wires which potentially leads to a lower power factor. By substituting the relationship into eq (3-4), the input energy E_{in} will all be dissipated by the damper E_d . In the absence of mechanical damping ($c_m = 0$), all the input power will be absorbed by the electrical damper, the energy harvesting efficiency then becomes 100%. However, this conclusion may not valid for a nonlinear or piecewise linear system as the system applied power becomes nonharmonic.

3.2 Piecewise linear model of MMR regenerative shock absorber

The mechanical motion rectifier (MMR) is able to provide a unidirectional rotational input for the coupled generator due to the compound one-way clutch. Figure 3-2 shows the schematic diagram of the motion rectifier gear system, no matter the shaft rotates in clockwise or anti-clockwise direction, the connected generator always works in one single direction.

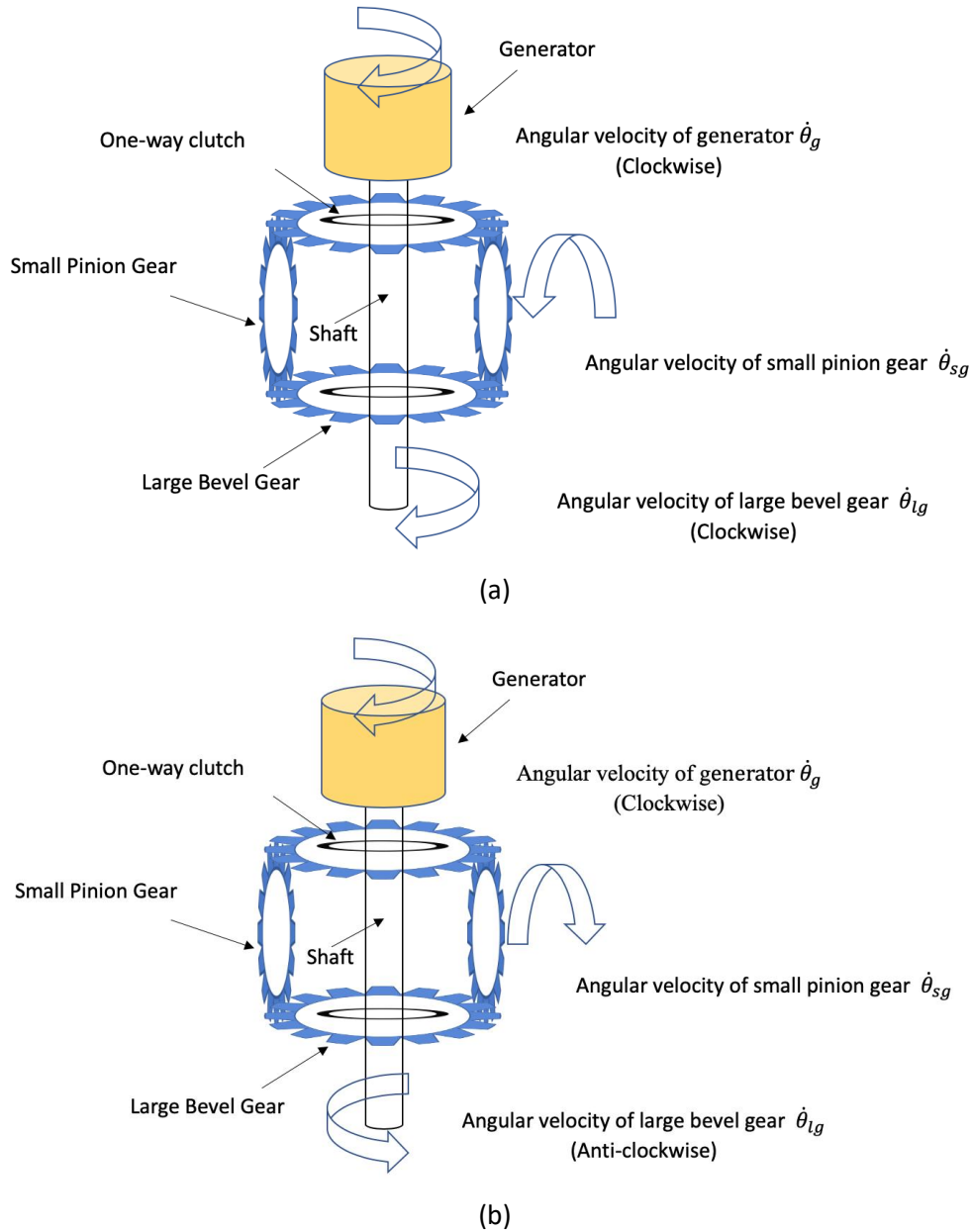


Figure 3-2: Schematic diagram of motion rectifier gear module (a) Clockwise direction (b) Anti-clockwise direction

It was demonstrated that the MMR based regenerative shock absorber behaves as a piecewise linear system due to the engagement and disengagement of the one-way

clutch.[84] At the time instant where the external force acting on the generator coupled electrical system reduces to zero, the one-way clutch tends to disengage the generator coupled electrical system from the vibration source. As a result, the model will be separated into two systems undergoing motions independently until the speed of primary system catching up with the generator. Different from the design which Zuo proposed in [53], the input and output shaft of the proposed design is in the same axis which yielding different torque transmission relationship. In this section, two piecewise linear systems will be introduced depending on the prescribed vibration source. Moreover, time instants of sprag-clutch engaging and disengaging generator from the vibration source are predicted, which allows to evaluate the performance of the MMR system.

3.2.1 Dynamics of piecewise linear systems

Based on the paper [52], similar theoretical approach is adopted. Considering the system is excited by a harmonic waveform, it is defined that when the system applied force/torque to the generator reduces to zero, the sprag-clutch inside MMR will disengage the generator from the vibration source which leads zero torque/power transmission between them. During the disengagement period, generator will release the residual kinetic energy stored on the shaft to electrical power doing a decaying vibration with an initial velocity. Once the driving speed catches up with the output, sprag-clutch will reconnect the generator with the vibration source and restart transmitting torque and power to it.

At the engaged state, the torque transmission relationship according to Figure 3-2 can be obtained as follows:

From the lead-screw to the large bevel gear:

$$T_{ls} - T_{lg} = J_{lg} \ddot{\theta}_{lg} \quad \text{eq (3-8)}$$

From the large bevel gear to the small bevel gear

$$T_{lg} - T_{sg} = J_{sg} \ddot{\theta}_{sg} \quad \text{eq (3-9)}$$

From the small bevel gear to the large bevel gear

$$T_{sg} - T_{lg} = J_{lg} \ddot{\theta}_{lg} \quad \text{eq (3-10)}$$

From large gear to the generator and idle small bevel gear

$$T_{lg} - T_{emf} - T_m = J_g \ddot{\theta}_g + J_{sg} \ddot{\theta}_{sg} \quad \text{eq (3-11)}$$

Where T_{emf} is the electromagnetic torque produced by the generator $T_{emf} = c_e \dot{\theta}_g$. T_m is the mechanical damping torque $T_m = c_m \dot{\theta}_g$. c_e, c_m is the rotational electrical and mechanical damping coefficient, $J_g, J_{lg}, J_{sg}, J_{ls}$ is the rotary inertia of the generator, large bevel gear, small bevel gear and lead screw respectively. $\dot{\theta}_g$ is the rotary velocity of the generator, $\dot{\theta}_{ls}$ is the angular velocity of lead screw which equals to the large bevel gear $\dot{\theta}_{lg}$. r_N is the gearhead ratio inside the generator. In addition to that, due to the gear ratio r_g between large and small bevel gear, the relationship of angular velocity between each part can be obtained as

$$\dot{\theta}_{sg} = r_g \dot{\theta}_g = r_g \dot{\theta}_{lg} = r_g \dot{\theta}_{ls} \quad \text{eq (3-12)}$$

Substituting eq (3-8) to eq (3-10) into eq (3-11)

$$T_{ls} = (J_{ls} + 2J_{lg} + 2r_g J_{sg} + r_N J_g) \ddot{\theta}_g + r_N c_e \dot{\theta}_g + c_m \dot{\theta}_g \quad \text{eq (3-13)}$$

Then, the equivalent moment of inertia can be formed by

$$J_{eq} = J_{ls} + 2J_{lg} + 2r_g J_{sg} + r_N J_g \quad \text{eq (3-14)}$$

The relationship between translational and angular velocity can be obtained as

$$\dot{\theta}_g = \left(\frac{2\pi}{l}\right) \dot{x}_{in} \quad \text{eq (3-15)}$$

Where l is the lead-screw pitch.

The applied force on the lead-screw and nut during engagement period is proportional to the input torque

$$F_e = \left(\frac{2\pi}{l}\right) T_{ls} \quad \text{eq (3-16)}$$

By taking eq (3-15) and eq (3-16) into eq (3-13), the relationship between the applied force and the linear motion is

$$F_e = \left(\frac{2\pi}{l}\right)^2 (J_{ls} + 2J_{lg} + 2r_g J_{sg} + r_N J_g) \ddot{x}_{in} + \left(\frac{2\pi}{l}\right)^2 (r_N c_e + c_m) \dot{x}_{in} \quad \text{eq (3-17)}$$

Equivalently, the system can be modelled as a switchable inerter in parallel with switchable damper. Since one terminal of the design is clamped, inerter behaves as a mass. Therefore, the equivalent inertance during engagement period can be obtained as

$$b_{eq} = \left(\frac{2\pi}{l}\right)^2 (J_{ls} + 2J_{lg} + 2r_g J_{sg} + r_N J_g) \quad \text{eq (3-18)}$$

While the sum of equivalent translational electrical and mechanical damper is

$$c_{eq} = \left(\frac{2\pi}{l}\right)^2 (r_N c_e + c_m) \quad \text{eq (3-19)}$$

The eq (3-18) shows the equivalent inrtance of the proposed design in Figure 3-2 which is directly proportional to the sum of rotary inertia. By placing the output gear in the same axis, the torque transmission relationship is relative straightforward, while the small bevel gear works as an idler gear, changes the direction of the large gear.

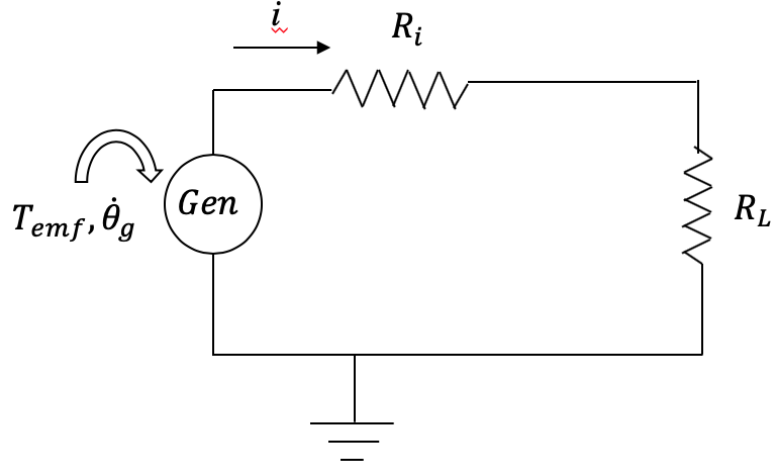


Figure 3-3: Equivalent diagram of the electrical load

Figure 3-3 shows the equivalent diagram of the coupled DC generator to the output shaft of MMR in the electrical system. R_i and R_L is the internal resistance of the generator and external load resistance respectively. To make the system easier to understand, the inductance effect is ignored here.

The induced electromagnetic torque T_{emf} produced by the generator is related to the current i which can be given by:

$$T_{emf} = k_t i \quad \text{eq (3-20)}$$

Where the torque coefficient k_t has units of [Nm/amp], and voltage (back emf) is related to the angular velocity $\dot{\theta}_g$ and the voltage coefficient k_e which units is [Volts/rad/s]

$$V_{emf} = k_e \dot{\theta}_g \quad \text{eq (3-21)}$$

According to the Kirchhoff's voltage law for the electrical circuit gives:

$$i(R_L + R_i) = k_e \dot{\theta}_g \quad \text{eq (3-22)}$$

Substituting eq (3-21) and eq (3-22) into eq (3-20)

$$T_{emf} = \frac{k_t k_e}{R_L + R_i} \dot{\theta}_g \quad \text{eq (3-23)}$$

The rotational electrical damping coefficient can be expressed as:

$$c_e = \frac{k_t k_e}{R_L + R_i} \quad \text{eq (3-24)}$$

The sum of equivalent translational damping coefficient can then be reformed by taking eq (3-24) into eq (3-19)

$$c_{eq} = \left(\frac{2\pi}{l} \right)^2 (r_N \frac{k_t k_e}{R_L + R_i} + c_m) \quad \text{eq (3-25)}$$

According to the Newton's second law, by assuming that there is no friction in the torque transmission, the applied torque T_G from the vibration source to the generator and coupled electrical load in Figure 3-4 is given by

$$T_G = J_g \ddot{\theta}_g + c_e \dot{\theta}_g \quad \text{eq (3-26)}$$

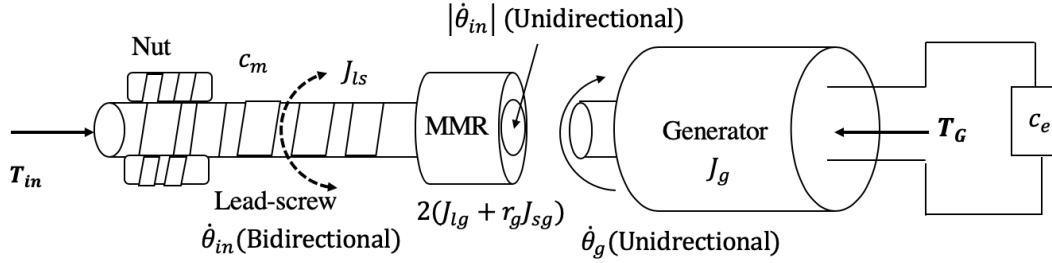


Figure 3-4: Schematic of dynamics of switching inside MMR

Disengagement happens when the applied torque on the generator and coupled electrical load (T_G) in eq (3-26) reduces to zero based on the mechanism of sprag-clutch

$$T_G = 0 \quad \text{eq (3-27)}$$

Once the disengagement happens, generator as well as coupled electrical load can be considered as disconnected from the vibration source, the torque transmission relationship can then be obtained as

Lead-screw to large gear

$$T_{ls} - T_{lg} = J_{lg} \ddot{\theta}_{lg} \quad \text{eq (3-28)}$$

Large gear to small gear

$$T_{lg} - T_{sg} = J_{sg} \ddot{\theta}_{sg} \quad \text{eq (3-29)}$$

Small gear to large gear

$$T_{sg} - T_{lg} = J_{lg} \ddot{\theta}_{lg} \quad \text{eq (3-30)}$$

The torque transmitted to the large gear then becomes

$$T_{lg} = J_{lg} \ddot{\theta}_{lg} + J_{sg} \ddot{\theta}_{sg} + T_m \quad \text{eq (3-31)}$$

Substituting eq (3-29) to eq (3-31) into eq (3-28), the force applied on the device during disengagement can be expressed as

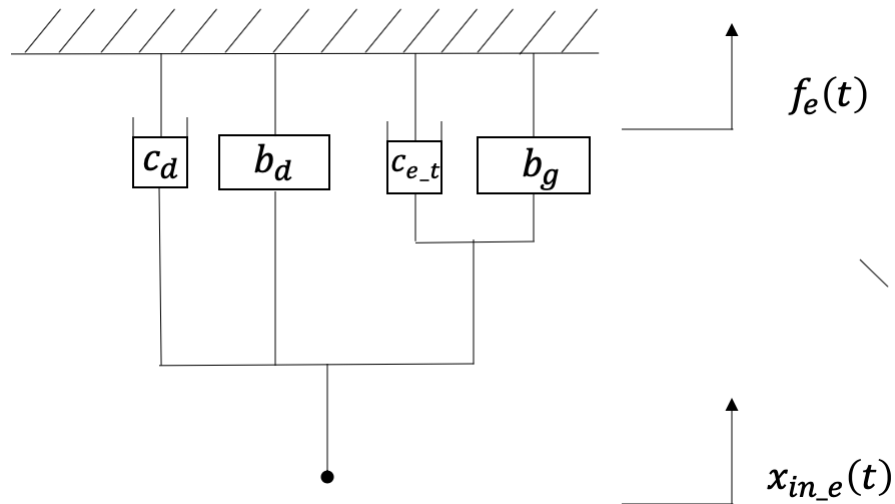
$$F_d = \left(\frac{2\pi}{l}\right) (J_{ls} + 2J_{lg} + 2r_g J_{sg}) \ddot{x}_{in} + \left(\frac{2\pi}{l}\right) c_m \dot{x}_{in} \quad \text{eq (3-32)}$$

The proposed regenerative shock absorber during disengaging period still can be modelled as an inerter in parallel with a translational mechanical damper. The equivalent inertance and translational damper then becomes

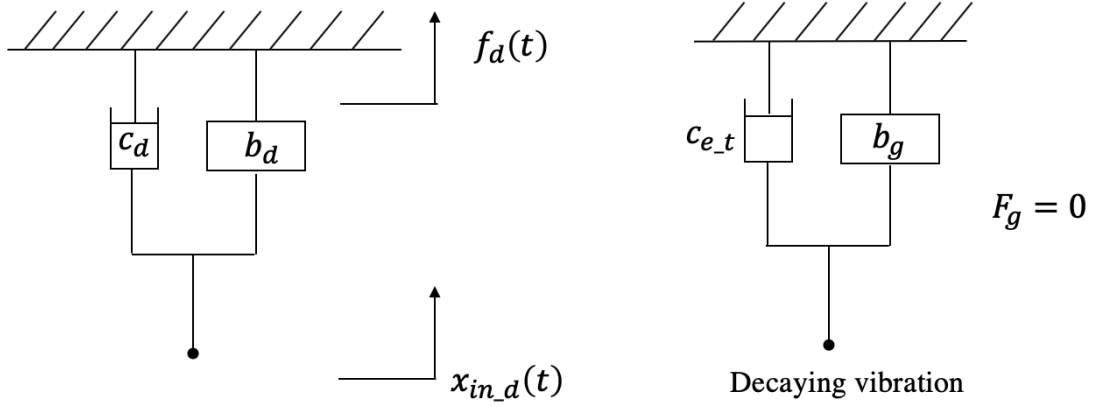
$$b_d = \left(\frac{2\pi}{l}\right)^2 (J_{ls} + 2J_{lg} + r_g J_{sg}) \quad \text{eq (3-33)}$$

$$c_d = \left(\frac{2\pi}{l}\right)^2 c_m \quad \text{eq (3-34)}$$

To sum up, applying the concept of MMR in regenerative shock absorber introduces a piecewise linear compound model, a secondary electrical generator coupled system is allowed to engage and disengage from the vibration source through sprag-clutch. Figure 3-5(a) shows the schematic diagram of vibration system during engaged state with a translational response \dot{x}_{in_e} . It shall be noted as the schematic diagram in Figure 3-5(a) is translational, c_{e_t} and b_g is defined by the translational electrical damping ($c_{e_t} = \left(\frac{2\pi}{l}\right)^2 c_e$) and generator inertance ($b_g = \left(\frac{2\pi}{l}\right)^2 J_g$) respectively. Spring was removed from the MMR model, as the system dynamics in this Chapter correspond to the lab-test discussion in Chapter 5. Figure 3-5(b) shows the schematic of system dynamics during disengaged state with translational response \dot{x}_{in_d} for the primary system, while the secondary system undergoes a decaying vibration with an initial velocity. Once the secondary switchable system is allowed to reconnect with the vibration source through the sprag-clutch, the vibration input will continuously transfer power into the generator. It shall be noted that as the secondary generator coupled electrical system will undergo a decaying vibration during disengagement period, it is important to ensure the primary and secondary system has the same initial condition when the switching happens. If this can be achieved, dynamics of primary and secondary systems will coincide at the correct time during engaged state, while the oscillation of both systems do not coincide during disengaged state.



(a) Engaged state



(b) Disengaged State

Figure 3-5: Mass clamped SDOF system with on-off switchable inerter and damper

(a) Engaged state (b) Disengaged state

At this stage, it still remains unknown that whether the switching between engaged and disengaged state of secondary system can enhance the energy harvesting performance. In the next section, two different dynamic models depending on the prescribed vibration source (Velocity/Force) according to Figure 3-5 will be presented.

3.2.2 Dynamics of velocity source

In this section, the dynamic of proposed design when one terminal of design is blocked will be analysed when it is excited by a prescribed single harmonic velocity input x_{in}

$$\begin{cases} x_{in} = X \sin(\omega t) \\ \dot{x}_{in} = X \omega \cos(\omega t) \\ \ddot{x}_{in} = -\omega^2 X \sin(\omega t) \end{cases} \quad \text{eq (3-35)}$$

Where X and ω is the amplitude and angular frequency of the velocity input. In this case, the vibration input behaves as a prescribed velocity source regardless the dynamics of switching. When the sprag-clutch inside mechanical motion rectifier allows the generator engaging with the vibration source, the applied torque ($T(t) = \frac{l}{2\pi} f(t)$) on the proposed regenerative shock absorber can be obtained according to Figure 3-6 :

$$T_e = (J_{ls} + 2J_{lg} + 2r_g J_{sg} + r_N J_g) \ddot{\theta}_{in} + (r_N c_e + c_m) \dot{\theta}_{in} \quad \text{eq (3-36)}$$

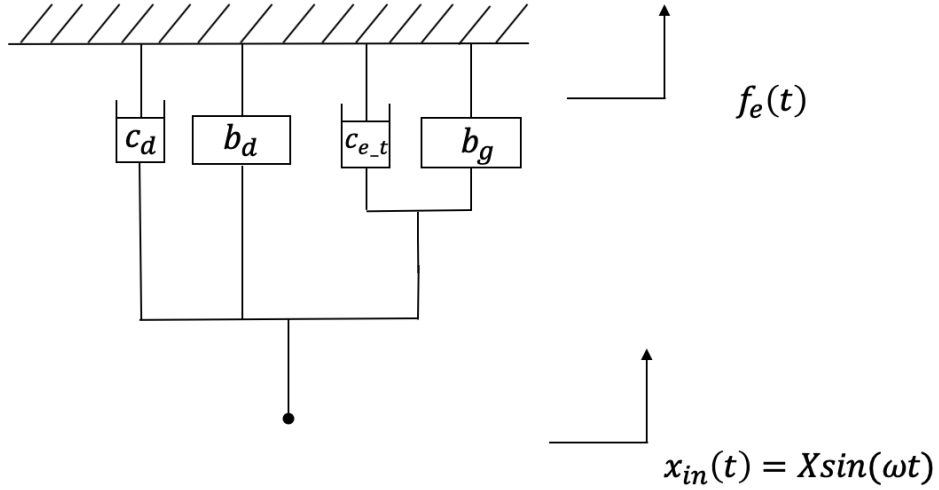


Figure 3-6: Engaged state of MMR based regenerative shock absorber (Velocity Input)

The relationship between the angular speed $\dot{\theta}_{in}$ and translational input speed \dot{x}_{in} can be obtained from eq (3-15). As the vibration source is described by a sinusoidal function, when the velocity of input reaches to its maximum amplitude and changing the direction of motion. At time instant t_1 where the external torque acting on the generator reduces to zero, the one-way clutch inside the motion rectifier module will disengage the generator from the vibration input which results no torque/power transmission between them. Figure 3-7 shows the schematic diagram during the disengagement period where the whole system splits into two parts (Primary unswitchable system and secondary switchable system) undergoing motions independently. Meanwhile, the applied torque from the actuator is requested to be varied in order to satisfy the prescribed velocity input in the absence of switchable electrical damper and generator inertia which leads to

$$T_d = (J_{ls} + 2J_{lg} + 2r_g J_{sg}) \ddot{\theta}_{in} + r_N c_m \dot{\theta}_{in} \quad \text{eq (3-37)}$$

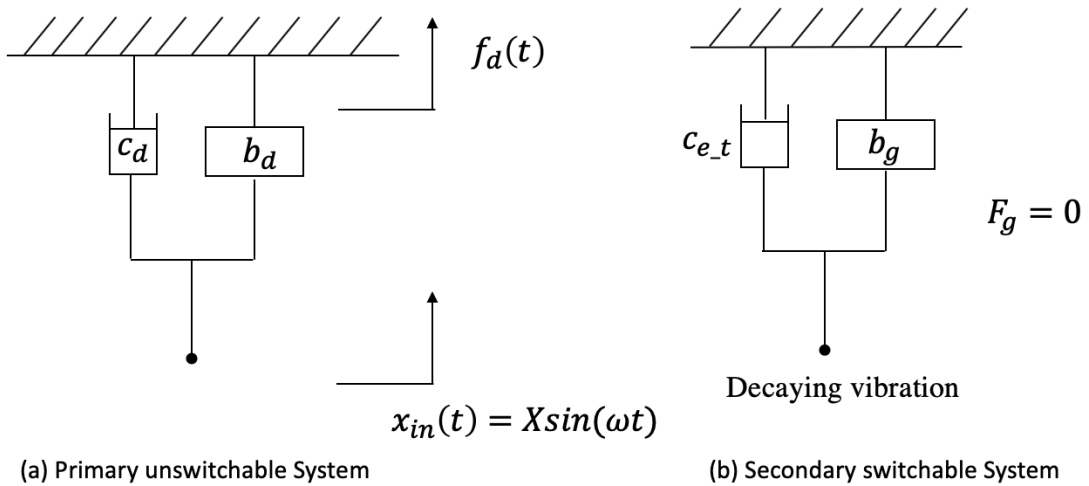


Figure 3-7: Disengaged state of MMR based regenerative shock absorber (Velocity Input)

(a)Primary unswitchable system (b)Secondary switchable system

The governing equation of the secondary switchable system when it is disconnected from the vibration source can be given by

$$J_g \ddot{\theta}_g + c_e \dot{\theta}_g = 0 \quad \text{eq (3-38)}$$

As there is no torque transmitted to the generator, it will release the kinetic energy stored on the shaft, and converting to electrical power which can be considered as a decaying vibration according to Figure 3-7(b). By assuming the switchable system starts transferring from engaged state into disengaged state at t_1 , while the output speed of MMR system (unidirectional) $|\dot{\theta}_{in}(t_1)|$ equals to the generator speed $\dot{\theta}_g$

$$|\dot{\theta}_{in}(t_1)| = \dot{\theta}_g(t_1) \quad \text{eq (3-39)}$$

The angular acceleration of the generator at t_1 instant can be obtained by employing eq (3-39) in eq (3-38)

$$\ddot{\theta}_g(t_1) = -\frac{c_e}{J_g} \dot{\theta}_{in}(t_1) \quad \text{eq (3-40)}$$

In the meantime,

$$\ddot{\theta}_{in}(t_1) = \ddot{\theta}_g(t_1) \quad \text{eq (3-41)}$$

Substituting equations eq (3-40) and eq (3-41) to eq (3-35), t_1 can be solved as

$$\tan(\omega t_1) = \frac{c_e}{\omega J_g} \quad \text{eq (3-42)}$$

Thus, for every half cycle the instant t_1 when the secondary system starts disengaging from the vibration source is

$$t_1 = \frac{1}{\omega} \arctan\left(\frac{c_e}{\omega J_g}\right) + \frac{k\pi}{\omega}, \quad k = 0, 1, 2, 3 \dots \quad \text{eq (3-43)}$$

During the disengaging period, the rotational speed of the generator can be solved by a 1st order linear homogeneous function. Assuming the angular position of generator from t_1 to t_2 is

$$\theta = Ae^{\lambda(t-t_1)} \quad \text{eq (3-44)}$$

By taking eq (3-40) into eq (3-44), the constant λ can be obtained as

$$\lambda = 0 \text{ or } -\frac{c_e}{J_g} \quad \text{eq (3-45)}$$

The general solution of the angular position during t_1 and t_2 can be derived as:

$$\theta = A_1 e^0 + A_2 e^{-\frac{c_e}{J_g}(t-t_1)} \quad \text{eq (3-46)}$$

By differentiating the angular position θ to get speed, the value of A_1 disappears. As the primary driving speed equals to the generator speed at t_1 , so that

$$\dot{\theta}_{in}(t_1) = -\frac{c_e}{J_g} A_2 \quad \text{eq (3-47)}$$

A_2 can be solved:

$$A_2 = -\dot{\theta}_{in}(t_1) \frac{J_g}{c_e} \quad \text{eq (3-48)}$$

Therefore, the rotational speed of the generator during the disengaging period can be obtained as:

$$\dot{\theta}_g = \dot{\theta}_{in}(t_1) e^{-\frac{c_e}{J_g}(t-t_1)}, t_1 \leq t \leq t_2 \quad \text{eq (3-49)}$$

Figure 3-8 simulates the dynamics of switching between engagement and disengagement within the MMR with given parameters in Table 3-1 (shown in section 3.3). As the vibration source is described by a prescribed sinusoidal velocity input, once the speed of the MMR driving shaft (unidirectional) catches up with the generator at time instant t_2 , the sprag-clutch will allow it to reconnect with the primary system.

$$\dot{\theta}_g = |\dot{\theta}_{in}(t_2)|, t_1 \leq t_2 \leq t_1 + \frac{\pi}{\omega} \quad \text{eq (3-50)}$$

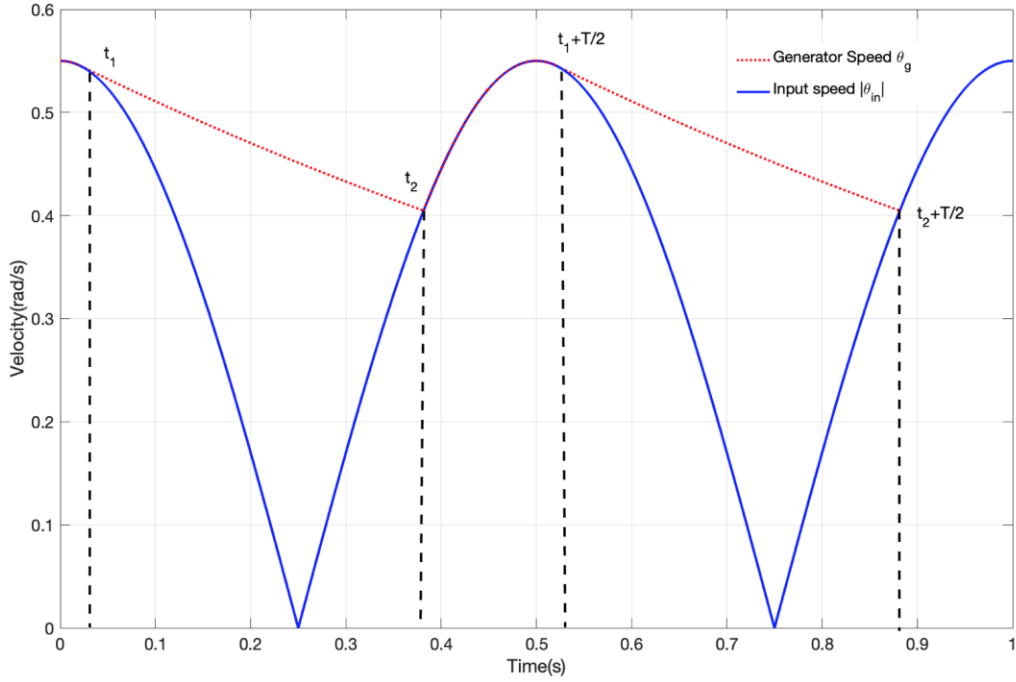


Figure 3-8: The dynamic of switching between engagement and disengagement inside MMR
(Velocity Input)

The re-engagement time instant t_2 can be solved from $\dot{\theta}_g = |\dot{\theta}_{in}(t_2)|$, $t_1 \leq t_2 \leq t_1 + \frac{\pi}{\omega}$ eq (3-50) for every t_1 with different k . To sum up, when the system is excited by a prescribed velocity input, the rotational speed of generator can be governed by the following equations

$$\begin{cases} \dot{\theta}_g = \dot{\theta}_{in} & t_2 \leq t \leq t_1 + \frac{\pi}{\omega} \\ \dot{\theta}_g = \dot{\theta}_{in}(t_1) e^{-\frac{c_e}{J_g}(t-t_1)} & t_1 < t < t_2 \end{cases} \quad \text{eq (3-51)}$$

Based on the model developed in this section, the energy being harvested by the electrical damper over half cycle between t_1 and $t_1 + \frac{\pi}{\omega}$ is

$$E_{out-v} = \int_{t_1}^{t_2} c_e \dot{\theta}_g^2 dt + \int_{t_2}^{t_1 + \frac{\pi}{\omega}} c_e \dot{\theta}_{in}^2 dt \quad \text{eq (3-52)}$$

Where the time instant of disengagement t_1 and re-engagement of the sprag-clutch t_2 can be obtained from eq (3-43) and eq (3-50) respectively, and the generator speed $\dot{\theta}_g$ during disengagement period can be found in eq (3-49).

Moreover, the input mechanical energy over half cycle can be formed by

$$E_{in-v} = \int_{t_1}^{t_2} T_d \dot{\theta}_{in} dt + \int_{t_2}^{t_1 + \frac{\pi}{\omega}} T_e \dot{\theta}_{in} dt \quad \text{eq (3-53)}$$

Where T_e and T_d is the applied torque during engagement and disengagement period respectively defined in eq (3-36) and eq (3-37).

Due to the absence of generator inertia and electrical damper, the amount of input torque/power tends to be lower during the disengagement period. For any cases of system without mechanical damper ($c_m = 0$), it is no doubt that the system will always be 100% effective. Since the switching between engagement and disengagement state raises changes on the input torque as well as the corresponded applied power, system efficiency might not be necessary to discuss in this case.

3.2.3 Dynamics of Torque/Force source

When the system is excited by a prescribed torque/force input, the relationship between the applied torque T ($T(t) = \frac{l}{2\pi} f(t)$) and angular velocity $\dot{\theta}_{in_e}$ of the design during engagement according to Figure 3-9 can be obtained as:

$$T = (J_{ls} + 2J_{lg} + 2r_g J_{sg} + r_N J_g) \ddot{\theta}_{in_e} + r_N (c_e + c_m) \dot{\theta}_{in_e} \quad \text{eq (3-54)}$$

The prescribed torque vibration source can be represented by a sinusoidal function

$$T = T_0 \sin \omega t \quad \text{eq (3-55)}$$

In this case, the vibration input behaves as a prescribed force/torque source regardless the dynamics of switching.

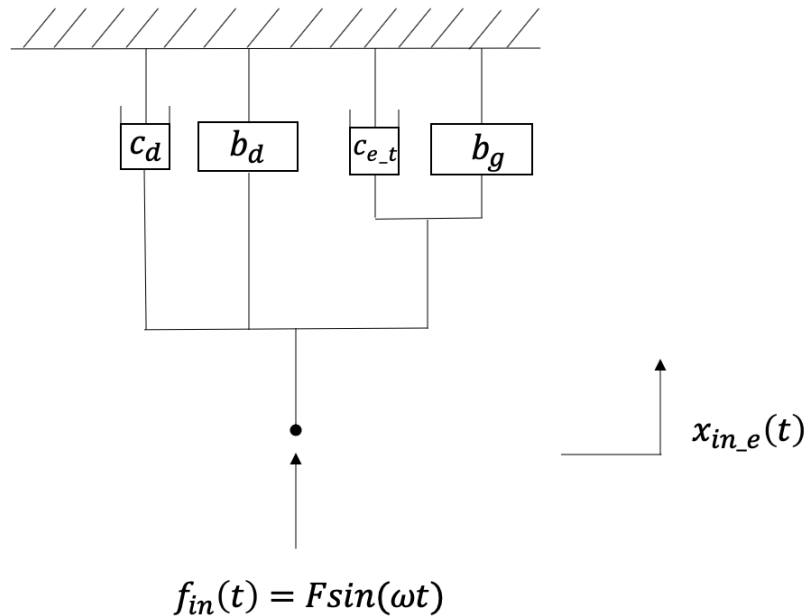


Figure 3-9: Engaged state of MMR based regenerative shock absorber (Torque/Force Input)

By assuming initial conditions $\theta_{in_e}(0) = 0$, $\dot{\theta}_{in_e}(0) = 0$, the angular speed and position for both primary and secondary systems during engagement period can be numerically solved

by using a 1st order Nonhomogeneous equation through MATLAB ode45. The corresponding motions in state-space form can be expressed as

$$\frac{d}{dt} \begin{bmatrix} \theta_{in_e}(t) \\ \dot{\theta}_{in_e}(t) \end{bmatrix} = \begin{bmatrix} 0 & 1 \\ 0 & \frac{-r_N(c_e+c_m)}{J_{ls}+2J_{lg}+2r_gJ_{sg}+r_NJ_g} \end{bmatrix} \begin{bmatrix} \theta_{in_e}(t) \\ \dot{\theta}_{in_e}(t) \end{bmatrix} + \begin{bmatrix} 0 \\ \frac{T(t)}{J_{ls}+2J_{lg}+2r_gJ_{sg}+r_NJ_g} \end{bmatrix} \quad \text{eq (3-56)}$$

Where the acceleration $\ddot{\theta}_{in_e}$ can be obtained by back substituting numerical solutions of θ_{in_e} and $\dot{\theta}_{in_e}$ into eq (3-54).

As mentioned in the previous section, the one-way clutch disengages the coupled generator from the vibration source when T_g reduces to zero. It is assumed that initial conditions of primary driving system (MMR and lead-screw) including velocity and acceleration equal to the driven part (generator) at time instant t_1 where system transfers from engaged state to disengaged state.

$$\dot{\theta}_g(t_1) = \dot{\theta}_{in_e}(t_1) \quad \text{eq (3-57)}$$

$$\ddot{\theta}_g(t_1) = \ddot{\theta}_{in_e}(t_1) \quad \text{eq (3-58)}$$

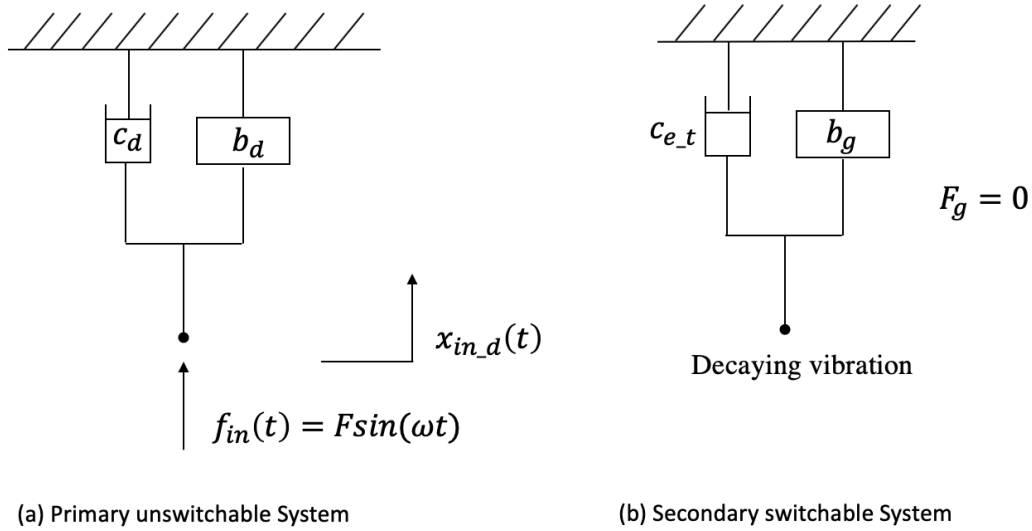


Figure 3-10: Disengaged state of MMR based regenerative shock absorber (Torque/Force Input) (a)Primary unswitchable system (b)Secondary switchable system

Figure 3-10 shows the schematic diagram of MMR system in disengaged state. During the period, the generator will undergo a decaying vibration in the absence of vibration input. Due to the connected electrical load, generator consumes the kinetic energy stored on the shaft to electrical power. The governing equation of motion is given by

$$J_g \ddot{\theta}_g + c_e \dot{\theta}_g = 0 \quad \text{eq (3-59)}$$

The time instant of disengagement t_1 can be solved by substituting numerical results of eq (3-57) and eq (3-58) into eq (3-59) within a defined tolerance. The form of angular speed of generator during disengagement can be solved by a similar way in Section 3.2.2. By taking the numerical solution of the angular speed at t_1 into the decaying function, it becomes

$$\dot{\theta}_g = \dot{\theta}_{in_e}(t_1)e^{-\frac{c_e}{J_g}(t-t_1)}, t_1 \leq t \leq t_2 \quad \text{eq (3-60)}$$

Different from prescribed velocity input which varies applied torque to consistent velocity, the vibration input in Figure 3-10 (a) is requested to adjust the primary system velocity and acceleration to keep the input force/torque consistent during disengagement period. The governing equation of primary system in the absence of secondary switchable system can be obtained by subscribing eq (3-59) into eq (3-54):

$$T = (J_{ls} + 2J_{lg} + 2r_g J_{sg})\ddot{\theta}_{in_d} + r_N c_m \dot{\theta}_{in_d} \quad \text{eq (3-61)}$$

The angular speed, position and acceleration of the primary system during disengagement period can be numerically solved by another 1st order Nonhomogeneous equation in eq (3-61) with initial conditions $\theta_{in_e}(t_1) = \theta_{in_d}(t_1)$, $\dot{\theta}_{in_e}(t_1) = \dot{\theta}_{in_d}(t_1)$ through ode45, its state space form can be expressed as

$$\frac{d}{dt} \begin{bmatrix} \theta_{in_d}(t) \\ \dot{\theta}_{in_d}(t) \end{bmatrix} = \begin{bmatrix} 0 & 1 \\ 0 & \frac{-r_N c_m}{J_{ls} + 2J_{lg} + 2r_g J_{sg}} \end{bmatrix} \begin{bmatrix} \theta_{in_d}(t) \\ \dot{\theta}_{in_d}(t) \end{bmatrix} + \begin{bmatrix} 0 \\ \frac{T(t)}{J_{ls} + 2J_{lg} + 2r_g J_{sg}} \end{bmatrix} \quad \text{eq (3-62)}$$

With given parameters in Table 3-1, Figure 3-11 demonstrates the dynamics of switching between engagement and disengagement when system is subjected to a prescribed torque input. Once the output speed of MMR $|\dot{\theta}_{in_d}|$ matches with the generator speed at t_2 , the generator will be allowed to reconnect with the vibration source. The corresponding time instant of re-engagement t_2 can then be numerically obtained by

$$\begin{cases} |\dot{\theta}_{in_d}(t_2)| = \dot{\theta}_g(t_2) \\ \theta_{in_d}(t_2) = \theta_{in_e}(t_2) \end{cases} \quad \text{eq (3-63)}$$

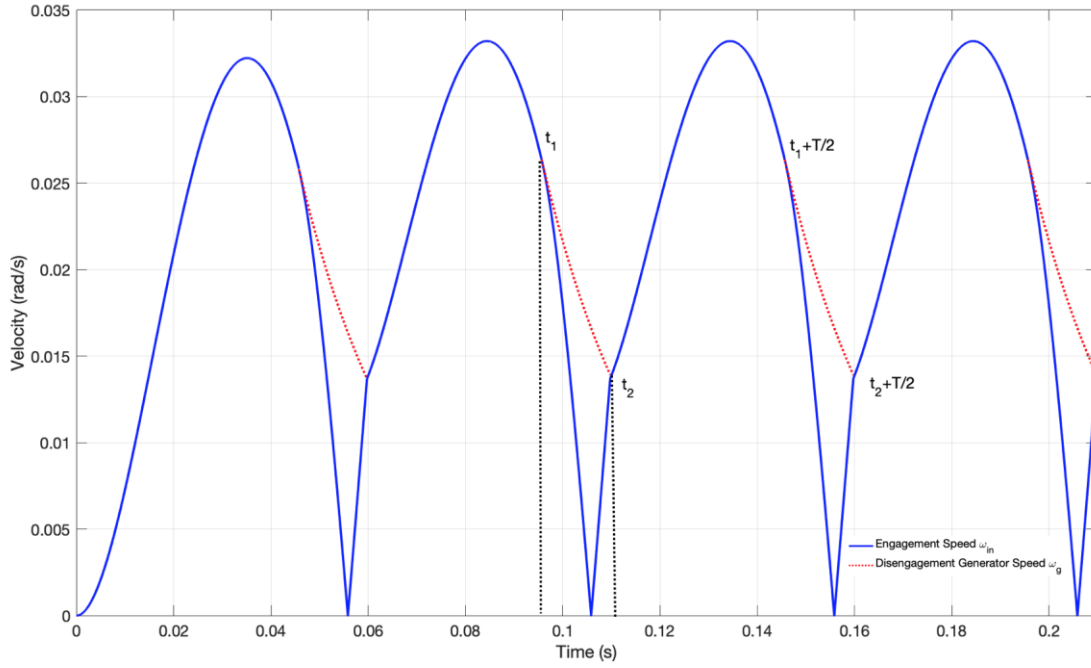


Figure 3-11: The dynamic of switching between engagement and disengagement inside MMR (Force/Torque Input)

Once the generator re-engages with vibrations source through the sprag-clutch, the corresponding motions from t_2 to $t_1 + T/2$ can be numerically solved by taking initial conditions of system converting from disengaged state back into engaged state at t_2 given by eq (3-63) into eq (3-56) through ode45 again.

Figure 3-11 also shows that due to zero initial condition $\dot{\theta}_{in-e}(0) = 0$, the angular speed in the first half cycle of time scale is unsymmetrical, while it decays as far as the time going. The system eventually becomes steady-state and the time instants of disengagement and re-engagement tend to be periodical.

Based on the above discussion, the regenerated electrical energy in steady state condition over half cycle E_{out-f} when it is subjected to a prescribed torque input can be expressed by

$$E_{out-f} = \int_{t_1}^{t_2} c_e \dot{\theta}_g^2 dt + \int_{t_2}^{t_1 + \frac{T}{2}} c_e \dot{\theta}_{in-e}^2 dt \quad \text{eq (3-64)}$$

Where time instant of disengagement t_1 and re-engagement t_2 are solved in eq (3-59) and eq (3-63) respectively.

In terms of prescribed velocity input varying the applied force/torque to produce a consistent velocity, the dynamic behaviour of torque input behaves the other way around. The primary system velocity and acceleration becomes discontinuous to consistent the torque input during disengagement period, the input mechanical energy over half cycle E_{in-f} can be obtained by substituting eq (3-56) and eq (3-62) in eq (3-65)

$$E_{in-f} = \int_{t_1}^{t_2} T \dot{\theta}_{in-d}^2 dt + \int_{t_2}^{t_1 + \frac{\pi}{\omega}} T \dot{\theta}_{in-e}^2 dt \quad \text{eq (3-65)}$$

Where $\dot{\theta}_{in-d}$ and $\dot{\theta}_{in-e}$ are output speed of MMR which corresponds to the period of disengagement and engagement.

Unlike the model developed for velocity input in Section 3.2.2, where switching is ineffective to the mechanical power loss. For a prescribed torque/force input, all system parameters become relevant which potentially affects the system dynamics including the switching time instant, speed and acceleration; these problems will be addressed in more details in the next section. Moreover, the mechanical power loss can no longer be solved with linear steady-state frequency function by adding viscous damper into the model as the motion of primary system becomes discontinuous, it might attempt to alter the mechanical power loss as well as the power flow according to the piecewise linear properties of MMR. Therefore, it becomes necessary to explore the dynamics of mechanical power dissipation over a full cycle to identify whether MMR reduces mechanical loss comparing to linear system.

3.3 Performance evaluation of MMR based regenerative shock absorber

As discussed in Section 3.1, whether a linear system is excited under on-resonance or off-resonance frequency does not really affect the energy harvesting performance, the amount of input mechanical energy always equals to the energy absorbed by the damper over a cycle. However, in the concept of mechanical motion rectified regenerative shock absorber, the change of input mechanical power arising from the switching of engagement and disengagement has not been addressed yet. The applied mechanical power becomes non-harmonic as the secondary electrical system disconnecting and reconnecting from the primary vibration system through sprag-clutch. To access the performance of MMR based regenerative shock absorber, it is essential to clarify the associated power input, transmission and dissipation of the system. In this section, the concept of mechanical active/reactive power flow based on force-current analogy was implemented to evaluate the performance of MMR based piecewise linear system. The use of active/reactive power flow is quite useful as it combines the force and velocity characteristics and can better reflect vibration transmission between unswitchable primary and switchable secondary system. In the meantime, a comparison between MMR based piecewise linear system and non-switching linear system is presented to identify whether MMR can enhance the performance, it might

draw different conclusions depending on the prescribed vibration input. Moreover, a numerical study will be presented to determine how system parameters affecting the dynamics of switching and corresponded energy harvesting performance. System parameters of MMR based regenerative shock absorber prototype (Referring to Chapter 5) are listed in Table 3-1

PARAMETERS	VALUE	DESCRIPTION
l	0.025[m]	Lead-screw pitch
J_g	1.21 [kgm ²]	Generator inertia
J_{ls}	0.02 [kgm ²]	Lead-screw inertia
J_c	0.05 [kgm ²]	Coupling inertia
J_{lg}	0.1[kgm ²]	Large-gear inertia
J_{sg}	0.0065[kgm ²]	Small-gear inertia
c_e	10[Nms/rad]	Electrical damping
c_m	15[Nms/rad]	Mechanical damping
T_m	1[Nm]	Applied Torque
X	± 0.01 [m]	Displacement Input

Table 3-1: System parameters of mechanical motion rectified regenerative shock absorber

3.3.1 Linear system

First of all, numerical study for linear system was conducted in this section to evaluate its power flow, extraction and dissipation characteristics. According to Figure 3-1, when the system is excited at its natural frequency $\omega_n = \sqrt{\frac{k}{b}} = 2\pi \text{ rad/s}$. By assuming electrical and mechanical damping coefficient $c_e = 10\text{Ns/m}$, $c_m = 15\text{Ns/m}$, inertance $b = 10\text{kg}$, spring stiffness $k = 394\text{N/m}$, Figure 3-12 describes the system dynamics (Power and velocity) when it is subjected to a harmonic force input $f(t) = F\sin(\omega_n t)$ with amplitude $F = 1\text{N}$.

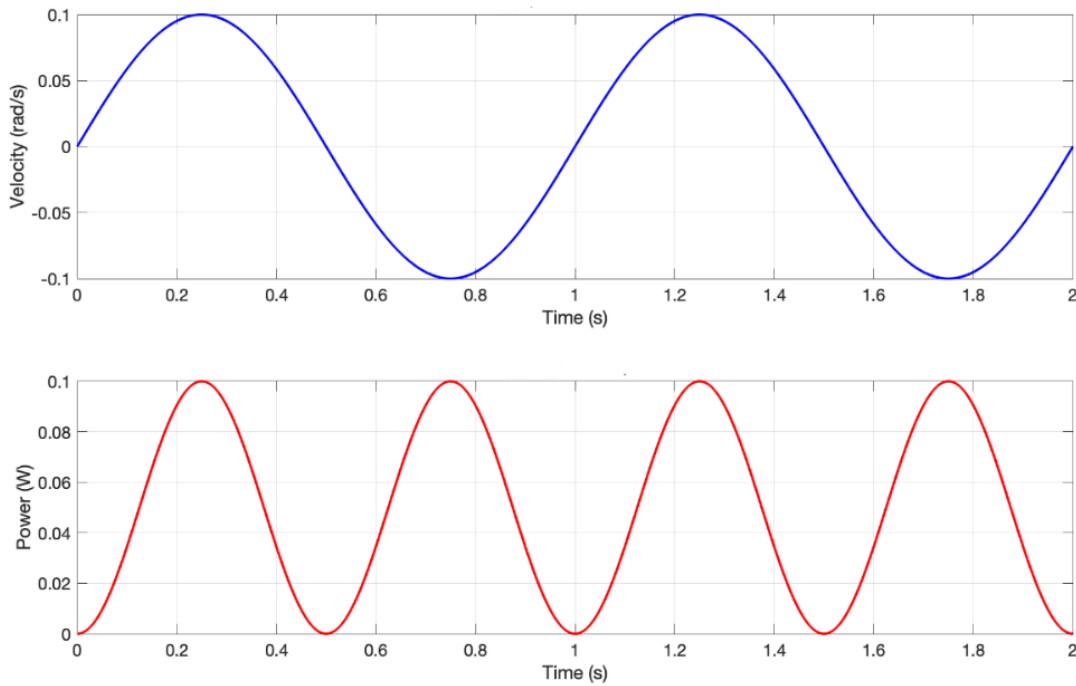


Figure 3-12: System dynamics at its natural frequency ($f = 1\text{Hz}$) (a) Excitation velocity (b) Total input power

As discussed in Section 3.1, when the system is excited at its natural frequency, the instantaneous changing rate in its mechanical power flow ($\dot{K} + \dot{U}$) always equals to zero as effects of mechanical reactive elements (spring and inerter) cancelled each other. All the vibration input power will be dissipated by the resistive damping. By looking at the simulation result in Figure 3-12, the applied mechanical power never falls down below zero as the damping force is always in phase with velocity. According to the theory, power dissipation is an irreversible process in which energy is transferred into the final form.[129] If the energy consumed by the load never flows back in the other direction, the amount of power can be given by the name of active power. Therefore, the in-phase product of force and velocity called mechanical active power can be analogized in the same way as electrical active power. The numerical study in this section was conducted for the case of off-resonance frequency as well. By removing the spring stiffness from the model ($k = 0$), where system does not have natural frequency (Further used to compare with MMR piecewise linear system as the developed prototype in Chapter 5 does not have spring as well). Figure 3-13 shows the dynamic of mechanical input power when the system is excited at the same frequency $\omega = 2\pi \text{ rad/s}$. Due to the existence of active power being absorbed by the damper, the amplitude of total input power is asymmetrical in positive and negative parts of y axes. It can be found that the positive part happens when the vibration source provides power for all

elements, while part of the power is given back to the vibration source in the other direction. By looking at the reactive power curve in Figure 3-13, the amount of power which system provides for reactive elements (inertor) in half cycle will flow back to the vibration source in the next half cycle. As a result, there will be zero change of mechanical energy over a full cycle which verify the observation in eq (3-6). In a similar way of electrical reactive elements, even though mechanical reactive elements (spring, inertor) within the model ideally do not consume any power, but it requires force from the vibration source. In order to harvest power, vibration source needs to provide sufficient power for reactive elements to achieve relative velocity between two terminals of damper.

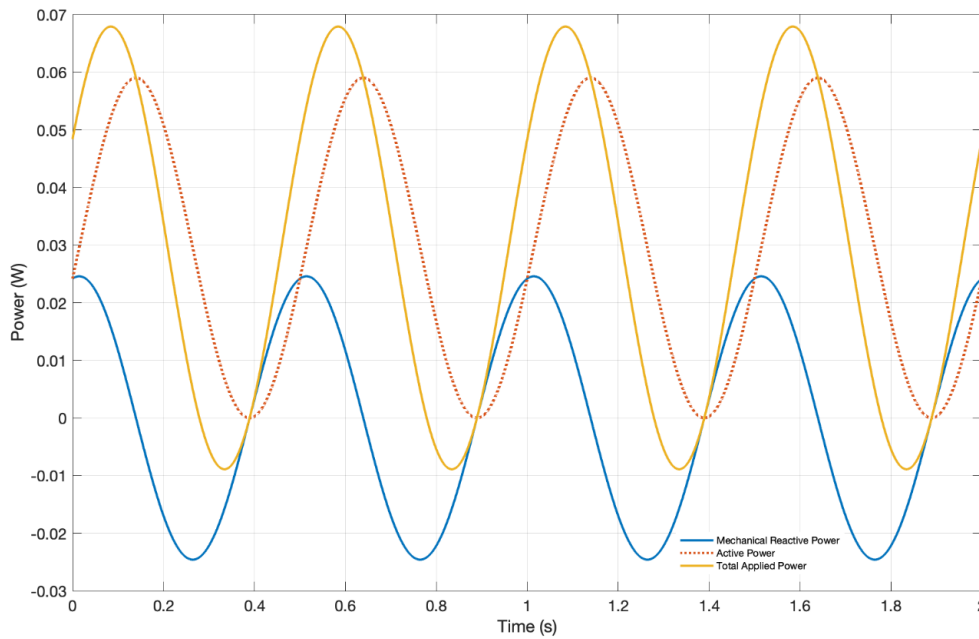


Figure 3-13: Dynamic of system subjected to its off-resonance frequency

Based on the above observation, the concept of active and reactive power can also be applied in mechanical system. To have a clear understanding of mechanical active and reactive power, it is necessary to develop an analogy between electrical and mechanical systems based on force-current analogy. Force-current analogy [86] between quantities in electrical and mechanical system are shown in Table 3-2

Electrical System	Mechanical System
Voltage v [V]	Velocity v [m/s]
Current i [A]	Force F [N]
Inductor L [H]	Spring k [N/m]
Capacitor C [F]	Inertor b [kg]
Resistor R [Ω]	Damper c [Ns/m]
Power p [W]	Power p [W]
Impedance Z [Ω]	Impedance [Ns/m]

Table 3-2: Force-current analogy between electrical and mechanical networks [86]

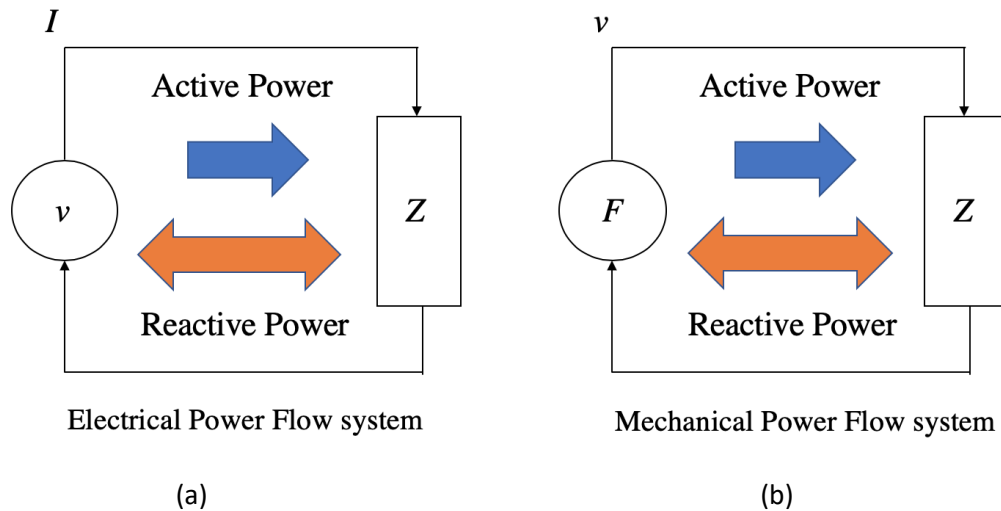


Figure 3-14: Electrical/Mechanical equivalent circuit (a)Electrical power flow system (b)
Mechanical Power flow system

Figure 3-14 illustrates the active/reactive power analogy between electrical and mechanical systems, the vibration source applies force F to the mechanical load impedance Z with a corresponding velocity v . The vibration source needs to apply sufficient power for all elements in order to produce velocity across the load impedance. However, the instantaneous active power applied on the mechanical load does not necessarily equal to the input power from the source due to the existence of reactive elements. This behaviour is similar to the electrical system shown in Figure 3-14 (a), the input power from the source would not equal to the active power on the load, as the reactive power is returned back to the source without working. To sum up, the electrical-mechanical power analogy allows deeper understanding of the power flow and dissipation in mechanical system. Moreover, the analogy can be further used to investigate the active and reactive power flow of MMR based piecewise linear system.

3.3.2 Piecewise linear system (Velocity source)

After studying characteristics of mechanical power flow and dissipation of linear system, the next step is to compare the energy harvesting performance between the MMR based piecewise linear system and non-switching linear system ($t_1 = t_2$). Figure 3-15 shows the simulation result of harvested electrical power excited by a 1Hz, $\pm 10mm$ harmonic input (Linear system (without sprung) versus MMR system). From the graph, the switching enables generator to work more continuously and the produced power never falls down to zero which results higher DC offset. Figure 3-16 describes the simulated system dynamics of MMR based

regenerative shock absorber including velocity, torque and power. According to the discussion in Section 3.2, disengagement happens when the applied torque on the switchable system reduces to zero. In the meantime, it can be identified from Figure 3-16(a) that the generator speed $\dot{\theta}_g$ is much greater than the output speed of MMR $|\dot{\theta}_{in}|$ during disengagement period. As a result, MMR can significantly improve the corresponding harvested energy (53.9%) comparing to the linear system without switching.

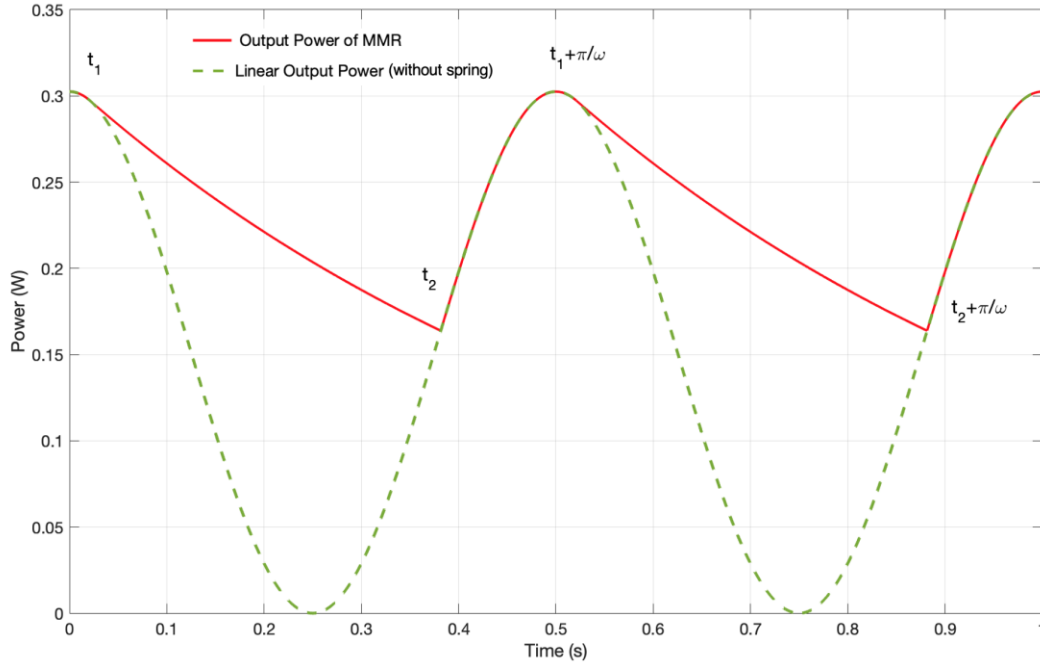


Figure 3-15: Harvested power comparison between Linear case (without spring) and MMR case under velocity vibration source excitation

Instead of individually describing the total input power (active + reactive), the simulation result in Figure 3-16 (c) shows the reactive power flow as well. The applied reactive power from the vibration source during engagement period can be formed by

$$P_{r_e} = (J_{ls} + 2J_{lg} + 2r_g J_{sg} + r_N J_g) \ddot{\theta}_{in} \dot{\theta}_{in} \quad \text{eq (3-66)}$$

While the reactive power during disengagement in the absence of generator inertia

$$P_{r_d} = (J_{ls} + 2J_{lg} + 2r_g J_{sg}) \ddot{\theta}_{in} \dot{\theta}_{in} \quad \text{eq (3-67)}$$

In order to make the curve easier to understand, it is assumed that there is no mechanical damping within the model ($c_m = 0$). According to the mechanical active/reactive power analogy, reactive power happens when the applied force and velocity are not in phase, the vibration source needs to provide power (positive direction) for reactive elements and it will eventually flow back (negative direction) to the source without working. By looking at the curve in Figure 3-16 (c), the generator disconnects from the vibration source at t_1 , where the

reactive power starts flowing back to the vibration source. Instead of giving the reactive power stored on the generator shaft back to the vibration source, the switching of disengaged state of sprag-clutch allows it being harvested between t_1 and t_2 shown in Figure 3-15. When the sprag-clutch allows generator to re-engage at t_2 , where system restarts involving electrical damping c_e and generator inertia J_g . Consequently, there will be an instantaneous changing on the corresponding applied torque as well as mechanical power shown in Figure 3-16 (b) and (c). Note that as the spring is not included in the model, there will not be any transient response. By looking at the waveform in Figure 3-16 (c) between t_2 and $t_1 + \pi/\omega$, the blue curve is the total input power which comprises both active and reactive power, while the pink curve is just the reactive power itself. The re-engaged electrical damper and generator inertia requires power from the vibration source.

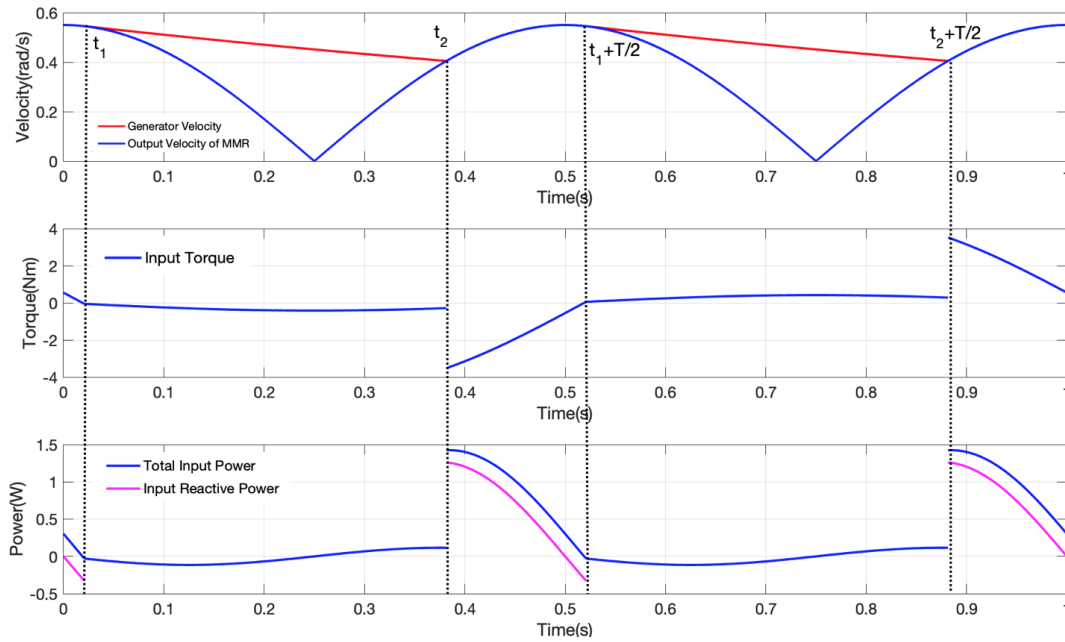


Figure 3-16: Simulated system Dynamics of MMR based regenerative shock absorber(a)

Rotational velocity of each part (b) Input torque (c) Input mechanical power

Since there is no mechanical damping within the model, the input mechanical energy defined in eq (3-53) shall be equal to the output electrical energy in eq (3-52) every half cycle in all aspects

$$E_{out_v} = E_{in_v} \quad \text{eq (3-68)}$$

By substituting eq (3-52) and eq (3-53) into eq (3-68), as unswitchable reactive terms such as lead-screw and MMR gear inertia consume zero energy over half cycle, it is found that the integration of reactive power on the generator shaft during engagement period t_2 and $t_1 + \pi/\omega$ equals to the total electrical energy between t_1 and t_2

$$\int_{t_1}^{t_2} c_e \dot{\theta}_g^2 dt = \int_{t_2}^{t_1 + \frac{\pi}{\omega}} J_g \dot{\theta}_{in} \ddot{\theta}_{in} dt \quad \text{eq (3-69)}$$

The observation in eq (3-69) verifies the energy conservation law, the amount of harvested energy during disengagement shall be equal to the integration of kinetic energy variation on the generator inertia over the engagement period.

After physically interpreting the dynamics of switching inside MMR when the system is subjected to a prescribed velocity input, it is necessary to conduct a numerical study to determine the impact of each element on system dynamics.

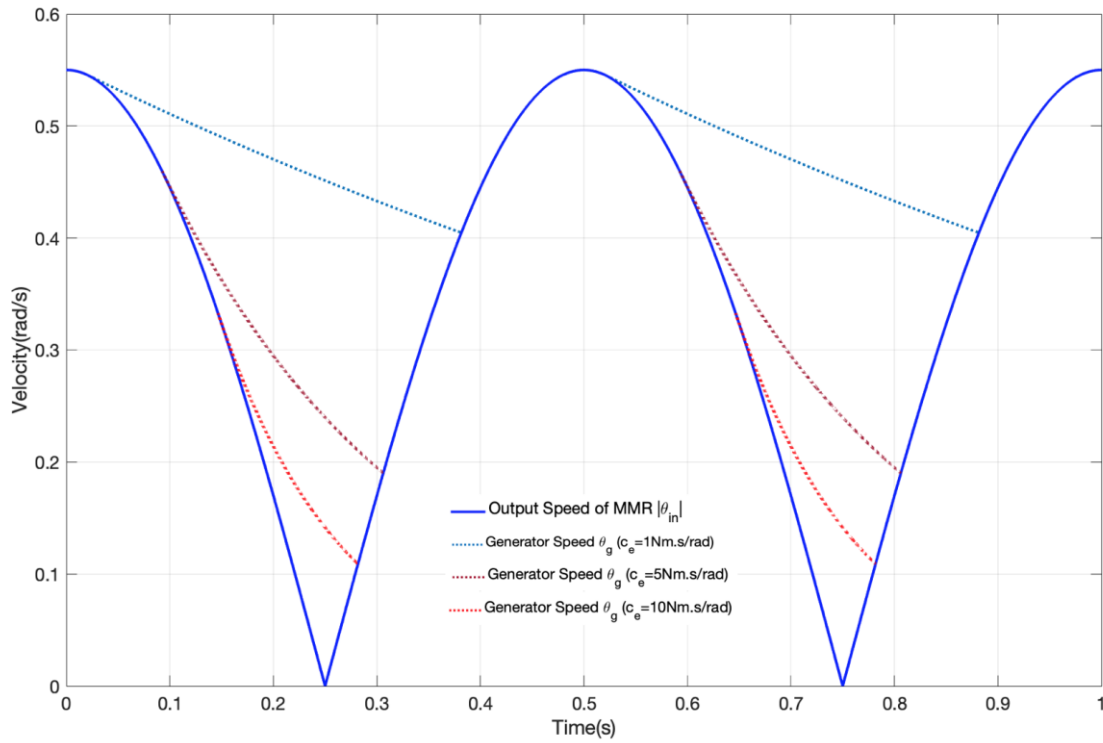


Figure 3-17: Dynamics of generator speed with different electrical damping c_e ($f = 1\text{Hz}$)

Figure 3-17 shows dynamics of switching between engagement and disengagement by varying the amplitude of electrical damping coefficient c_e . It is evident from eq (3-24), heavier electrical damping c_e increases the current flowing through the circuit, which allows the residual kinetic energy being consumed faster. In which case, it significantly shortens the disengagement period. However, this might raise another problem is it better to reduce the disengagement duration to let more current flow through the electrical circuit or to extend the disengagement period as the produced voltage and power are more continuous.

Table 3-3 shows numerical study results by varying the electrical damping. It was found that when system is heavily electrical damped, the energy harvesting performance of MMR based system is quite close to linear system as the disengagement period is significantly shortened. Assuming c_e is chosen to maximize P_e for energy harvesting purposes, system gains less

benefits from the switching inside MMR. Therefore, MMR might be more suitable for lighter electrical damped system, as it enables more continuous voltage and power with less ripple which is desirable for both supplying power electronic device and energy storage.

Electrical damping coefficient (Nms/rad)	P_e (MMR) (W)	P_e (Linear) (W)
$c_e = 1$	0.2339	0.1513
$c_e = 5$	0.8336	0.7563
$c_e = 10$	1.5487	1.5125
$c_e = 20$	3.0366	3.025

Table 3-3: Harvestable Power with different electrical damping coefficient (MMR versus Linear system (without spring))

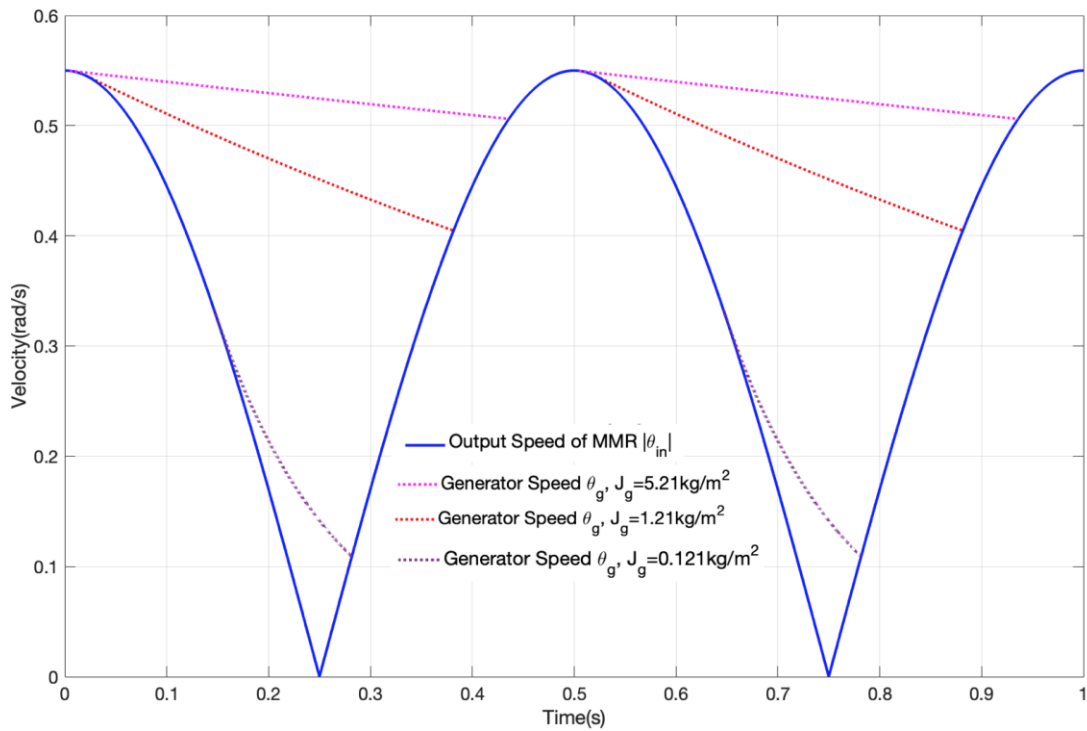


Figure 3-18: Dynamics of generator speed with different generator inertia J_g ($f = 1Hz$)

After discussing the impact of electrical damping on system dynamics, the next step is to evaluate the generator inertia on the performance. Figure 3-18 shows the simulation result with different generator sizes. By fixing the electrical damping $c_e = 1Nms/rad$, it is seen that with the increasing of generator inertia, the disengagement period becomes longer. The main reason is that more kinetic energy can be stored on the generator shaft by increasing its size. Once the sprag-clutch disengages the coupled generator from the vibration input, the amount of increasing kinetic energy smooths the rotational speed. As the electrical

damping is fixed, the corresponding regenerated voltage will have a higher DC offset which significantly improves the energy harvesting performance.

Generator inertia (kgm^2)	P_e (MMR) (W)	P_e (Linear) (W)
$J_g = 0.121$	0.1549	0.1513
$J_g = 1.21$	0.2339	0.1513
$J_g = 3.21$	0.2686	0.1513
$J_g = 5.21$	0.2798	0.1513

Table 3-4: Harvestable Power with different generator inertia (MMR versus Linear system (without spring))

Table 3-4 shows the numerical study results of harvestable power by implementing different generator inertia for both MMR and unswitchable linear systems at same excitation frequency ($f = 1 \text{ Hz}$). It is evident that the performance of MMR based system is quite close to linear system with smaller size generator. According to the simulation result in Figure 3-18, the velocity of generator becomes more continuous with greater generator inertia. As a result, it improves the average electrical power being harvested by the load.

The next step of the discussion is to identify whether excitation velocity will affect time instants of engagement and disengagement inside MMR. In order to well address the problem, the system is examined with different amplitudes of excitation displacement and frequencies respectively in Figure 3-19 and Figure 3-20. It is no doubt that the amount of harvestable power will be improved by amplifying the input velocity, so the energy harvesting performance will not discuss here. According to switching criterion of sparg-clutch, when the applied force/torque on the generator reduces to zero, generator is disconnected from the primary system undergoes a decaying vibration with its initial condition. By looking at the analytical solution of disengagement time instant in eq (3-38), it is found that the amplification of displacement X will be cancelled out in the velocity and acceleration terms when solving t_1 . Even though it will amplify the initial velocity of generator switching from engagement to disengagement at t_1 , but it will be compensated eventually by solving the time instant of re-engagement t_2 in eq (3-50). Therefore, varying the amplitude of displacement will not affect the time instant of switching and the simulation result in Figure 3-19 illustrates this.

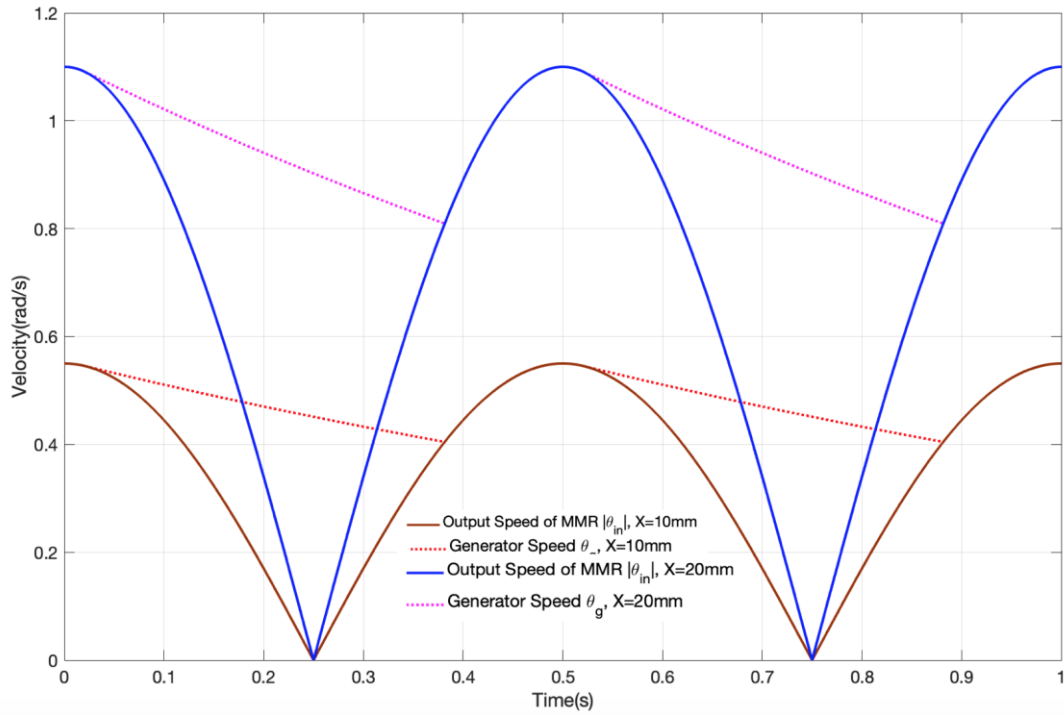


Figure 3-19: Dynamics of generator speed with different displacement amplitudes X

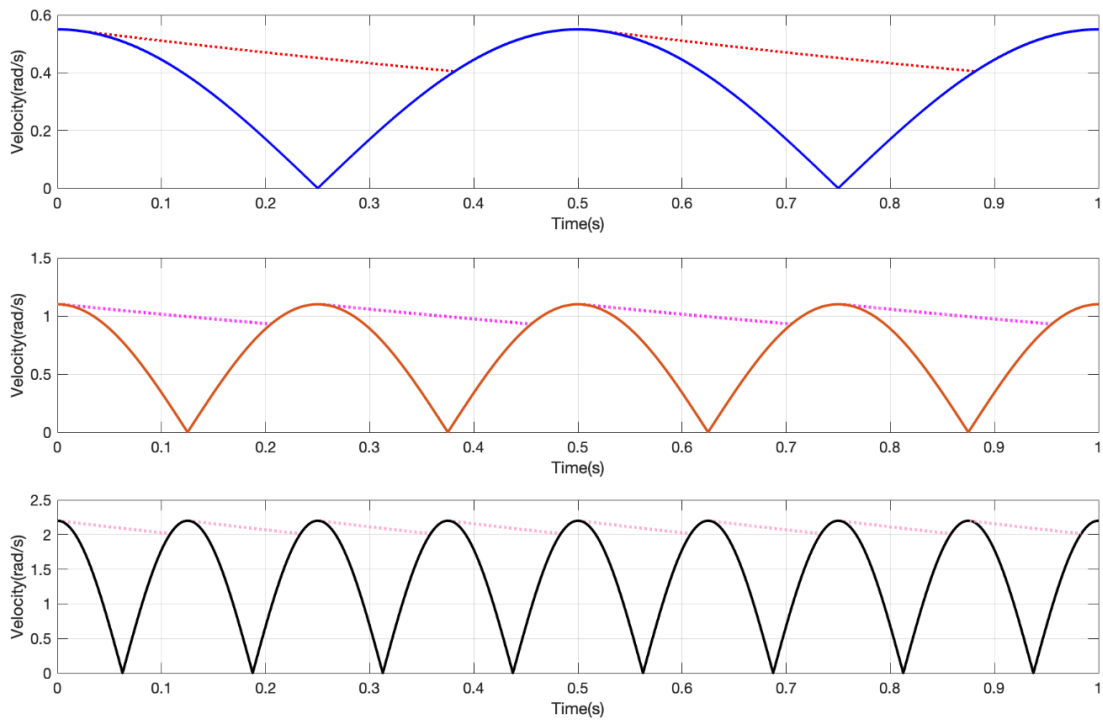


Figure 3-20: Dynamics of generator speed with different excitation frequencies f (a) $f = 1\text{Hz}$ (b) $f = 2\text{Hz}$ (c) $f = 4\text{Hz}$

Figure 3-20 describes dynamics of MMR system by varying the excitation frequency. As the vibration input is periodical, the switching happens more frequently when the excitation

frequency goes up. It can be counted that for a time scale equals to 1 second, there is 0.7216s disengaging duration for 1Hz with given system parameters, while it becomes 0.8576s when the frequency is increased to 4Hz. Even though the extended disengagement duration is desirable for energy harvesting, but it is not the case with the increasing of excitation frequency. To solve the disengagement duration, it is found that its amplitude $t_2 - t_1 \approx 0$ by setting $\omega \rightarrow \infty$. Meanwhile, it was also identified in Figure 3-20 that the engagement duration becomes shorter with the increasing of excitation frequency. The engagement duration eventually becomes zero when $\omega \rightarrow \infty$. As both engagement and disengagement period tend to be zero, the MMR based regenerative shock absorber might not able to work under higher frequency excitation.

3.3.3 Piecewise linear system of MMR (Torque/Force source)

Based on the piecewise linear model developed in Section 3.2.3, Figure 3-21 shows the harvested power comparison between linear system (purple curve) and MMR based piecewise system (red curve) when the vibration source is considered as a prescribed torque input.

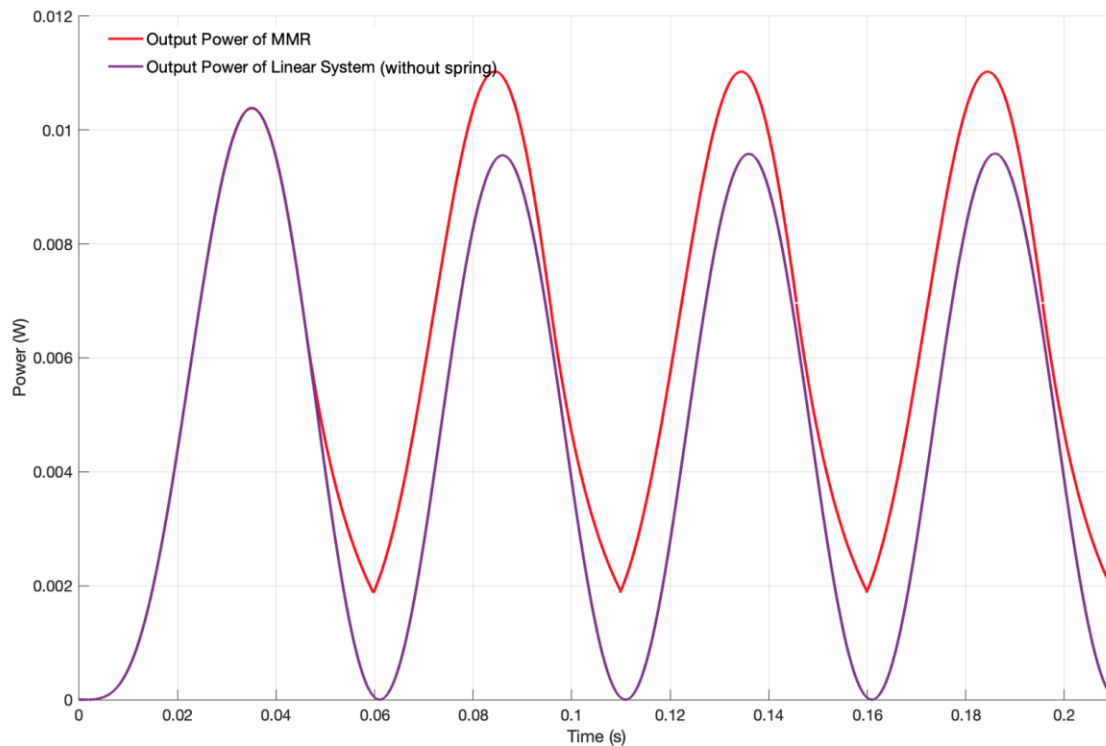


Figure 3-21: Harvested electrical power comparison between Linear (without spring) and MMR case under force input excitation ($T=1\text{Nm}$, $f=10\text{Hz}$)

The result shows that the MMR coupled regenerative shock absorber could harvest more electrical power comparing to linear system, when the system reaches to its steady state

condition (switching becomes periodical). In the same way as velocity source, the switching between engagement and disengagement allows the generator to work more continuously, the generated voltage and power potentially never falls down to zero. With given system parameters in Table 3-1, the average power of MMR based system equals to $6.58mW$ which is 27.5% better than the linear system without switching ($4.77mW$).

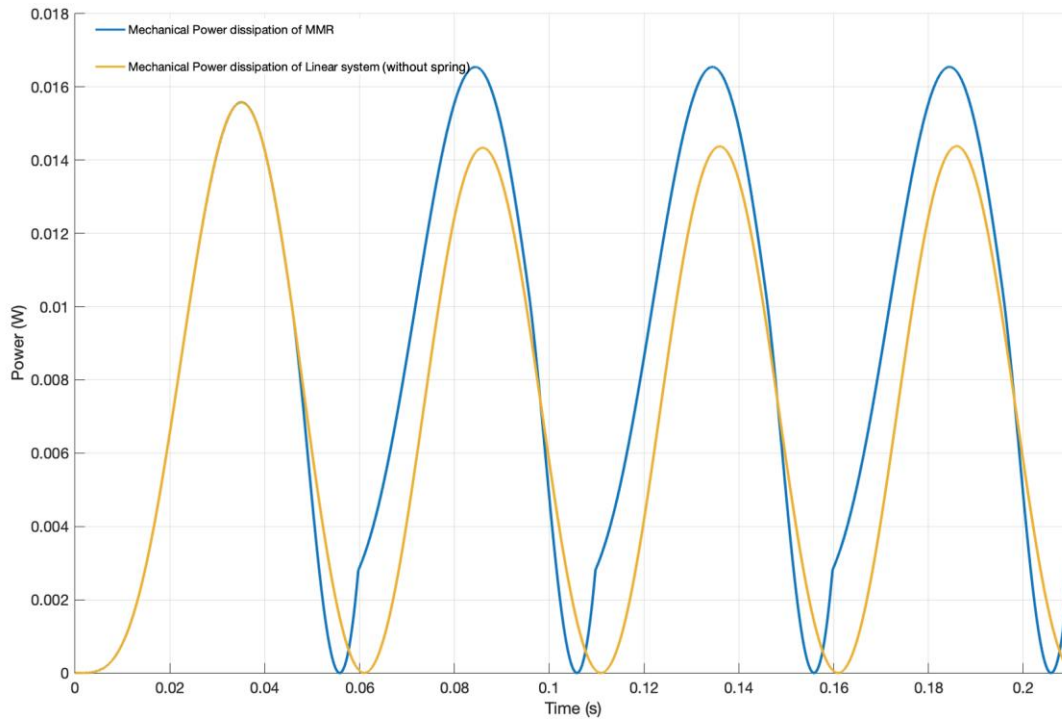


Figure 3-22: Mechanical Power loss comparison between Linear (without spring) and MMR system under torque input excitation($T=1Nm$, $f=10Hz$)

As mentioned in the Section 3.2.3, the switching brings a transient response to the primary system as well when system is subjected to a force excitation, the mechanical power loss can no longer be solved by steady-state frequency function. Figure 3-22 shows the mechanical power loss comparison between linear and MMR system. It can be identified that the mechanical power loss is increased by employing MMR. With a mechanical damper $c_m = 15Nms/rad$, the numerical study result shows that for a linear system, the average mechanical power is $7.17mW$, while the amplitude is increased to $9.17mW$ by employing MMR.

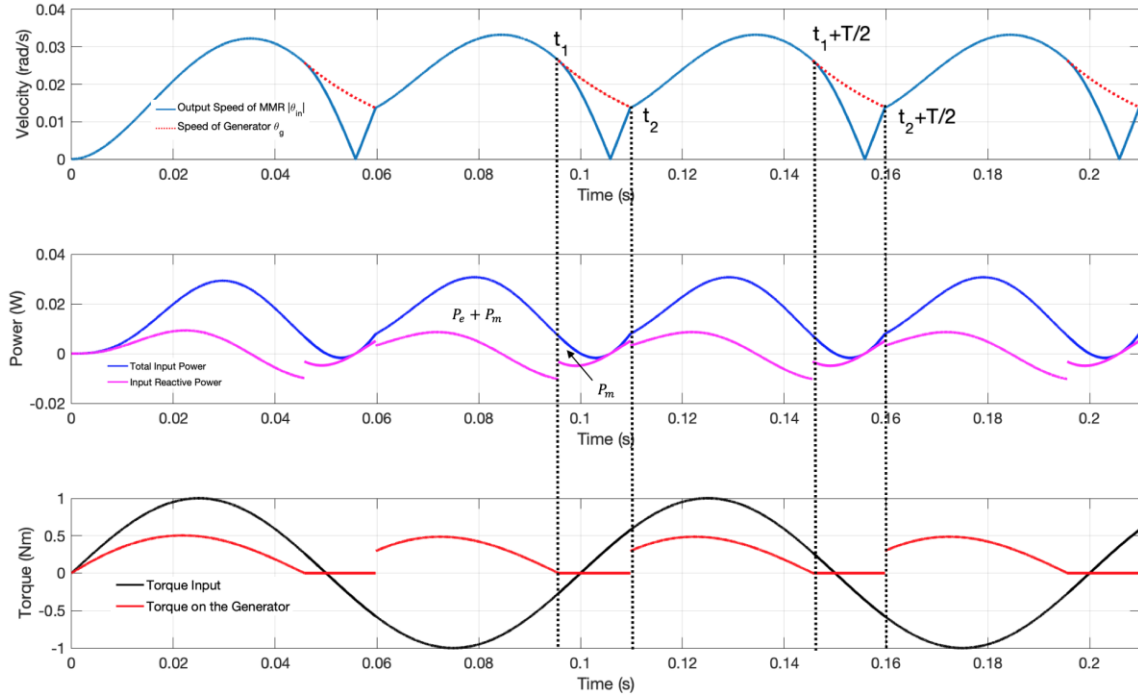


Figure 3-23: Simulated System Dynamics (a) Rotational speed of each part (b) Total input Power & Reactive Power Flow (c) Total input torque & torque acting on the generator

Up till now, it looks like the switching within MMR increases both harvestable electrical power and mechanical power loss, but whether it is beneficial for mechanical power flow is still unknown yet. According to the model developed in Section 3.2.3, dynamics of MMR based regenerative shock absorber when it is subjected to a prescribed torque input are presented and simulation results are shown in Figure 3-23. Figure 3-23 (a) describes output speed of primary system ($|\dot{\theta}_{in}|$) and generator speed ($\dot{\theta}_g$) respectively. Due to the compound sprag-clutch, the torque and velocity transmitted to the generator is unidirectional. It can be identified from Figure 3-23 (c), when the torque acting on the secondary switchable system reduces to zero at t_1 instant, the generator inertia and electrical damping disconnects from the vibration source undergoing a decaying vibration. Unlike velocity input varies applied torque to keep the velocity of primary system remaining consistent, the force/torque source behaves as the other way around. When J_g and c_e are unloaded from vibration source during disengagement period, the primary velocity (unidirectional) falls down from its initial condition and speed up quickly. At t_2 instant, when the output speed of primary system (unidirectional) catches up with the generator speed ($|\dot{\theta}_{in_d}| = \dot{\theta}_g$), the generator and electrical load are allowed to reconnect with the vibration source through the sprag-clutch. Figure 3-23 (b) describes dynamics of applied mechanical power given by the product of applied torque and velocity ($P_{total} = T\dot{\theta}_{in}$). During the engagement period, the vibration source provides power for all of the resistive and reactive elements, the difference between

total input power (blue curve) and the reactive power (pink curve) gives the sum of power absorbed by electrical and mechanical damper. When the generator disengages from the vibration source at t_1 , where the reactive power was feeding back to the vibration source. In the same way as velocity input, part of mechanical reactive power is converted into harvestable electrical power by the secondary system. As there is no electrical damper in the primary system during disengagement period, the difference between total power and reactive power is mechanical power loss only. As there is no electrical damper and generator inertia resisting applied force during disengagement, which results more mechanical power loss between t_1 and t_2 . When the generator is allowed to reconnect with vibration source at t_2 , there is an instantaneous drop on the reactive power. The main reason is according to re-engaged generator inertia and electrical damper restarts resisting the applied force which causes a reduction on the system acceleration. As discussed in the start of this section, the disengagement of secondary system allows the generator to work more continuously, while the corresponding dynamics during re-engagement period will increase both electrical and mechanical power. Even though, increasing mechanical power loss is undesirable, whereas more electrical power is being harvested compared to linear system as a trade-off.

After interpreting the consequence of implementing MMR in regenerative shock absorber when the vibration source is a prescribed torque input, the next step is to determine how system parameters affecting the dynamics of switching. Figure 3-24 shows dynamics of generator speed by varying the amplitude of electrical damping c_e . It is evident that the speed of generator system becomes greater and more continuous with lower c_e . The primary system takes longer period to catch up with the generator speed, as the kinetic energy stored on the generator shaft during disengagement will be consumed slower. As a result, system with lighter electrical damping (i.e. $c_e = 1 \text{ Nms/rad}$) has much longer disengagement durations compared to others in Figure 3-24, and the dynamics of switching allow the coupled generator to produce more continuous voltage.

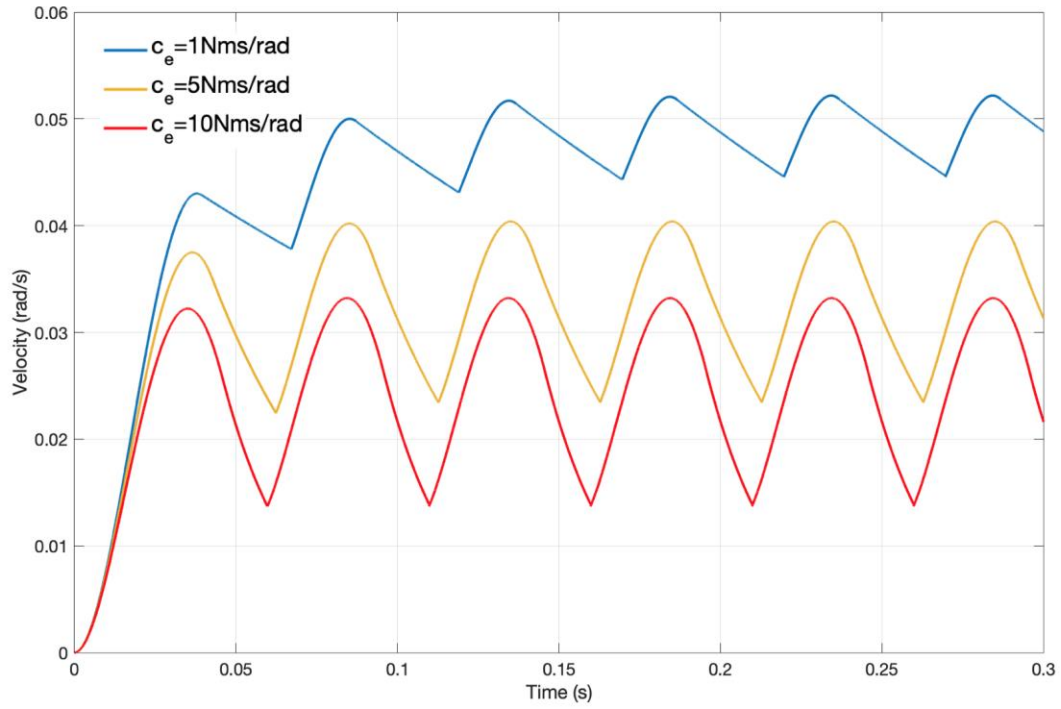


Figure 3-24: Dynamics of generator speed with different electrical damping c_e
($f=10\text{Hz}$)

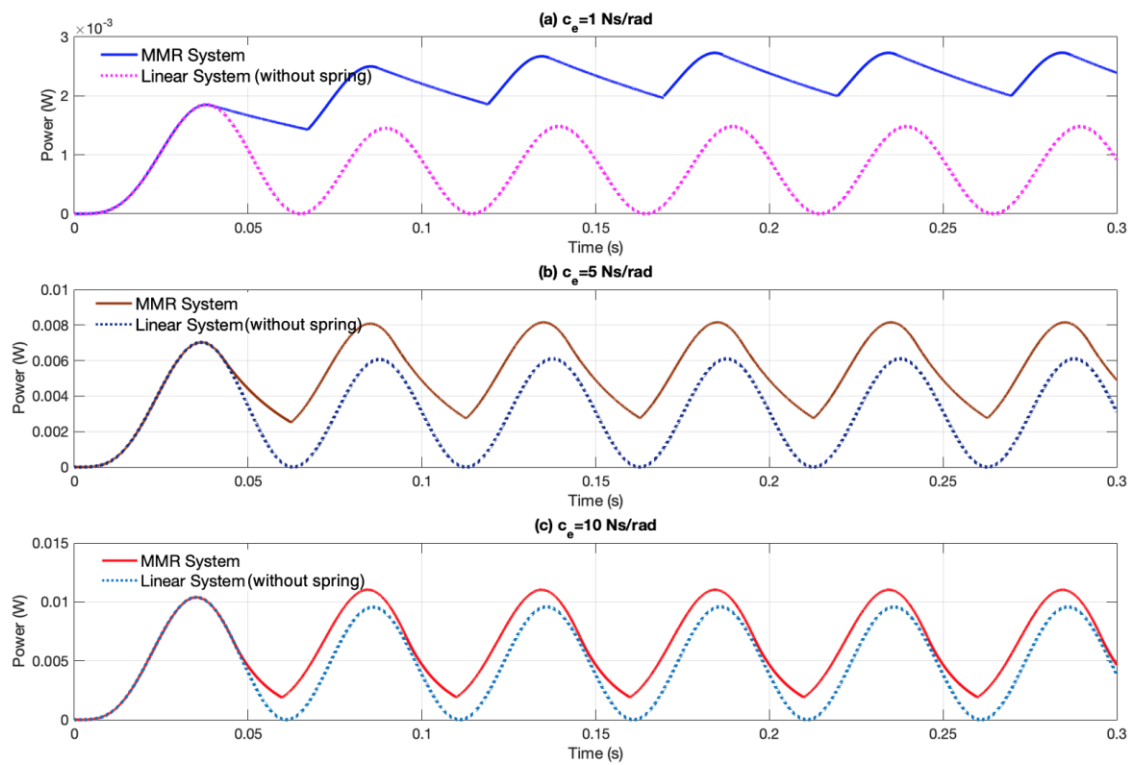


Figure 3-25: Harvested electrical power of MMR vs linear system (without spring) with different electrical damping c_e ($f=10\text{Hz}$) (a) $c_e = 1\text{Nms/rad}$ (b) $c_e = 5\text{Nms/rad}$ (c) $c_e = 10\text{Nms/rad}$

Figure 3-25 shows a comparison of harvestable electrical power between MMR and linear system by varying c_e . It is clearly from the curve that lighter electrical damped system will gain more benefits by employing MMR comparing to linear system. The numerical study result in Table 3-5 shows that the average harvestable power for linear system is only $0.74mW$, while the amplitude will be triple with MMR. As far as the electrical damping increases, the performance tends to be closer to the linear system. The main reason is according to the residual reactive power will be consumed faster with heavier c_e which shortens the disengagement period. Throughout the numerical study, it was found that when the amplitude of electrical damper is closer or greater than the mechanical damper ($c_e \geq c_m$), $t_1 \approx t_2$. In this case, the sprag-clutch allows the generator to engage with the vibration source all the time and ideally the MMR based regenerative shock absorber works exactly the same as linear system. In the same way as the conclusion drawn in Section 3.3.3, system cannot take additional advantages from the switching when it is heavily electrical damped. According to the mechanical power loss quantification result in Table 3-5, it is found that even though switching within the MMR system significantly enhance the energy harvesting performance comparing to unswitchable linear system, but it results much more mechanical power loss. Increasing the electrical damping shortens the disengaging duration, energy harvesting performance takes less advantages from the switching, while it decreases the mechanical power loss as a trade-off.

c_e (Nms / rad)	$P_e(MMR)$ (mW)	$P_m(MMR)$ (mW)	$P_e(Linear)$ (mW)	$P_m(Linear)$ (mW)
1	2.35	23	0.74	10
5	5.55	14	3.04	9.135
10	6.585	9.17	4.79	7.18

Table 3-5: Average harvestable electrical power and mechanical power loss with different electrical damping coefficient (MMR versus Linear system (without spring))

The next step of the discussion is to identify how generator inertia affecting the dynamics of switching as well as energy harvesting performance. Figure 3-26 shows the dynamics of generator speed by varying J_g . As the vibration source is considered as a prescribed torque, the maximum amplitude of steady-state velocity becomes lower by increasing the generator inertia. From the generator speed waveform in Figure 3-26, it is also found that system takes longer durations to reach its steady-state response (switching becomes periodical) with greater generator inertia. Once the system reaches to its steady-state condition, the generator speed becomes more continuous with less ripple. Increasing the generator inertia allows more reactive power stored on the shaft which extends the disengagement duration.

Furthermore, it is also found that smaller generator inertia significantly shortens the disengagement period, and characteristics of MMR system become closer to the linear system in Figure 3-27. There will be no switching happening when the value of J_g is far below the primary system inertia, as the residual kinetic energy on the generator inertia vanishes in a second when the applied torque reduces to zero. Numerical study results in Table 3-6 illustrate that larger generator inertia enables much greater harvestable power comparing to linear system. However, unreasonably increasing the generator inertia will not bring any advantages especially when the amplitude of input torque is fairly small. By setting $J_g \rightarrow \infty$ in eq (3-54), it is found that system might not harvest any energy as the applied torque is not enough to produce a velocity across the damper.

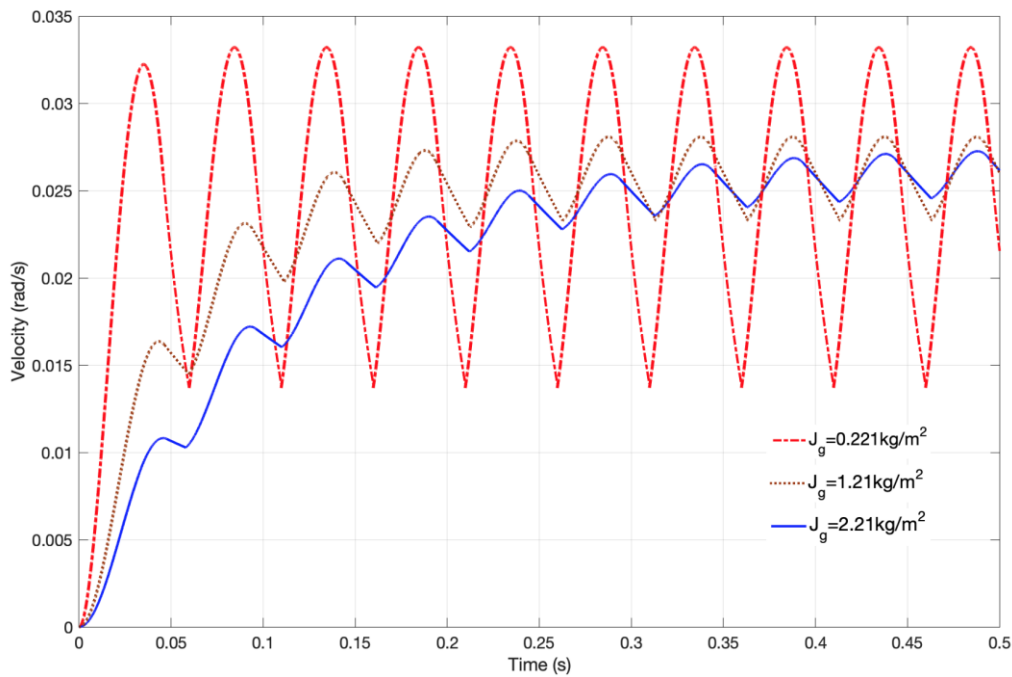


Figure 3-26: Dynamics of generator speed with different generator inertia J_g ($f=10\text{Hz}$)

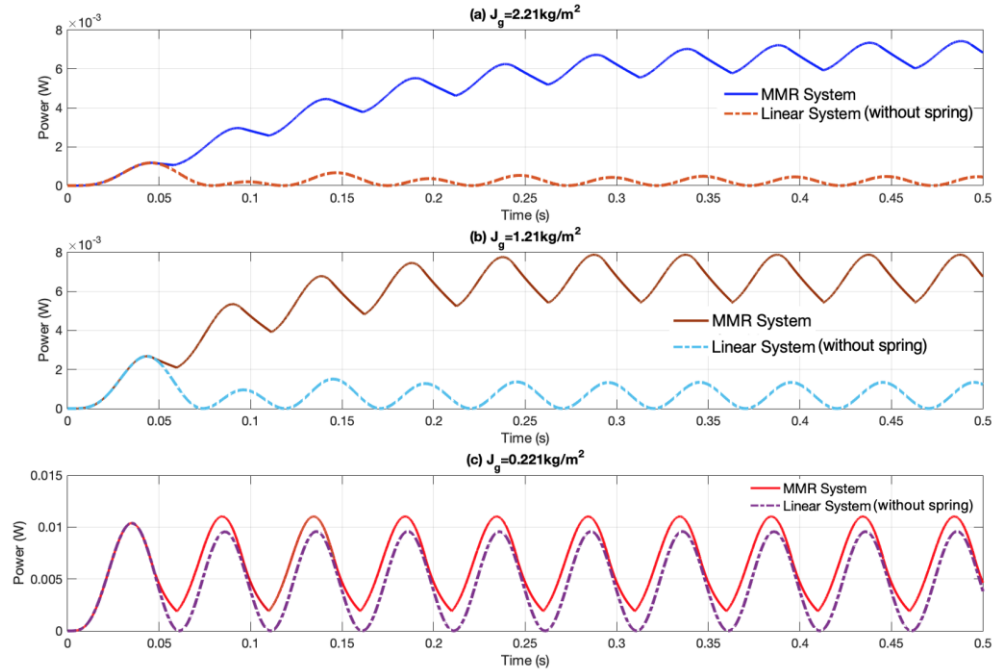


Figure 3-27: Instantaneous harvested electrical power with different generator inertia J_g

($f=10\text{Hz}$) (a) $J_g = 2.21\text{kgm}^2$ (b) $J_g = 1.21\text{kgm}^2$ (c) $J_g = 0.221\text{kgm}^2$

J_g (kgm^2)	$P_e(\text{MMR})$ (mW)	$P_m(\text{MMR})$ (mW)	$P_e(\text{Linear})$ (mW)	$P_m(\text{Linear})$ (mW)
0.221	6.585	9.17	4.79	7.18
1.21	6.75	8.13	0.677	1.02
2.21	6.79	8.04	0.2336	0.3504

Table 3-6: Harvestable Power with different generator inertia (MMR versus Linear system (without spring))

According to eq (3-54) and eq (3-61), varying the amplitude of torque T_0 in eq (3-55) will change the system velocity and acceleration whenever the secondary is under engaged or disengaged state. Figure 3-28 presents dynamics of generator speed with different input torque. It is seen that the amplitude of generator speed in both the engaged and disengaged state is improved by increasing T_0 , while the time instant of switching remains unchanged. This is according to system dynamics is still linear under certain time durations even though it is discontinuous. In a similar way of changing the amplitude of velocity input, the variation of velocity and acceleration will mathematically compensate each other in real time. As a result, the switching time instants of MMR will not be affected by varying the amplitude of applied torque.

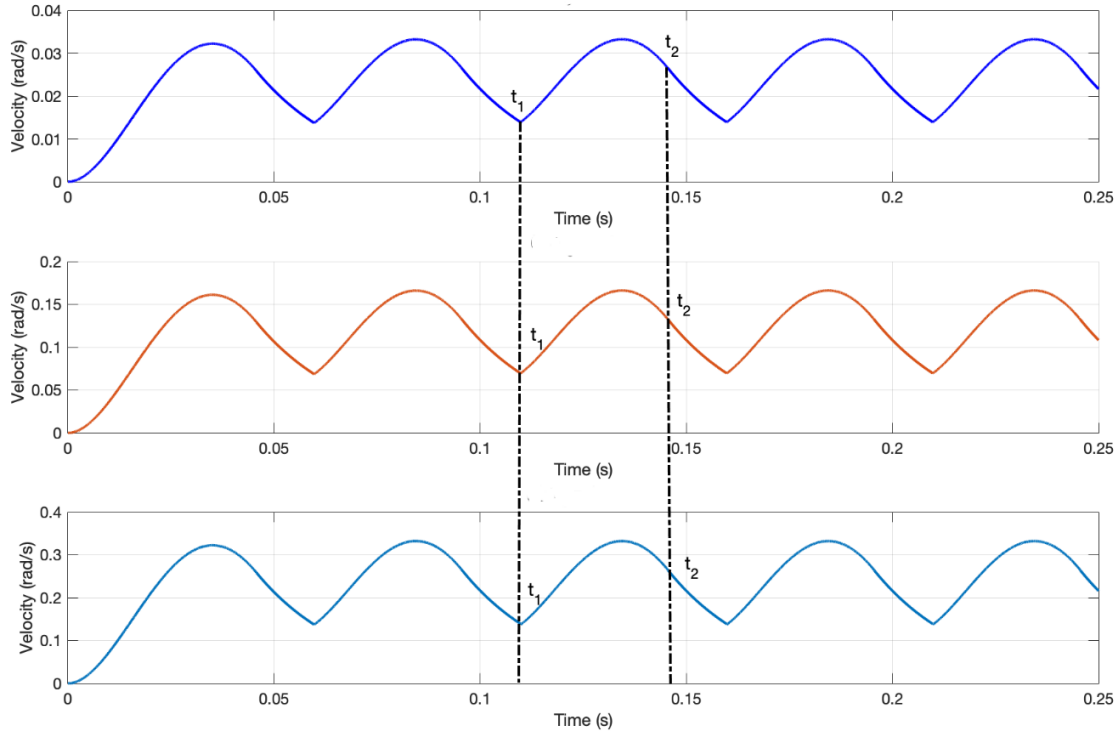


Figure 3-28: Dynamics of generator speed with different amplitudes of applied torque T_0

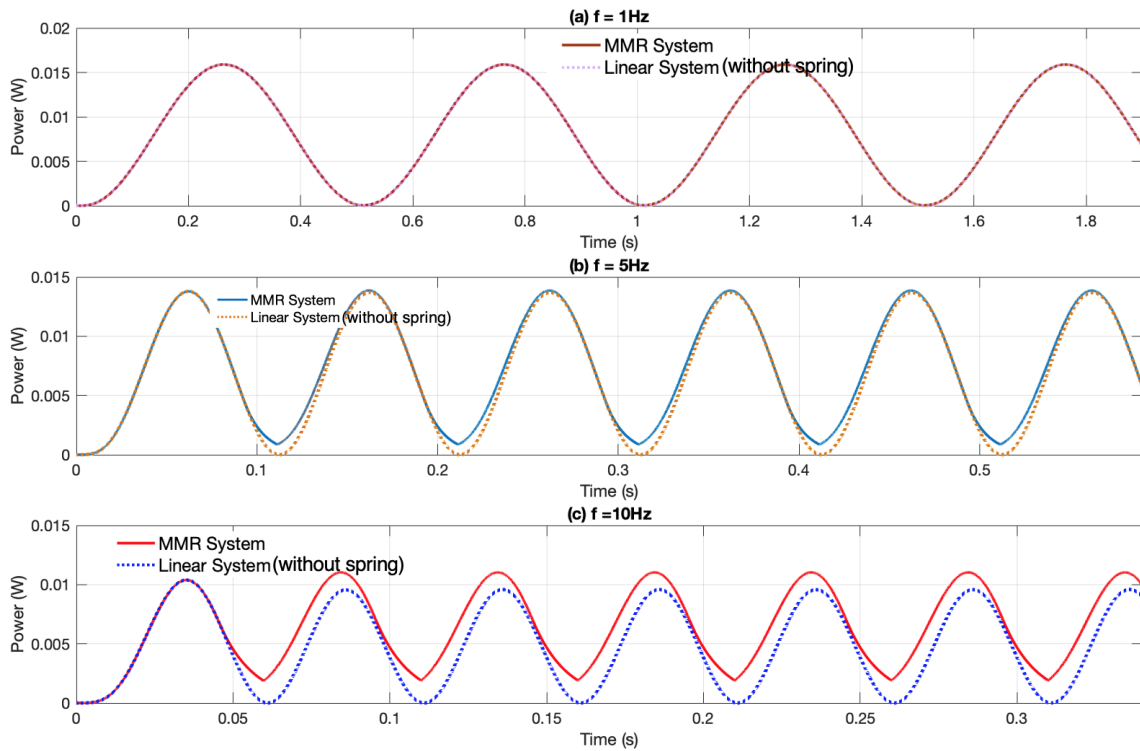


Figure 3-29: Instantaneous harvested electrical power under different frequency excitations (MMR versus Linear system (without spring)) (a) $f=1\text{Hz}$ (b) $f=5\text{Hz}$ (c) $f=10\text{Hz}$

Finally, whether MMR is desirable at different excitation frequency ranges is investigated, a comparison between MMR and linear system is shown in Figure 3-29. It is a bit surprised that

the disengagement duration is shorter in lower excitation frequency, the energy harvesting performance is quite close to a linear system when it is excited at 1Hz with given parameters. As there is no spring in the system, majority of torque and power flows into damper instead of inertia elements under lower frequency region which results less kinetic energy stored on the generator shaft. Since the amount of kinetic energy willing to convert into useful power is reduced, the disengagement period is significantly shortened as a result. Therefore, for a force/torque vibration input, the impact of switching on system dynamics is negligible when the excitation frequency is fairly low. However, this does not mean the performance becomes better under higher frequency excitation. As stated earlier, system is gradually dominated by mass or inertance with the increasing of frequency. By setting $\omega \rightarrow \infty$ in eq (3-54), it is found that there will be no velocity or acceleration output from the device. For a finite vibration input, either the linear inerter based regenerative shock absorber or MMR based piecewise linear system would not be able to work under higher frequency excitation as the vibration source cannot provide enough power for reactive elements to produce output velocity across the damper.

3.4 Multiple harmonics input

In section 3.2 and 3.3, dynamics of regenerative shock absorber with MMR under single frequency excitation has been modelled and analysed. However, the device might be subjected to vibration which is disturbed over a broadband of frequencies and random in physics. The frequency range may vary one the other depends on the vibration environment. Generally, an ideal random excitation with equal power spectral density over broadband frequency called broadband white noise is taken into account. However, this only valid in a quite narrow frequency band in nature. Broadband vibration is a stationary random process whose mean square spectral density has a significant value over considered range. The filtered vibration signal transmitted to the receiver is typically dominated by one or two harmonics according to the system natural frequency. A random vibration input can be constructed mathematically from a series of sinusoids with different periods, amplitudes and phases. [130] In this section, the performance of MMR based regenerative shock absorber will be evaluated when it is subjected to multiple harmonics input. In order to simplify the discussion, the vibration input here is assumed to be velocity source only as a combination of force and velocity input might cause confusion in understanding it in physics. Meanwhile, it is necessary to identify whether the switching of engagement and disengagement will be dominated by one single frequency or all of them.

Employing system parameters in Table 3-1, Figure 3-30 shows the simulation result of time duration of secondary system switching on/off from the vibration source when it is excited by single harmonic input with frequency range ($1\text{Hz} \leq f \leq 5\text{Hz}$). It was also found that the period of engagement (Yellow area) and disengagement (White area) for each frequency tend to be conflict with the other (single frequency excitation). Based on the discussion in the section 3.3.2, the switching inside MMR happens more frequently with higher excitation frequency, and the ratio of disengagement period over given time scale increases as well. For a 1Hz excitation input, the percentage of disengagement period over a cycle is 72.16%, while it reaches to 87.16% when the frequency is 5Hz. As stated earlier in this section, system may be subjected to a random excitation in a physical vibration environment which comprised multiple harmonics. By other means, one frequency may require the sprag-clutch inside MMR to disengage generator with the vibration source during certain periods while the other may not want to. Therefore, it becomes necessary to investigate how the system reacts when the conflict happens.

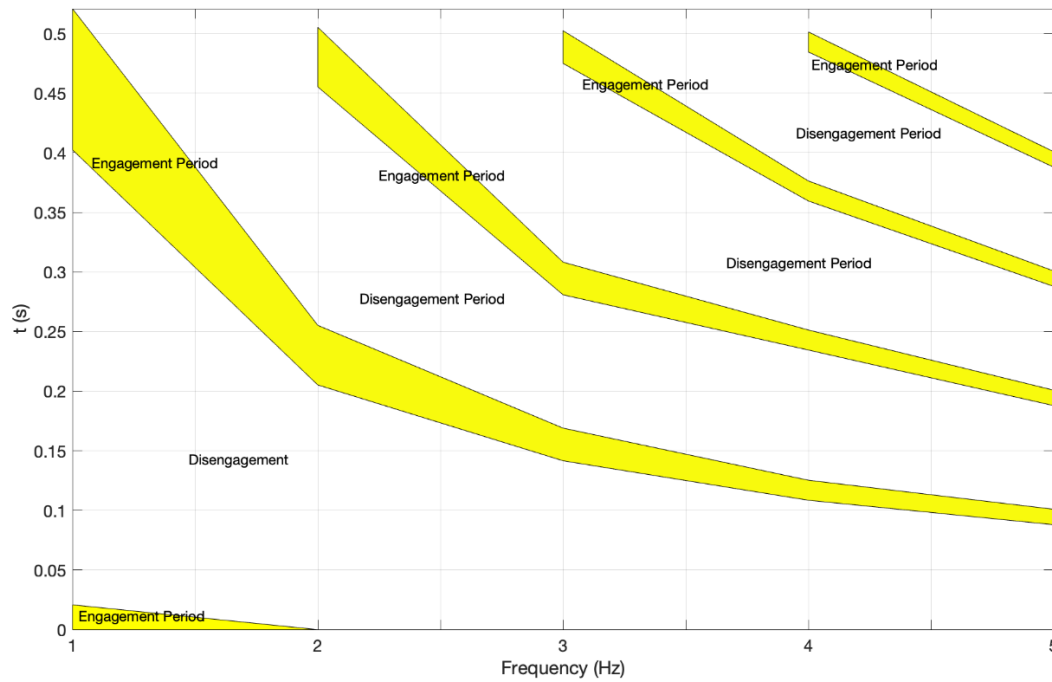


Figure 3-30: Time instant of switching on/off in different frequencies ($1\text{Hz} \leq f \leq 5\text{Hz}$)

By adopting parameters from Table 3-1, Figure 3-31 shows the simulation result of system dynamics when it is excited by dual harmonics velocity input (1&2Hz) with same phase ($\varphi = 0$) at starting point $t = 0$ and equal maximum rotary input velocity $Max(\dot{\theta}_{in}) = 1.1\text{rad/s}$ for both 1&2Hz. It shall be noted that the in a real application, the amplitude and phase angle for each frequency component will not be the same, the value here is only chosen for

demonstration purposes. It is seen that the generator tends to disengage from the vibration input three times over 1 second by combining these two frequencies in Figure 3-31(c). Considering the consequence for single harmonic excitation in Figure 3-31(a) (1Hz) and Figure 3-31(b) (2Hz), it is found that at t_1 instant the 1Hz applied waveform is allowed the vibration source transferring power to the generator while the 2Hz component tries to disengage the generator from the vibration input. Furthermore, the generator re-engages with the primary system at t_2 instant in Figure 3-31(c), while the generator is still at disengaged state for 1Hz input. The similar result can be observed in the rest of time span.

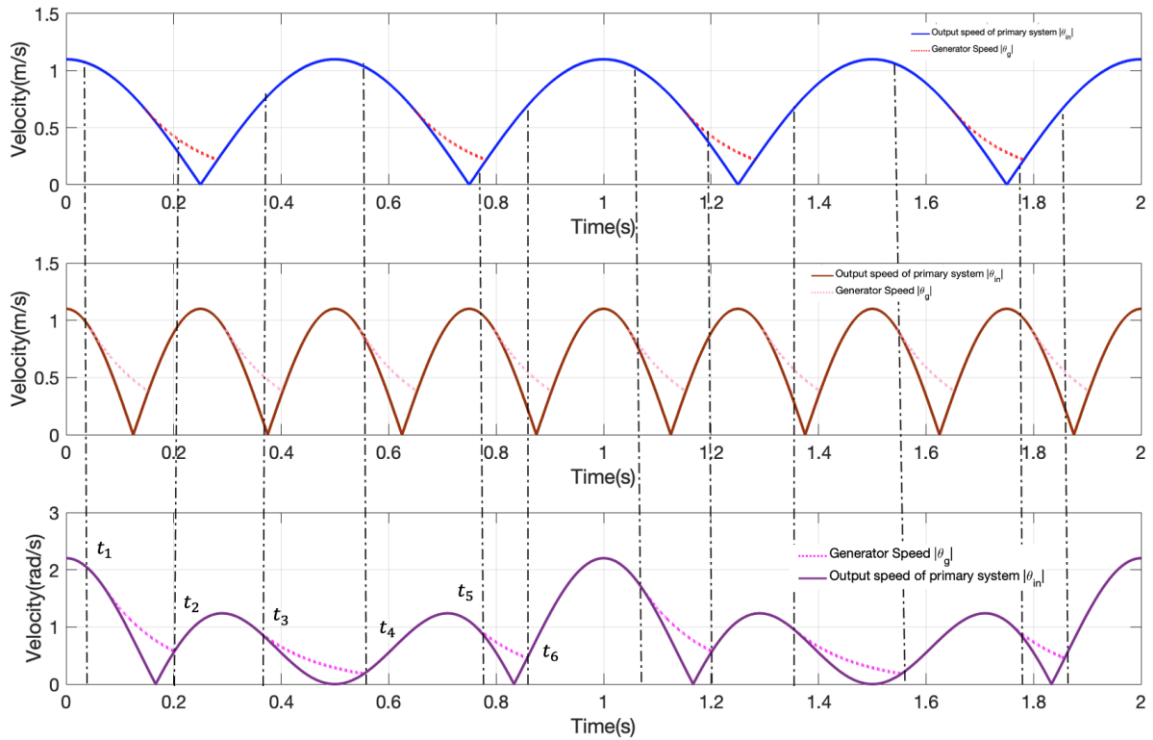


Figure 3-31: Consequences of switching on system dynamics (1&2Hz excitation) (a)1Hz, $\text{Max}(\dot{\theta}_{in}) = 1.1\text{rad/s}$ (b) 2Hz, $\text{Max}(\dot{\theta}_{in}) = 1.1\text{rad/s}$ (c) 1&2Hz, $\text{Max}(\dot{\theta}_{in}) = 2.2\text{rad/s}$

After discussing how the MMR based regenerative shock absorber system reacting to multiple harmonics input, it is necessary to evaluate its performance including energy harvesting as well as mechanical power flow. Figure 3-32 shows the power extraction and flow when the MMR based regenerative shock absorber is subjected to a dual harmonics velocity input (1&2Hz) with same amplitude of velocity ($\text{Max}(\dot{\theta}_{in}) = 1.1\text{rad/s}$). It is clear from Figure 3-32 (a) that system with MMR stills harvests more electrical power comparing to conventional linear regenerative shock absorber without MMR. Throughout the numerical study, there will be an 8% improvement over a cycle with given parameters in Table 3-1.

Figure 3-32(b) describes the dynamic of mechanical active and reactive power flow of MMR based piecewise linear system (without spring). In the same way as single harmonic input, switching stops part of the kinetic energy stored on the generator shaft returning back to the vibration source and discharging the electrical load. Once the generator and coupled electrical load reconnects with the vibration source, the source will restart providing both active and reactive power for them until next disengagement happens.

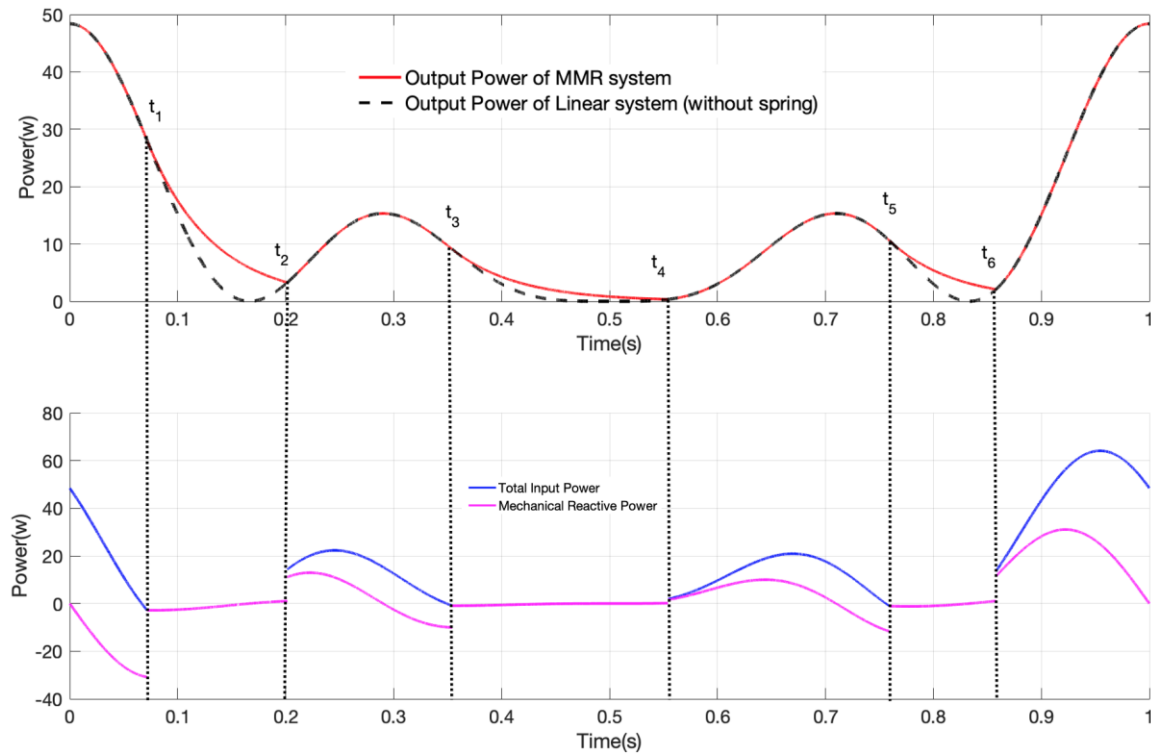


Figure 3-32: Power dissipation/flow of MMR based regenerative shock absorber under 1&2Hz excitation (a)Electrical power dissipation (b)Mechanical reactive power flow

From the above observation, it can be obtained that whenever the MMR based regenerative shock absorber is excited by single harmonic or multiple harmonics velocity input will not affect the consequence of switching, system still enables greater harvestable power over linear system by its discontinuous power transmission between the vibration source and secondary switchable system.

3.5 Summary

In this chapter, characteristics of regenerative shock absorber with MMR are modelled and analysed when one terminal of the design is blocked which allows to be experimentally

validated in Chapter 5. Due to the sprag-clutch inside MMR gear module, system is able to unidirectionally drive the coupled generator. However, when the external torque on the generator reduces to zero, the sprag-clutch will disengage the generator from the vibration source until the unidirectional output speed of the primary system catching up with the secondary system. The switching between engage and disengage state of generator allows system comprising a switchable inertia and electrical damper. In order to comprehensively investigate the energy harvesting performance of the MMR coupled system, two piece-wise linear models including velocity and torque input are developed. It was found that the engagement and disengagement of MMR potentially enables generator to work more continuously and the produced voltage and power never falls down to zero. Furthermore, a comparison between MMR based piecewise linear system and linear system without switching is presented. To have a clearer understanding of how power flow works in mechanical system, an analogy of active and reactive power between electrical and mechanical system is proposed based on force-current analogy. It is seen that the amount of power which system provides for reactive elements will eventually give back to the source without working. The discontinues power transmission between primary and secondary system stops part of the mechanical reactive power flowing back and converting it into useful electrical power which significantly improves the energy harvesting performance. In order to well interpret the system dynamics, numerical study for both velocity and torque input systems are conducted. The main conclusion obtained is that when the system is heavily electrical damped, implementing MMR in regenerative shock absorber allows less benefits from the switching and system dynamics is quite close to the linear system. Whereas MMR enables lightly electrical damped system much more improvement over linear system. It is feasible to provide a more continuous voltage with higher DC offset and less ripple. Moreover, reasonably increasing the generator inertia can somehow smooth the generator speed and extend the disengagement period which further improves the energy harvesting performance for both vibration input systems. It was also identified that MMR is not desirable for higher frequency vibration environment, since the whole structure might not be able to produce output velocity across the damper. Furthermore, dynamics of MMR based regenerative shock absorber are investigated when it is subjected to multiple harmonics input to identify whether the time instant of switching will be dominated by one single frequency. Based on the simulation result, it is found that the switching time instant will be decided by all frequency components unless one single harmonic dominates the excitation waveform. Finally, it was demonstrated that MMR still enables improvement on the energy

harvesting performance over unswitchable linear system whenever the vibration input is single harmonic or multiple harmonics.

Chapter 4 Regenerative shock absorber with electrical rectifier

Rotary regenerative shock absorber converts translational vibration into a bi-directional rotational oscillation of coupled electrical generator. In order to charge batteries or provide power for electronic devices, the oscillating motion/voltage needs to be commutated with either mechanical or electrical rectification to rectify the AC input signal to a DC signal. The argument so far has not made any recommendation in which rectification module is more suitable for various applications. To be more specific, the literature focused on physical mechanism problems rather than the delivery of useful power to an electrical load, while the power loss has not been quantified yet.[82] Although much work has been conducted to maximize the vibration power transferred to the electrical load, the definition of useful power still needs further clarification. In this chapter, a study of electrical rectifier coupled regenerative shock absorber is presented. The impact of voltage drop across the diode is evaluated in more detail in both electrical and mechanical systems. The discussion can be extended to compare the performance between the electrical rectifier and mechanical motion rectifier. By combining the piecewise linear model developed for MMR in Chapter 3, a numerical study is conducted to justify the usage of each rectifier in different scenarios.

4.1 Dynamics of electrical rectification

Electrical rectifier is a circuit which converts the Alternating Current (AC) input into a Direct Current (DC) output. In this section, a brief introduction of full-wave bridge rectified electrical circuit including its fundamental operating principle and nonlinear dynamics will be presented. The full wave electrical rectifier in Figure 4-1 consists four diodes connected to the load resistance R_L . During each positive half cycle of the AC sine wave, two diodes (D_1 and D_2) are forward biased as the anode is positive with respect to the cathode resulting in current flowing through the diodes. While during the negative half cycle of the AC input, D_1 and D_2 are reverse biased as the anode is negative with respect to the cathode. Therefore, no current flows through these two diodes, while D_3 and D_4 starts conducting the current through the load.

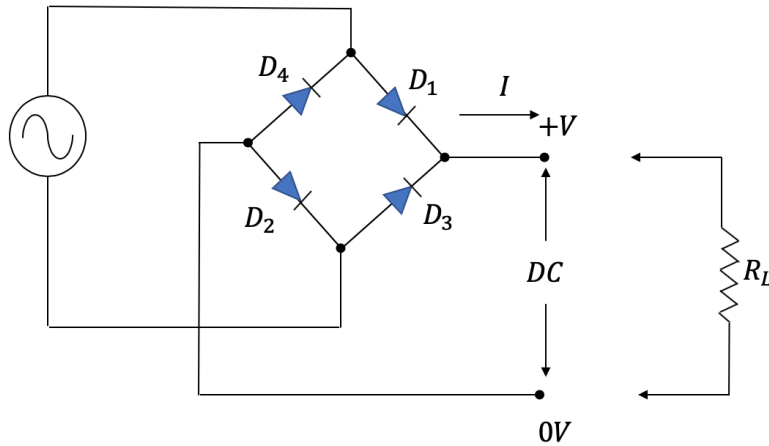


Figure 4-1: AC/DC circuit with electrical rectification

As the current flowing through the load is unidirectional, thus, the voltage across the load is unidirectional as well. For the DC electromagnetic generator, the back emf voltage is related to the angular velocity and voltage coefficient k_e of the electrical transducer

$$v_{emf} = k_e \dot{\theta} \quad \text{eq (4-1)}$$

During each half cycle, the current flows through electrical rectification causing voltage drops across the rectifying diodes in practice. This voltage drop cannot be ignored unless the produced emf voltage is much greater than it. It should be noted that the voltage drop across a current-conducting diode does change with the amount of current passing through, but this change is fairly small over a wide range of currents. Therefore, it is assumed that the voltage drop across each diode remains constant at 0.7 volts for silicon and 0.3 volts for germanium. [131] Dynamic effects of diodes are not considered here. The voltage drop V_D can then be described as a constant, acting in the opposite direction of back emf voltage (v_{emf}) and driving velocity of the electromagnetic transducer ($\dot{\theta}$) in Figure 4-2.

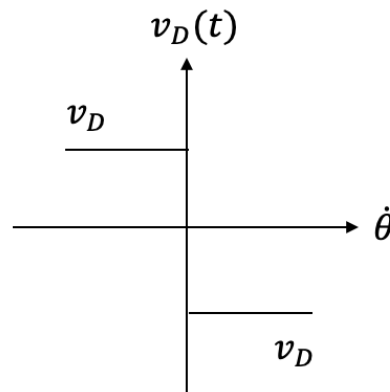


Figure 4-2: Diode voltage drop characteristic

Where

$$v_D(t) = -V_D \text{sgn}(\dot{\theta}(t)) \quad \text{eq (4-2)}$$

By assuming the electrical circuit is purely resistive, the governing equation of electrical circuit can be obtained according to the Kirchhoff's voltage law:

$$i(R_L + R_i) = v_{emf} + v_D \quad \text{eq (4-3)}$$

Where R_L and R_i is the load and internal resistance respectively, v_D is the voltage drop across the diode bridge.

The induced electromagnetic torque is proportional to the current through the coil and the coupling coefficient of the dc generator k_e which can be given by

$$T_{EM} = k_e i \quad \text{eq (4-4)}$$

The final model is a combination of eq (4-1) to eq (4-4). It can be found that the voltage drop of the electrical rectification attenuates the current through the electrical circuit and brings a threshold to the system, it starts conducting only if the back EMF voltage greater than the forward bias voltage V_D , otherwise there is no current flowing through the electrical circuit. In the meantime, it weakens the electromagnetic torque giving back to the mechanical system according to eq (4-4). In the next section, a detailed performance quantification of electrical rectified regenerative shock absorber in both electrical and mechanical systems will be presented.

4.2 Regenerative shock absorber with electrical rectifier

The primary measurement used to quantify the performance of rectifier is defined by the conversion from AC input power to DC output power. This has not been well considered in electrical-mechanical system, as the previous study [56, 63] generally assumes all the power transmitted to the electrical load rather dissipated by mechanical damping or internal resistor is the useful power. This approach is inaccurate since useful power for off-grid system generally refers to the DC term of the total power with zero frequency. Furthermore, the raw output of a passive rectifier cannot give a constant DC voltage output, the power conversion between the AC input power to the output DC power will always be less than 100%, even for an ideal case (81%). Some of the output power is AC power rather than DC which manifests as ripple superimposed on the DC waveform. [132] In this section, characteristics of a full-wave electrical rectifier will be investigated in both electrical and mechanical domains. In order to well evaluate the performance of the electrical rectifier and its coupled regenerative shock absorber, the effect of AC power oscillation and diode conducting voltage drop are essential to be addressed in the discussion.

4.2.1 Electrical system analysis

The electrical system of regenerative shock absorber in this section is comprised of a generalized electrical load via an electromagnetic generator and a full-wave rectifier. This is illustrated in a schematic form in Figure 4-3. By assuming the steady-state response of input displacement is a sinusoidal waveform $x(t) = X\sin(\omega t)$, and by adopting the relationship between the linear and angular speed $\dot{\theta} = \frac{2\pi}{l}\dot{x}$, where l is the screw pitch. The output voltage produced by the generator is related to the angular velocity in the time domain can be obtained by

$$v(t) = V_{max}\cos(\omega t) \quad \text{eq (4-5)}$$

Where

$$V_{max} = k_e X \omega \left(\frac{2\pi}{l} \right) \quad \text{eq (4-6)}$$

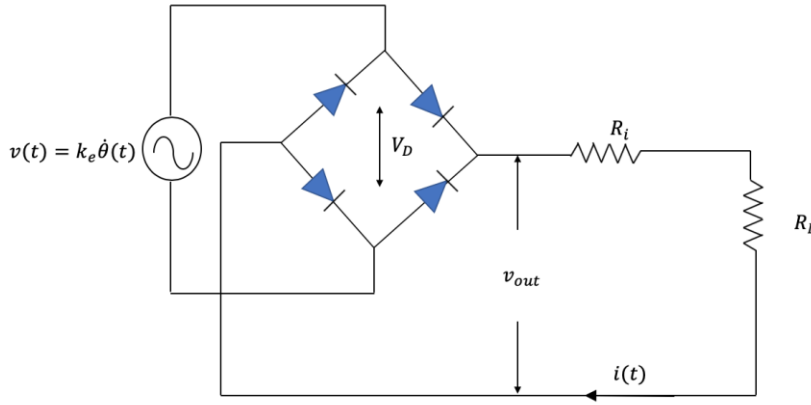


Figure 4-3: Schematic representation of full-wave electrical rectifier circuit

When the produced voltage goes through a full-wave rectification, there will be a voltage drop across the diode bridge in order to conduct the current through the circuit. The output voltage of the electrical rectifier in the time domain becomes

$$v_{out}(t) = |V_{max}\cos(\omega t)| - V_D \quad \text{eq (4-7)}$$

It shall be noted that there will be no output voltage from the electrical rectifier unless the amplitude of $v(t)$ is able to cover the conducting voltage. Therefore, the output voltage of electrical rectifier can be expressed as

$$\begin{cases} v_{out}(t) = 0, & |v(t)| \leq V_D \\ v_{out}(t) = |V_{max}\cos(\omega t)| - V_D, & |v(t)| > V_D \end{cases} \quad \text{eq (4-8)}$$

It can be observed from eq (4-8) that the output voltage of electrical rectifier becomes discontinuous according to the voltage drop across the diode bridge. Figure 4-4 shows the theoretical output voltage of the electrical rectifier by assuming $V_{max} = 3.14 \text{ V}$, $V_D = 0.7 \text{ V}$, $f = 1 \text{ Hz}$.

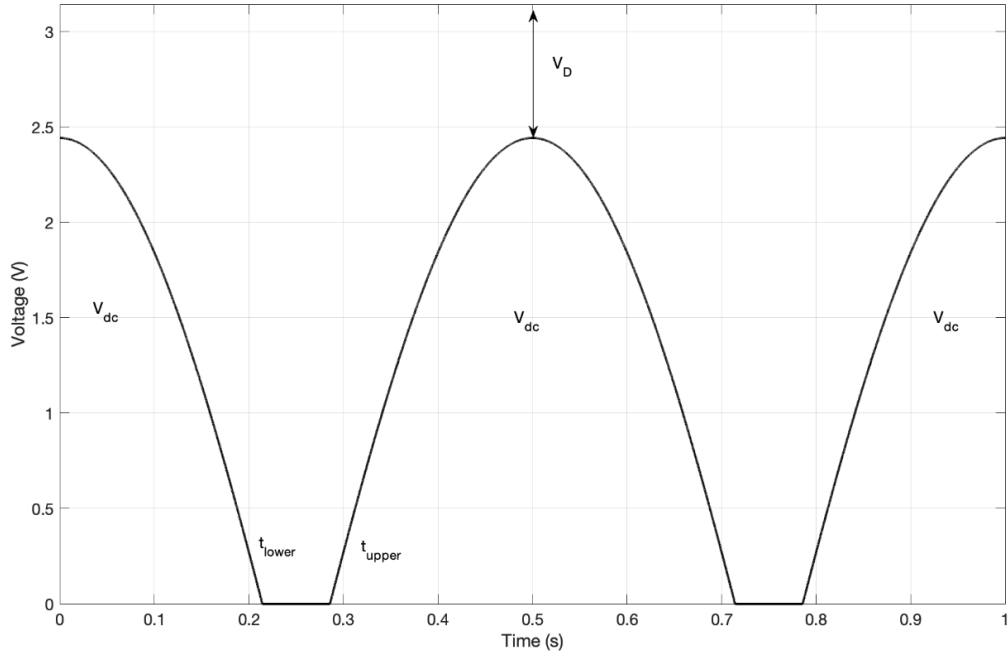


Figure 4-4: Theoretical output voltage of the electrical rectifier

From the curve, it is found that the voltage drop across the electrical rectifier brings a threshold to the system, it stops conducting at t_{lower} ($|v| = V_D$) and restarts at t_{upper} where the input voltage is above the DC offset V_D . As a result, the output voltage will not be transmitted to the load continuously. By assuming $V_{max} \geq V_D$, the time instant of t_{lower} and t_{upper} can be solved in eq (4-9) and eq (4-10) respectively when $V_{out} = 0$

$$t_{lower} = \frac{1}{\omega} \cos^{-1}\left(\frac{V_D}{V_{max}}\right) \quad \text{eq (4-9)}$$

$$t_{upper} = \frac{\pi}{\omega} - \frac{1}{\omega} \cos^{-1}\left(\frac{V_D}{V_{max}}\right) \quad \text{eq (4-10)}$$

As the output voltage of electrical rectifier is unidirectional, its average value over a half cycle is exactly the same as full cycle. Therefore, the output DC voltage in a half cycle can be obtained by

$$V_{dc} = \frac{2}{T} \left[\int_0^{t_{lower}} (V_{max} \cos(\omega t) - V_D) dt + \int_{t_{upper}}^{T/2} (V_{max} \cos(\omega t) - V_D) dt \right] = \frac{2}{\pi} \left[\sqrt{V_{max}^2 - V_D^2} + V_D \sin^{-1}\left(\frac{V_D}{V_{max}}\right) \right] - V_D \quad \text{eq (4-11)}$$

It can be observed from eq (4-11) that if V_{max} is below or equal to the voltage drop V_D , the diode is not able to work (no solutions for t_{lower} and t_{upper} as well) and of course there will not be any voltage output from the electrical rectifier ($V_{dc} = 0$).

Furthermore, the DC current through the internal and load resistance is

$$i_{dc} = \frac{V_{dc}}{R_L + R_i} \quad \text{eq (4-12)}$$

Assuming $V_{max} > V_D$, the DC power delivered to the electrical load becomes

$$P_{dc_L} = i_{dc}^2 R_L = \left(\frac{\frac{2}{\pi} \left[\sqrt{V_{max}^2 - V_D^2} + V_D \sin^{-1} \left(\frac{V_D}{V_{max}} \right) \right] - V_D}{R_L + R_i} \right)^2 R_L \quad \text{eq (4-13)}$$

Therefore, the useful power transmitted to the electrical load can be modelled with a discontinuous function of V_{max} and V_D

$$P_{dc_L}(\omega) = \begin{cases} 0, & V_{max} \leq V_D \\ P_{dc_L}, & V_{max} > V_D \end{cases} \quad \text{eq (4-14)}$$

It is incomprehensive to individually study how much DC power is transmitted to the electrical load as it is determined by the voltage source only. The diode conduction loss, internal power dissipation and AC power oscillation are not taken into account.

The average AC input power transferred from the electromagnetic generator to the electrical rectifier in Figure 4-3 is

$$P_{ac} = \frac{2}{T} \int_0^{\pi/\omega} \frac{v(t)^2}{R_L + R_i} dt = \frac{V_{max}^2}{2(R_L + R_i)} \quad \text{eq (4-15)}$$

The electrical power conversion efficiency can be defined by the ratio between the DC power delivered to the electrical load and the AC input power

$$\eta_e = \begin{cases} 0, & V_{max} \leq V_D \\ \frac{P_{dc_L}}{P_{ac}}, & V_{max} > V_D \end{cases} \quad \text{eq (4-16)}$$

To verify the approach, eq (4-15) and eq (4-16) were solved numerically to identify the impact of voltage drop on the system performance whose parameters (Design prototype referring to Chapter 5) are listed in Table 4-1

Parameter	Value
k_e	0.114 rad/v · s
X	20 mm
l	25 mm
f	1-10 Hz
V_D	0.7 V
R_L	10 Ω

Table 4-1: System parameters within the electrical domain

By assuming the internal resistance $R_i = 0$, Table 4-2 shows the numerical study results of electrical rectifier

Frequency (Hz)	$P_{dc_L} (W)$	$\eta_e (\%)$
1	0	0
2	$4.07 \cdot 10^{-6}$	0.0016
4	0.1072	10.34
6	0.5597	23.9
8	1.41	34.02
10	2.67	41.27

Table 4-2: Performance quantification of electrical rectifier-based regenerative shock absorber

For an unrectified harmonic voltage signal, the ratio between DC output and AC input power should be 20.25% without considering other internal losses. Based on numerical study results in Table 4-2, the system performance becomes even worse by using electrical rectifier when V_D is significant comparing to V_{max} . There will be no power transmitted to the load unless the input voltage is able to conduct the diode which results in a discontinuous power transmission system. With the increasing of excitation velocity, the influence of voltage drop becomes less significant, and eventually negligible when $V_{max} \gg V_D$. Note that reverse recovery behaviour through the diode bridge is the other source of power loss in practise, the transition between conducting-state to the blocking-state leads to a large instantaneous power loss, where its value depends on the switching frequency and recovery energy from the manufacture data sheet which further reduces the electrical efficiency. [133]

4.2.2 Mechanical system analysis

Individually studying electrical rectifier within the electrical domain is not the best way to characterise the coupled regenerative shock absorber, as it does not demonstrate its behaviour in mechanical system. According to eq (4-4), the voltage drop across the diode alters the current flowing through the circuit which reduces the electrical damping force giving back to the mechanical system. These issues are discussed in more detail in this section for the case of system excited by a prescribed velocity input.

A schematic diagram of an inerter based regenerative shock absorber with electrical rectifier when one terminal of the design is clamped is shown in Figure 4-5, k is the spring stiffness, c_m is the mechanical damping coefficient, F_{EM} is the back emf force, b is the system inerter.

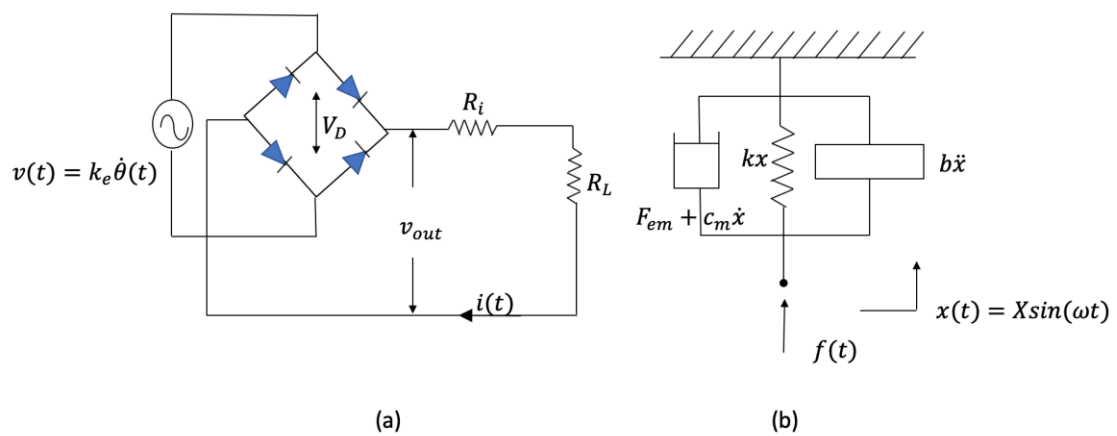


Figure 4-5: Schematic of regenerative shock absorber with electrical rectifier (a) Electrical circuit (b) mechanical schematic diagram

The governing equation of motion according to Figure 4-5(b) is written as

$$b\ddot{x} + c_m\dot{x} + kx + F_{EM} = f(t) \quad \text{eq (4-17)}$$

While the back emf force reflected into the mechanical domain due to the creation of an opposing magnetic field by the current flowing through the coil [134] is related to the applied angular velocity $\dot{x}(\frac{2\pi}{l})$ and the translational electromechanical coupling coefficient k_e , by assuming the electrical circuit is non-reactive, it can be obtained by

$$F_{EM}(t) = \begin{cases} 0, & V_{max} \leq V_D \\ (\frac{l}{2\pi})k_e i, & V_{max} > V_D \end{cases} \quad \text{eq (4-18)}$$

While i is the current flowing through the circuit, which can be expressed as

$$i = \frac{V_{max} - V_D \cdot \text{sign}(\dot{x})}{R_L + R_{in}} \quad \text{eq (4-19)}$$

As stated in section 4.2.1, when the DC offset of the $v(t)$ is less than the diode voltage drop V_D , no current is flowing through the electrical circuit. As a result, there will be no electrical damping force giving back to the mechanical system ($F_{EM} = 0$), all the input mechanical energy $\int f(t) \cdot \dot{x}$ will be dissipated by the viscous damper c_m and diode conduction.

Maximum vibration power is transmitted into the device when system is excited at its undamped natural frequency $\omega_n = \sqrt{k/b}$ according to Figure 4-5(b). The energy conversion efficiency in an electric-mechanical system η_m is defined by the ratio between DC load power P_{dc_L} and the total amount of power absorbed by the device P_{total} , it is straightforward to show the power conservation relationship

$$P_{ac} + P_{dc_L} + P_{int} + P_m + P_{cond} = P_{total} \quad \text{eq (4-20)}$$

P_{ac} is the AC power oscillations, P_{int} is the internal losses within the generator, P_{cond} is the diode conducting power and P_m is the mechanical power loss

$$\eta_m = \frac{P_{dc_L}}{P_{total}} \quad \text{eq (4-21)}$$

The translational electrical damping coefficient in a unit of Ns/m can be obtained by

$$c_e = \frac{k_e^2}{R_L + R_{in}} \quad \text{eq (4-22)}$$

The sum of power absorbed by the electromechanical system in the time domain can be given by

$$P_{total}(t) = P_e + P_m = (c_e + c_m)\dot{x}^2 \quad \text{eq (4-23)}$$

The average power dissipation including electrical and mechanical over half cycle can be obtained by

$$P_{ave-total} = \frac{2}{T} \int_0^{\frac{T}{2}} P_m(t) + P_e(t) dt = \frac{1}{2}(c_e + c_m)\omega^2 X^2 \quad \text{eq (4-24)}$$

By assuming the maximum input voltage V_{max} defined in eq (4-6) into the electrical rectifier is greater than the diode conducting voltage V_D ($V_{max} \geq V_D$), the energy conversion efficiency η_m can be reformed by substituting eq (4-13) and eq (4-24) into eq (4-21)

$$\eta_m = \frac{\left(\frac{\frac{2}{\pi} \left[\sqrt{V_{max}^2 - V_D^2} + V_D \sin^{-1} \left(\frac{V_D}{V_{max}} \right) \right] - V_D}{R_L + R_i} \right)^2 R_L}{\frac{1}{2} (c_e + c_m) \omega^2 X^2} \quad \text{eq (4-25)}$$

In the same way as electrical system analysis, the voltage drop across the diode bridge significantly reduces the useful power transferred to the electrical load. Meanwhile, the current flowing through the electrical load as well as the corresponded damping force becomes discontinuous. For a more physical mechanical vibration system (one terminal of the design is not clamped in Figure 4-5(b)), the existence of voltage drop attenuates the current and associated electrical damping force F_{EM} which potentially leads more relative displacement between the mass and base especially at system natural frequency. This is undesirable for both vibration isolation and energy harvesting performances. It can be observed that amplifying the angular speed $\dot{\theta}$, scaling the electromechanical coupling coefficient k_e can significantly improve the harvestable electrical power and minimise the effect of diode voltage drop. It is suggested that using high flux density electromagnetic transducer with smaller internal resistance. Then, for an ideal case ($c_m \rightarrow 0$), more useful power can be harvested on the electrical load by employing electrical rectifier.

4.3 Theoretical comparison between electrical rectifier and MMR

For a conventional regenerative shock absorber, the generated voltage by the electromagnetic generator needs to commute through electrical rectifier to provide power for electronic device or charge the battery. Based on earlier discussion, it can be identified that the voltage drop across the diode significantly reduces the energy harvesting efficiency especially for low power application. However, its influence becomes less significant with the increasing of voltage flowing through the electrical rectifier. In this section, a theoretical comparison between electrical rectifier and mechanical motion rectifier will be presented through a series of numerical examples to distinguish which one is more desirable in different scenarios. System parameters for both rectifiers are fixed to match the experimental testing discussion in Chapter 5 and shown in Table 3-1 and Table 4-1 respectively.

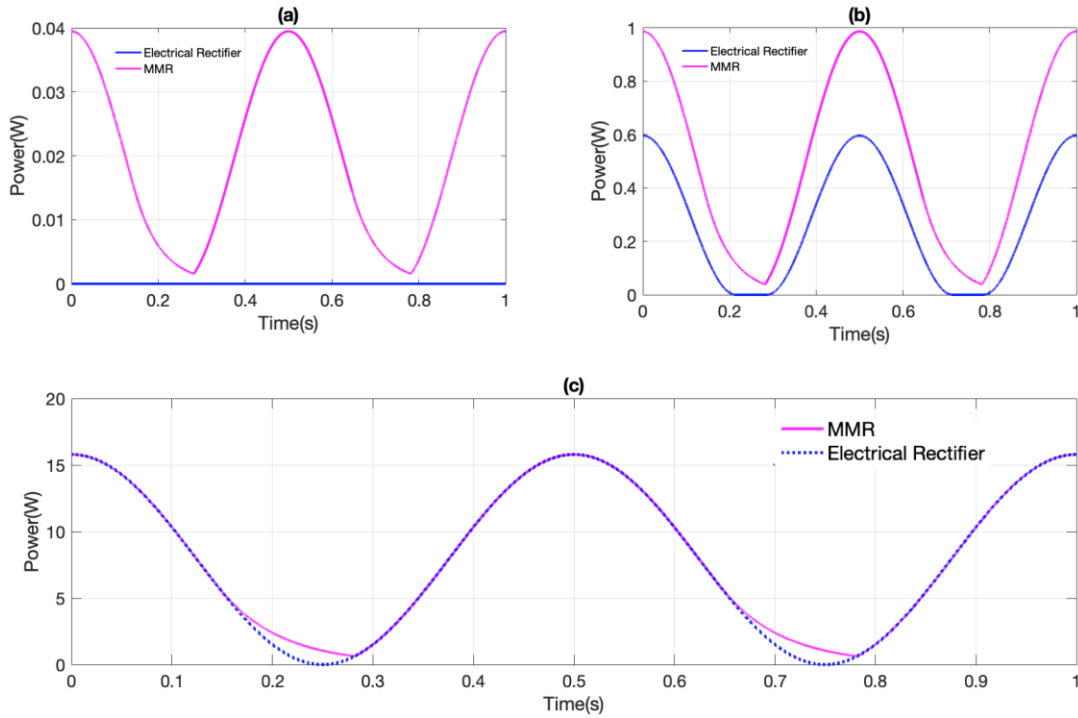


Figure 4-6: Energy harvesting performance comparison between electrical rectifier and mechanical rectifier with different input displacement ($f = 1\text{Hz}$, $c_e = 10\text{Ns/m}$) (a) $X = \pm 10\text{mm}$ (b) $X = \pm 50\text{mm}$ (c) $X = \pm 200\text{mm}$

Figure 4-6 shows the energy harvesting performance comparison between electrical rectifier and MMR by varying input displacement. It is found that the diode conduction loss becomes significant when the displacement amplitude X is relatively low. When the generated voltage across the electromagnetic transducer is below the voltage drop across the diode, no energy can be extracted by the electrical damper in Figure 4-6(a). Even though with the increasing excitation displacement, the diode voltage drop becomes less significant in in Figure 4-6(c), the MMR based regenerative shock absorber still can offer more harvestable power according to the switching within the gear module converting part of the mechanical reactive power into harvestable electrical power. In this case, the performance of MMR is better than the electrical rectifier.

The next step of the discussion is to find out how electrical damper affecting the selection of rectifier. Figure 4-7 shows the simulated energy harvesting comparison between electrical rectifier and MMR with different electrical damper c_e . As stated in Chapter 3, MMR is more beneficial for lightly electrical damped system comparing to linear system. It can be observed from Figure 4-7 (a) and (b), the MMR enables much greater performance in terms of electrical rectifier, since diode conducting loss significantly reduces the power transmitted to the load especially for lighter electrical damped system. However, the disengagement duration is

significantly shortened with greater electrical damping, the sprag-clutch eventually engages the generator with the vibration source all the time in Figure 4-8(c) when system is heavily electrical damped. As a result, no additional benefits can be found by using MMR compared to electrical rectifier as the diode conduction loss can be ignored. Moreover, the MMR gear module unavoidably brings additional viscous damper and friction into the design in physics. When the regenerative shock absorber no longer gains advantages from the switching, the additional mechanical damping within MMR gear module results more mechanical power loss and hence reduce the energy harvesting efficiency. Therefore, it is suggested that MMR is more suitable for a lighter electrical damped system, while electrical rectifier is more beneficial for heavily electrical damped regenerative shock absorber.

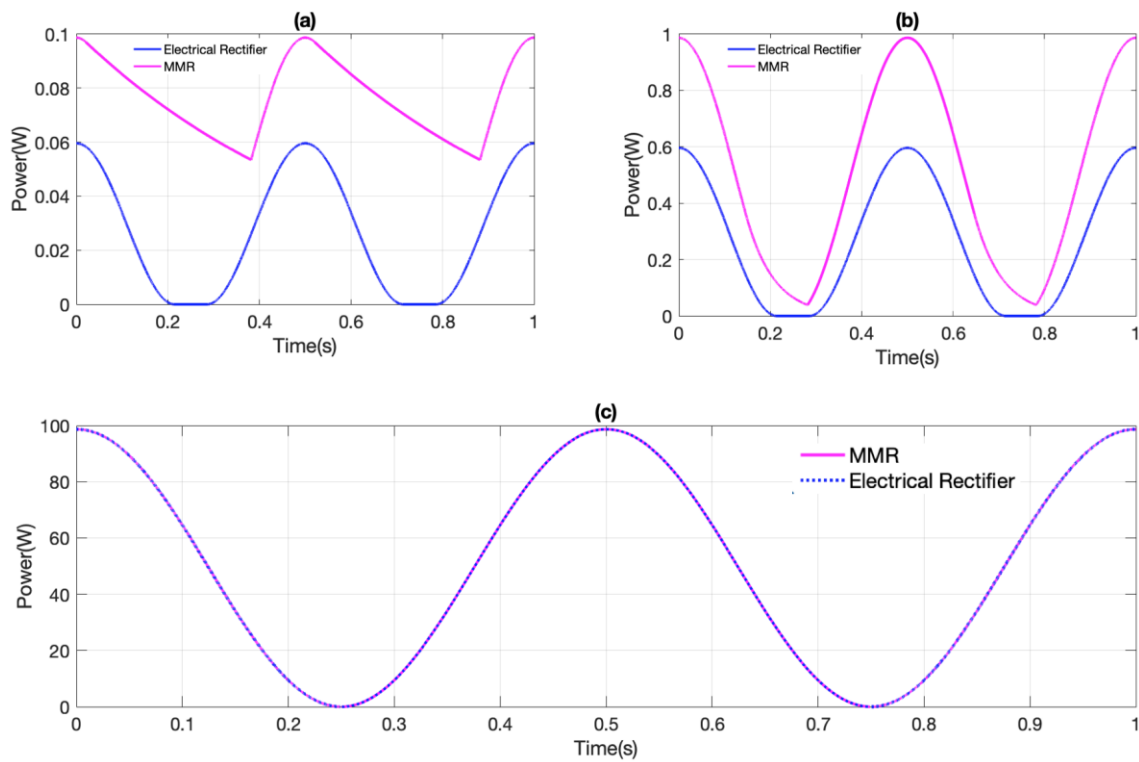


Figure 4-7: Energy harvesting performance comparison between electrical rectifier and mechanical rectifier with different c_e ($f = 1\text{Hz}$, $X = \pm 50\text{mm}$) (a) $c_e = 1\text{Ns/rad}$ (b) $c_e = 10\text{Ns/rad}$ (c) $c_e = 500\text{Ns/rad}$

Finally, both electrical rectifier and MMR are examined in different excitation frequencies in Figure 4-8. Under lower frequency region, it is no doubt that MMR is more desirable to regulate the input signal due to the switching within the gear module. With the increasing of excitation frequency, the performance of MMR is further improved as more mechanical reactive power is able to transfer into useful electrical power, once the sprag-clutch disengages the generator from the vibration input. It can be identified from Figure 4-8(c),

even though the diode conduction loss becomes less significant when the excitation frequency increases to 5Hz, but MMR still allows more harvestable electrical power. However, this does not mean the MMR gear module is always more beneficial comparing to electrical rectifier among all frequency range. As discussed in Chapter 3, the MMR based regenerative shock absorber is undesirable under higher frequency excitation. For a prescribed velocity source, the switching might result no power transmitting to the coupled generator, and the additional inertia/inertance introduced by the MMR gear module requires much more mechanical reactive power from the vibration source especially under mass or inerter controlled frequency region. Failure to provide this amount of reactive power leads to zero velocity across the electrical damper. Therefore, it is not a good idea to implement MMR in energy harvesting device in high frequency region.

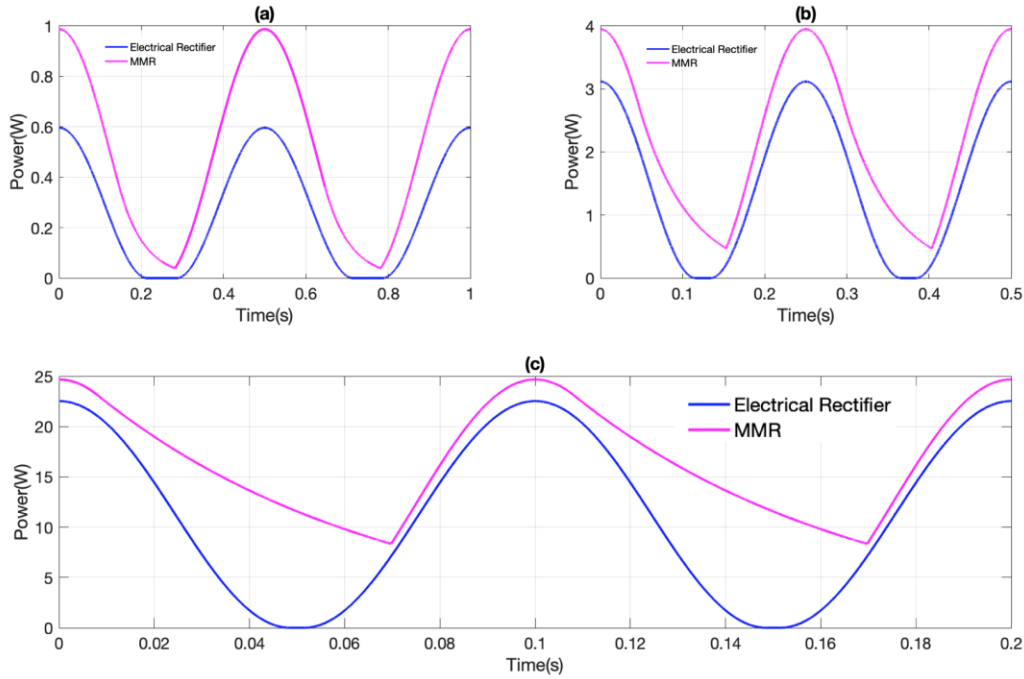


Figure 4-8: Energy harvesting performance comparison between electrical rectifier and mechanical rectifier in different excitation frequency ($X = \pm 50\text{mm}$, $c_e = 10\text{Ns/rad}$) (a) $f = 1\text{Hz}$ (b) $f = 2\text{Hz}$ (c) $f = 5\text{Hz}$

4.4 Summary

In this chapter, characteristics of regenerative shock absorbers with electrical rectifier are investigated in both electrical and mechanical systems. Based on the theory, adding electrical rectifier enables the current unidirectionally flowing through the circuit in order to charge the battery or supply power electronic device. For an ideal full-wave electrical rectifier circuit,

the conversion ratio between the DC power consumed by the load to the AC power input is around 81%, while 19% is AC power oscillation. The conduction losses in a diode appear when the diode is forward conduction mode due to the on-state voltage. The diode can work only if the input voltage is greater than its on-state voltage, which leads a discontinuous transmission system. Considering the electrical rectifier in the mechanical domain, it is found that the voltage drop weakens the current flowing through the circuit as well as the corresponding back emf force. This behaviour potentially results more displacement of seismic mass, meanwhile it brings additional mechanical power loss and reduce the power delivered to the electrical load. Finally, a theoretical comparison between electrical and mechanical rectifier is presented. It is suggested that MMR is more desirable for low power/voltage application, as the diode conducting voltage significantly reduces amount of power flowing into the electrical load. Even though with the increasing excitation displacement, the diode voltage drop becomes less significant, the MMR based regenerative shock absorber still can offer more harvestable power according to the switching within the gear module. However, it is found that when the system is heavily electrical damped or under high frequency excitation, the implementation of MMR might lead the system performance even worse. When the regenerative shock absorber can no longer take advantages from the switching, the amount of additional friction and viscous damping within the MMR gear module causes more mechanical power losses in terms of electrical rectifier, a physical comparison will be experimentally addressed in Chapter 5.

Chapter 5 Experimental characteristic of regenerative shock absorber with MMR

Several motion rectified regenerative shock absorber prototypes have been developed and tested. Li [17] proposed a motion rectifier module attached to a rack-pinion type regenerative shock absorber. Road tests were conducted to demonstrate its feasibility in a vehicle suspension system. Zhang [22] developed a portable high-efficiency electromagnetic energy harvesting system with super capacitors and one-way clutch which converts the energy track vibrations into electrical power. Bench tests demonstrated its performance in a railroad application. Liu et al. [53] developed a motion rectified regenerative shock absorber by adopting a ball-screw mechanism. Due to the engagement and disengagement of the sprag-clutch within such a motion rectifier, the dynamics of the motion rectifier-based regenerative shock absorber was modelled as a piecewise linear system. Laboratory tests were also conducted to characterise the dynamic behaviour of the design.

This chapter mainly concerns the testing of a similar motion rectified regenerative shock absorber prototype. In order to physically study characteristics of MMR based regenerative shock absorber, a similar design prototype was developed and tested. A dynamic model of the proposed design was implemented, and parameter values were estimated from measured data. The model compares favourably with measurements which confirms that the model has the correct physical ingredients for the frequency range of interest. Variance in the load resistor is investigated as a way to influence engagement durations of the generator with the vibration source and hence energy harvesting performance. Moreover, according to the theoretical analysis of electrical rectifier in Chapter 4, it was found that the voltage drop across the diode unavoidably reduces the power transmitted to the electrical load. When the conducting voltage is significant comparing to the input voltage produced by the electromagnetic generator, MMR might be a better choice. Specifically, MMR potentially allows part of mechanical reactive power converting into useful electrical power instead of giving it back to the vibration source which enhances the system performance. However, when the diode voltage drop is negligible and system cannot take advantages from the switching, applying MMR in regenerative shock absorber might not be desirable, as it brings additional mechanical power losses and backlash effect in practice. Therefore, it is necessary to experimentally compare the performance between electrical and mechanical rectifier to give a more insight understanding which one is more suitable in different scenarios.

5.1 Mechanism of the design

The proposed MMR based regenerative shock absorber is shown in Figure 5-1. It is composed of four parts which are the lead-screw and nut, spring, motion rectifier gear module and the generator, which are assembled through shaft coupling. Two grips on each terminal of prototype are used to attach to the actuator and load cell of test machine respectively. When the device is subjected to a vertical excitation which leads one terminal to oscillate around its equilibrium point. The lead-screw and nut is able to convert the translational motion into bi-directional rotational motion, the bi-rotational rotational motion will become unidirectional via a motion rectifier module. The shaft of the motion rectifier is then connected to the inner race of a one-way clutch while the outer racer is coupled to a flywheel which drives the generator.

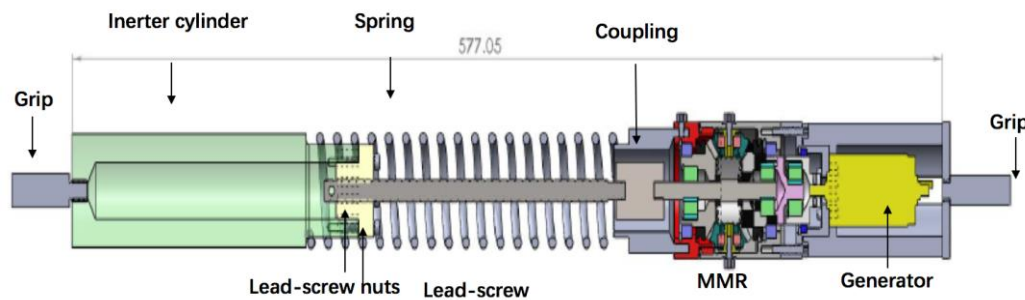


Figure 5-1: Final design of prototype

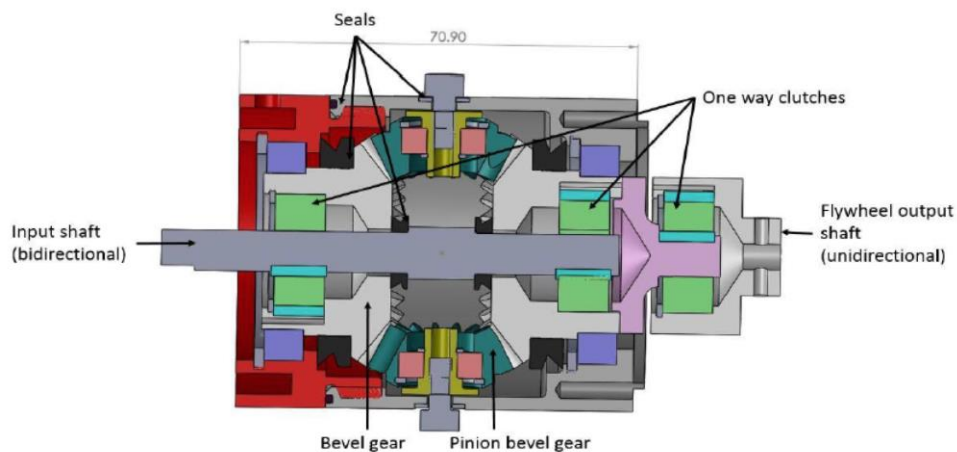


Figure 5-2: Motion rectifier module layout of principle components

Figure 5-2 shows the structure of the motion rectifier gear module, which is composed of a screw shaft with two sprag-clutches, two large and two small spiral bevel gears and bearings. Sprag-clutches are installed between input shaft and large bevel gear. The sprag-clutch only

transmits the torque in one direction and idly rotates in the other direction. Due to these two sprag-clutches, only one large bevel gear is engaged with the shaft and transmit torque while the other one is free-wheeling.

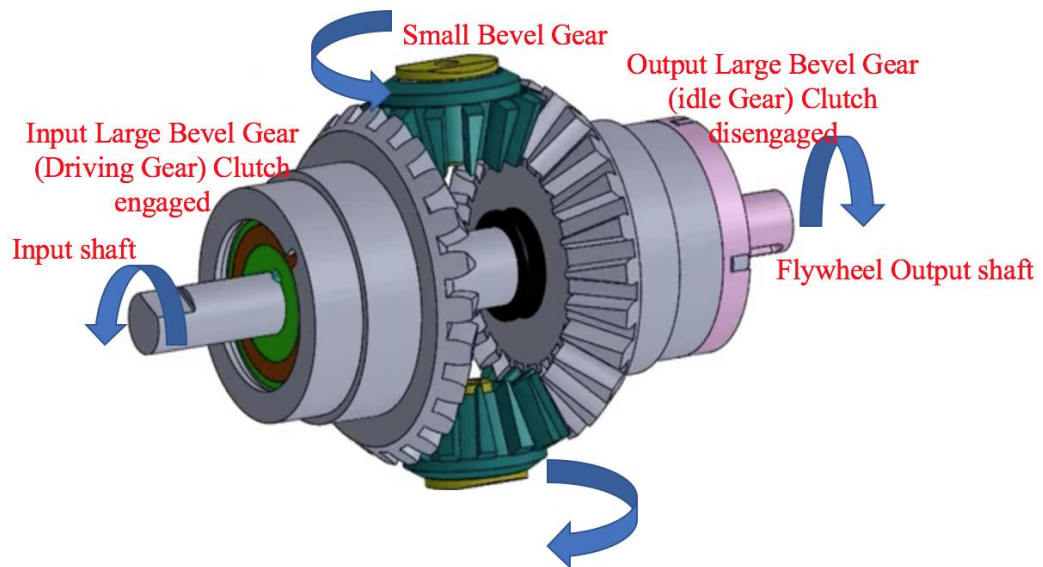


Figure 5-3: Counter-clockwise torque transmission path

According to Figure 5-3, if the lead screw and shaft rotate in counter-clockwise direction, the first large bevel gear is engaged to transmit torque via sprag-clutch. The small bevel gear rotates in the opposite direction and transmit torque to the output gear. The output gear will work as a bearing and always rotate in the same direction, irrespective of the input.

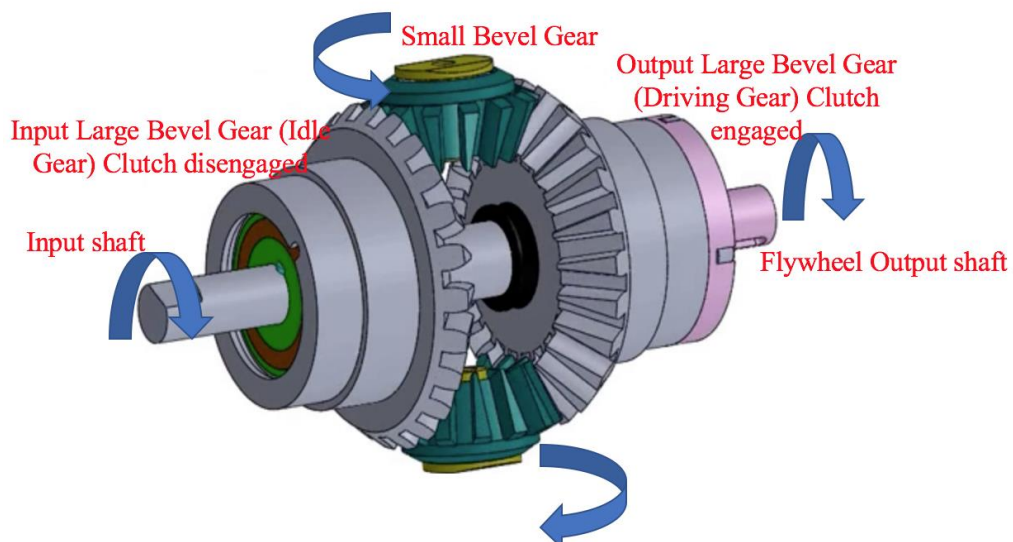


Figure 5-4: Clockwise torque transmission path

Similarly, the clockwise rotation of the shaft also drives the generator to rotate in clockwise direction, in which the previous input large bevel gear will disengage and work as a bearing. In Figure 5-4, the torque is directly transmitted to the output side via the shaft. Therefore, the motion-rectifier can convert the bi-directional rotation of the screw to the unidirectional rotation of the generator. In this way, the coupled generator always rotates in one direction regardless of upwards to downwards direction of the vibration input. Note that when neither terminal of design is blocked, the lead-screw and nut behave as an inerter since their rotation is proportional to relative acceleration across the terminals.

5.2 Experimental set up

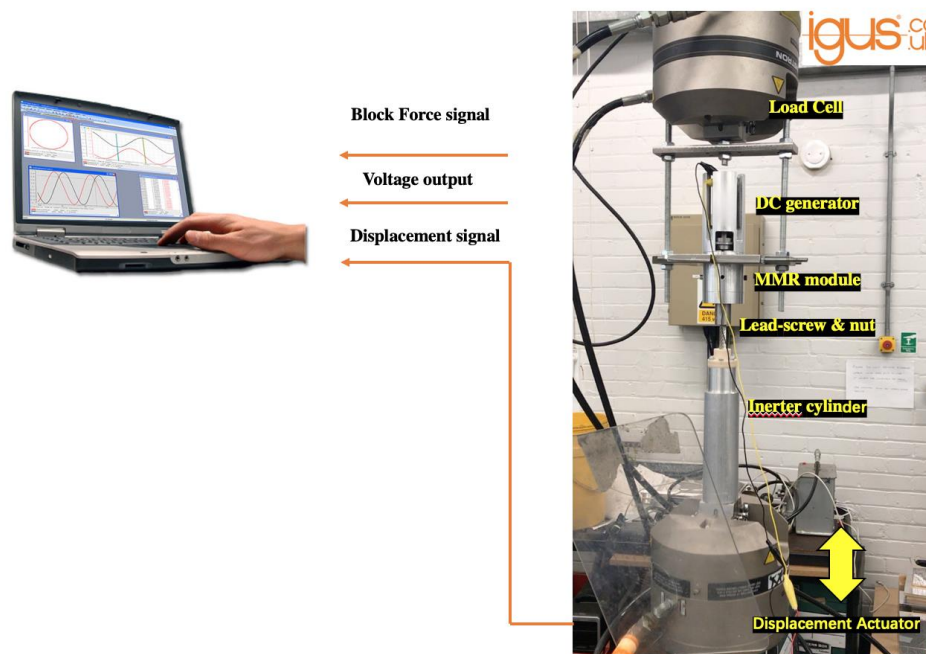


Figure 5-5: Schematic of the experimental set up of MMR based regenerative shock absorber

Figure 5-5 shows the schematic of the experimental set up for testing the proposed MMR based regenerative shock absorber. The testing platform is an actuator driven by a cyclic load provided by an Instron hydraulic test machine. The hydraulic actuator was controlled by Instron's WaveMatrix controller to create a relative movement between the machine frame and the piston rod. The inbuilt data acquisition system was used to record the input displacement and blocked force signals in real time. A rotary electrical generator was coupled to the output shaft of the motion rectifier in order to determine the energy harvesting performance as well as identifying periods of engagement and disengagement due to the

switching within the gear module. A simple electrical circuit was built which consists of a dc generator in series with a resistor. A Picoscope data acquisition system was used to record the output voltage signal across the load resistor.

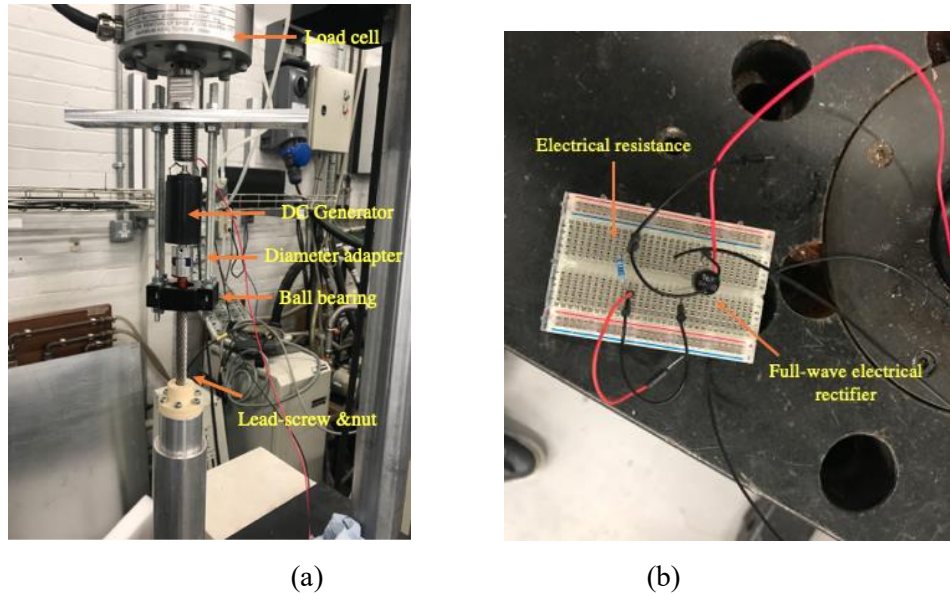


Figure 5-6: Experimental setup of electrical rectifier based regenerative shock absorber
(a)Test rig setup (b)Electrical circuit configuration

Moreover, in order to validate the analytical model and physically compare the performance between electrical and mechanical rectifier, prototype was also developed and tested in a hydraulic Instron machine as well. Figure 5-6(a) shows the test rig set up, a DC generator was directly coupled to the end of lead-screw shaft through the diameter-adapter. Figure 5-6 (b) describes the configuration of electrical circuit, where the full-wave bridge rectifier is purchased from Surge.

5.3 Testing results and discussion

In this section, testing results of regenerative shock absorber with MMR and electrical rectifier are presented. The discussion is conducted steps by steps. In Section 5.3.1, mechanical properties of MMR based regenerative shock absorber were investigated at different excitation frequencies. According to the curving fitting result (Fourier Series) from the blocked force measurement, a comparison between predicted and measured force was achieved, which allow to build and verify a physical model. Furthermore, the output voltage across the load resistance was measured in order to validate the piecewise linear model built in Chapter 3. By varying the value of load resistance, it is supposed to affect the engagement

and disengagement durations according to the theoretical analysis. In Section 5.3.2, the MMR gear module was removed from the design prototype, the lead-screw is directly coupled with the generator and the electrical rectifier. The main purpose of section 5.3.2 is to find out the additional inertance, viscous damper and friction which the MMR gear module potentially brings to the whole design. In the meantime, the experimental study is able to physically justify the usage of each rectifier and validate the hypothesis in Chapter 4.

5.3.1 Characteristics of MMR based regenerative shock absorber

First of all, preliminary tests are conducted to characterize the MMR based regenerative shock absorber prototype which allows to validate the dynamic model of the system. The proposed design was initially modelled in Chapter 3 which corresponding to the discussion here. One terminal of the prototype is put in the vertical actuator, while the other terminal is clamped by the fixture. Hence, the relative displacement between two terminals equals to the absolute input displacement from the actuator and the inerter behaves as mass in this case. Therefore, the design prototype ideally behaves as an inerter-spring-damper system. As the spring might shadow the nonlinearities within the design and the characteristic of the inerter, it was removed from the design.

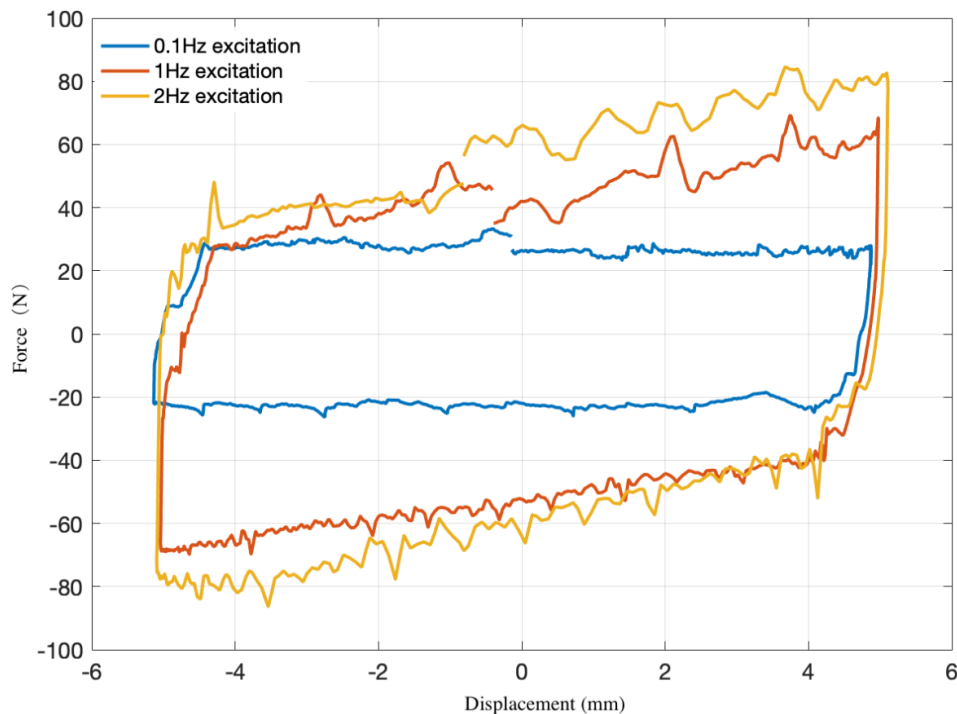


Figure 5-7: Force-displacement curves for 0.1-2Hz excitation frequencies, ± 5 mm sinusoidal excitation

Figure 5-7 shows a graph of the blocked force against displacement with amplitude $\pm 5\text{mm}$ under excitation frequencies ranging from 0.1Hz to 2Hz. As mentioned in the literature, the effects of viscous damping and inertance are negligible under lower frequency excitation, and the measured blocked force is dominated by coulomb friction. At higher frequencies, the gradient of the hysteresis curve steepens as the blocked force becomes dominated by the inertance. It can be observed from the blue curve (0.1 Hz) in Figure 5-7, the blocked force is almost a square wave with amplitude around 25N, implying a coulomb friction effect which only changes direction when the velocity changes sign. It should be noted the quality of measured curves in Figure 5-7 is very poor which comprised noise and discontinuities. The noise mainly comes from the Instron machine as the excitation displacement from the actuator is not perfect single harmonic waveform. Also, since the dynamics of load cell is far too large for the device (50N), which limits the accuracy of the force measurement.

Since the input displacement and blocked force are both periodical signals of known fundamental frequency, the system parameters can be determined from fundamental terms of a Fourier series. By curve fitting the data obtained at 2Hz, the equivalent viscous damping coefficient and inertance (a_1, b_1 terms of Fourier series model) were estimated to be 640Ns/m and 45.5kg respectively. By adopting these parameter values into a damper-inerter-coulomb friction model [5], where the estimated blocked force F_b can be expressed by

$$F_b = b\ddot{x} + c_v\dot{x} + f_c \text{sgn}(\dot{x}) \quad \text{eq (5-1)}$$

Where b and c_v is the equivalent inertance and viscous damper respectively, f_c is the coulomb friction damper. Thus, a comparison between predicted and measured blocked force is shown in Figure 5-8.

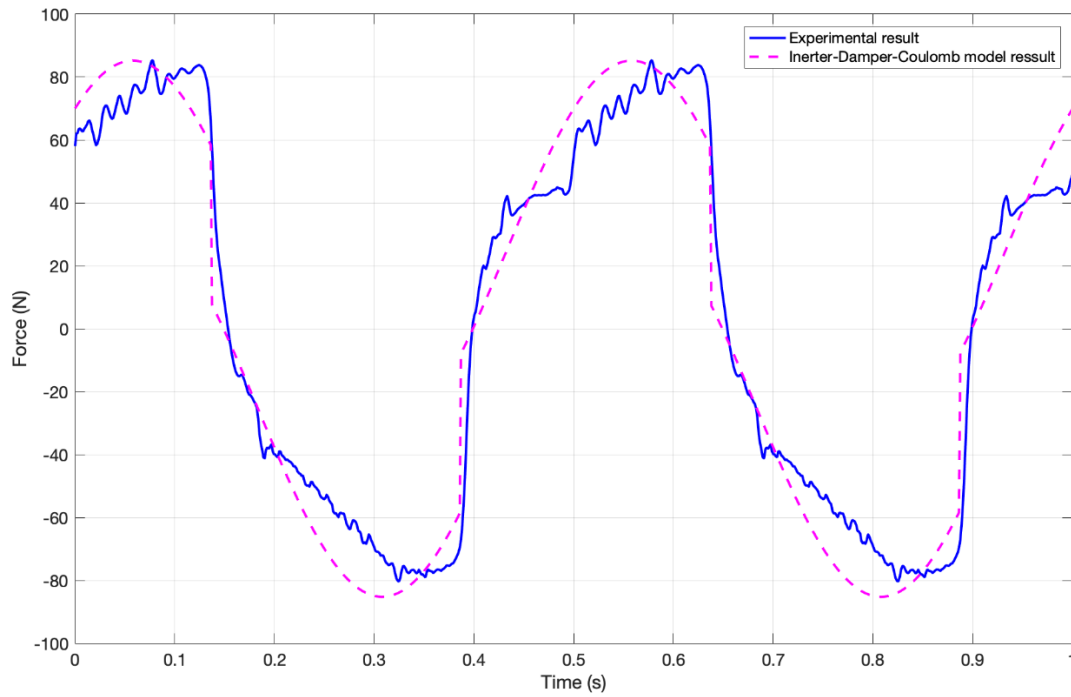


Figure 5-8: Measured and simulated blocked force of MMR based regenerative shock absorber at 2Hz, $\pm 5\text{mm}$ sinusoidal excitation

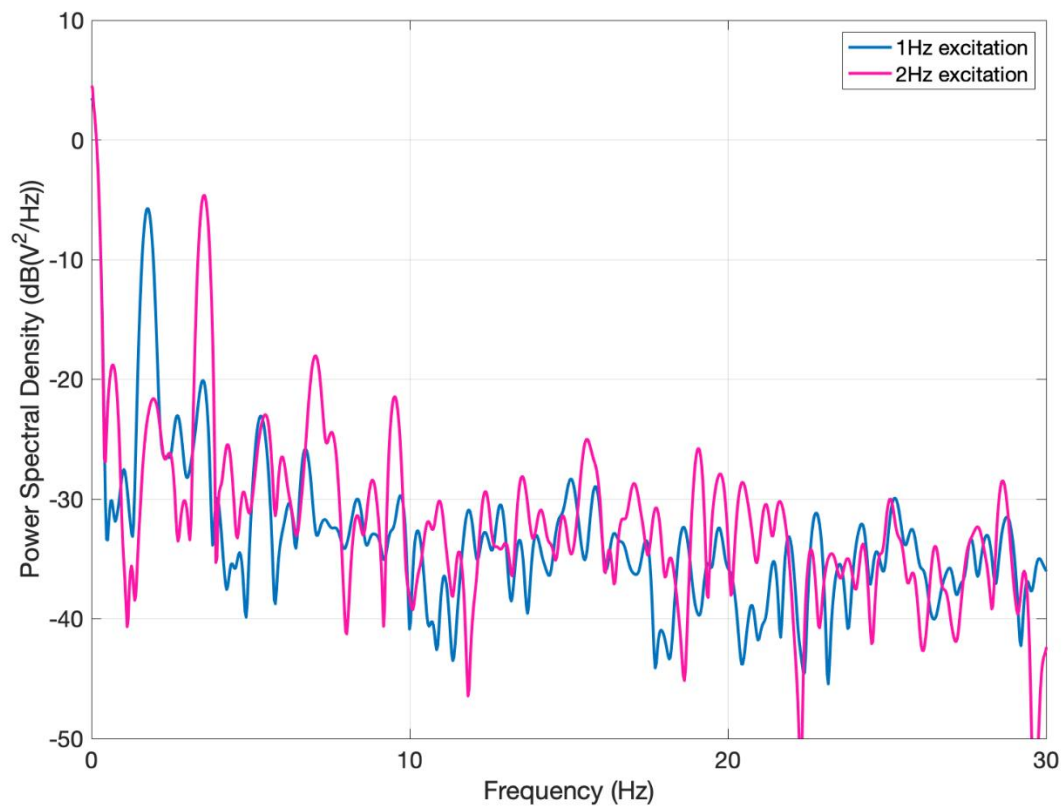


Figure 5-9: Power spectral density of the output voltage under 1.0Hz $\pm 10\text{mm}$ and 2.0Hz, $\pm 5\text{mm}$ excitation

Figure 5-9 shows the power spectral density (PSD) of the output voltage across the load resistance (100Ω) under $1\text{Hz } \pm 10\text{mm}$ and $2\text{Hz}, \pm 5\text{mm}$ excitation. It is desirable that the dc component contributes most to the PSD of the output voltage since this can be directly used for battery charging or other power electronic usage. The fundamental frequency of the output signal is observed to be double that of the input signal owing to motion rectification by the MMR gear module. Based on the result in Figure 5-9, the total regenerated power over a frequency range of 0Hz to 30Hz can be obtained by

$$P_v = \int_0^{30} \frac{S_v(f)}{R_L} df \quad \text{eq (5-2)}$$

For $1\text{Hz}, \pm 10\text{mm}$ excitation and load resistance equal to 100Ω , the dc to ac power ratio can be computed as 67%, while the corresponding average dc power in one cycle is around 3.64mW .

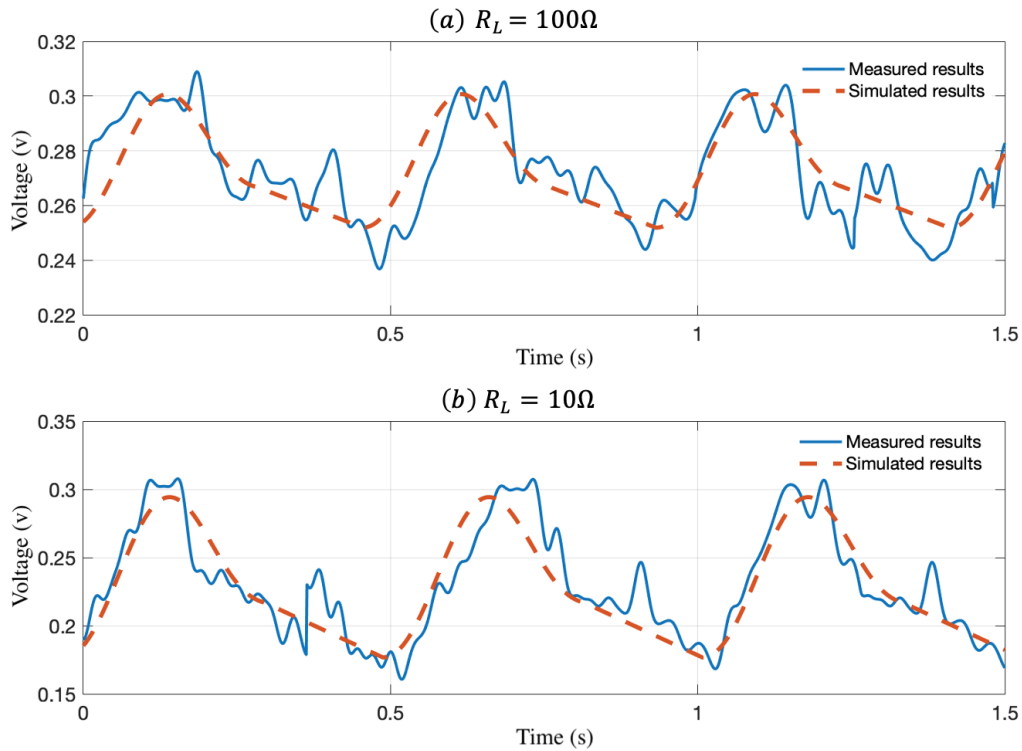


Figure 5-10: Measured and simulated voltage under $1\text{Hz}, \pm 10\text{mm}$ excitation ($R_{Load} = 10\Omega, 100\Omega$)

Figure 5-10 shows the comparison between the measured and simulated output voltages. The large dc offset illustrates that the proposed motion rectifier can provide a unidirectional rotary output speed for the generator. It is observed that the output voltage of the generator in half a cycle has an asymmetrical shape, and the positive slope is sharper than the negative slope. The latter occurs when the generator disengages from the vibration input through the sprag-

clutch. The generator transforms the residual kinetic energy stored by the shaft to the electrical energy which results in a slower deceleration. Note that for a 100Ω load resistance, the period of disengagement is around 0.33s which is shorter than the theoretical prediction (0.48s) for a half cycle. The main reason for the shorter disengagement period is the existence of viscous damper inside the generator, resulting in the stored kinetic energy being partially wasted as heat. From Figure 5-10, it can be seen that by adapting the load resistance to 10Ω , the disengagement duration is further reduced. According to the relationship between the resistance and electrical damping coefficient, reducing load resistance allows more current flowing through the circuit. Therefore, the adapted load consumes the stored kinetic energy faster, i.e., the rotary speed of generator shaft drops faster, which shortens disengagement duration. As a result, the primary system takes less time to catch up with the generator speed via the sprag-clutch. This implies that by varying the load resistance or the electrical damping enables to control the duration of engagement and disengagement. Selecting heavier electrical damping is more suitable for energy storage purposes while the system potentially takes less advantages from the MMR. Whereas the switching inside MMR offers lighter electrical damped system more continuous voltage and power. It might not be desirable for energy harvesting in terms of heavier electrical damped system, but it is beneficial for providing power supplementary for electronic device. It should be noted that the voltage signal in Figure 5-10 is quite noisy, the main reason might be according to the excitation waveform is closer to the threshold of Instron machine. The harmonic from the actuator might distort the shape of voltage signal. For this reason, Instron machine is not desirable for high frequency (velocity) excitation testing. Also, as the prototype is assembled through various mechanical adapters, the rig resonance or other dynamic nonlinearities i.e. backlash, cubic damping etc. might bring the harmonic distortions to the coupled generator as well.

5.3.2 Characteristics of electrical rectified regenerative shock absorber

After characterising the MMR based regenerative shock absorber, the next step is to experimentally study electrical rectified regenerative shock absorber with a focus on the output power and energy conversion efficiency. The dynamic of the electrical rectifier system was initially discussed in Chapter 4, it is shown that voltage drop across the diode causes major loss within the electrical domain. To validate this, it is necessary to experimentally quantify the loss. Moreover, a series of dynamic tests of proposed device at different excitation frequencies and amplitudes are conducted to investigate its mechanical properties. The comparison between the mechanical input power and electrical DC output power can

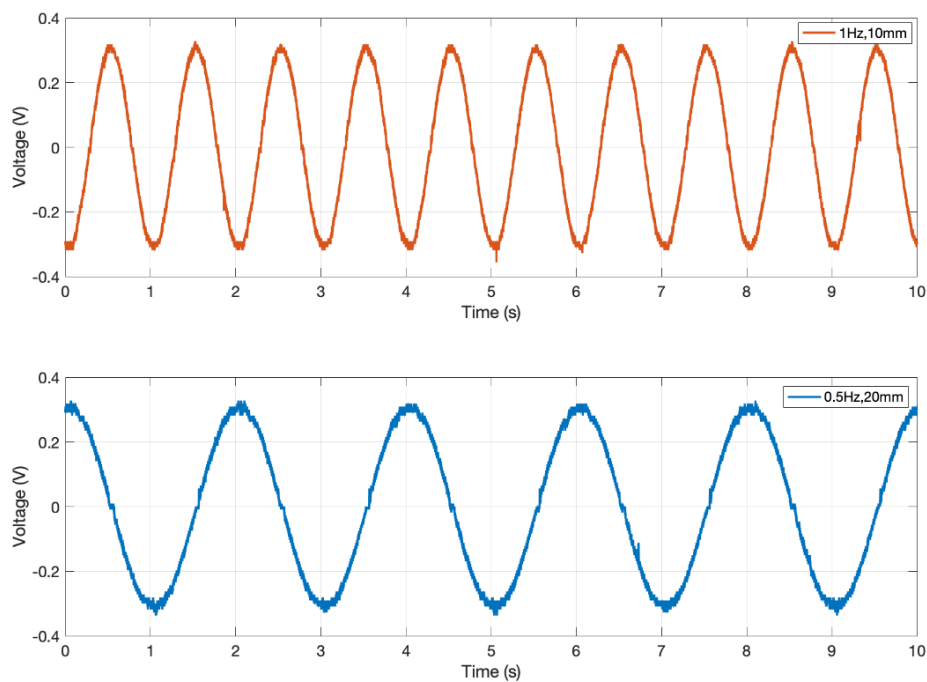
physically demonstrate the performance of electrical rectifier coupled regenerative shock absorber. Based on the testing result in Section 5.3.1, the discussion can be expanded to justify the usage of each rectifier.

Case 1: Open circuit

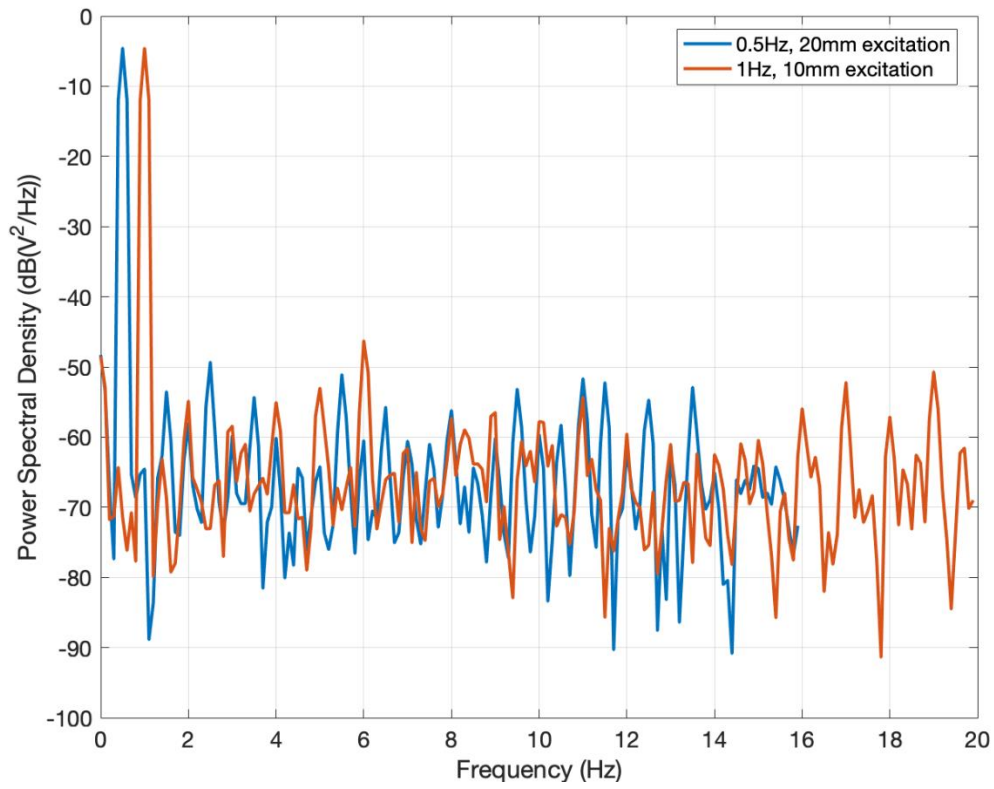
In order to clearly identify the consequence of employing electrical rectifier, the electrical circuit is initially open in Figure 5-6(b). The voltage across two terminals of the electromagnetic generator was directly measured in this case at different frequencies and amplitudes. Figure 5-11(a) shows the measured open circuit voltage when the sampling prototype was excited under $1\text{Hz}, \pm 10\text{mm}$ and $0.5\text{Hz}, \pm 20\text{mm}$ harmonic input. From both time and frequency domain analysis in Figure 5-11, the measured generated voltage is nearly linear and proportional to the driving angular speed $\dot{\theta}$

$$\dot{\theta} = \frac{2\pi}{l} \dot{x} \quad \text{eq (5-1)}$$

According to the data sheet, the lead-screw pitch l equals to 25mm. Based on the voltage measurement result in Figure 5-11(a) and the known translational excitation velocity, the back EMF constant of the electromagnetic generator k_e was estimated as $19.1\text{mV} \cdot \text{s/rad}$. Furthermore, by comparing the DC power across the generator internal resistance (0.00625mW) with the total electrical power dissipation without using electrical rectifier between 1 to 25Hz (0.1028W) according to Figure 5-11(b), the DC power conversion efficiency is nearly zero as majority is AC oscillations.



(a)



(b)

Figure 5-11: Open circuit voltage(a) Time domain results (b) Power Spectral Density

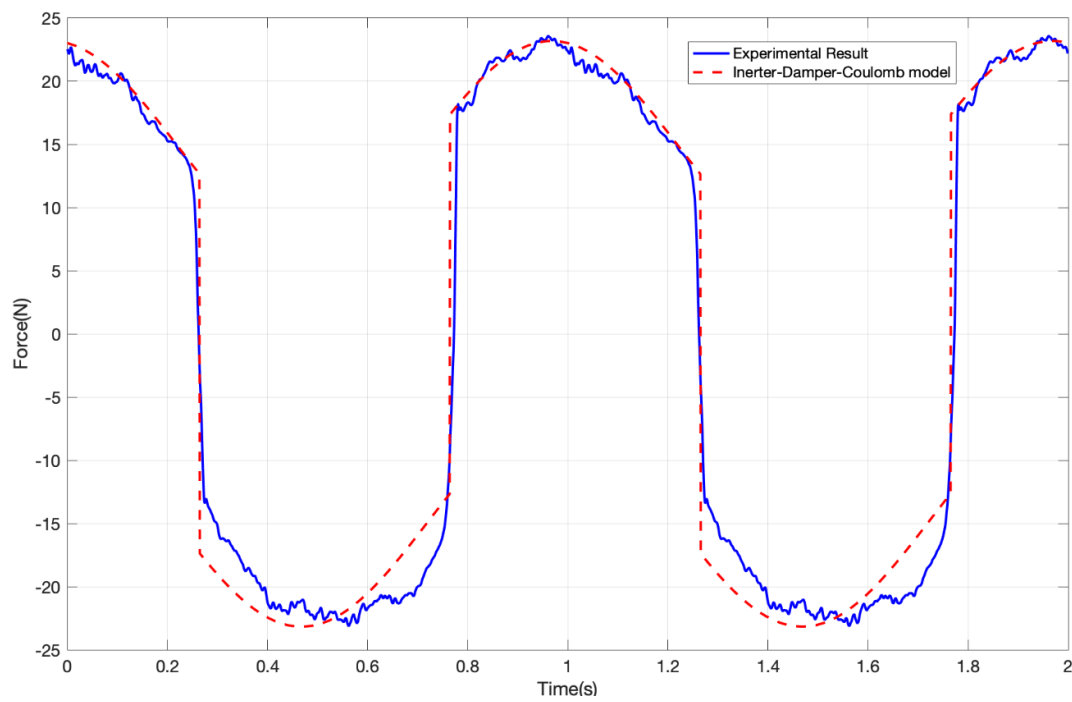
Figure 5-12: Measured and simulated blocked force of regenerative shock absorber without any rectifier at 1Hz, $\pm 10\text{mm}$ sinusoidal excitation

Figure 5-12 shows the experimental results of the blocked force excited at the frequency of 1Hz with displacement $\pm 10mm$. As the fundamental system parameters can be determined by applying Fourier series into the measured data, the amplitude of equivalent damping coefficient and inertance were estimated to be $205 N \cdot s/m$ and $7.2 kg$ respectively. The coulomb friction force can be identified by blocked force at zero velocity in Figure 5-12, which is approximately $17N$. By adopting these parameters in a damper-inerter-coulomb friction model, a comparison between simulated and measured waveforms was achieved in Figure 5-12.

Case 2: General electrical rectifier circuit with constant resistor

The next step of the experimental work is to connect the DC generator with an external load resistance through a full-wave electrical rectifier in Figure 5-6(a). The internal coil resistance is 1.63Ω , the voltage across the resistor with 10Ω and 100Ω were measured in this case. Due to the restriction of the testing bench and generator, the output voltage was not able to cover the conducting voltage through the rectifier ($1.2V$). As a result, no current flows through the electrical circuit which leads to zero harvestable electrical power.

Case 3: MATLAB Simulink

In case 3, the acquired voltage signal in case 1 was imported into a Simulink model of full-wave electrical circuit. It allows the user to numerically amplify the voltage signal in order to conduct the diode which can be ideally considered the same way as amplifying the displacement amplitude. In the meantime, the input mechanical power from the machine can be predicted by adopting equivalent system parameters from case 1 into the damper-inerter-coulomb friction model. In this the way, it was feasible to evaluate the performance of electrical rectified regenerative shock absorber without any technical restriction and it can give a more insight comparison with MMR.

Figure 5-13 shows the Simulink model of the full-wave electrical rectifier, the forward voltage for each diode is $0.6V$ and a 10Ω load resistance is chosen at output.

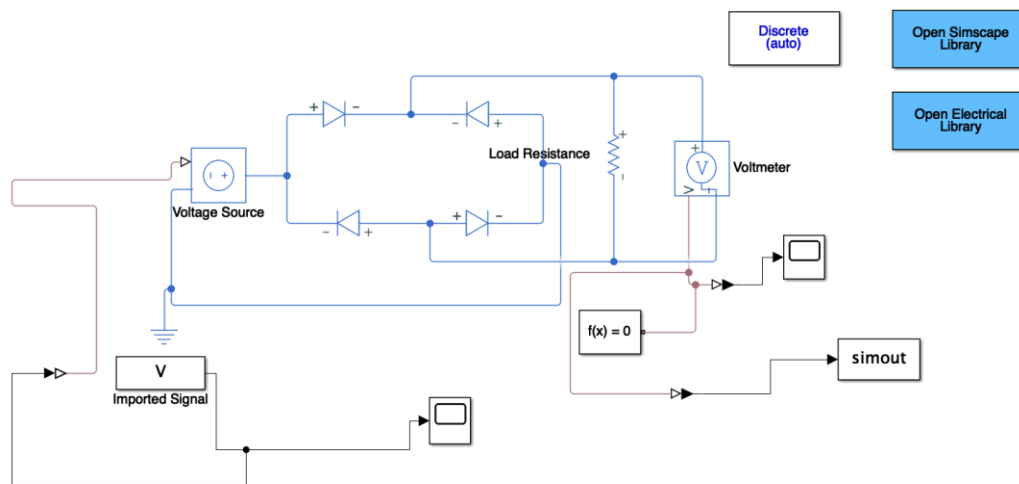


Figure 5-13: Simulink model of the full-wave electrical rectifier

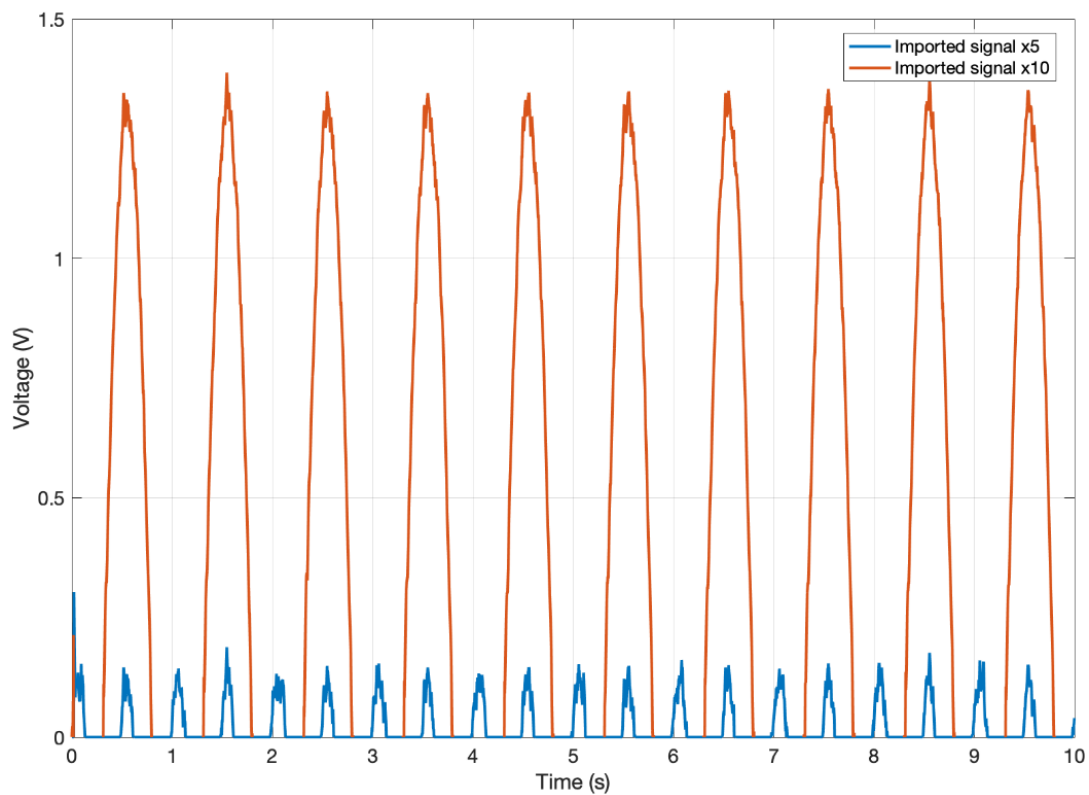
Figure 5-14: Simulated output voltage across the load resistance ($R_L = 10\Omega$)

Figure 5-14 shows a comparison between the output voltage across the load resistance in the time domain by amplifying the acquired experimental data (5&10 times). Due to the voltage drop across the diode, the output voltage of electrical rectifier transmitted to the load is discontinuous. It is clearly from the curve that conducting voltage causes; major loss within the electrical domain. For a peak voltage equals to 1.5V, the maximum amplitude of output is only 0.3V which significantly reduces the amount of power being harvested by the

load and the system efficiency as well. For an amplification factor of 5, the DC power (average power) over a cycle is only 1.4 mW with 21.5% DC to AC (RMS power) electrical power conversion efficiency. By looking at the result with amplification of 10, the DC power is 0.15W and the output DC to input AC power ratio is approximately 30.3%. Even though the result is much greater than the system without using electrical rectifier in case 1, but most of the useful power is still wasted on the diode conduction. As a result, electrical rectifier is not suitable for low power application, especially when diode voltage drop is significant.

5.4 Summary

In this chapter, experimental results of regenerative shock absorber with electrical and mechanical rectifiers are presented respectively. The primary intention of conducting experiment is to physically demonstrate the performance of proposed mechanical motion rectified regenerative shock absorber prototype, validate the dynamic model and justify the usage of each rectifier. It is seen that the blocked force of the proposed design is mainly influenced by coulomb friction at low frequencies and inertance at high frequencies. Comparing to the measured force, the damper-inerter-coulomb friction model gives a reasonable prediction of the behaviour, and this can be further used as a basis to determine optimum system parameters for different applications. Switching durations were estimated from periodic features of the voltage measurement curves. It can be observed that the shape of produced voltage is asymmetric due to the engagement and disengagement of the one-way clutch. It is seen that the disengagement period can be controlled by varying the electrical load resistance, while this can be further implemented in accordance with operating conditions. Moreover, the performance of regenerative shock absorber with electrical rectifier was physically quantified as well. It can be identified that the voltage drop across the diode significantly reduces the system efficiency especially for low power application. In this case, it is suggested to use mechanical motion rectifier to rectify the AC signal as it achieves fairly well electrical power conversion efficiency. However, the manufactured MMR gear module is found to have a coulomb friction around 8N, inertance 38 kg and mechanical damping coefficient 435Ns/m. According to the conclusion drawn in Chapter 4, when system can longer take advantages of switching within MMR and the diode conducting effect is negligible, i.e. high-power application. In this case, implementation of electrical rectifier in the regenerative shock absorber might be more desirable, as MMR gear module brings additional mechanical power loss.

Chapter 6 Analysis of regenerative shock absorber in quarter car model

A regenerative shock absorber with MMR can be modelled as a piecewise linear system, the secondary switchable generator coupled electrical system can be engaged and disengaged from the primary system according to the mechanism of sprag-clutch. In Chapter 3, it was demonstrated that the switching inside MMR is able to improve the amount of harvested electrical power over linear system despite the vibration source (Force & Velocity). However, the model developed in Chapter 3 refers to the experimental test in Chapter 5, where one terminal of the design is clamped. In the case of vehicle suspension system, the implementation of MMR based regenerative shock absorber on system dynamics still needs further investigation.

Primary intentions of this chapter can be split into two purposes: First, studying characteristics of vibration input when the linear regenerative shock absorber is installed in a road vehicle by using the mechanical impedance/mobility approach. It is initially unclear to assume the system is excited by force/velocity, as all parameters are frequency dependent which affects the dynamic behaviour of vibration source. The investigation can be extended to identify typical frequency where primary maximum power is delivered to the electrical damper. It is evident that primary resonance of harvestable power happens when system behaves as a velocity source. Moreover, the force source usually happens in higher frequency, while the regenerative shock absorber can only extract tiny amount of electrical power. As a result, the main focus of this study should be on velocity source. Second, the performance of employing regenerative shock absorber with MMR in vehicle suspension system is evaluated. Based on the result of vehicle vibration source characteristics, dynamics of implementing regenerative shock absorber with MMR in suspension system can be modelled and investigated. The result can be used to justify whether the implementation of MMR is able to improve both ride comfort and energy harvesting over non-switching linear system or it is a trade-off between these performances. Finally, a numerical study is conducted to determine the impact of each element on system dynamics.

6.1 Vehicle suspension model

First of all, the linear vehicle suspension system is investigated. Different from the model in Chapter 3 where one terminal of the design is blocked in Figure 6-1, the discussion here corresponds to a more physical system. A simplified quarter car model is shown in Figure 6-2 which consists of the wheel mass m_{us} , the tyre stiffness k_t , and the sprung mass of the vehicle body m_s . The suspension structure/isolator provides an equal and opposite force on the sprung and unsprung masses and it is assumed to have a massless passive mechanical impedance Z_I . The road input applies a displacement $x_o(t)$ to the vehicle wheel in the vertical direction as it is driven along the road.

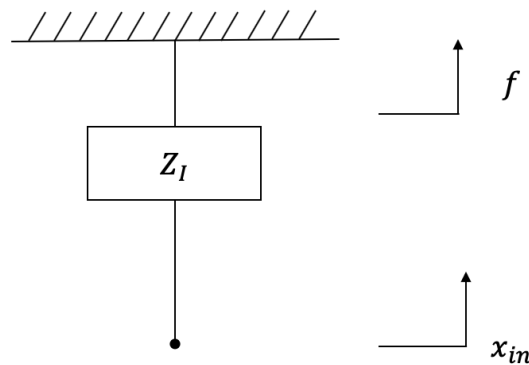


Figure 6-1: Schematic diagram of isolator (one terminal is clamped) excited by a velocity input

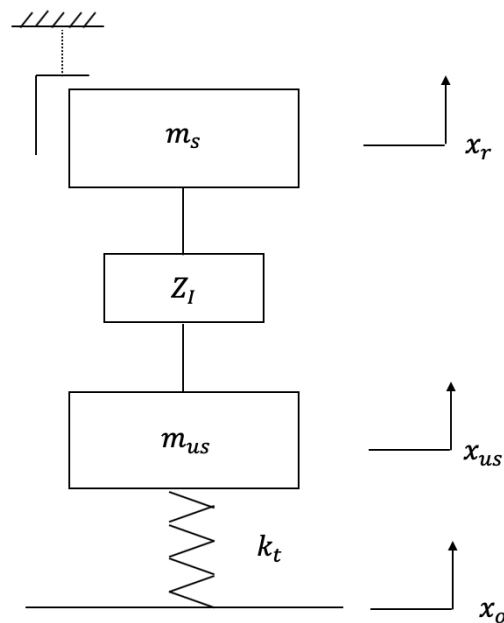


Figure 6-2: Quarter car suspension model

Governing equations of motion according to Figure 6-2 can be obtained as

$$m_s \ddot{x}_r = -Z_I(\dot{x}_r - \dot{x}_{us}) \quad \text{eq (6-1)}$$

$$m_{us} \ddot{x}_{us} = Z_I(\dot{x}_r - \dot{x}_{us}) + k_t(x_o - x_{us}) \quad \text{eq (6-2)}$$

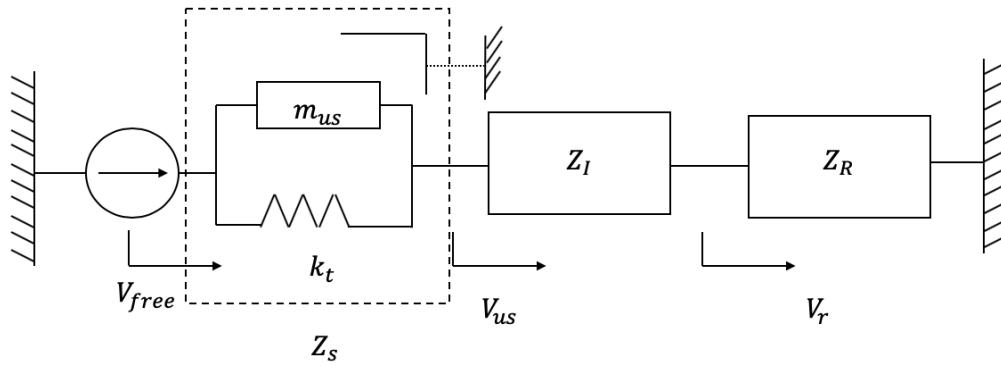
In linear mechanical system, it is straightforward to combine the lumped parameters to give a single impedance/mobility at a selected point. [115] Concepts of impedance/mobility are quite useful in discussing the dynamics of vibration system in the frequency domain, and it provides a convenient way to describe vibration source characteristics. Generally, the vibration isolation problem involves a source of vibration, a receiver and an isolator inserted between the source and receiver. The main function of isolator is to reduce the vibration transmitted to the receiver to acceptable levels. In the case of road vehicle, the vibrating source can be obtained as a free velocity \dot{x}_{free} in series with a source impedance Z_s which consists of unsprung mass and tyre stiffness. [Norton equivalent system] One terminal of vibration isolator Z_I is connected to the vibration source, while the other terminal is coupled to the sprung mass which is the receiver. The most commonly used measurement of isolator performance is the transmissibility between sprung mass and road input. When the isolator is considered as a regenerative shock absorber, the vibration isolation is not the only criterion to define whether it is good or not, the ability to develop maximum useful power to the electrical load is important as well.

6.2 Mobility/Impedance model of quarter car system

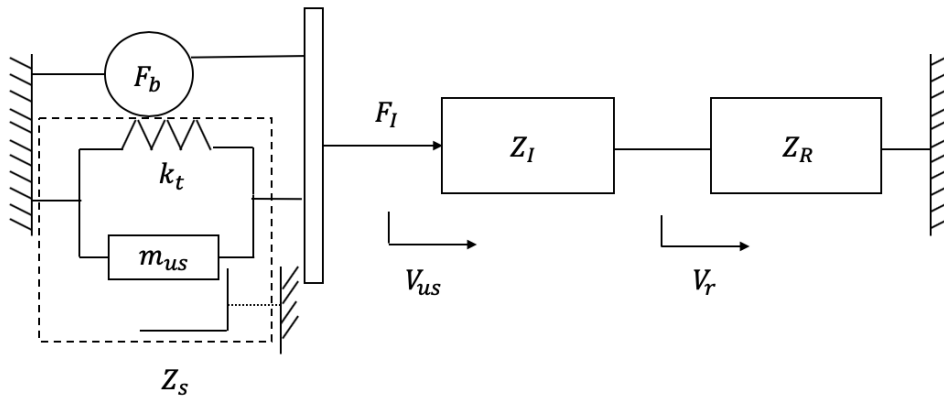
In this section, the 2dof quarter car suspension system is represented by a generic vibration system (source, isolator and receiver). By using mechanical impedance/mobility methods [112], characteristics of vibration source and receiver are investigated in different frequency ranges. The approach is then used to study dynamics of linear regenerative shock absorber in vehicle suspension system when the isolator is considered as an electrical-mechanical system. The intention of this section is to understand in which scenario the vibration source behaves as a velocity/force source and identify typical frequency where maximum power is delivered to the electrical damper. The result provides important references for investigating dynamics of implementing MMR in a quarter car suspension system.

6.2.1 Source characteristic of suspension system

In the frequency domain, the vibration source can either be represented by a blocked force F_b in parallel with source impedance Z_s (Thévenin equivalent source) or a free velocity V_{free} in series with source impedance Z_s (Norton equivalent source). The equivalent diagrams of quarter car model are shown in Figure 6-3. These source elements are in series connected to the isolator impedance, while the receiver (sprung mass) is on the other terminal.



(a) A Norton equivalent system



(b) A Thévenin equivalent system

Figure 6-3: Quarter-car equivalent diagrams (a) Norton equivalent system (b) Thévenin equivalent system

The relationship between the blocked force, source free velocity and the source impedance is given by

$$F_b = Z_s V_{free} \quad \text{eq (6-3)}$$

Either Thévenin or Norton equivalent system can be used to represent the vibration source by using the relationship in eq(6-3). According to the literature [115], characteristics of the vibration source may affect the isolator performance and thus influence the choice of an optimum isolator.

For a blocked vibration source in Figure 6-3(b), the source output velocity V_{us} can be obtained by

$$V_{us} = V_{free} - \frac{F_I}{Z_s} \quad \text{eq (6-4)}$$

F_I is the applied force from the vibration source through the massless isolator to the receiver in Figure 6-3(b) can be obtained by

$$F_I = Z_I(V_{us} - V_r) \quad \text{eq (6-5)}$$

Where F_I can also be solved in terms of blocked receiver according to Figure 6-3(b)

$$F_I = Z_r V_r \quad \text{eq (6-6)}$$

The ratio between output velocity and free velocity of the source can then be obtained by substituting eq(6-5) and eq(6-6) into eq(6-4)

$$\frac{V_{us}}{V_{free}} = \frac{1}{1 + \frac{Z_I Z_R}{(Z_I + Z_R) Z_s}} \quad \text{eq (6-7)}$$

The load impedance is defined by

$$Z_{Load} = Z_I + Z_R \quad \text{eq (6-8)}$$

The form of eq (6-7) can be alternatively rewritten in terms of mobility given by $Y = V/F$

$$\frac{V_{us}}{V_{free}} = \frac{1}{1 + \frac{Y_s}{Y_R + Y_I}} \quad \text{eq (6-9)}$$

Similarly, the ratio between the isolator force F_I and blocked force F_b can be obtained by applying eq (6-3), eq (6-5) and eq (6-6) into eq (6-4)

$$\frac{F_I}{F_b} = \frac{1}{1 + \frac{(Z_I + Z_R) Z_s}{Z_I Z_R}} \quad \text{eq (6-10)}$$

Where it can be also expressed in terms of mobility

$$F_I = \frac{F_b}{1 + \frac{Y_R + Y_I}{Y_s}} \quad \text{eq (6-11)}$$

From eq (6-9) and eq (6-11), it is clear that the vibration source produces output velocity V_{us} and force F_I to the isolator and receiver depending on the relative mobility of source, isolator and receiver. It was also found that the receiver acting in parallel with isolator according to eq (6-7) and eq (6-10), also referred as the load. As the receiver for a quarter car model is just sprung mass itself, then the load (isolator and receiver) effectively acting as a vibration absorber above source. Moreover, the characteristic of vibration source is determined upon the ratio between load mobility $Y_R + Y_I$ and source mobility Y_s , while all these elements are

frequency dependent. In order to study the quarter-car suspension dynamics, typical parameters of road vehicles in Table 6-1 are evaluated within the model.

	$m_s(\text{kg})$	$m_{us}(\text{kg})$	$k_s(\text{kN/m})$	$k_t(\text{kN/m})$	$c(\text{Ns/m})$
Passenger car	240	36	16	160	980

Table 6-1: Road vehicle parameters [135, 136]

A simple suspension/isolator system is introduced as a parallel arrangement of spring-damper-inerter system in Figure 6-4, where its mechanical mobility is formed by

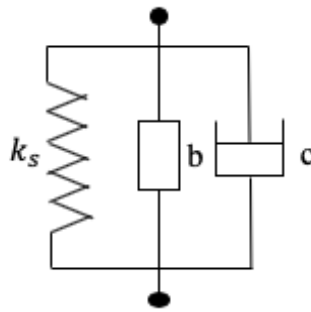


Figure 6-4: Isolator layout

$$Y_I = \frac{j\omega}{k_s} + c + \frac{1}{bj\omega} \quad \text{eq (6-12)}$$

Combining lumped parameter elements according to Figure 6-2, the source and receiver mobility can be obtained by

$$Y_S = \frac{j\omega}{k_t} + \frac{1}{j\omega m_{us}} \quad \text{eq (6-13)}$$

$$Y_R = \frac{1}{j\omega m_s} \quad \text{eq (6-14)}$$

Assuming the value of inertance b in eq (6-12) equals to 500kg and employing the quarter car parameters from Table 6-1, Figure 6-5 shows the vibration source characteristics of vehicle suspension system. Referring to eq (6-11), when the source mobility is much greater than the load mobility ($|Y_S| \gg |Y_R + Y_I|$), then the force applied to the isolator equals to the blocked force ($F_I \approx F_b$). For an undamped system ($c = 0$), when the system is excited at load natural frequency ($IM(Y_R + Y_I) = 0$) or the source natural frequency at 10Hz ($|Y_S| \rightarrow \infty$), the isolator force tends to equal to the blocked force in Figure 6-5 (a) and (c). In this case, the vibration source behaves as a force source, which means the force applied to the isolator is insensitive to the dynamic behaviour of the load (isolator and receiver). [115]

Whereas, if the source mobility is much less than load mobility ($|Y_R + Y_I| \gg |Y_S|$) in eq (6-9), then the free velocity of the unsprung mass equals to its output velocity ($V_{free} \approx V_{us}$). For an undamped system ($c = 0$), this happens when the driving frequency is below the load natural frequency ($|Y_S| \approx 0$) or around isolator natural frequency at 0.9Hz ($|Y_I| \rightarrow \infty$) shown in Figure 6-5 (a) and (b). In this case, the vibration source behaves as a velocity source, which means the free velocity to the isolator is insensitive to the dynamic behaviour of the load. [115]

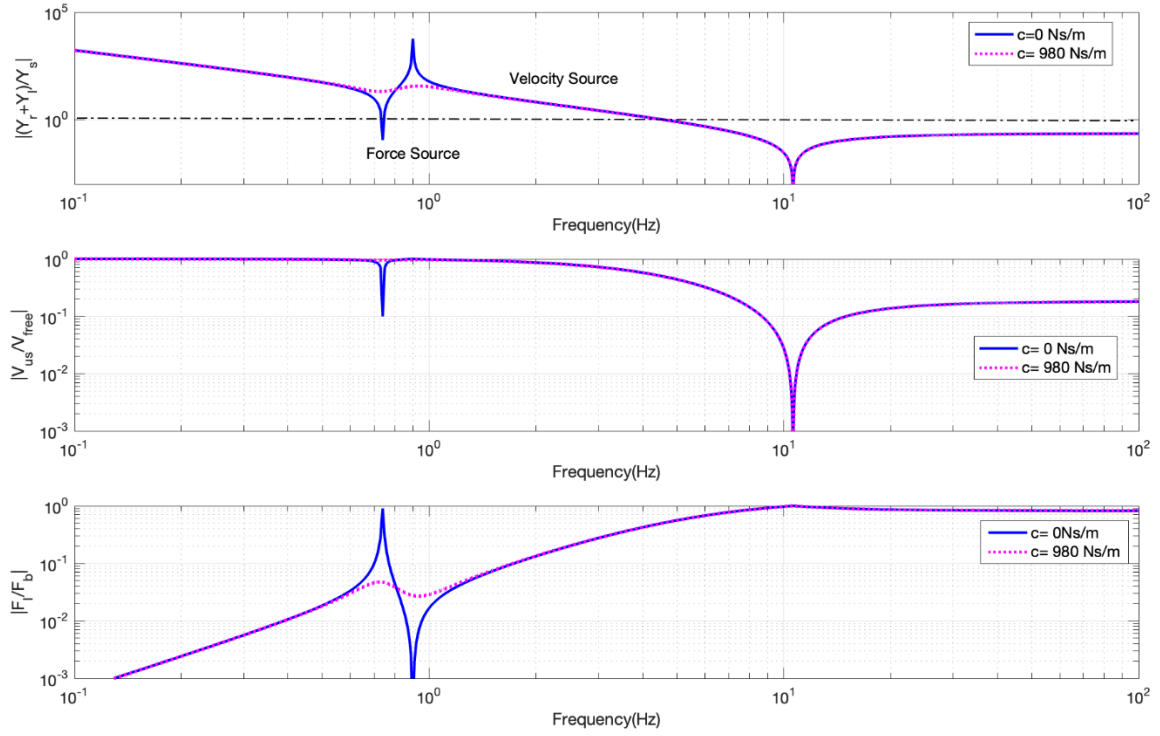


Figure 6-5: Source Characteristic (a) $|Y_R + Y_I|/Y_S$ (b) $|V_{us}/V_{free}|$ (c) $|F_I/F_b|$

It should be noted that the source mobility is really small in low frequency region ($|Y_S| \approx 0$), e.g. source is massive. For a damped system, the load/vibration absorber effect is slight in practise at its natural frequency ($IM(Y_R + Y_I) = 0$), because $|Y_R + Y_I|$ becomes small but not zero, due to damping. As a result, the anti-peaks at $IM(Y_R + Y_I) = 0$ disappears in Figure 6-5 (a), where the vibration source behaves as velocity source at corresponding frequency 0.7 Hz in Figure 6-5 (b).

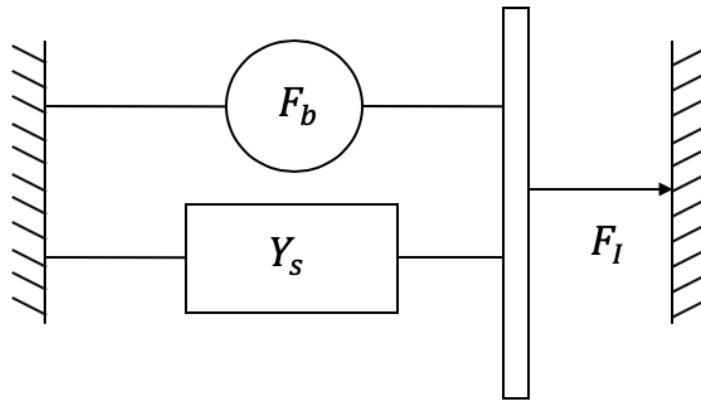
To sum up, for a damped system, the vibration source behaves as a velocity source at “lower frequency” ($f < 5\text{Hz}$) according to Figure 6-5, while it starts to behave as force source at “higher frequency” ($f > 5\text{Hz}$).

Two equivalent representations of vibration sources are sketched in Figure 6-6, while the vibration source can be identified by

$$F_I = F_b|_{V_{us} \approx 0} \quad \text{eq (6-15)}$$

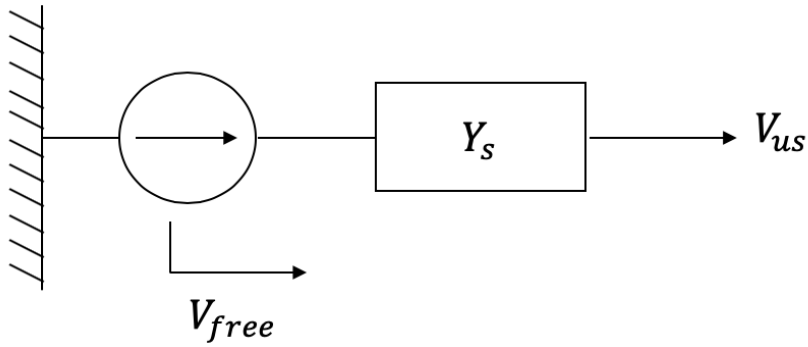
$$V_{free} = V_{us}|_{F_I \approx 0}$$

eq (6-16)



$$V_{us} \approx 0$$

(a) Force source



(b) Velocity source

Figure 6-6: Two equivalent representations of vibration source (a)Force source (b)Velocity source

For an infinite source mobility $|Y_s| \rightarrow \infty$ or $|Y_R + Y_I| \approx 0$ (undamped, otherwise velocity source), the vibration source behaves as a force source and the force applied to the isolator F_I equals to the blocked force F_b ; for $|Y_R + Y_I| \rightarrow \infty$ or $|Y_s| \approx 0$, the vibration source behaves as a velocity source and the free velocity V_{free} equals to the output velocity of source V_{us} .

6.2.2 Vibration isolation

For a vehicle suspension system, the main role of isolator is to reduce the vibration transmitted to the vehicle body. By substituting eq (6-6) and eq (6-19) into eq (6-5), the transmissibility between receiver and source free velocity can be written as

$$\left| \frac{V_r}{V_{free}} \right| = \left| \frac{1}{1 + \frac{Y_s + Y_I}{Y_R}} \right| \quad \text{eq (6-17)}$$

The free velocity of the source (no isolator and sprung mass) V_{free} equals to its output velocity (with isolator and sprung mass) V_{us} by assuming $m_s = 0, Z_I = 0$ in eq (6-1) and eq (6-2) respectively, which results

$$V_{free} = \frac{k_t}{k_t - \omega^2 m_{us}} V_o \quad \text{eq (6-18)}$$

The transmissibility between the free velocity of unsprung mass (source) and road input can then be expressed by

$$T = \left| \frac{V_{free}}{V_o} \right| = \left| \frac{k_t}{k_t - \omega^2 m_{us}} \right| \quad \text{eq (6-19)}$$

Substituting eq (6-19) into eq (6-17), the transmissibility between the receiver and road velocity can be formed as

$$\left| \frac{V_r}{V_o} \right| = \left| \frac{T}{1 + \frac{Y_s + Y_I}{Y_R}} \right| \quad \text{eq (6-20)}$$

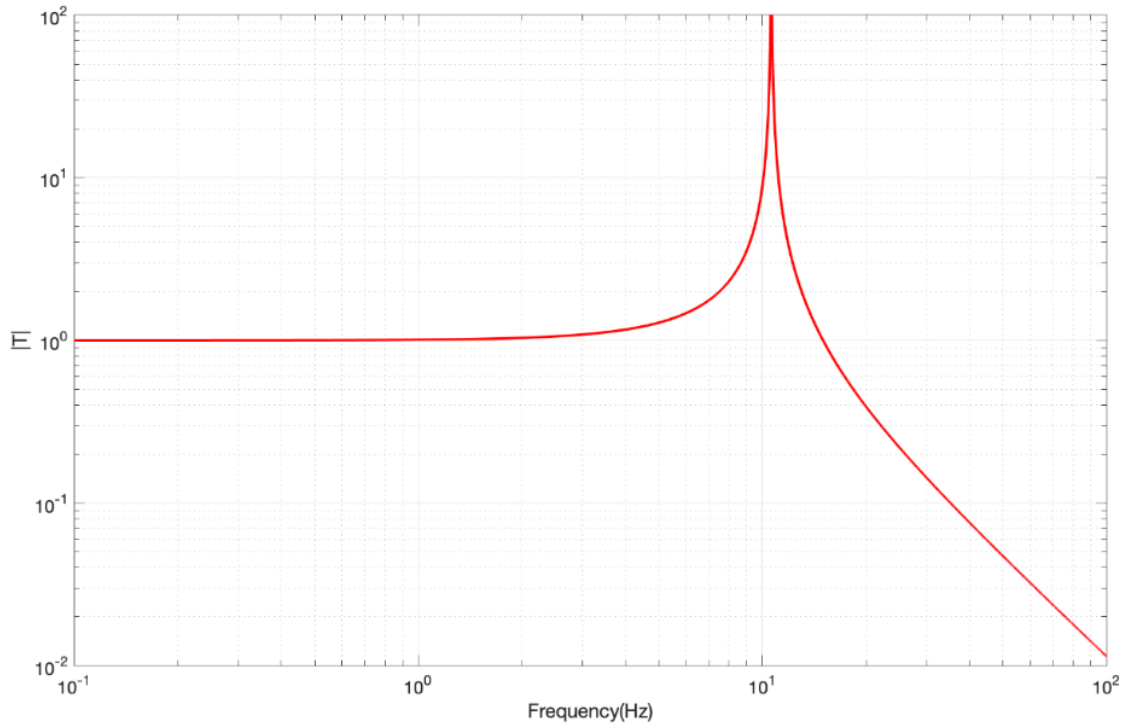
It is apparent from eq (6-20) that the vibration transmissibility between sprung mass (receiver) and road input depends upon $|T|$ as well as mobility ratio between $|Y_s + Y_I|$ and $|Y_R|$.

The transmissibility between free velocity of unsprung mass and road input $|T|$ is determined by the tyre stiffness and the unsprung mass. By varying the excitation frequency

$$|T| \approx 1, \quad \omega \ll \sqrt{k_t/m_{us}} \quad \text{eq (6-21)}$$

$$|T| \approx \frac{k_t}{m_{us}\omega^2}, \quad \omega \gg \sqrt{k_t/m_{us}} \quad \text{eq (6-22)}$$

Figure 6-7 shows the dynamics of transmissibility $|T|$, it is clearly that the amplitude of $|T|$ tends to be 1 below 3Hz. It starts increasing until the source natural frequency (10Hz), while its value decreases with a rate of ω^{-2} afterwards.

Figure 6-7: Characteristic of transmissibility $|T|$

For a good vibration isolation performance, the sum of source and isolator mobility should be much greater than the receiver mobility ($|Y_s + Y_I| \gg |Y_R|$) in order to reduce the vibration transmitted to the receiver according to eq (6-20). It happens when the sum of source and isolator mobility tends to be infinite ($|Y_s + Y_I| \rightarrow \infty$) or the receiver mobility tends to zero ($|Y_R| \approx 0$).

Figure 6-8 (a) simulates the mobility ratio between $(Y_s + Y_I)$ and receiver Y_R by varying the excitation frequency. Considering the conventional spring-damper isolator system ($b=0$), the mobility ratio $|\frac{Y_s + Y_I}{Y_R}|$ increases along with the excitation frequency shown in Figure 6-8 (a).

Meanwhile, the amplitude of free vibration transmissibility $|T|$ decreases with a rate of ω^{-2} above the source natural frequency 10 Hz ($|Y_s| \rightarrow \infty$). Therefore, the higher of excitation frequency, the better isolation performance can be achieved.

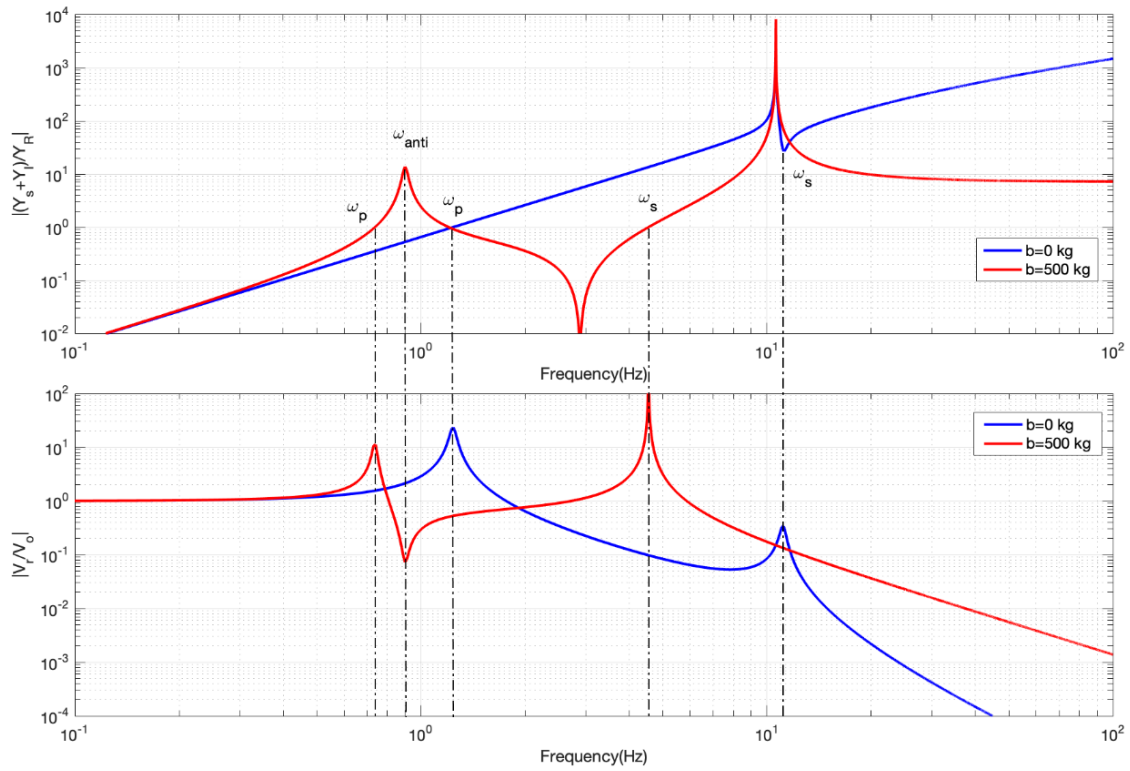


Figure 6-8:(a) Mobility ratio amplitude ($|Y_s + Y_I|/|Y_R|$) (b) Transmissibility between sprung mass and road ($|V_r/V_o|$)

In terms of conventional spring-damper isolator, adding inerter introduces an upward on the mobility ratio between $|Y_s + Y_I|$ and $|Y_R|$ at 0.9Hz in Figure 6-8(a), as it corresponds to the isolator natural frequency ($|Y_I| \rightarrow \infty$). A minimum transmissibility can be found at the same frequency in Figure 6-8(b) which suggests the appearance of anti-resonance. As the excitation frequency around the anti-resonance frequency, there is a significant improvement of the vibration isolating performance with the inerter, the closer to the anti-resonance frequency, the better isolation performance system can gain. By increasing the value of inertance, the peak value of isolator mobility is shifted to lower frequency range. This is desirable as the isolation band becomes wider.

Two local peaks can be found in Figure 6-8 (b) when the denominator of eq (6-20) is minimised, while each peak behaves differently with inerter. It attenuates the primary resonance of vibration transmissibility at 0.7Hz, while the secondary resonance at 4.5Hz is increased in contrast. The corresponded resonance frequency can be obtained by solving

$$IM(1 + \frac{Y_s + Y_I}{Y_R}) = 0 \quad \text{eq (6-23)}$$

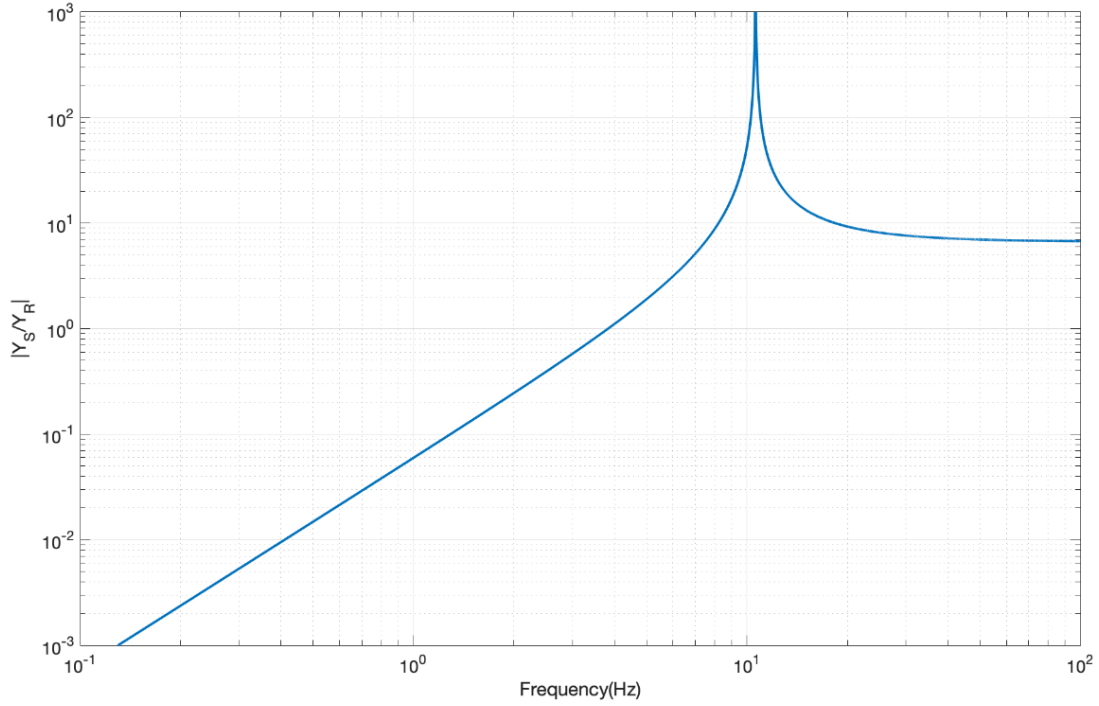
Figure 6-9: Relative mobility $|Y_S/Y_R|$

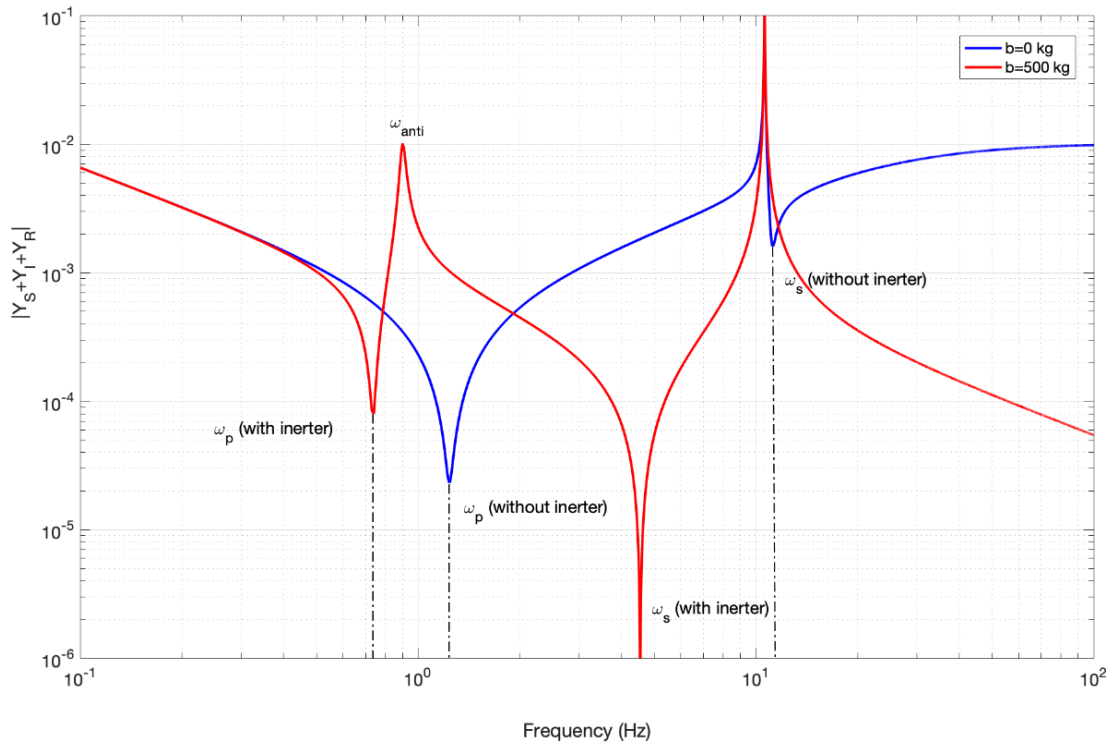
Figure 6-9 shows the relative mobility between source and receiver $|Y_S/Y_R|$. It can be observed from the curve that the source mobility is negligible compared to receiver below 1Hz where $|Y_S/Y_R| \approx 0$. In this case, eq (6-20) can be simplified by

$$\left| \frac{V_r}{V_o} \right| \approx \left| \frac{T}{1 + Y_R} \right| \quad \text{eq (6-24)}$$

The primary resonance can be identified in Figure 6-8 when $IM(Y_R + Y_I) = 0$ at 0.7Hz which corresponds to the primary undamped natural frequency ω_p

$$\omega_p = \sqrt{\frac{k_s}{m_s + b}} \quad \text{eq (6-25)}$$

It is clearly from eq (6-25) that inerter shifts the primary natural frequency ω_p to lower region. Since the denominator of eq (6-25) is minimised, the amplitude of primary resonance is determined by $|T|$. It is evident from eq (6-19) that its amplitude decreases by lowering the excitation frequency below source natural frequency according to Figure 6-7. As a result, the added inertance shifts the natural frequency to lower value which attenuates the primary resonance value in Figure 6-8(b).

Figure 6-10: Characteristics of $|Y_s + Y_l + Y_R|$

The secondary resonance frequency ω_s can be obtained by solving $IM(Y_s + Y_l + Y_R) = 0$ in eq (6-23). Figure 6-10 simulates the amplitude of $|Y_s + Y_l + Y_R|$ in different frequency band. It is evident from the curve that adding inverter shifts the secondary undamped natural frequency to lower value as well. In a similar way of primary natural frequency, the secondary peak value of transmissibility is determined by $|T|$. As stated earlier, the amplitude of $|T|$ decreases with a rate of ω^{-2} above source natural frequency (10Hz). By shifting the secondary resonance frequency of non-inverter isolator (11.2Hz) to lower region with inverter, the secondary peak of vibration transmissibility $\left|\frac{V_r}{V_o}\right|$ becomes larger.

As the excitation frequency continues to climb, the sum of source and isolator mobility eventually becomes much greater than the receiver ($|Y_s + Y_l| \gg |Y_R|$) according to Figure 6-8(a), the transmissibility between receiver and road input will be

$$\lim_{\omega \rightarrow \infty} \left|\frac{V_r}{V_o}\right| \approx 0 \quad \text{eq (6-26)}$$

It can be observed from Figure 6-8(b) that the amplitude of vibration transmissibility of inverter based isolator decreases with a rate of ω^{-2} while the non-inverter isolator decreases with ω^{-4} . This confirms the conclusion drawn in the literature [137], inverter is undesirable for vibration isolation performance at higher frequency region.

6.2.3 Energy harvesting analysis

When the isolator is considered as a regenerative shock absorber which consists electrical damper c_e , the power harvested by electrical damper is proportional to the relative velocity between the sprung and unsprung mass. The velocity of the unsprung mass can be solved in terms of the receiver (sprung mass) velocity according to eq (6-5) and eq (6-6)

$$V_{us} = (1 + \frac{Y_I}{Y_R})V_r \quad \text{eq (6-27)}$$

Substituting eq (6-18) and eq (6-27) into eq (6-20), the relative velocity between the sprung and unsprung masses can be expressed as

$$V_{us} - V_r = \frac{T}{1 + \frac{Y_R + Y_S}{Y_I}} V_o \quad \text{eq (6-28)}$$

The electrical damping force is

$$F_e = c_e(V_{us} - V_r) \quad \text{eq (6-29)}$$

For a given harmonic road profile V , the average electrical power can be obtained by

$$P_e = F_e(V_{us} - V_r)^* = \frac{1}{2} c_e V^2 \left| \frac{T^2}{(1 + \frac{Y_R + Y_S}{Y_I})^2} \right| \quad \text{eq (6-30)}$$

Where * denotes the complex conjugate.

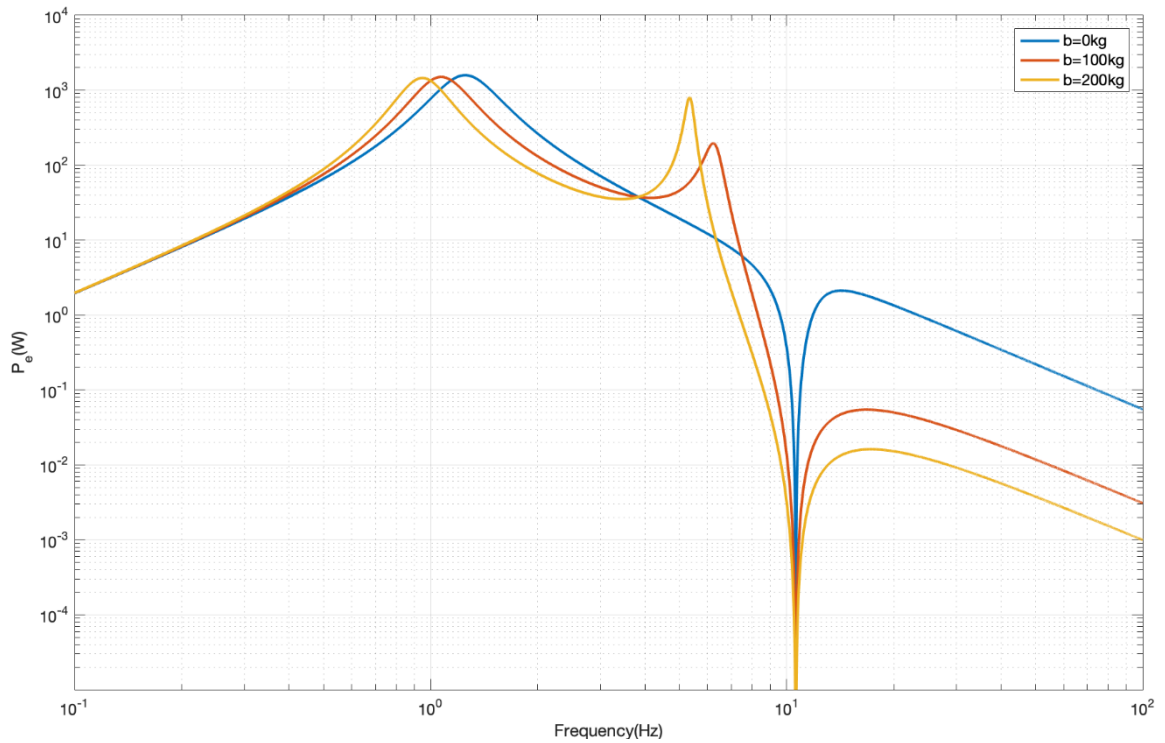


Figure 6-11: Average harvestable electrical power generation in different excitation frequencies

From eq (6-30), it is clearly that the generated electrical power is dependent upon the transmissibility T , mobility of isolator Y_I , receiver Y_R and source Y_S . By assuming V is constant in the frequency domain with an amplitude equals to 1 m/s , Figure 6-11 shows the simulation result of the average electrical power generation under different excitation frequencies. There are few extreme cases that may occur in practice at particular frequencies. Maximum electrical power can be found when the denominator of eq (6-30) is minimised. According to the discussion in the Section 6.2.2, the source mobility is negligible ($Y_S \approx 0$) compared to other terms below 1Hz. The primary resonance is found when the system is excited at load undamped natural frequency $\omega_p = \sqrt{\frac{k_s}{m_s+b}}$ ($IM(Y_I + Y_R) = 0$). Due to the existence of inerter b , the primary natural frequency is shifted to lower frequency region. Meanwhile, it can be identified from Figure 6-11 that inerter attenuates the amplitude of primary peak harvestable power. The main reason can be explained similarly to the primary resonance of vibration transmissibility in Section 6.2.2.

The secondary resonance on the electrical power extraction can be identified when $IM(Y_I + Y_R + Y_S) = 0$ according to eq (6-30). Furthermore, it can be observed from Figure 6-11 that adding inerter improves the amplitude of secondary peak which is contrast to primary resonance. The main reason is according to power expression in eq (6-30) is dominated by T^2 at system resonance. According to the discussion in Section 6.2.2, the amplitude of transmissibility T becomes greater by shifting the secondary resonance frequency below 10 Hz (source natural frequency). As a result, there will be more electrical power generation with higher inertance.

When the excitation frequency continues increasing and tends to be infinite,

$$\lim_{\omega \rightarrow \infty} |P_e| \approx 0 \quad \text{eq (6-31)}$$

No matter the regenerative shock absorber with or without inerter, there will be less and less power extracted from the road input in high frequency region. Note that by adding inerter into the regenerative shock absorber at high frequencies in Figure 6-11, the harvestable electrical power is further reduced with a rate approximately ω^{-6} (non-inerter isolator ω^{-4}), since the amplitude of isolator mobility Y_I with inerter is decreased along with the frequency as well.

To sum up, this section analyses the characteristic of linear regenerative shock absorber in vehicle suspension system by introducing electrical damper into the isolator. Maximum power is delivered to the electrical damper when $\text{Im}(Y_I + Y_R + Y_S) = 0$. The primary resonance happens when the system is excited at $IM|Y_I + Y_R| = 0$, where the vibration source behaves as a velocity source according to the discussion in Section 6.2.1. With the

increasing of excitation frequency, the relative velocity between the sprung and unsprung masses becomes fairly small. The regenerative shock absorber can only extract tiny amount of electrical power from the road input in higher frequency (i.e. $f > 5 \text{ Hz}$), where the vibration source starts behaving as a force source. These observations provide a better understanding of the influence of vibration source on energy harvesting performance and can assist to physically demonstrate the performance of MMR based regenerative shock absorber in suspension of road vehicles.

6.3 Application of MMR in Vehicle suspension system

Mechanical motion rectifier (MMR) is able to convert a bi-directional rotational motion into unidirectional. It was demonstrated that when the input torque acting on the generator reduces to zero, sprag-clutch will stop the power transmission between the vibration source and generator. Due to the absence of vibration input, the generator undergoes a decaying vibration motion until the output speed of primary system (unidirectional) catching up with it. Even though the dynamics of MMR based regenerative shock absorber have been demonstrated in Chapter 3, but the developed model is corresponding to the lab-test case in Chapter 5 where one terminal of the design was clamped by the fixture. The effect of switching between engagement and disengagement state on vehicle dynamics still needs further clarified.

In this section, a regenerative shock absorber with MMR was implemented in the vehicle suspension system. Based on the vibration source characteristics of quarter car system in Section 6.2.1, influences of switching between engaged and disengaged state on energy harvesting as well as ride comfort performance will be evaluated, the result can justify whether MMR based regenerative shock absorber is beneficial for vehicle suspension system. Consistent to Chapter 3, a simple parallel layout of MMR based regenerative shock absorber with switchable inerter and damper was considered in this study, where suspension stiffness k_s , a translational mechanical damper c_m (non-switchable) plus an electrical damper c_e (switchable), total inertance of lead-screw, MMR module b_1 (non-switchable) and generator inertance b_2 (switchable) are placed between sprung and the unsprung masses. It should be noted that both switchable and unswitchable inerter b_1 and b_2 , like other suspension elements such as spring and damper are considered as massless. Generally, the energy harvesting performance is discussed at its primary resonance ($IM|Y_l + Y_R| = 0$), where the vibration source behaves as a velocity source according to Figure 6-5. Moreover, as the force source usually happens in higher frequency region, where the regenerative shock absorber

can only extract tiny amount of power from the vibration input in Figure 6-11. Therefore, the main focus of this study should be on velocity source.

As discussed in Section 6.2.1, when the vibration source behaves as a velocity source, the free velocity of the road transmitted to the isolator is insensitive to the dynamic behaviour of the load. As a result, it can be assumed that the unsprung mass is placed on the ground where the movement of unsprung mass approximately equals to the road input x_o , the 2dof quarter car model can then be simplified by a 1dof system, a schematic diagram is shown in Figure 6-12

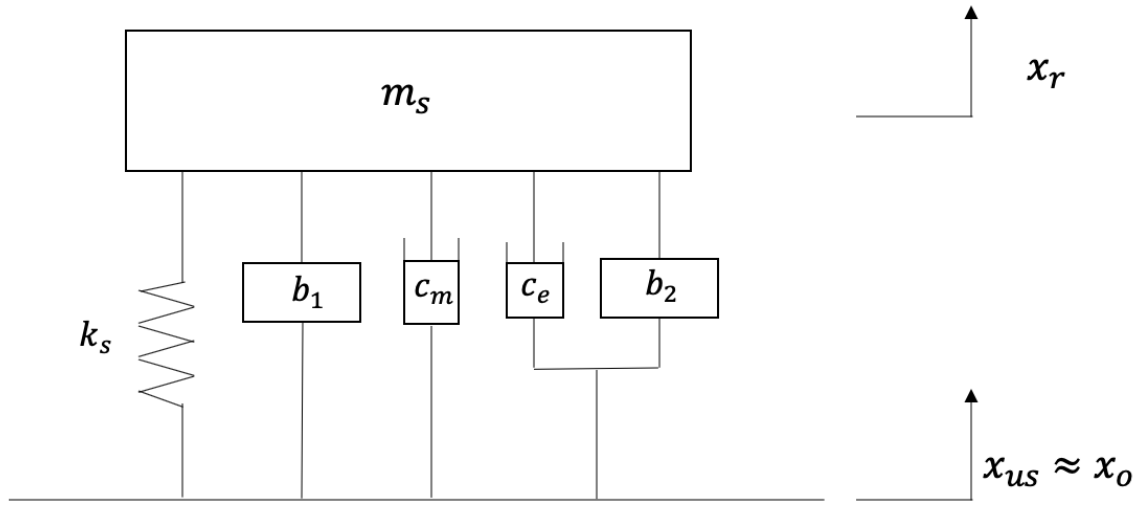


Figure 6-12: Schematic diagram of applying MMR in quarter car model during engaged state (Velocity Source)

As mentioned in Chapter 3, the switchable secondary system can be engaged or disengaged from the vibration source according to the mechanism of the sprag-clutch. In order to evaluate influences of switching inside MMR on the vehicle dynamics, the governing equation of MMR based regenerative shock absorber in a quarter car model according to Figure 6-12 can be analytically represented as

At engaged state

$$m_s \ddot{x}_r + k_s(x_r - x_o) + (c_e + c_m)(\dot{x}_r - \dot{x}_o) + (b_1 + b_2)(\ddot{x}_r - \ddot{x}_o) = 0 \quad \text{eq (6-32)}$$

At disengaged state

$$m_s \ddot{x}_r + k_s(x_r - x_o) + c_m(\dot{x}_r - \dot{x}_o) + b_1(\ddot{x}_r - \ddot{x}_o) = 0 \quad \text{eq (6-33)}$$

$$b_2(\ddot{x}_r - \ddot{x}_o) + c_e(\dot{x}_r - \dot{x}_o) = 0 \quad \text{eq (6-34)}$$

The total inertance of lead-screw and MMR gear module b_1 according to Chapter 3 can be formed by

$$b_1 = (J_{ls} + 2J_{lg} + 2r_g J_{sg}) \left(\frac{2\pi}{l} \right)^2 \quad \text{eq (6-35)}$$

The switchable inertance b_2 contributed by the generator is given by

$$b_2 = r_N J_g \left(\frac{2\pi}{l} \right)^2 \quad \text{eq (6-36)}$$

Agostinacchio et al [138] categorize the road profile into four grades when the vehicle is travelling at the speed of 40 km/h, which defined a very good surface (ISO A-B class) with amplitude $X_o = \pm 15 \text{ mm}$, good (ISO B-C class) with amplitude $X_o = \pm 25 \text{ mm}$, average (ISO C-D class) with amplitude $X_o = \pm 50 \text{ mm}$, and poor (ISO D-E class) with amplitude $X_o = \pm 100 \text{ mm}$. Generally, random road profile is used to emulate the vertical excitation from the ground. However, it is quite difficult to interpret physical consequences of switching of engagement and disengagement by injecting a noisy signal. A harmonic road profile with average road quality $X_o = 50 \text{ mm}$ at vehicle body bounce frequency $f = 1 \text{ Hz}$ (velocity source) was considered in this case.

During the engagement period, the generator velocity can be solved by the relative velocity between the sprung mass and the road input. By setting $z_e = x_r - x_o$, and $x_o = X_o \sin \omega t$, eq (6-32) can be rearranged by

$$(b_1 + b_2 + m_s) \ddot{z}_e + (c_e + c_m) \dot{z}_e + k_s z_e = m_s \omega^2 X_o \sin \omega t \quad \text{eq (6-37)}$$

As the characteristic of MMR system is described by a piecewise linear model, the initial condition of relative displacement and velocity at the starting point can be written by

$$z_e(0) = 0 \quad \text{eq (6-38)}$$

$$\dot{z}_e(0) = 0 \quad \text{eq (6-39)}$$

The system relative displacement, velocity and acceleration during engagement period can be numerically solved by taking zero initial conditions from eq (6-38) and eq (6-39) into the second ordinary differential equation form of eq (6-37) through Matlab ODE45. Disengagement happens when the external force acting on the secondary switchable electrical system reduces to zero ($F_G = 0$). As a result, the initial velocity at the time instant t_1 where switchable system transferring from engaged state into disengaged state can be obtained by

$$\dot{\theta}_g(t_1) = |\dot{\theta}_e(t_1)| \quad \text{eq (6-40)}$$

$|\dot{\theta}_e|$ is the output angular velocity of the primary system (unidirectional) during engagement period which can be formed by $\dot{\theta}_e = \dot{z}_e \left(\frac{2\pi}{l} \right)$, while $\dot{\theta}_g(t_1)$ is the initial velocity of generator transfers from engaged state to disengaged state. Furthermore, the time instant of generator

disengaging from the primary system t_1 can be numerically solved by rotational form of eq (6-34)

$$J_g \ddot{\theta}_g + c_{e_r} \dot{\theta}_g = 0 \quad \text{eq (6-41)}$$

In a similar way of discussion in Chapter 3, dynamics of generator speed in the absence of vibration input during disengagement period according to Figure 6-13(b)

$$\dot{\theta}_g = \dot{\theta}_e(t_1) e^{-\frac{c_{e_r}}{J_g}(t-t_1)}, t_1 \leq t \leq t_2 \quad \text{eq (6-42)}$$

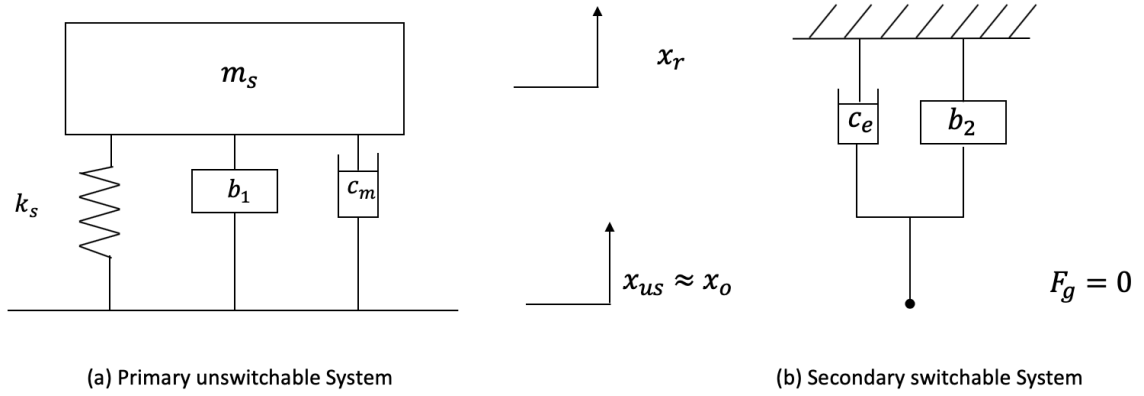


Figure 6-13: Schematic of disengaged state of the system (a)Primary unswitchable system
(b)Secondary switchable system

In the absence of generator inertance b_2 and electrical damper c_e , the governing equation of motion for the primary system according to Figure 6-13(a) can be obtained as

$$(b_1 + m_s) \ddot{z}_d + c_m \dot{z}_d + k_s z_d = m_s \omega^2 X_o \sin \omega t \quad \text{eq (6-43)}$$

Where $\ddot{z}_d, \dot{z}_d, z_d$ is the relative acceleration, velocity and displacement between the sprung mass and road input during the disengagement period.

Initial conditions of relative displacement and translational velocity of primary system at the time instant t_1

$$\dot{z}_d(t_1) = \dot{z}_e(t_1) \quad \text{eq (6-44)}$$

$$z_d(t_1) = z_e(t_1) \quad \text{eq (6-45)}$$

As the vibration input from the road x_o is prescribed, the relative displacement z_d and velocity \dot{z}_d between the sprung mass and road during disengagement period can then be obtained by another second order differential equation form of eq (6-43) with the initial condition eq (6-44) and eq (6-45).

Based on the vehicle parameters in Table 6-2 and assuming MMR system parameters ($b_1 = 60kg, b_2 = 70kg, c_m = 750Nsm^{-1}, c_e = 400Nsm^{-1}$), Figure 6-14 simulates the dynamics of MMR based regenerative shock absorber. The generator is allowed to re-engage with the

vibration source at t_2 in Figure 6-14 (a), where the output angular velocity of primary system $|\dot{\theta}_d|$ (unidirectional) catches up with the generator velocity

$$|\dot{\theta}_d(t_2)| = \dot{\theta}_g(t_2) \quad \text{eq (6-46)}$$

Once the sprag-clutch reconnects the generator inertance and electrical damper with the vibration source, the system dynamics according to re-engagement can then be solved by taking initial conditions at eq (6-47) and eq (6-48) at t_2 back to eq (6-37)

$$\dot{z}_d(t_2) = \dot{z}_e(t_2) \quad \text{eq (6-47)}$$

$$z_d(t_2) = z_e(t_2) \quad \text{eq (6-48)}$$

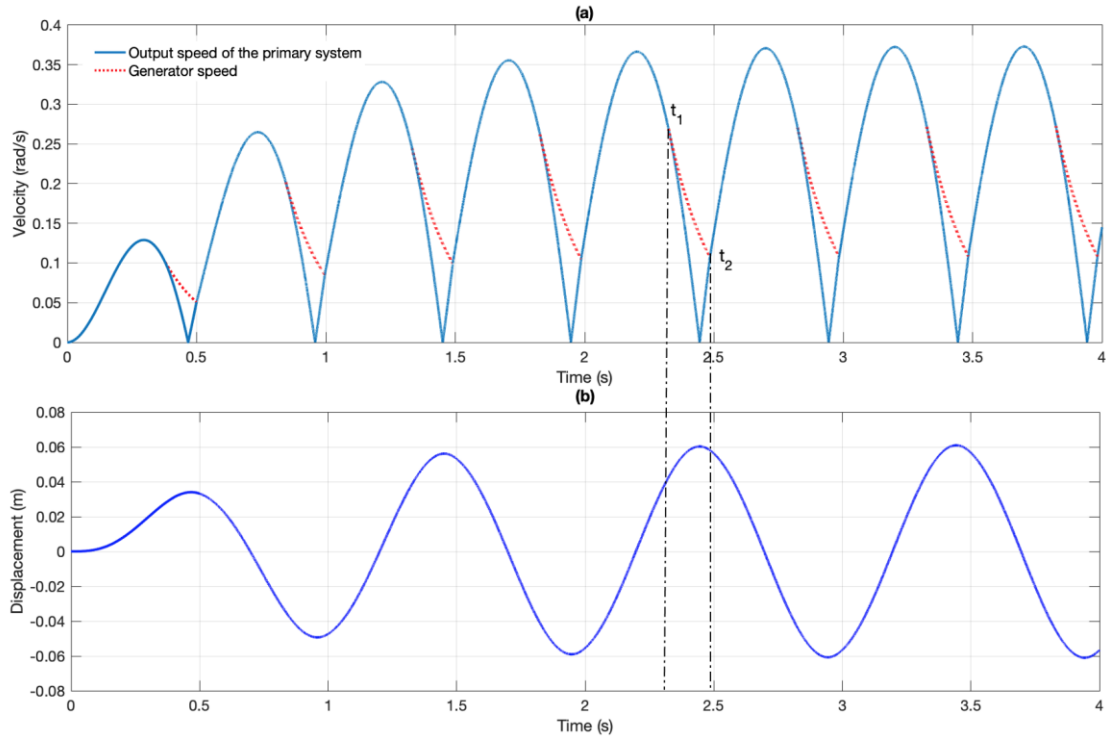


Figure 6-14: Vehicle dynamics with MMR (a) Relative rotational speed across the electrical damper (b) Relative displacement between the sprung mass and road

In this section, the MMR based regenerative shock absorber was implemented in a quarter car model at vehicle body bounce frequency, where primary maximum power is delivered to the electrical damper. Different from the model developed in Chapter 3, where one terminal of the design is clamped, the dynamic model here takes the sprung mass and suspension stiffness into account. Once the switchable secondary electrical system disconnects from the primary system, the output velocity of primary system no longer remains prescribed. During the disengagement period, the non-switchable primary system and the switchable secondary system undergo independent motions until re-engagement. In this way, the consequence of implementing MMR based regenerative shock absorber in vehicle suspension system can be

obtained based on the newly developed piecewise linear model where it can be further used to demonstrate whether MMR is still able to enhance the system performance.

6.4 Performance evaluation of MMR based regenerative shock absorber in quarter car model

As discussed in Chapter 3, the MMR based regenerative shock absorber improves the energy harvesting performance as the switching between engagement and disengagement allows part of the mechanical reactive power converting into useful electrical power instead of giving back to the vibration source. However, this observation only validates lab-test case in Chapter 5, where one terminal of the design is clamped. In this section, the performance of MMR based regenerative shock absorber is evaluated in a quarter car system. Based on the piecewise linear model developed in Section 6.3, the influence of switching on the system performance including energy harvesting, mechanical power flow and the sprung mass acceleration (ride comfort) will be discussed. Moreover, a comparison between linear system without switching and MMR based piecewise linear system is presented to identify whether switching within MMR is still able to improve the performance. Passenger car is selected as the implementing object, where parameters are shown in Table 6-2. Moreover, numerical study is also conducted to insightfully explain how system parameters affecting the vehicle dynamics, which can be further used to justify the usage of MMR based regenerative shock absorber.

	$m_s(kg)$	$k_s(kN/m)$	$c_e(Ns/m)$	$c_m(Ns/m)$
Passenger car	240	16	400	750

Table 6-2: Quarter car parameters

6.4.1 Energy harvesting performance quantification

Based on the model developed in Section 6.3, the amount of energy harvested by the electrical damper during disengagement period from t_1 to t_2

$$E_d = \int_{t_1}^{t_2} c_{e_r} \dot{\theta}_g^2 dt \quad \text{eq (6-49)}$$

Where the generator speed during disengagement is obtained from eq (6-42), the time instant of the secondary system starts disengagement t_1 and reconnect with the vibration source t_2 can be numerically solved from eq (6-41), eq (6-46) respectively.

As far as the time going, the transient response of system due to the zero initial condition will eventually disappear, while the switching time instant becomes periodical. The harvestable electrical energy during the engagement period between t_2 and $t_1 + \frac{T}{2}$

$$E_e = \int_{t_2}^{t_1 + \frac{T}{2}} c_{e-r} \dot{\theta}_e^2 dt \quad \text{eq (6-50)}$$

Where $\dot{\theta}_e$ is the angular speed of the primary system during engagement period provided by $\dot{\theta}_e = \dot{z}_e \left(\frac{2\pi}{l} \right)$.

The amount of mechanical energy losses over half cycle can be formed in a similar way

$$E_m = \int_{t_1}^{t_2} c_m \dot{z}_d^2 dt + \int_{t_2}^{t_1 + \frac{T}{2}} c_m \dot{z}_e^2 dt \quad \text{eq (6-51)}$$

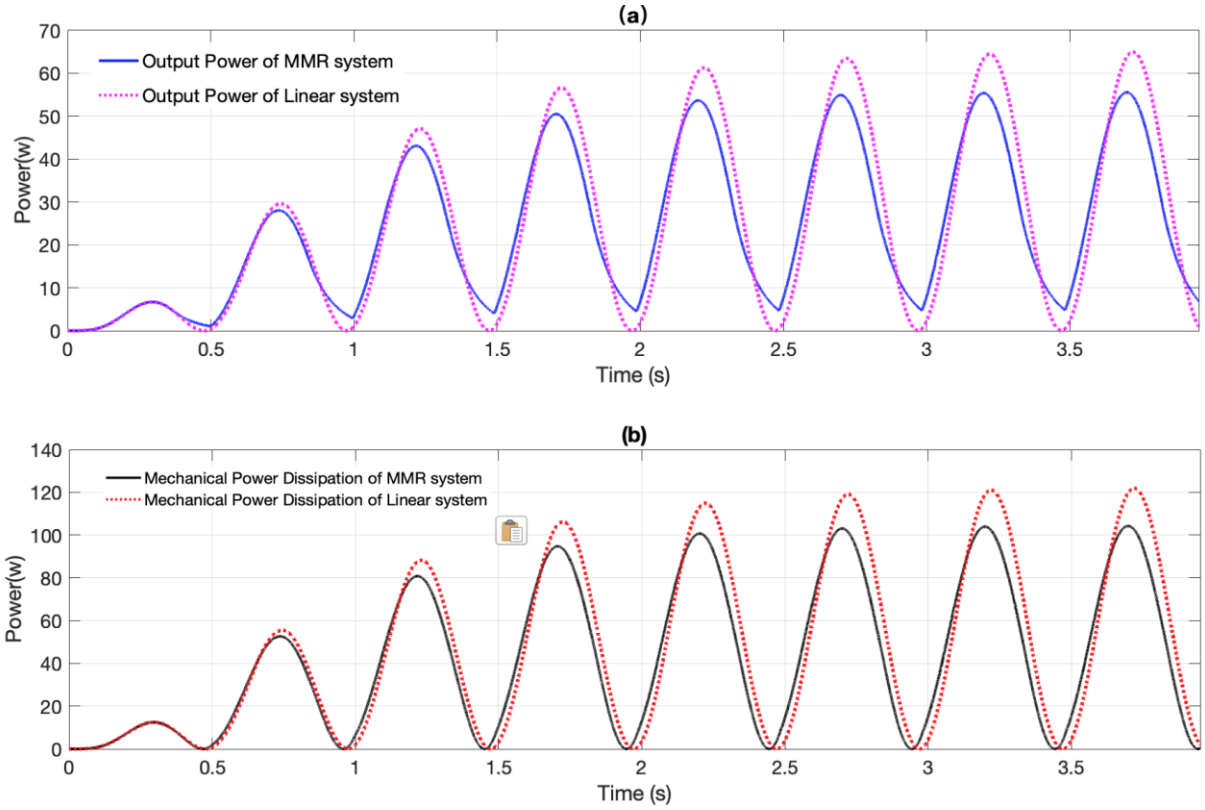


Figure 6-15: Power extraction and dissipation comparison between MMR and Linear system

(a) Electrical harvestable power (b) Mechanical Power loss

Applying system parameters in eq (6-49) to eq (6-51), Figure 6-15 shows the power extraction and dissipation comparison between MMR and linear system without switching excited at vehicle body bounce frequency $f = 1\text{Hz}$. Since the developed prototype in Chapter 5 is not scaled up, it is assumed that the primary unswitchable inertance (b_1) and switchable generator inertance (b_2) equals to 60kg and 70kg respectively. As can be seen in Figure 6-15(a), generator during disengagement period consumes the residual kinetic energy stored

on the shaft and produce a more continuous voltage and power due to the absence of the vibration input. By setting $t_1 = t_2$, which means the switchable secondary system engages with the primary system all the time. The pink dotted line in Figure 6-15(a) shows the output electrical power for non-switchable linear system as well. From the waveform, it is found that the amount of power extraction for linear system is greater than the MMR system when the switching becomes periodical, even though the mechanical power loss is reduced. The numerical study result shows that for a steady-state condition, the system average electrical power for a linear system is 32.03W, while the useful power is decreased to 30.28w by employing MMR. Although MMR allows less mechanical power loss (10%) compared to linear system, but it reduces the amount of useful power harvested by the electrical damper as well. This observation is quite different from the result drawn in Chapter 3, where MMR enables better energy harvesting performance despite the vibration source when the design is installed in a testing machine.

In order to understand the reason why the MMR based regenerative shock absorber generates less electrical energy than the linear system, it is necessary to look at the mechanical active and reactive power flow to identify whether the switching time instant is desirable.

During the engaged state, the mechanical active/reactive power flow can be formulated by multiplying \dot{x}_r (sprung mass absolute velocity) on eq (6-32)

$$m_s \ddot{x}_r \dot{x}_r + k_s (x_r - x_o) \dot{x}_r + (c_e + c_m) (\dot{x}_r - \dot{x}_o) \dot{x}_r + (b_1 + b_2) (\ddot{x}_r - \ddot{x}_o) \dot{x}_r = 0 \quad \text{eq (6-52)}$$

Where it can be rearranged by

$$-k_s z_e \dot{x}_o - (c_e + c_m) \dot{z}_e \dot{x}_o - (b_1 + b_2) \ddot{z}_e \dot{x}_o = (c_e + c_m) \dot{z}_e^2 + \frac{d}{dt} \left(\frac{m_s \dot{x}_r^2}{2} + \frac{k_s z_e^2}{2} + \frac{(b_1 + b_2) \dot{z}_e^2}{2} \right) \quad \text{eq (6-53)}$$

eq (6-53) is the expression of power conservation, the instantaneous power into the electrical-mechanical system (left hand side) equals to the power either dissipated or absorbed by the damper plus the sum of change of the mechanical kinetic and potential energies (right hand side).

Similarly, the energy conservation during disengagement period can be formed by multiplying \dot{x}_{r_d} (sprung mass absolute velocity during disengagement) on eq (6-43)

$$-k_s z_d \dot{x}_o - c_m \dot{z}_d \dot{x}_o - b_1 \ddot{z}_d \dot{x}_o = c_m \dot{z}_d^2 + \frac{d}{dt} \left(\frac{m_s \dot{x}_{r_d}^2}{2} + \frac{k_s z_d^2}{2} + \frac{b_1 \dot{z}_d^2}{2} \right) \quad \text{eq (6-54)}$$

In this way, the total mechanical input power from the road to create the prescribed velocity input \dot{x}_o for engagement and disengagement can be expressed respectively by

$$P_{in_e} = -k_s z_e \dot{x}_o - (c_e + c_m) \dot{z}_e \dot{x}_o - (b_1 + b_2) \ddot{z}_e \dot{x}_o \quad \text{eq (6-55)}$$

$$P_{in_d} = -k_s z_d \dot{x}_o - c_m \dot{z}_e \dot{x}_o - b_1 \ddot{z}_e \dot{x}_o \quad \text{eq (6-56)}$$

The sum of reactive power during engagement and disengagement can be formed respectively by

$$P_{react_e} = \frac{d}{dt} \left(\frac{m_s \dot{x}_{r_e}^2}{2} + \frac{k_s z_e^2}{2} + \frac{(b_1 + b_2) \dot{z}_e^2}{2} \right) \quad \text{eq (6-57)}$$

$$P_{react_d} = \frac{d}{dt} \left(\frac{m_s \dot{x}_{r_d}^2}{2} + \frac{k_s z_d^2}{2} + \frac{b_1 \dot{z}_d^2}{2} \right) \quad \text{eq (6-58)}$$

While the applied reactive power from the vibration source into secondary system for each state is

$$P_{s_e} = \frac{d}{dt} \left(\frac{b_2 \dot{z}_e^2}{2} \right) \quad \text{eq (6-59)}$$

$$P_{s_d} = 0 \quad \text{eq (6-60)}$$

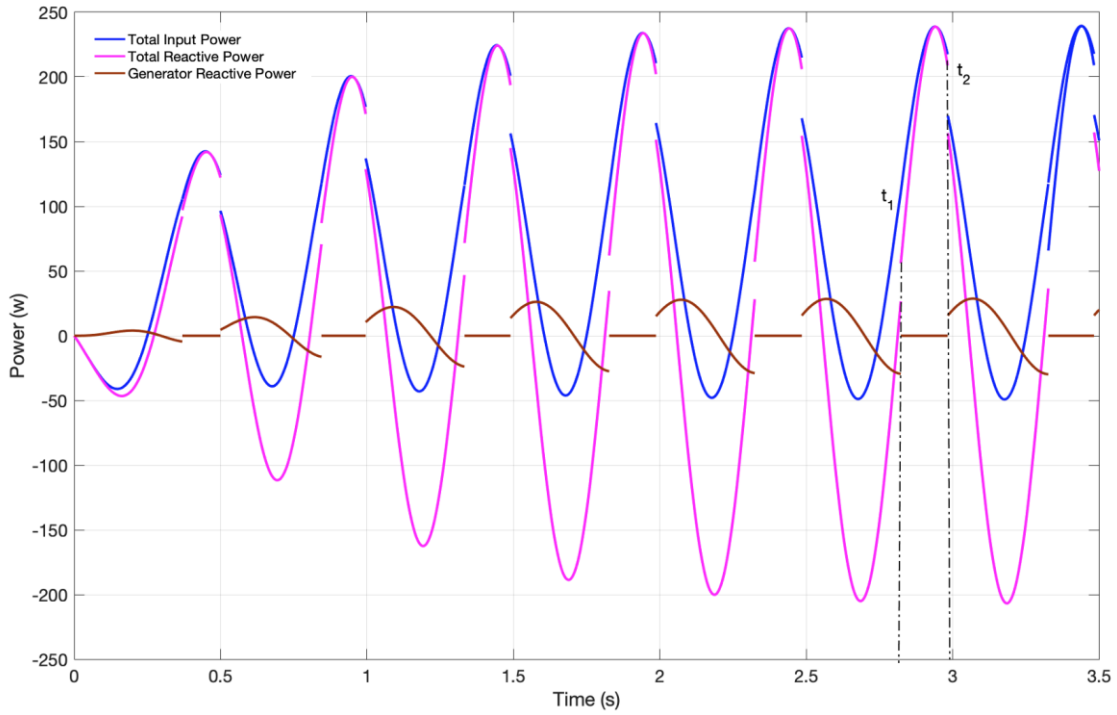


Figure 6-16: Mechanical active/reactive power flow of quarter car system with MMR

Figure 6-16 shows the mechanical active/reactive power flow of quarter car system with MMR based regenerative shock absorber. Unlike the discussion in Chapter 3 where either the force or velocity through the electro-mechanical system is harmonic, both terms become discontinuous to create a prescribed road velocity input \dot{x}_o . By looking at the total reactive power (pink curve) in Figure 6-16, it can be identified that since the primary system involves

less inertance and less damper due to switching, there is an instantaneous jump on the reactive power at t_1 . This is unbeneficial, as the amount of increasing on reactive power partially flows into sprung mass which may affect the ride comfort (sprung mass acceleration). Next, by considering the applied reactive power to secondary system (brown curve) in Figure 6-16. Consistent to the result in Chapter 3, switching stops part of the reactive power on secondary system giving back to the vibration source at t_1 and converting into useful electrical power which is desirable. Since the secondary system disengages from the vibration source doing decaying vibration motion from t_1 to t_2 , there is no reactive power transmitting to the generator which results a plain curve during the period. When the sprag-clutch re-engages the secondary system with the vibration source at t_2 , the vibration source restarts transmitting power to the secondary switchable system. As the system comprises more inertance and damper to resist the road input, which leads to a drop on the corresponding power at t_2 .

Even though switching is beneficial for reactive power flow of secondary system, but it is still questionable why the implementation of MMR in vehicle suspension system is not able to enhance the energy harvesting performance over linear system. In order to address the problem, it is necessary to increase the value of sprung mass to infinite ($m_s \rightarrow \infty$), such that its movement x_r tends to be zero ($x_r \approx 0$). The model in Figure 6-12 behaves exactly the same as Chapter 3 while the mass can be considered as clamped, the relative displacement between the sprung mass and road input z equals to the absolute displacement of road input x_o .

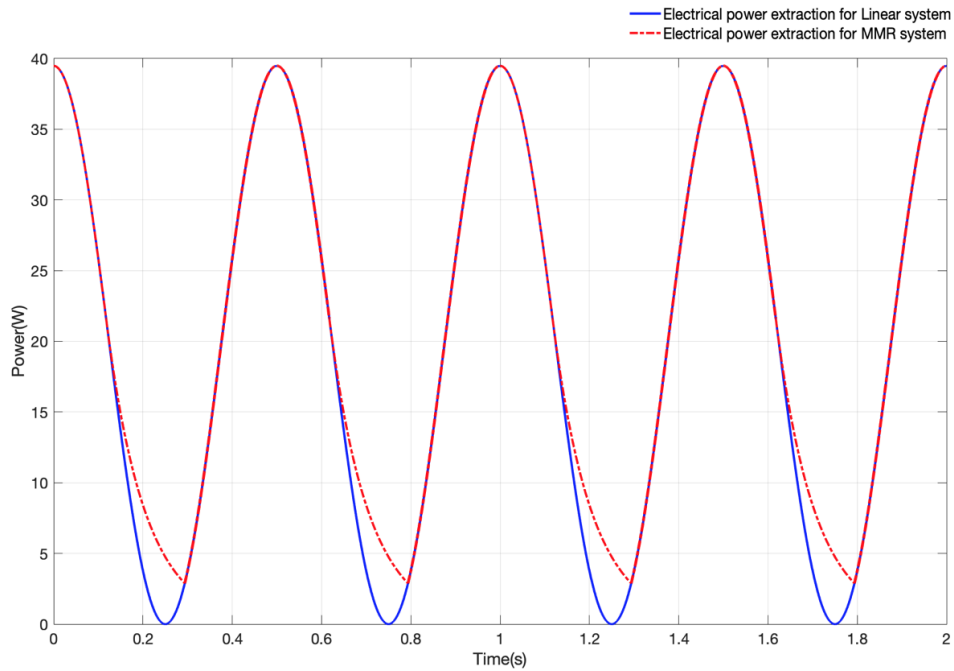


Figure 6-17: Electrical power extraction between linear and MMR system ($m_s \rightarrow \infty$)

Figure 6-17 shows the electrical power extraction between linear and MMR system by setting $m_s \rightarrow \infty$. Apparently, the energy harvesting performance of MMR system becomes better than the linear system, which consistent the result in Chapter 3. Therefore, it can be concluded that the energy harvesting performance of regenerative shock absorber with MMR becomes worse when it is implemented in vehicle suspension system is mainly according to the movement of sprung mass.

Up till now, it is still unknown that how system parameters especially secondary system affecting the dynamics of switching. Moreover, it is necessary to investigate whether it is desirable to extend disengagement durations as it potentially allows more harvestable electrical power. According to the discussion in Chapter 3, MMR is more beneficial for lightly electrical damped system as the extension of disengagement period can offer a more continuous output voltage and power. Meanwhile, increasing the generator inertia improves more electrical power extraction as well. These hypotheses need to be validated through a numerical study. It should be noted that the suspension stiffness k_s , sprung mass m_s , primary unswitchable inertance b_1 and mechanical damper c_m here are fixed in order to identify influences of electrical damping c_e and generator inertance b_2 on the system performance.

Figure 6-15, Figure 6-18 and Figure 6-19 describe the harvested electrical power and mechanical power loss respectively (MMR Versus Linear) by varying the value of electrical damping coefficient c_e . It was demonstrated in Chapter 3 that lighter electrical damper improves the velocity of output generator which somehow extends the disengagement duration. Consequently, the generator can work more continuously and produce voltage with higher offset in terms of linear system. As shown in Figure 6-18 and Figure 6-19, even though the maximum power of linear system is much greater than the MMR system, but MMR can offer a more continuous power rather than falling up and down. Throughout the numerical study result in Table 6-3, it was found that MMR is still more suitable for lightly electrical damped vehicle suspension system i.e. $c_e = 50Ns/m$, as it can enhance both amount of harvestable power on the electrical load and system efficiency at the same time. With the increasing of electrical damping, system performance might become even worse with MMR comparing to linear system. When the system is heavily electrical damped $c_e \geq c_m$, the sprag-clutch tends to engage the switchable part with the primary system all the time. Even though increasing c_e is desirable for energy harvesting, but no advantages can be found by using MMR comparing to linear system according to Table 6-3.

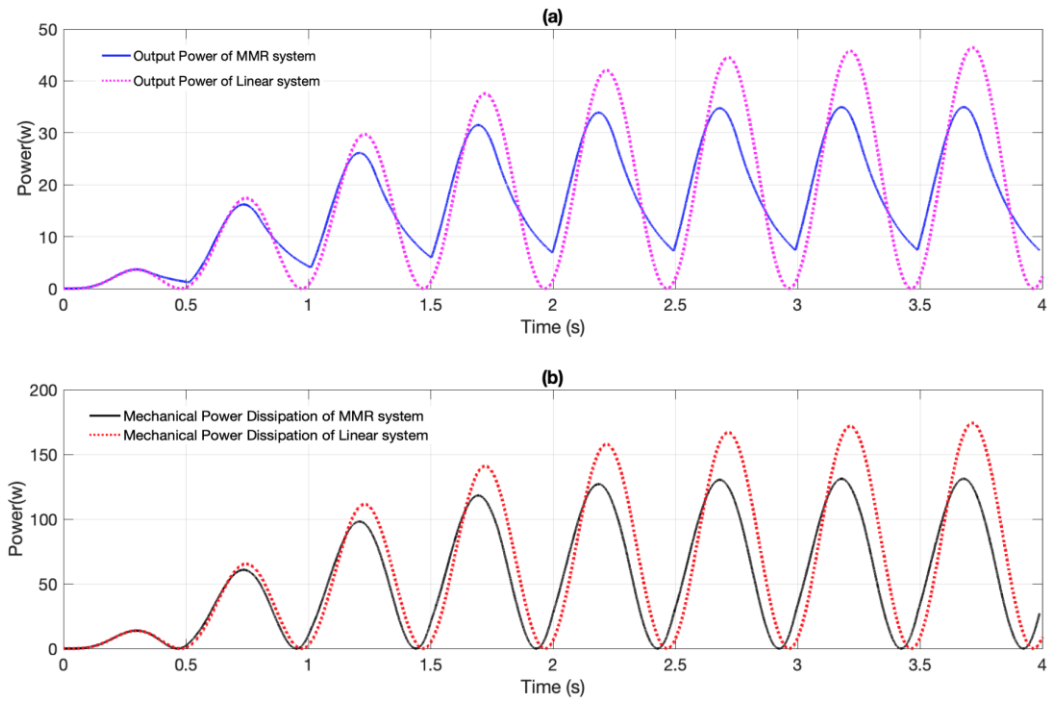


Figure 6-18: Power extraction and dissipation comparison between MMR and Linear system ($c_e = 200Ns/m$) (a) Electrical harvestable power (b) Mechanical power loss

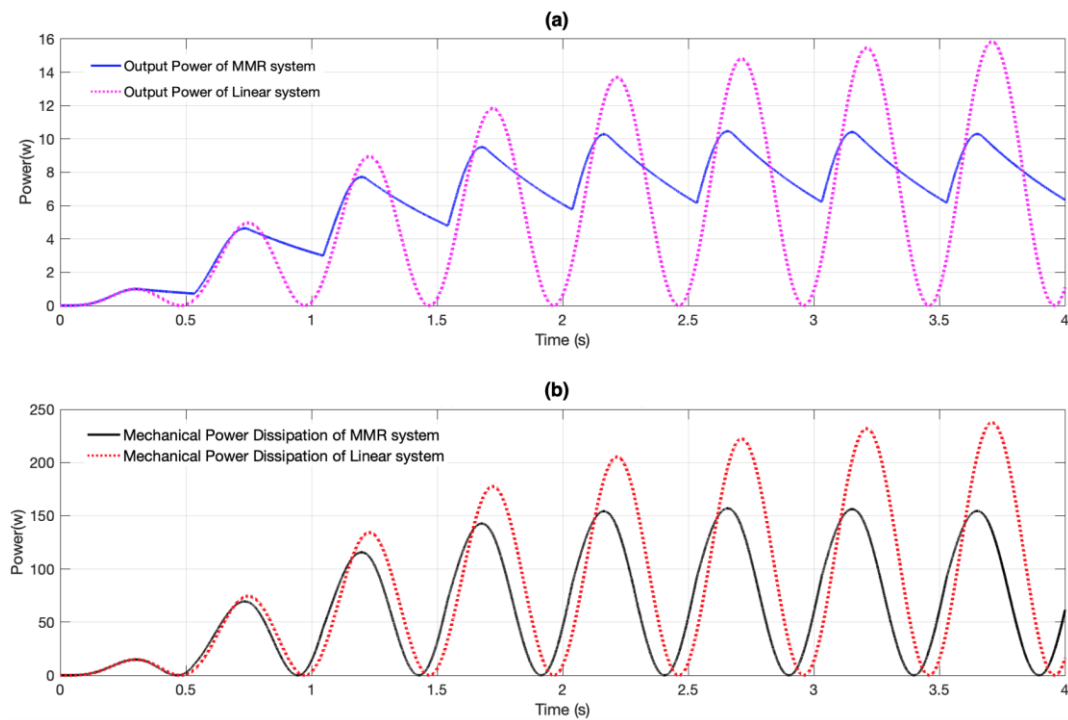


Figure 6-19: Power extraction and dissipation comparison between MMR and Linear system ($c_e = 50Ns/m$) (a) Electrical harvestable power (b) Mechanical power loss

c_e (Ns/m)		P_e (W)	P_m (W)	η (%)
50	MMR	8.328	80.5	9.38
	Linear	7.7582	116.37	6.25
100	MMR	13.64	75.73	15.26
	Linear	14.05	105.37	11.76
200	MMR	21.32	68	23.86
	Linear	22.62	84.83	21.05
400	MMR	30.28	53.94	35.95
	Linear	32.03	60.06	34.78

Table 6-3: Energy harvesting performance comparison between MMR and Linear system with different c_e

Figure 6-20 to Figure 6-22 describe the performance comparison between MMR and linear system by varying the generator inertance b_2 ranging from 10 to 200kg. According to the discussion in Chapter 3, increasing the generator inertance can potentially enhance the energy harvesting performance as it allows more reactive power being converted into useful power once it is disconnected from the primary system. In this way, the disengagement period can be extended which smooth out the output voltage and power in Figure 6-20. Furthermore, it is found that the effect of switching on energy harvesting can be ignored when the generator size is relatively small, i.e. $b_2 = 10kg$, while the dynamics of MMR system tend to overlap the linear system in Figure 6-22.

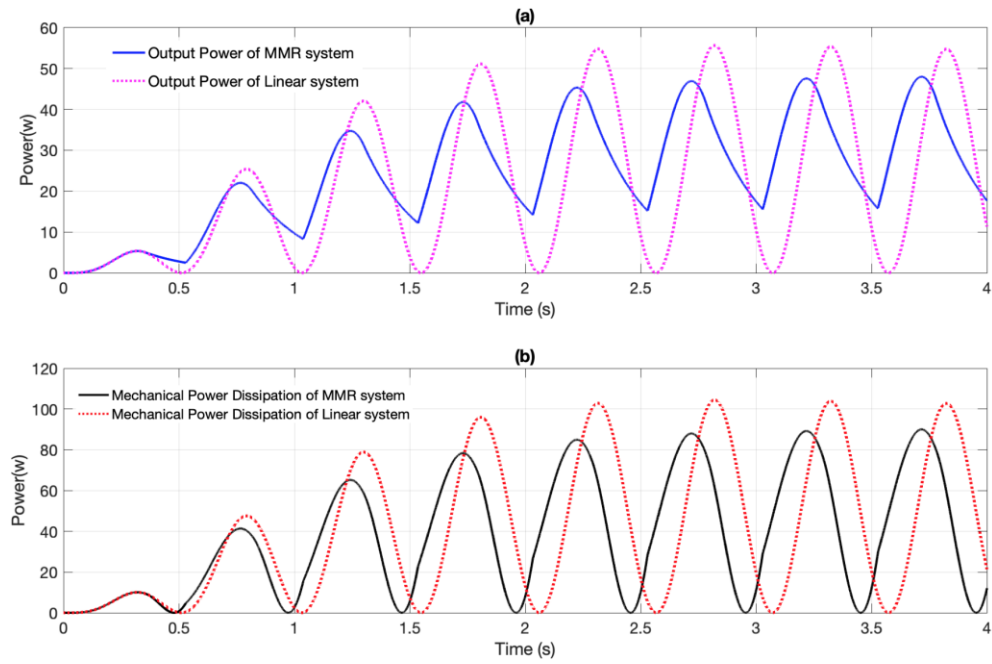


Figure 6-20: Power extraction and dissipation comparison between MMR and Linear system
 $(b_2 = 200\text{kg})$ (a) Electrical harvestable power (b) Mechanical power loss

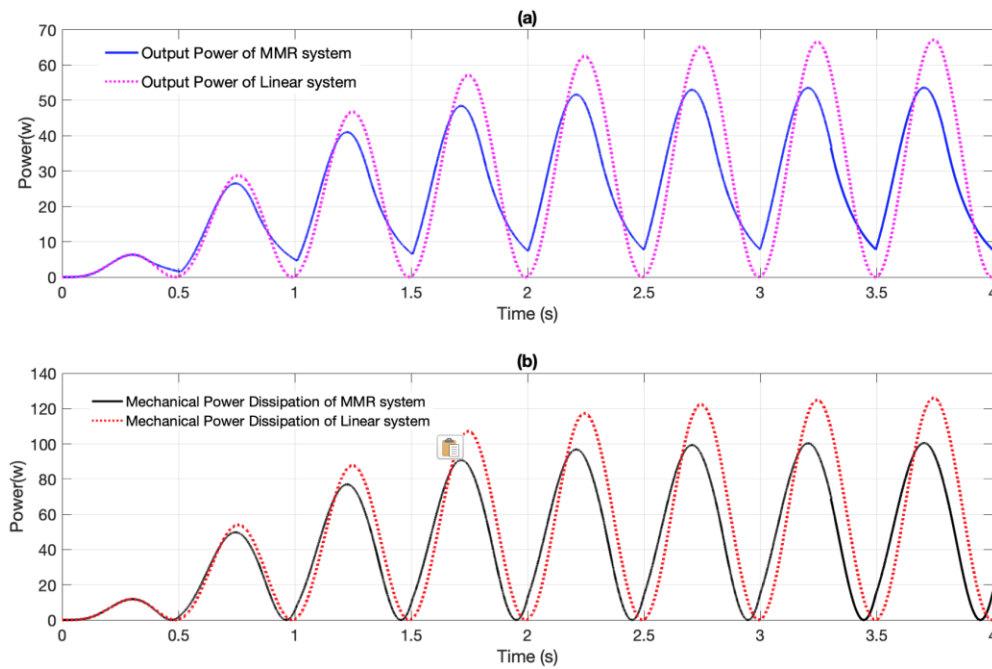


Figure 6-21: Power extraction and dissipation comparison between MMR and Linear system
 $(b_2 = 100\text{kg})$ (a) Electrical harvestable power (b) Mechanical power loss

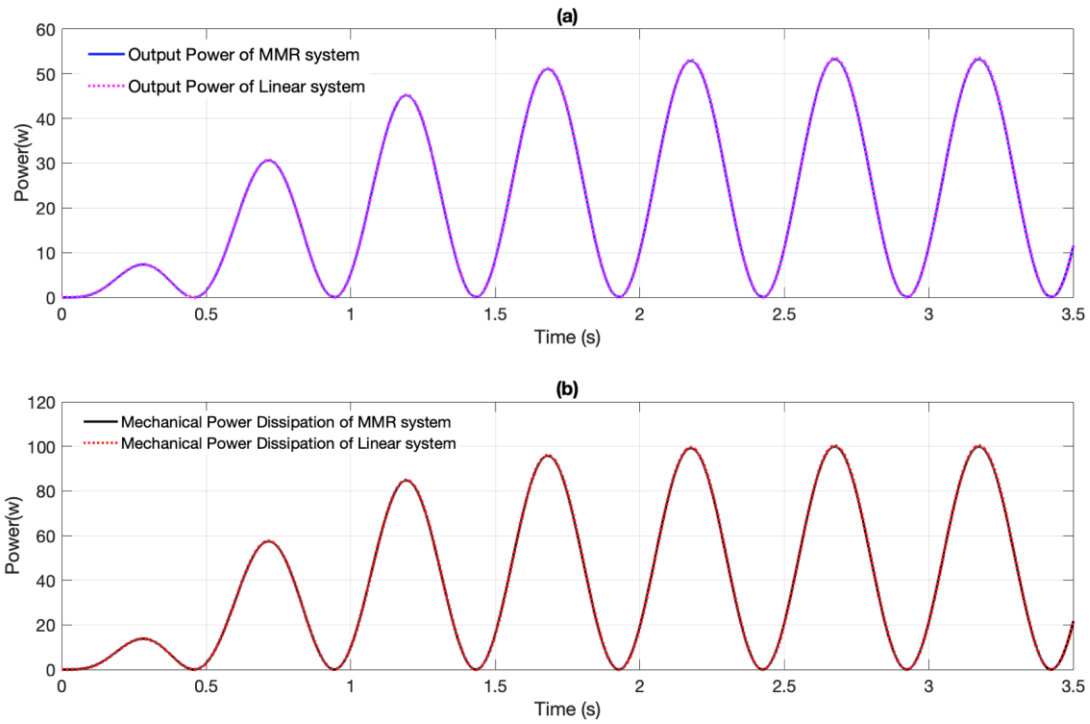


Figure 6-22: Power extraction and dissipation comparison between MMR and Linear system

($b_2 = 10\text{kg}$) (a) Electrical harvestable power (b) Mechanical power loss

$b_2(\text{kg})$		$P_e(\text{W})$	$P_m(\text{W})$	$\eta(\%)$
10	MMR	26.62	49.91	34.8
	Linear	26.16	49.06	34.78
70	MMR	25.53	75.73	25.21
	Linear	32.03	60.06	34.78
100	MMR	31	52.9	36.9
	Linear	32.69	61.29	34.78
200	MMR	32.91	49.68	35.95
	Linear	26.26	49.24	34.78

Table 6-4: Energy Harvesting Performance comparison between MMR and Linear system with different generator inertance b_2

Table 6-4 shows the numerical study results by varying the generator inertance with fixed electrical damping $c_e = 400\text{Ns/m}$. It can be observed that better energy harvesting performance can be achieved over linear system by increasing generator size. Note that the average electrical power for linear system is reduced with larger generator inertance. This is mainly according to the system natural frequency $\sqrt{k_s/(m_s + b_1 + b_2)}$ is shifted to a lower

region, the system transfers from spring controlled frequency region ($\omega < \omega_n$) into mass/inertance dominated region ($\omega > \omega_n$). In this case, more vibration power flows into inerter and mass rather than being harvested by the electrical damper.

6.4.2 Ride comfort evaluation

The main function of the isolator placed between the sprung and unsprung mass is to mitigate the vibration induced by the road irregularity to achieve better ride comfort. In this section, the influence of switching inside MMR on ride comfort performance is investigated based on the piecewise linear model built in Section 6.3. A comparison between MMR based piecewise linear system and no switching linear system is presented to identify whether the engagement and disengagement of MMR is able to offer better ride quality.

To assess the levels of ride comfort, the dynamic response of the vehicle body of passenger car is generally measured by sensors. Indicative of ride comfort (e.g. vertical acceleration, absorbed power) have been laid down in standards such as ISO 2631-1 [139], BS 6841 [140], and VDI 2057 [141]. In this study, ISO 2631-1 was used to identify the switching between engaged and disengaged state on the ride comfort performance at system resonance frequency (1Hz), while is generally determined by the sprung mass acceleration in the z-axis (vertical). According to ISO 2631-1, the following values in Table 6-5 give approximate indications of likely reactions to various magnitudes of overall vibration total values in public transport.

Acceleration Level	Passenger Reaction
Less than $0.315m/s^2$	Not uncomfortable
$0.315m/s^2$ to $0.63m/s^2$	A little uncomfortable
$0.5m/s^2$ to $1m/s^2$	Fairly uncomfortable
$0.8m/s^2$ to $1.6m/s^2$	Uncomfortable
$1.25m/s^2$ to $2.5m/s^2$	Very uncomfortable
Greater than $2m/s^2$	Extremely uncomfortable

Table 6-5: Comfort reactions to vibration environments [139]

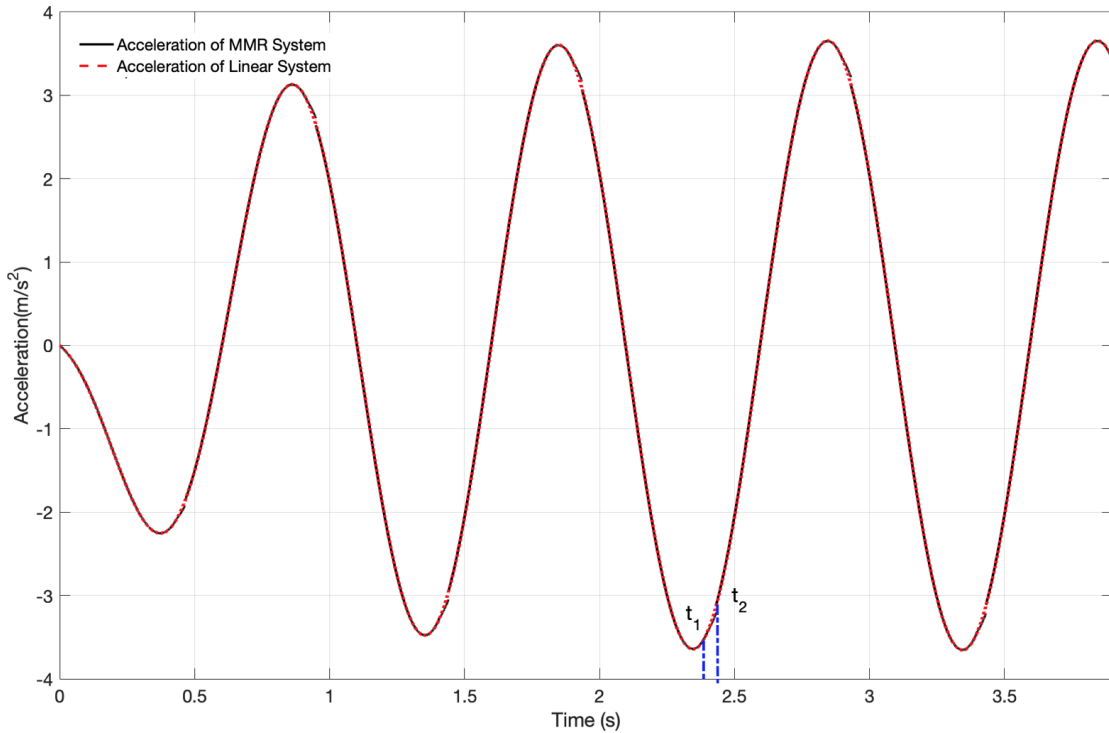
For the MMR based piecewise linear system, the absolute sprung mass acceleration during engagement period \ddot{x}_{r_e} can be obtained by

$$\ddot{x}_{r_e} = \ddot{z}_e + \ddot{x}_o \quad \text{eq(6-61)}$$

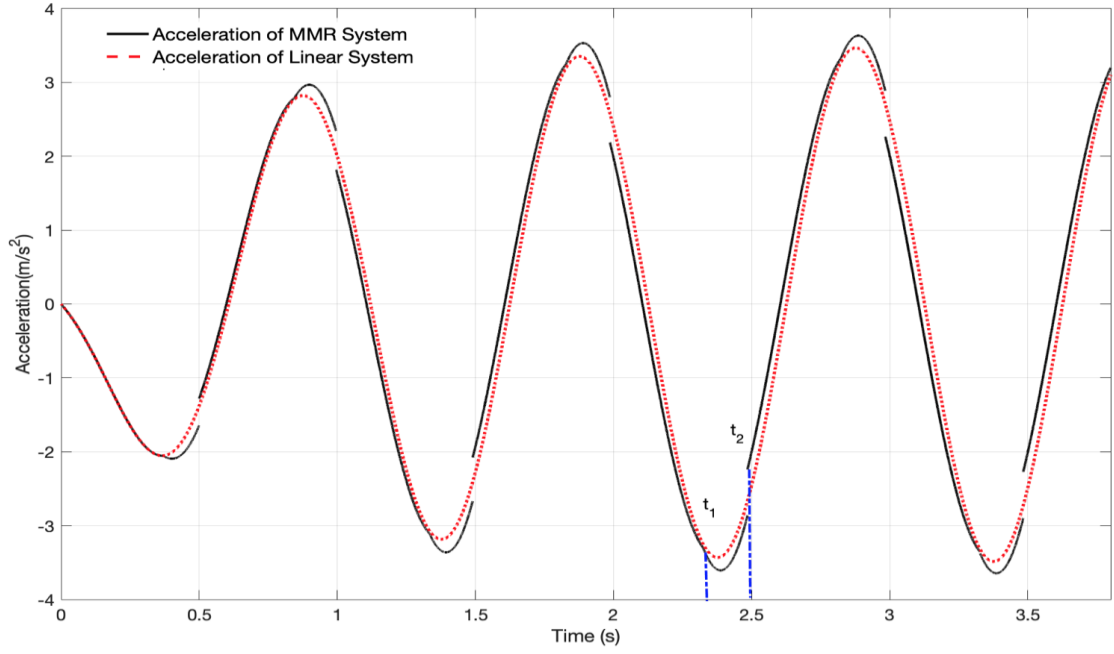
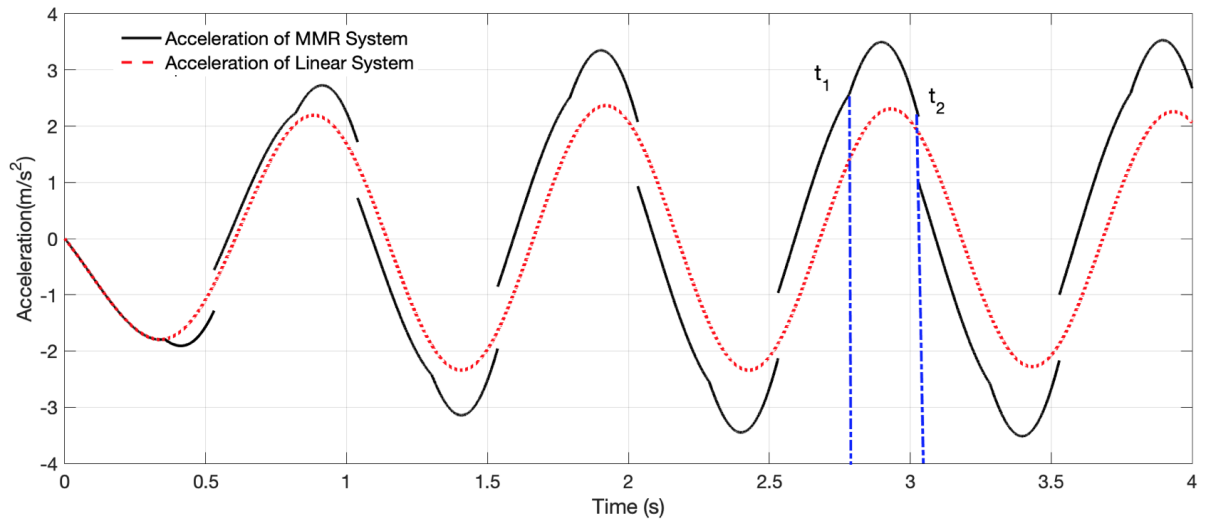
While the sprung mass acceleration during disengagement \ddot{x}_{r_d} is expressed by

$$\ddot{x}_{r_d} = \ddot{z}_d + \ddot{x}_o \quad \text{eq(6-62)}$$

Figure 6-23 shows the simulation result of the absolute sprung mass acceleration \ddot{x}_r for a generator inertance range ($10kg \leq b_2 \leq 200kg$). It is seen that when the switchable secondary system starts disengaging from the primary system at t_1 causes excessive jerk motions (changing rates of acceleration). This is undesirable as a high value of acceleration or jerk might result discomfort even for a very short period. Passenger might not be able to balance under influences of switching. In the meantime, this gives a deeper understanding of reactive power flow curve in Figure 6-16. The instantaneous jump on total reactive power at t_1 instant due to the absence of electrical damper and generator inertance, while part of them is used to accelerate the sprung mass. Once the secondary switchable system is allowed to re-engage with the vibration source, there will be an instantaneous reduction on the acceleration amplitude as the system restarts involving generator inertance and electrical damper to resist motion from the road. Figure 6-23 also shows the influence of switching on sprung mass acceleration by varying the switchable generator inertance. It is found in Figure 6-23 (c) that the passenger tends to suffer from longer duration of jerk motion and feel extremely discomfort with larger generator size according to Table 6-5, while in Figure 6-23 (a) the impact of switching on sprung mass acceleration is negligible if b_2 is small.

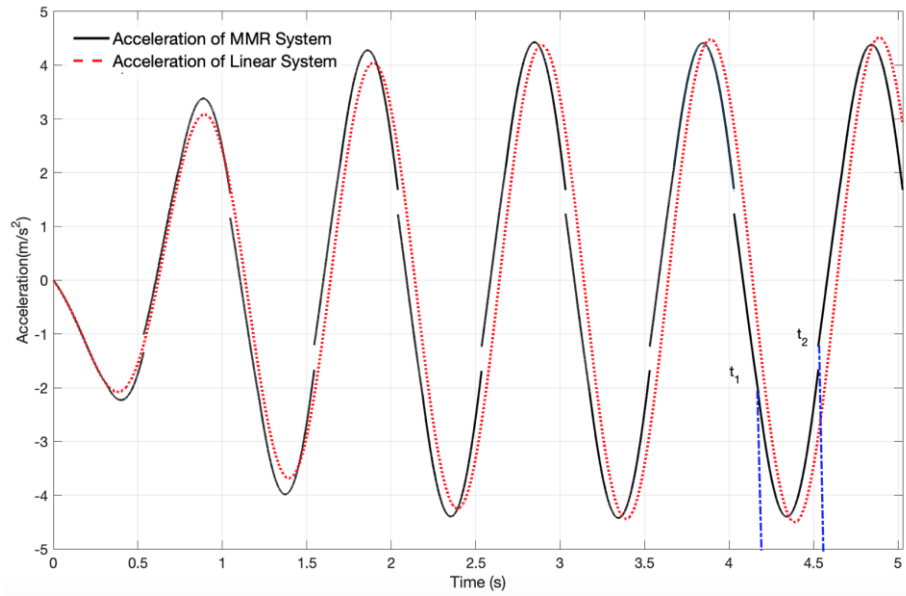


(a) $b_2 = 10kg$

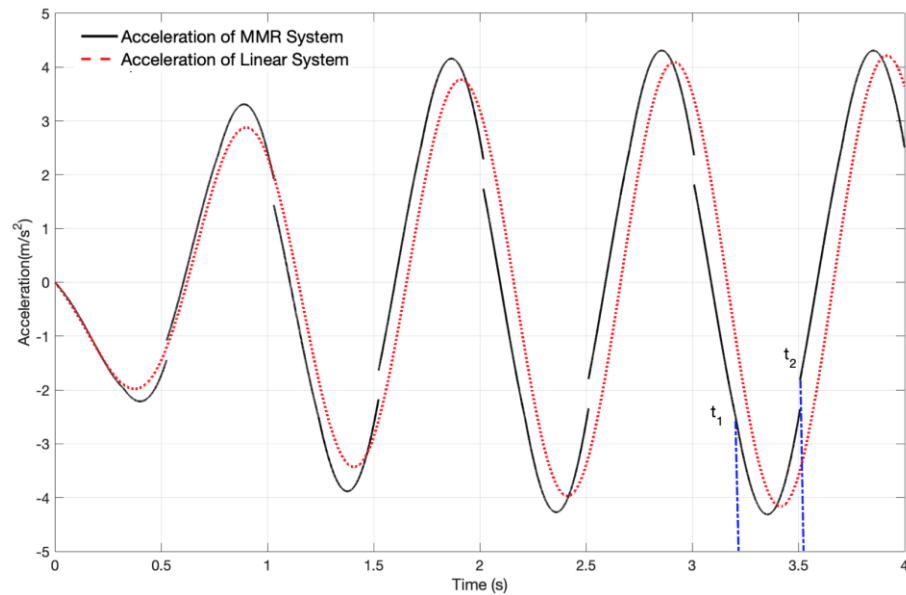
(b) $b_2 = 70\text{kg}$ (c) $b_2 = 200\text{kg}$ Figure 6-23: Sprung mass absolute acceleration $\ddot{x}_r (10\text{kg} \leq b_2 \leq 200\text{kg})$

Based on the above observation, it is seen that increasing the generator size results a bad ride experience for passenger especially when switching happens. Moreover, the extended disengaging duration of secondary switchable system influences the dynamics of ride comfort (sprung mass acceleration) as well. As stated in Section 6.4.1, MMR is more desirable for lightly electrical damped system in terms of energy harvesting. In a similar way of increasing generator inertia/inertance, lighter electrical damper enables more continuous generator speed once it disconnects from the primary system. Therefore, it becomes necessary to find out how the ride comfort being affected by varying electrical damping.

Figure 6-24 shows the dynamics of sprung mass acceleration by varying the switchable electrical damping. It can be identified from Figure 6-24(a) that the changing rate of the acceleration nearly remains at t_1 when the switchable electrical damper is fairly light, while its influence on sprung mass acceleration becomes more remarkable by increasing the amplitude of c_e . Moreover, when the switchable part is allowed to reconnect with the primary system at t_2 , the reduction on the sprung mass acceleration becomes more significant with heavier electrical damper.



(a) $c_e = 50\text{Ns/m}$



(b) $c_e = 200\text{Ns/m}$

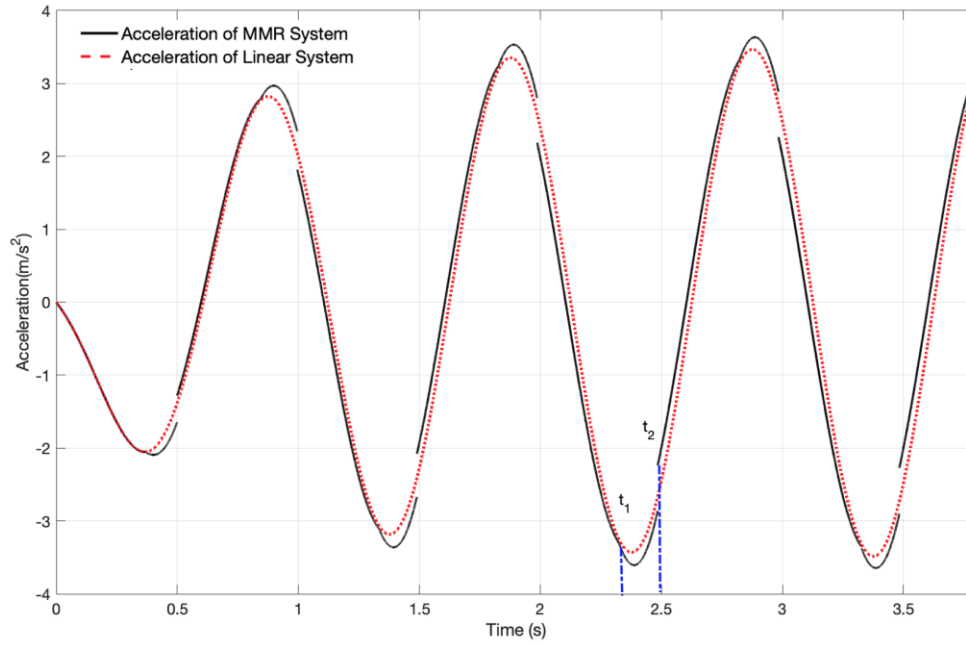
(c) $c_e = 400 \text{Ns/m}$

Figure 6-24: Sprung mass acceleration \ddot{x}_r by varying electrical damping ($50 \text{Ns/m} \leq c_e \leq 400 \text{Ns/m}$)

It is seen that even though decreasing c_e extends the disengagement period, but it seems to offer slight better ride comfort to the passenger compared to linear system i.e. $c_e = 50 \text{Ns/m}$ in Figure 6-24(a). Improving its value potentially causes excessive jerk motion, but it reduces the disengagement duration as well. Passengers might feel difficult to remain their seating posture according to the switching, but the duration of awful experience is shortened with the increasing of c_e . Unlike the generator inertance has significant influences on the ride comfort performance, the effect of electrical damper is fairly tiny. The MMR based regenerative shock absorber eventually works as a linear system when $c_e \approx c_m$.

6.5 Summary

In this chapter, the MMR based regenerative shock absorber was implemented in a quarter car model to identify whether the switching within the gear module is able to offer better performances. In order to well address the problem, vibration source characteristics of vehicle suspension system are firstly presented. The primary intention of the study is to find out the typical frequency for discussing the energy harvesting performance, while it normally refers to the system primary resonance frequency. Meanwhile, it is necessary to clearly understand the dynamic behaviour of the vibration source in different frequency range

instead of assuming the system is excited by force/velocity input. It was found that the vibration source behaves as velocity source in lower frequency, and force source in higher frequency. Primary peak power extraction can be found when the quarter car model is excited at load natural frequency, while the vibration source behaves as a velocity source. Meanwhile, it is evident that the regenerative shock absorber can only extract tiny amount of electrical power in higher frequency (force source). Therefore, the main focus of this study should be on velocity source. Based on source characteristics results, the dynamic behaviour of MMR based regenerative shock absorber in quarter car system subjected to a velocity input is discussed. Consistent to the piecewise linear model developed in Chapter 3, the secondary electrical system is able to engage and disengage from the vibration source through the mechanism of the sprag-clutch. However, it is found that the implementation of MMR in quarter car system might not be able to enhance the energy harvesting performance over linear system due to the movement of sprung mass. Throughout the numerical study, it is desirable to extend the disengagement period which smooth out the voltage and improve the harvested power over linear system. In the same way as Chapter 3, MMR is more suitable for lightly electrical damped system. The module enhances both amount of harvestable power on the electrical load and the influence of switching on sprung mass acceleration (ride comfort) is negligible. Even though increasing the generator size/inertance allows more electrical power generation, but it causes jerk motion on the passenger ride comfort as a trade-off.

Chapter 7 Design procedure of MMR based regenerative shock absorber for road vehicle

Generally, the main scope of regenerative shock absorber is developed to absorb maximum power from the vibration environment, which typically featured a resonant system. It has been demonstrated that the MMR based regenerative shock absorber can be modelled as a piecewise linear system introduced by the switching within the gear module. As discussed in Chapter 3, the discontinuous power transmission between the vibration source and switchable electric-mechanical system enables more harvestable power compared to linear system. However, when it is applied in the suspension of road vehicle in Chapter 6, it was identified that the switching between engage and disengage state still offers more continuous voltage and power, but it might not be beneficial for energy storage due to the movement of sprung mass. It is desirable to extend the disengagement duration to improve the energy harvesting performance. The numerical study result shows that most efficient way is to increase the size of generator, as it allows more mechanical reactive power being converting into useful electrical power once it disengages from the vibration source. However, it was found that the passenger might feel discomfort as there will be a significant increase on the changing rates of sprung mass acceleration when the switching happens. Increasing the generator size will be a trade-off between the ride comfort and energy harvesting. Electrical rectifier has been theoretically and experimentally investigated respectively in Chapter 4 and Chapter 5; it was found that the diode conducting voltage reduces significant amount of harvestable electrical energy on the load especially for lower power application. In this case, mechanical motion rectifier seems to be the only option to harvest power from the road input even though it compromises ride comfort.

The manufactured prototype in Chapter 5 was developed for general application, while the size is not scaled up for vehicle suspension system. Based on the piecewise linear model in Chapter 6, a design procedure of mechanical motion rectified regenerative shock absorber for road vehicle suspension system is presented in this chapter. It is considered to be excited at vehicle body bounce frequency, where primary maximum vibration power is delivered to the electrical load. Meanwhile, it is necessary to set up several physical constraints such as maximum permissible movement distance, rpm, torque etc, exceeding setup limitations might result in damaging the device. In the meantime, the system damping ratio of vehicle suspension is generally fixed for vibration suppression purpose in physics. In this way, a reliable design guideline can be developed to provide important reference for its applications

in vehicle suspension system. It shall be noted that the main focus of design procedure is developed to improve the system energy harvesting performance. The ride comfort is not considered in the guidance as there is always a conflict between energy regeneration and vibration control.

7.1 Design requirements

Before discussing the selection of system parameters, it is necessary to define several requirements in designing MMR based regenerative shock absorber for road vehicle:

- A mechanical motion rectifier module should be able to convert bidirectional rotational motion of the lead-screw into unidirectional input to the generator
- Mechanical friction within the design should be minimized
- The proposed design should be effective in the considered frequency range
- The size of the MMR based regenerative shock absorber is defined by the allowable space of vehicle suspension
- Design parameters should ensure that system does not reach its constraints during operation
- For a physical suspension system, the vehicle body bounce natural frequency $\omega_n = \sqrt{k_s/(m_s + b)}$, damping ratio $\zeta = \frac{c}{2\sqrt{k_s(m_s+b)}}$ and inertance to mass ratio $\beta = \frac{b}{m_s}$ are generally selected in the following ranges: $0.3 < \omega_n < 100$, $0.01 \leq \zeta \leq 10$ and $0 \leq \beta \leq 10$. These three parameters are generally kept constant in accordance with the vibration suppression performance criteria. [142]

7.2 Design process

In this section, the design process of selecting physical parameters of a motion rectified regenerative shock absorber for vehicle suspension is presented. A general passenger car is chosen as the implementing objective. The design guidance includes selecting the stroke length, lead-screw dimension, MMR gear module, generator, electrical load resistance and flywheel. Figure 7-1 shows the design flow chart for the MMR based regenerative shock absorber.

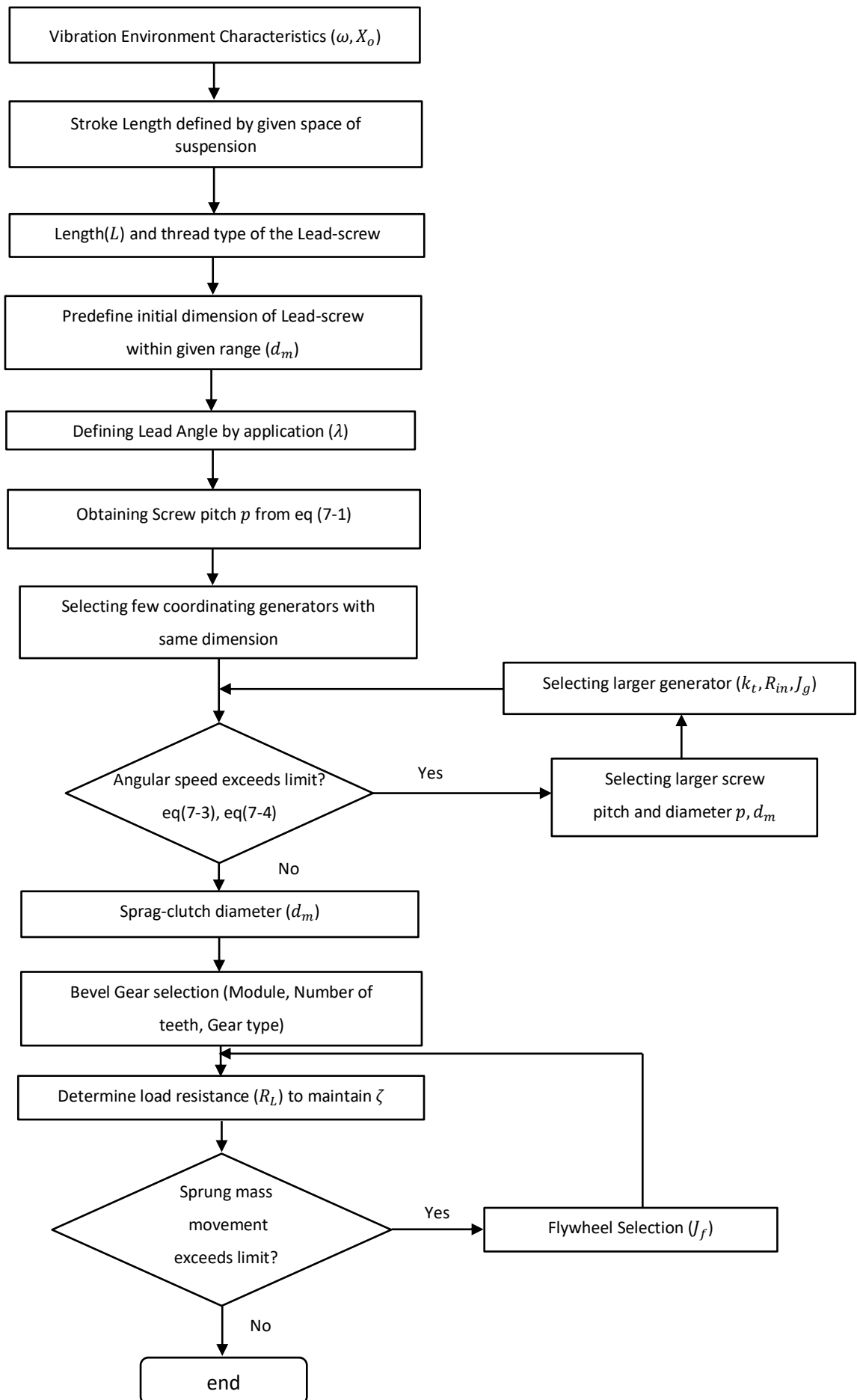


Figure 7-1: Design procedure of MMR based regenerative shock absorber

7.2.1 Vibration source characteristics

The first step of designing a regenerative shock absorber is to understand characteristics of the vibration source. In the case of vehicle dynamics, the vibration input acting on the vehicle suspension system depends on the driving velocity, frequency, road irregularities and wave amplitude. [143] Among all of these factors, road roughness plays an important role to both rider and the vehicle suspension itself. [144] Generally, the road roughness is represented as a stationary Gaussian stochastic process of a given displacement power spectral density, while the disturbance of road displacement input is modelled as white noise. [145] However, it is inaccurate to assume the power spectrum density of road input is flat among the considered frequency band, as the filtered vertical road input is typically dominated by one or two frequencies which depends on the system natural frequency. According to the discussion in Chapter 6, primary resonance power is delivered to the electrical load at the vehicle body bounce frequency (1-2Hz). The initial scope of work is to design the MMR based regenerative shock absorber where it is excited by a 1Hz harmonic waveform with amplitude $\pm 100mm$.

7.2.2 Selection of maximum stroke length

According to eq (6-30), maximum harvestable power for linear system does not rely on the vibration source characteristics (X_o, ω) only, but also the relative displacement between the sprung and unsprung masses. The maximum allowable length of the stroke should ideally be as long as possible to avoid system reaching its constraint during operation. If there is no space limitation, the priority is to improve the harvested energy. However, for an application of vehicle suspension system, the maximum allowable displacement is generally defined by the given space. Extending the length of the stroke will not increase the angular velocity as well as energy extraction from the vibration input. In the meantime, it might bring few practical problems such as misalignment, increasing the size and weight of the design prototype. In the design of a vehicle suspension system in this work, the maximum allowable displacement from its equilibrium position is defined to be $\pm 50 mm$.

7.2.3 Selection of the lead-screw

As mentioned in the previous section, the length of the lead-screw can be obtained from the maximum allowable traveling distance 100 mm plus a margin of 40 mm for safety purposes

and an extra length 60 mm to accommodate the nut and rigid shaft coupling. Therefore, the overall length of the lead-screw here is 200 mm.

The next step of design procedure is to determine the lead-screw diameter. Before that, there are few constraints that should be considered. The efficiency of a power screw mainly depends on three factors: friction, lead and lead angle. Lead angle is defined by the angle between the helix of the screw thread and line perpendicular to the axis of rotation.[146] Generally, a higher lead angle is more efficient since less energy is required to overcome the friction in order to drive the power screw. [147] The lead angle λ can be obtained by trigonometry in Figure 7-2

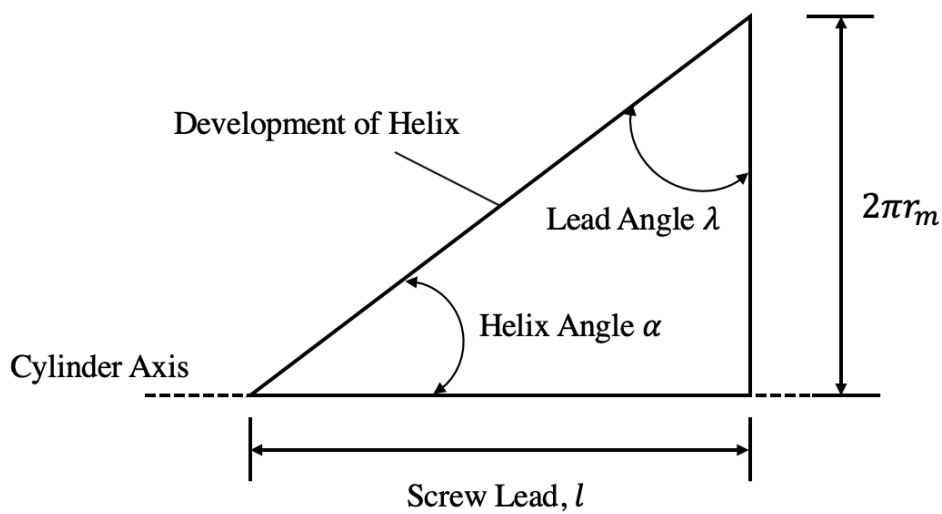


Figure 7-2: Lead-screw helix angle

$$\lambda = \arctan\left(\frac{l}{2\pi r_m}\right) \quad \text{eq (7-1)}$$

l is the screw lead, r_m is the radius of the screw thread. According to datasheet produced by THK[148], the efficiency of lead-screw reaches to its maximum value (typically around 80%) at a lead angle of 40 degrees. Note that, when the efficiency is greater than 50%, the lead-screw becomes back-drivable, which means it can be driven backwards by the load. [147] As the vibration input is considered as the up and down vertical motion, back-drivability is necessary in this case. Due to technical difficulties in forming the thread, lead angle greater than 30° is rarely used, while a reasonable efficiency can be achieved at 20° .

The second constraint of the lead-screw is its rotational speed ($\dot{\theta}$). The angular velocity should always below the maximum permissible speed of the lead-screw,

$$\dot{\theta} = \frac{2\pi}{p} \dot{z} \leq N_1 \quad \text{eq (7-2)}$$

Where p is the screw pitch and \dot{z} is the relative velocity between the sprung and unsprung masses. It is defined that the maximum allowable speed of lead-screw should be running under its critical speed (N_1). Critical speed is the theoretical angular velocity which the lead-screw is in resonance. When the speed of the lead-screw is close to its natural frequency, the object begins to resonate which dramatically increases system vibration and noise regardless of orientation. [149] Generally, the lead-screw is allowed to rotate at a speed less than 80% of the calculated critical speed where it can be formed by

$$N_1 = \frac{(4.76 \cdot 10^6) d C}{l_b^2} \quad \text{eq (7-3)}$$

l_b is the length of the unsupported lead-screw, C is a constant which depends on the configuration of lead-screw ends. Maximum value of C can be achieved when both ends are fixed and d is the minor diameter of the screw thread.

Another consideration corresponds to the velocity of the ball bearing driven by the screw shaft (N_2). Exceeding the speed limit results in the temperature of the bearing becoming higher, which might breakdown its lubrication. The amplitude of the limit can be obtained from

$$N_2 = \frac{C_r}{D_m} \quad \text{eq (7-4)}$$

Where D_m is the centre to centre diameter of the ball bearing and C_r is the speed limit factor which depends on the manufacturing details of the bearing type. Therefore, the maximum allowable rotational speed is obtained by the lower value of N_1 and N_2 , while the initial dimension of the lead-screw d_m can be determined from eq (7-3) to satisfy the condition of eq (7-4). Note that N_1 and N_2 are determined based on the material regardless of application, the relative velocity between the sprung and unsprung mass is supposed to be far below the maximum allowable speed N_1 and N_2 based on the considered road excitation displacement and frequency. It is desirable to define this criterion to check system safety before operation, but it might not be that important in this work.

The most efficient way to increase the translational to angular speed is to use a higher screw lead. However, due to the limitations of the stroke length, increasing the screw lead unavoidably reduces the number of effective turns in the nut which results in a lower load capacity. [150] It is evident that multi-start screw threads offer better load capacity and a safety mechanism compared to single-start screws. In the meantime, multi-start thread allows more contact surface in a single thread rotation which significantly reduces the backlash effect. Another way to improve the angular speed is to shorten the screw pitch which reduces the axial distance to complete one rotation of the screw. However, selecting a shorter screw pitch reduces the load capacity of the lead-screw and potentially adds more

contact between the nut and screw which results in lower efficiency and duty cycle. Meanwhile, shortening the screw pitch increases the apparent mass (inertance) of the system, according to eq (3-18) i.e. the whole structure requires more translational force to be driven and the inertance to mass ratio β might exceed the defined range.

Even though the minimum required diameter of the lead-screw is determined from eq (7-3) and eq (7-4), a larger diameter might be more desirable for the system. Selecting smaller dimension of the lead-screw reduces the load capacity and might cause the relative displacement between sprung and unsprung mass exceeding its maximum allowable travelling distance especially at high frequencies, according to its steady-state response.[151] On the other hand, selecting a lead-screw with unnecessarily large diameter increases its size and cost, and vibration source might fail to provide sufficient reactive power to achieve relative velocity between the electrical damper. According to the developed prototype in Chapter 5, the lead-screw is coupled with the generator through the MMR gear module in the same axis. Generally, the dimension of the lead-screw is chosen with equal size of the MMR shaft as well as the generator shaft in order to reduce torque loss during transmission. Having selected a reasonable screw diameter, the dimension of shaft inside MMR gear module can then be determined.

7.2.4 Selection of MMR gear module

Sprag-clutch selection

In order to convert the bi-directional rotary motion of the lead-screw into unidirectional input to the generator, employing a sprag-clutch within the design is a cost-effective approach. Sprag-clutch works in a similar way as roller-bearings, instead of allowing the object to rotate in both directions, sprag-clutch only enables the element to roll freely in one direction, and locks when driven in the opposite direction. Generally, the sprag-clutch bearing consists cage, sprags and spring to preload the friction contact between sprags and the mating parts. [152] As the initial dimension of the lead-screw is predefined by the size of the generator shaft in Section 7.2.3, the diameter of the sprag-clutch is also required to match it. Note that, the sprag-clutch bearing is usually considered with smaller mass and inertia free in lower frequency region, in order to improve the bearing torque capacity, it is suggested to install a number of sprags in a given space.

Bevel Gear selection

The easiest way to design a MMR module is to put the input and output gears in the same axis by using bevel gears with speed ratio 1:1. The outer diameter is generally required to be as small as possible, while the dimension of the sprag-clutch and the overall size constraints determine its minimum and maximum permissible diameters.

Unlike the design prototype in Chapter 5 employing straight-cut gear with straight teeth, spiral bevel gear with helical teeth might be more desirable as it is stronger and operate more quietly. Different from straight bevel gears, the spiral types have curved teeth at an angle allowing tooth contact to be gradual and smooth [153] Generally, the ratio between bevel gear and pinion is selected as high as possible in order to save space. However, it increases the speed of pinion gear at the same time. This is potentially undesirable as the abrupt tooth engagement causes noise especially at high speed, and impact stress on the teeth which leads them unable to support heavier load hence noise and vibration. Therefore, allowing for a minimum requirement of the pinion gear size to maintain the load capacity (for this reason, spiral bevel gear is better) and speed limitations of the device, the outer diameter of pinion can be identified. Given the bevel gear dimensions and the maximum rpm constraint, it is straightforward to define the number of teeth and module ($Module = \frac{Diameter}{Number\ of\ teeth}$).

7.2.5 Selection of generator, electrical load and flywheel

As a general requirement for regenerative shock absorber, the internal resistance (R_{in}) and viscous damper (c_v) within the generator should be minimize. In terms of using an AC generator, a PMDC (Permanent Magnet DC) generator does not necessarily require an inverter for lower power generation which reduces the cost and difficulty of running the generated current. Additionally, brushless generators offers numerous advantages over brushed DC generators, including higher torque to weight ratio, higher efficiency (no direct contact between stator with rotor), increased reliability, lower noise, longer duty cycle (no brush and commutator erosion) and overall reduction of electromagnetic interfacing (EMI), etc. [154] As there is no windings on its rotors, the moment of inertia and viscous damper tend to be lower which requires less torque to produce voltage. Moreover, it is evident that regenerated electrical power can be improved by increasing the back emf constant k_e , while its amplitude is proportional to the generator size according to [155]. For energy harvesting purpose, the generator is usually selected as large as possible.

Based on the developed piecewise linear model in Chapter 6, the engagement and disengagement durations depend on the electrical damping coefficient c_e and generator inertia J_g . It is evident in Chapter 6, extending disengagement period enables generator to work more continuously which consequently improves the dc voltage. Increasing generator size allows more reactive power converting into useful power once the secondary switchable system disconnecting from the vibration source. As a result, more electrical power can be extracted.

According to eq (3-24), greater k_e improves electrical damping c_e which is desirable for energy harvesting in the absence of MMR module. However, it increases the energy consumption rate which potentially shortens the disengagement duration for MMR system. As a result, the system might not be able to gain additional benefits from the switching within MMR by employing larger generator. An alternative solution is to couple a flywheel between the output shaft of MMR and generator. It was evident in Chapter 6, the added secondary system inertance/inertia improves the energy harvesting performance, while the ride comfort performance is compromised as a trade-off. Therefore, the size of generator and flywheel should be selected as large as possible for energy harvesting, while the maximum dimension is determined by the ride comfort.

After selecting the generator, the next step is to determine load resistance. According to the design requirement defined in Section 7.1, damping ratio of the vehicle is usually fixed for vibration suppression performance. Once the sum of system inertia/inertance is defined, the load resistance needs to be adjusted in accordance with the prescribed damping ratio. Hence, there will not be any space for choosing the load resistance once the generator and flywheel are selected.

In the above section, a process of designing regenerative shock absorber with MMR for road vehicle suspension system is presented. The design flow chart in Figure 7-1 gives a general guidance of selecting parameters to increase the harvestable electrical power from the road vibration input as well as maintaining system safety during operation. As stated earlier in section 7.1, the damping ratio of vehicle suspension system is generally fixed for vibration suppression performance criteria. In order to realistically study the implementation of MMR based regenerative shock absorber in a vehicle suspension system, it is helpful to conduct a numerical study to evaluate its performance for a given damping ratio.

7.3 Numerical Study

In this section, the performance of MMR based regenerative shock absorber coupled with different generator modules is evaluated. Table 7-1 shows parameters of six PMDC generators including size, internal resistance, back EMF constant, viscous damping constant and rotary inertia. As mentioned in section 7.2.1, the initial scope of the work is to develop the design specifically when it is excited at vehicle body bounce frequency 1Hz, with amplitude $\pm 100mm$. The sprung mass $m_s = 240kg$, suspension stiffness $k_s = 16kN/m$, system mechanical damper $c_m = 500Ns/m$ and overall damping ratio $\zeta = 0.25$ are fixed. Such that, the performance of MMR with different generators can be investigated.

Model	Diameter (mm)	Length (mm)	k_e (mNm/A)	R_{in} (Ω)	c_v (Nm/rads)	J_g (kgm^2)
a	23	84.6	30	0.64	13.6E-3	1.55E-5
b	23	101.6	50	1.2	17.6E-3	2.82E-5
c	23	114.3	105.5	3.9	22.6E-3	3.67E-5
d	34	127	127.7	4.3	32.6E-3	4.59E-5
e	34	138.4	217.6	6.4	37.1E-3	5.5E-5
f	42	152.4	280	10.5	53.6E-3	6.68E-5

Table 7-1: Parameters for PMDC generators [156]

For energy harvesting purpose, the screw pitch needs to be selected as small as possible in order to improve the angular to translational speed. However, it might lead the inertance to mass ratio exceeding the given range ($0 \leq \beta \leq 10$) as defined in Section 7.1. By selecting a typical lead angle around 20° , and the diameter of lead-screw is chosen in the same dimension of the generator to improve the torque transmission efficiency, the screw lead can be obtained at 44mm according to eq (7-1). As stated earlier, multi-start screw thread offers better load capacity and more contact between screw and nut compared to the single-start type. It is suggested to use a double-start screw in this case where the lead equals to the pitch times number of starts ($p = 22mm$). As suggested earlier in Section 7.2.4, spiral bevel gear is more suitable than the previous straight cut type as it provides higher strength and less vibration noise than the straight cut bevel gear. The gear ratio between bevel gear and pinion is more desirable to be higher to maintain a compact design. Allowing a minimum requirement of torque capacity, a typical gear ratio 3:1 is selected in this case to reduce the size of MMR module, while the inner diameter of bevel gear and sprag-clutch should be closer to each other.

Main materials of proposed design are aluminium and mild steel. Aluminium is desirable for designing cases for the MMR as it is light weight. Mild steel can be used to manufacture the MMR gears including the large bevel gears and small pinion gears to achieve high strength. To come up with similar design and same material in [157] (MSc design report of regenerative

shock absorber with MMR), an estimation of the system equivalent inertance, inertia and mass is shown in Table 7-2

Module	Equivalent Inertance (<i>kg</i>)	Inertia (<i>kgm²</i>)	Estimated mass (<i>kg</i>)
Lead-screw	25	6.47E-5	1.15
Sparg-clutch	0.63	0.16E-5	0.015
Large Bevel Gear	2.72	0.69E-5	0.123
pinion	0.06	0.015E-5	0.011
coupling	0.91	0.23E-5	0.041
Shaft	0.69	0.174E-5	0.031
Total	30.01	7.74E-5	1.371

Table 7-2: Estimation of inertia and mass of each module

The sum of the inertance of the lead-screw and the MMR module is 30.01 kg according to Table 7-2. By fixing the damping ratio $\delta = 0.25$, the system natural frequency, overall inertance, load resistance, electrical and mechanical damping coefficient for each generator model are obtained and shown in Table 7-3

Generator Model	ω_n (rad/s)	<i>b</i> (kg)	R_L (Ω)	c_e (Ns/m)	$c_m + c_v$ (Ns/m)
a	7.6	36.13	1	549	513.6
b	7.54	41.15	3.27	559	517.6
c	7.5	44.5	15.76	566	522.6
d	7.45	48.12	24.2	573	532.6
e	7.406	51.7	75.23	580	537.1
f	7.35	56.39	112.6	589	553.6

Table 7-3: Proposed regenerative shock absorber with six PMDC generator modules

Since the sprung mass is much bigger than the system equivalent inertance, minor changes are made on the vehicle body bounce frequency with given generator modules. Meanwhile, larger generator i.e. model *f* has to be connected with heavier external electrical load resistance (i.e. battery) in order to maintain the prescribed damping ratio.

Table 7-4 shows the performance quantification for each regenerative shock absorber model. It is seen that more electrical power can be harvested by increasing the generator size. Model *f* enables more power on the electrical load, but the energy harvesting efficiency is not satisfactory as the internal resistance and viscous damper within model *f* are greater than other modules according to Table 7-1.

Model	P_{e-L} (W)	P_m (W)	η_e (%)	η_{e-m} (%)
a	13.15(12.67)	20.47(20.94)	60.98	23.85
b	16.55(16.28)	21(21.71)	73.15	32.2
c	18.35(18.08)	21.2(20.84)	80.16	37.12
d	19.48(19.35)	21.17(21.17)	84.9	40.72
e	21.38(21.29)	21.44(21.88)	92.16	47.6
f	22.88(21.22)	21.9 (22.08)	91.4	46.94

Table 7-4: Performance quantification for each generator module (switching & non switching case)

Even though the proposed MMR based regenerative shock absorber is designed to maximize harvestable power at primary resonance frequency, while the regenerative shock absorber is subjected to a broadband frequency excitation in a physical environment. Generally, the vibration input from the road is considered to vary over the frequency range between 1 to 10Hz. When the vibration frequency is closer to the system resonance, the traveling distance of the lead-screw might exceed its allowable limit which is generally controlled by increasing system damping. However, adding more mechanical damping brings additional power losses, while increasing the electrical damping results the system taking less benefits from switching within MMR. Besides changing other system parameters, an alternative solution is to add flywheel within the design. By assuming no switching happens during operation, Figure 7-3 shows the relative displacement between the sprung mass and the road with different dimensions of flywheel alongside with the generator model f among the considered frequency range 1-10 Hz at the same displacement amplitude 100 mm. As can be seen in Figure 7-3, the system natural frequency is shifted below the considered frequency range by increasing the flywheel inertia. As a result, the travelling distance of the lead-screw can be controlled below its maximum permissible limit. It was identified in Chapter 6 that the energy harvesting performance of the MMR system can be improved by increasing the inertia/inertance of secondary switchable system (generator or flywheel) as it extends the disengagement duration. Even though the extended disengagement duration causes passenger discomfort especially at the time instant when switching happens, but it allows the generator to work more continuously and improve the voltage/power as a trade-off.

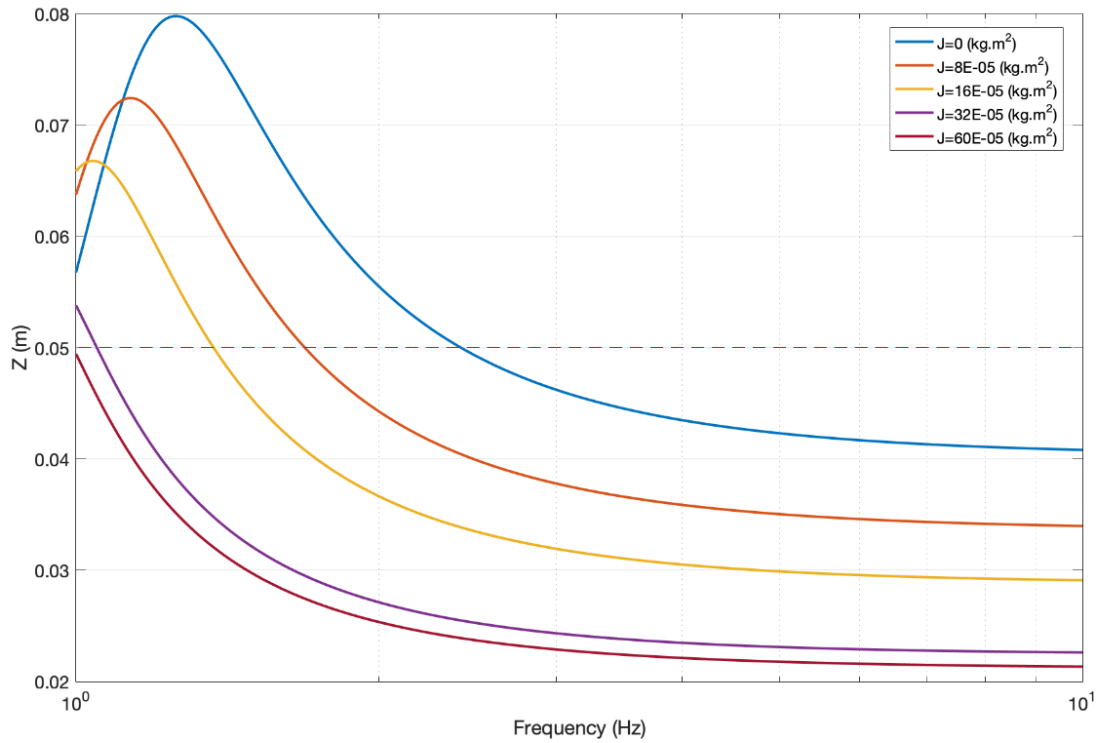


Figure 7-3: Relative displacement between sprung mass and the road for broadband frequency

Parameter	Value	Parameter	Value
l	44 mm	R_L	73.9 Ω
p	22 mm	R_{in}	10.5 Ω
λ	20°	J_{MMR}	1.3E-5 kgm^2
L	200 mm	J_{ls}	6.5E-5 kgm^2
d_m	42 mm	J_f	6E-4 kgm^2
r_g	3	J_g	6.7E-5 kgm^2
$c_m + c_v$	553.6 Ns/m		
c_e	928.6 Ns/m		

Table 7-5: Suggested parameters of regenerative shock absorber design with model f

By employing the flywheel with inertia $J_f = 6E - 4kgm^2$, the electrical damping coefficient c_e is obtained as 928.6Ns/m to maintain the prescribed damping ratio $\xi = 0.25$. Hence, the suggested parameters of the MMR based regenerative shock absorber is shown in Table 7-5. The average electrical power harvested on the load resistance is 24.83W with 57.7% mechanical to electrical power conversion efficiency when it is subjected to 1Hz, $\pm 100mm$ road input. With the given screw pitch $p = 22\text{ mm}$, the maximum rotational speed of the

lead-screw can go up to 89.7 rad/s or 925 rpm which satisfies the condition defined in eq (7-3) and eq (7-4).

7.4 Summary

In this chapter, procedure for the designing MMR based regenerative shock absorber is presented to maximize the harvestable energy from the vehicle suspension system at vehicle body bounce frequency. Note that ride comfort is not considered in the design procedure, as it generally conflicts the energy regeneration. The proposed design is able to convert the induced translational vibration of the road into the unidirectional rotary motion input to a PMDC generator through the MMR gear module. In order to provide a more reliable guidance of selecting system parameters, constraints involved in designing a typical regenerative shock absorber for road vehicle suspension are set including the maximum allowable displacement of the mass and fixed system damping ratio. Based on the numerical study results in Chapter 6, it is suggested to employ a larger generator in order to produce more continuous voltage hence improving energy harvesting performance. By selecting a larger size generator which offers greater electromagnetic coefficient, external load resistance is required to be adapted to maintain the prescribed damping ratio. A flywheel is chosen in order to keep the maximum displacement of mass from its equilibrium point below the permitted limit. In the meantime, the added inertia/inertance extends the disengagement duration of generator from the vibration source, which potentially improves the energy harvesting performance of the proposed design. With the selected parameters, the average electrical power extraction is estimated to be 24.83W with 57.7% mechanical to electrical power conversion efficiency when it is subjected to $1\text{Hz}, \pm 100\text{mm}$ input.

Chapter 8 Conclusions and future work

This thesis establishes a methodology of modelling and designing a mechanical motion rectified regenerative shock absorber for road vehicle suspension systems. In this chapter, a brief summary of results and conclusions are presented, along with a discussion of potential venues for future work.

8.1 Conclusions

Chapter 3: Regenerative shock absorber with MMR

In this chapter, dynamics of a regenerative shock absorber with MMR (with one terminal blocked) were modelled and investigated. This study started with the discussion of a linear regenerative shock absorber (i.e., without switching to include power flow and dissipation) and the result was further used to identify whether MMR enables more harvestable electrical energy. Based on the force-current analogy and power flow/dissipation characteristics of the linear system, an analogy of active and reactive power between electrical/mechanical systems was established. It was found that the instantaneous power applied to the mechanical load was not necessarily equal to the input power from the source. The amount of power that the system provides for reactive elements (i.e., spring, mass and inerter) will eventually flow back to the vibration source without doing any work. However, this conclusion is not valid for a piecewise-linear system as the applied power becomes nonharmonic.

Next, it was demonstrated that the MMR based regenerative shock absorber behaves like a piecewise linear system due to the engagement and disengagement of the one-way clutch within the MMR's gear module. When the external force acting on the generator reduces to zero, the sprag-clutch tends to disengage the coupled electrical generator from the vibration source. As a result, the model will be separated into two systems doing independent motions until the primary system's speed catches up with the generator. Based on the prescribed vibration input (Force and velocity), two piecewise linear systems were developed and analysed. It was found that the switching between the engagement and disengagement events prevents part of the mechanical reactive power from flowing back to the source and converts it into useful electrical power which significantly improves the energy harvesting performance. Numerical study showed that when the system is heavily electrically damped,

less advantage can be taken from the switching and its performance is fairly close to a linear system. However, MMR enables a lightly electrically damped system to be much more superior over a linear system. It is therefore feasible to provide a more continuous voltage output with a higher DC offset and less ripples. It was also found that MMR is not suitable for higher frequency vibration environments and for both velocity and force inputs, the MMR based regenerative shock absorber might not be able to function properly.

Finally, the dynamics of an MMR based regenerative shock absorber, when subjected to multiple harmonics input, were further investigated to identify whether the time instants of switching will be dominated by a single frequency. As one frequency requires the sprag-clutch to disengage generator with the vibration source during certain periods, while the other one does not want to. The results showed that the switching time instants of engagement and disengagement will be decided by all frequencies. It was demonstrated that, in comparison to a linear system, MMR generally improves the energy harvesting performance regardless of whether the vibration input is a single or multiple harmonic.

Chapter 4: Regenerative shock absorber with electrical rectifier

Chapter 4 presented a comparative study of a regenerative shock absorber with an electrical rectifier. The primary aim of this chapter was to investigate the suitability of each rectifier in different scenarios. In order to achieve this, characteristics of an electrical rectifier was initially modelled and analysed in both electrical and mechanical domains. It was shown that the diodes conducting voltage across the electrical rectifier significantly reduces the energy harvesting performance especially for lower power application. When the dc offset of the generated voltage is below the diode's voltage drop, there will not be any power delivered to the electrical load. By adding an electrical rectifier to a mechanical device, the voltage drop attenuates the current flowing through the circuit and hence reduces the corresponding back emf force. This behaviour potentially results in more displacement of the seismic mass especially at system's natural frequency and produces additional mechanical power losses that subsequently reduces the output power delivered to the load. Hence, based on the comparison between electrical and mechanical rectifiers, it was suggested that MMR is more suitable for low power applications. Even though with the increasing of displacement, the effect of diode conducting voltage becomes less significant, MMR still provides more harvestable power due to the switching between engagement and disengagement of the sprag-clutch within the module. However, it was found that when the system is electrically

heavily damped or is under high frequency excitations, the implementation of MMR might lead to the deterioration of the system's efficiency. In other words, the regenerative shock absorber can no longer take advantage of the switching and the amount of additional friction and viscous damping within the MMR gear module increases the mechanical power losses.

Chapter 5: Experimental characteristics of regenerative shock absorber with MMR

Chapter 5 presented an experimental study of a regenerative shock absorber with MMR. The main aim of conducting the experiments was to physically demonstrate the performance of a manufactured prototype, validate the dynamic model and experimentally justify the usage of each rectifier. It was shown that the blocked force of the proposed design is mainly influenced by coulomb friction at low frequencies and inertance at high frequencies. Confirmed by the measured results, a damper-inerter-coulomb friction model gave a reasonable prediction of the shock absorber's behaviour, which was further used as a basis to determine optimum system parameters for different applications. The engagement and disengagement durations were estimated from the periodic features of the voltage measurement curves. It was shown that the disengagement duration can be controlled by varying the electrical load resistance. This observation validated the model developed in Chapter 3, which could then be implemented in accordance with operating conditions. Moreover, the performance of electrical rectifier in a regenerative shock absorber was quantified as well. It was identified that the voltage drop across the diode significantly reduced the system efficiency especially for low power applications. In this case, MMR is a better choice as it enables a more continuous voltage and power. However, the manufactured MMR gear module introduced an additional coulomb friction of around 8 N, an inertance value of 30 kg and a mechanical damping coefficient of 435 Ns/m to the system. Hence, when the regenerative shock absorber can no longer take advantage of the switching inside MMR (in high-power applications), employing an electrical rectifier in the regenerative shock absorber may be more suitable as the MMR module brings about additional mechanical power losses.

Chapter 6: Analysis of regenerative shock absorber in a quarter car model

Chapter 6 presented a study of implementing a regenerative shock absorber in a quarter car model. In order to address the problem appropriately, vibration source characteristics of the vehicle suspension were firstly studied to identify the suitable frequency band for energy harvesting. A generic vibration system can be separated into three components: source, isolator and receiver. Mass, spring, damper and inerter are combined together to give a simple mobility at single point to interpret the dynamic behaviour of a vehicle suspension system. It was found that the characteristics of the vibration source is determined by the relative mobility between source, isolator and receiver, while all of these modules are frequency dependent. It was pointed out that vibration source behaves as a velocity source in lower frequencies, and a force source in higher frequency ranges. Primary peak power extraction can be found when the quarter car model is excited at load's natural frequency, whilst the vibration source behaves as a velocity source. Since the regenerative shock absorber can only extract tiny amount of electrical power at higher frequencies, the main focus of this study was on velocity source. Consistent with the piecewise linear model developed in Chapter 3, the secondary switchable system was able to engage and disengage from the vibration source. Even though MMR still allows part of the mechanical reactive power being converted into useful electrical power, in comparison with a linear system, the implementation of MMR in a quarter car system may not enhance the energy harvesting performance due to the movement of the sprung mass. Throughout the numerical study, it was desirable to extend the disengagement period which smooths out the output voltage and improves the harvested power. Similar to the conclusions in Chapter 3, it was also concluded here that MMR is more suitable for lighter electrically damped systems. The module enhances the harvestable output power whilst the influence of switching on sprung mass acceleration (i.e., ride comfort) is negligible. Even though increasing the generator size/inertance allows more electrical power generation, but it causes excessive jerk motion that consequently reduces the passenger ride comfort as a trade-off.

Chapter 7: Design procedure of MMR based regenerative shock absorber

Chapter 7 developed a process for designing a regenerative shock absorber with MMR. The proposed design flow chart provides guidance on selecting desirable device parameters including the lead-screw dimension, MMR gear module, generator, flywheel and load resistance. Ride comfort is not considered in the design procedure, as it generally conflicts with the energy regeneration. In line with discussions in Chapter 6, the proposed design flow chart takes physical constraints into account including the maximum allowable displacement of the sprung mass and fixed system damping ratio for vibration suppression purposes. In the context of energy harvesting, selecting a larger size generator is more beneficial as it offers a greater electromagnetic coefficient. In order to increase the tuning of the proposed design during operation, a flywheel is chosen whose added inertia/inertance extends the disengagement duration of the generator from the vibration source, i.e., potentially improves the energy harvesting performance of the design. With the selected parameters, the average electrical power extraction was shown to be 24.83 W with 57.7% mechanical to electrical power conversion efficiency when subjected to a 1 Hz, ± 100 mm road input.

8.2 Future Work

The research presented in this thesis has revealed a number of potential venues for further work and investigation which are briefly discussed in the following sections.

Model extensions

It was demonstrated in Chapter 3 that when the MMR based regenerative shock absorber is subjected to multiple harmonics vibration input, the time instance of switching will be decided by all the harmonics. This investigation can be extended to identify the consequence of switching when the proposed regenerative shock absorber is excited by random vibration. This study can insightfully demonstrate whether MMR is still able to improve the energy harvesting performance by varying the vibration input.

In Chapter 4, characteristics of an electrical rectifier coupled with a regenerative shock absorber were investigated. It was found that the voltage drop across the diode attenuates the current flowing through the circuit, which reduces the back EMF force given back to the mechanical system. The study focused on the lab-test case, while the discussion can be

expanded to include a mass within the system, i.e., a vehicle suspension system. This study can be interesting as the discontinuous current and back EMF force caused by the diode conducting voltage will influence the movement of sprung mass. Furthermore, it would be desirable to compare the performances between an electrical rectifier and MMR experimentally for different ranges of output power scenarios.

In Chapter 5, the engagement and disengagement durations were estimated from the periodic features of the voltage measurement curves. The switching inside the MMR gear module allows part of the mechanical reactive power being converted into harvestable electrical power. According to the conclusions in Chapter 3, MMR is more beneficial for lightly electrically damped system, as the disengagement allows more continuous voltage and power, but it might not be desirable for energy harvesting. By increasing the electrical damping, more electrical power can be extracted from the vibration source, but the disengagement duration is also significantly shortened, i.e., the system takes less advantage of the switching. Future work should include real time variation of the load resistance i.e. adding microprocessors in accordance with the operating conditions.

In Chapter 6, the implementation of MMR based regenerative shock absorbers in vehicle suspension systems was discussed. This study was focused on the vehicle body bounce frequency, where the primary resonance of the electrical power can be extracted from the vibration input. The model can be extended to investigate the performance of the proposed regenerative shock absorber under a road input. In addition, the impact of switching on ride comfort needs to be investigated as well. In terms of the discussion in Chapter 6 which considers a single harmonic only, the broadband road input can insightfully demonstrate the performance of the MMR based regenerative shock absorber and give recommendations on whether it is applicable to road vehicles.

In this work, the electrical system was viewed as a purely restive circuit, while the generator inductance was ignored. It is desirable to investigate its effect on system dynamics especially at higher excitation frequencies, its effect is negligible in lower frequency (ωL). This study could be very interesting as the electrical impedance becomes frequency dependent (due to inductance), which affects the relative movement between the mass and the base. Moreover, the inclusion of an inductance within the model may change the dynamics of MMR system. When the sprag-clutch disengages generator from the vibration source, the inductance

within the generator will discharge the load, which might be beneficial for energy harvesting as well.

8.2.1 Experimental validation and physical implementation

In chapter 5, characteristics of an MMR based regenerative shock absorber prototype was experimentally studied in a Hydraulic Instron testing machine. Due to the large scale of the load cell in use, the accuracy of the force measurement was limited. Furthermore, besides the Coulomb damping effect, there are other nonlinearities that need to be included to develop a more realistic dynamic model. Even though the engagement and disengagement time durations can be roughly identified from the periodic features of the voltage measurements, but the electromagnetic coefficient of the coupled generator is too small. The switching inside the MMR needs to be further investigated by varying different types of generator. Moreover, the inclusion of a load resistor was shown to alter the engagement period, which can potentially be designed as a smart device, i.e. adding microprocessors to control the switching duration in accordance with the operating conditions.

Furthermore, the prototype used in this work was designed for a generic application, and the design parameters were not chosen for a realistic vehicle suspension system. By following the design guidance presented in Chapter 7, a sustainable prototype can be manufactured. By implementing the newly developed prototype in a road vehicle, the performance of an MMR based regenerative shock absorber in a realistic setup can be demonstrated.

Bibliography

1. Zhang, Y., et al., *Energy conversion mechanism and regenerative potential of vehicle suspensions*. Energy, 2017. **119**: p. 961-970.
2. Pancharoen, K., D. Zhu, and S. Beeby, *Temperature dependence of a magnetically levitated electromagnetic vibration energy harvester*. Sensors and Actuators A: Physical, 2017. **256**: p. 1-11.
3. Zhao, D., *Waste thermal energy harvesting from a convection-driven Rijke–Zhao thermo-acoustic-piezo system*. Energy conversion and management, 2013. **66**: p. 87-97.
4. Pugi, L., et al., *Design of a hydraulic servo-actuation fed by a regenerative braking system*. Applied Energy, 2017. **187**: p. 96-115.
5. Itani, K., et al., *Comparative analysis of two hybrid energy storage systems used in a two front wheel driven electric vehicle during extreme start-up and regenerative braking operations*. Energy Conversion and Management, 2017. **144**: p. 69-87.
6. Li, L., et al., *Model predictive control-based efficient energy recovery control strategy for regenerative braking system of hybrid electric bus*. Energy conversion and management, 2016. **111**: p. 299-314.
7. Wei, C. and X. Jing, *A comprehensive review on vibration energy harvesting: Modelling and realization*. Renewable and Sustainable Energy Reviews, 2017. **74**: p. 1-18.
8. Zuo, L. and X. Tang, *Large-scale vibration energy harvesting*. Journal of intelligent material systems and structures, 2013. **24**(11): p. 1405-1430.
9. Abdelkareem, M.A., et al. *On-field measurements of the dissipated vibrational power of an SUV car traditional viscous shock absorber*. in ASME 2018 International Design Engineering Technical Conferences and Computers and Information in Engineering Conference. 2018. American Society of Mechanical Engineers Digital Collection.
10. Ali, M.K.A., et al., *Novel approach of the graphene nanolubricant for energy saving via anti-friction/wear in automobile engines*. Tribology International, 2018. **124**: p. 209-229.
11. Wang, H., A. Jasim, and X. Chen, *Energy harvesting technologies in roadway and bridge for different applications—A comprehensive review*. Applied energy, 2018. **212**: p. 1083-1094.
12. Ali, M.K.A., et al., *Fuel economy in gasoline engines using Al₂O₃/TiO₂ nanomaterials as nanolubricant additives*. Applied energy, 2018. **211**: p. 461-478.
13. Segel, L. and X. Lu, *Vehicular resistance to motion as influenced by road roughness and highway alignment*. Australian Road Research, 1982. **12**(4): p. 211-222.
14. Browne A, H., *Onroad measurement of the energy dissipated in automotive shock absorbers* Symposium on Simulation and Control of Ground Vehicles Transport, 1986: p. 167-186.
15. Fairbanks, J. *Vehicular thermoelectrics: a new green technology*. in Proc. 2011 Directions in Engine-Efficiency and Emissions Research (DEER) Conference, Detroit, Michigan. 2011.
16. Khoshnoud, F., et al., *Energy regeneration from suspension dynamic modes and self-powered actuation*. IEEE/ASME Transactions on Mechatronics, 2015. **20**(5): p. 2513-2524.
17. Abdelkareem, M.A., et al., *Vibration energy harvesting in automotive suspension system: A detailed review*. Applied energy, 2018. **229**: p. 672-699.
18. Tang, X., et al., *Energy harvesting technologies for achieving self-powered wireless sensor networks in machine condition monitoring: A review*. Sensors, 2018. **18**(12): p. 4113.
19. Li, Z., et al., *Electromagnetic energy-harvesting shock absorbers: design, modeling, and road tests*. IEEE Transactions on Vehicular Technology, 2013. **62**(3): p. 1065-1074.

20. Gysen, B.L., et al., *Efficiency of a regenerative direct-drive electromagnetic active suspension*. IEEE transactions on vehicular technology, 2011. **60**(4): p. 1384-1393.
21. Lu, S.-B., et al., *Integrated control on MR vehicle suspension system associated with braking and steering control*. Vehicle System Dynamics, 2011. **49**(1-2): p. 361-380.
22. Zhang, Z., et al., *A high-efficiency energy regenerative shock absorber using supercapacitors for renewable energy applications in range extended electric vehicle*. Applied Energy, 2016. **178**: p. 177-188.
23. Zhang, Z., et al., *Design, modelling and practical tests on a high-voltage kinetic energy harvesting (EH) system for a renewable road tunnel based on linear alternators*. Applied Energy, 2016. **164**: p. 152-161.
24. Chen, L., et al., *Energy conservation analysis and control of hybrid active semiactive suspension with three regulating damping levels*. Shock and Vibration, 2016. **2016**.
25. Wang, R., R. Ding, and L. Chen, *Application of hybrid electromagnetic suspension in vibration energy regeneration and active control*. Journal of Vibration and Control, 2018. **24**(1): p. 223-233.
26. Shi, D.H., et al., *Design and experiment study of a semi-active energy-regenerative suspension system*. Smart Materials and Structures, 2015. **24**(1).
27. Li, P., et al. *Electromagnetic regenerative suspension system for ground vehicles*. in *2014 IEEE International Conference on Systems, Man, and Cybernetics (SMC)*. 2014. IEEE.
28. Cassidy, I.L., et al., *Design and experimental characterization of an electromagnetic transducer for large-scale vibratory energy harvesting applications*. Journal of Intelligent Material Systems and Structures, 2011. **22**(17): p. 2009-2024.
29. Li, Z., G. Luhrs, and L. Zuo, *Energy-harvesting shock absorbers with motion magnification*. 2011 ASME IMECE, Denver Colorado, 2011.
30. Zhu, S., W.-a. Shen, and Y.-l. Xu, *Linear electromagnetic devices for vibration damping and energy harvesting: Modeling and testing*. Engineering Structures, 2012. **34**: p. 198-212.
31. Zhang, R., X. Wang, and Z. Liu, *A novel regenerative shock absorber with a speed doubling mechanism and its Monte Carlo simulation*. Journal of Sound and Vibration, 2018. **417**: p. 260-276.
32. Demetgul, M. and I. Guney, *Design of the hybrid regenerative shock absorber and energy harvesting from linear movement*. Journal of Clean Energy Technologies, 2017. **5**(1): p. 81-84.
33. Liu, S., H. Wei, and W. Wang. *Investigation on some key issues of regenerative damper with rotary motor for automobile suspension*. in *Proceedings of 2011 International Conference on Electronic & Mechanical Engineering and Information Technology*. 2011. IEEE.
34. Tonoli, A., et al., *Modelling and validation of electromechanical shock absorbers*. Vehicle System Dynamics, 2013. **51**(8): p. 1186-1199.
35. Sultoni, A.I., I.N. Sutantra, and A.S. Pramono, *Vibration Energy Harvesting on Vehicle Suspension Using Rotary and Linear Electromagnetic Generator*. IPTEK The Journal for Technology and Science, 2013. **24**(1).
36. Li, P. and L. Zuo, *Assessment of vehicle performances with energy-harvesting shock absorbers*. SAE International Journal of Passenger Cars-Mechanical Systems, 2013. **6**(2013-01-0170): p. 18-27.
37. Hendijanizadeh, M., M. Moshrefi-Torbati, and S.M. Sharkh, *Constrained design optimization of vibration energy harvesting devices*. Journal of Vibration and Acoustics, 2014. **136**(2).
38. Li, Z., Z. Brindak, and L. Zuo. *Modeling of an electromagnetic vibration energy harvester with motion magnification*. in *Proceedings of the ASME International Mechanical Engineering Congress and Exposition (IMECE), Denver, CO, November. 2011*.

39. Kim, B.-s., D.-w. Lee, and S.-j. Kwon. *Vehicle dynamic analysis for the ball-screw type energy harvesting damper system*. in *International Conference on Advanced Engineering Theory and Applications*. 2016. Springer.
40. Guo, S., et al., *Performance evaluation and parameter sensitivity of energy-harvesting shock absorbers on different vehicles*. *Vehicle System Dynamics*, 2016. **54**(7): p. 918-942.
41. Chen, C., et al., *Self-powered magnetorheological dampers for motorcycle suspensions*. *Proceedings of the Institution of Mechanical Engineers, Part D: Journal of Automobile Engineering*, 2018. **232**(7): p. 921-935.
42. Maravandi, A. and M. Moallem, *Regenerative shock absorber using a two-leg motion conversion mechanism*. *IEEE/ASME Transactions on Mechatronics*, 2015. **20**(6): p. 2853-2861.
43. Berg, N.I., R.K. Holm, and P.O. Rasmussen. *A novel magnetic lead screw active suspension system for vehicles*. in *2014 IEEE Energy Conversion Congress and Exposition (ECCE)*. 2014. IEEE.
44. Li, C. and W.T. Peter, *Fabrication and testing of an energy-harvesting hydraulic damper*. *Smart materials and structures*, 2013. **22**(6): p. 065024.
45. Galluzzi, R., et al., *Optimized design and characterization of motor-pump unit for energy-regenerative shock absorbers*. *Applied Energy*, 2018. **210**: p. 16-27.
46. Song, X. and Z. Li, *Regenerative damping method and apparatus*. 2005, Google Patents.
47. Song, X., Z. Li, and J.R. Edmondson, *Regenerative passive and semi-active suspension*. 2006, Google Patents.
48. Amati, N., et al., *Electromagnetic shock absorbers for automotive suspensions: Electromechanical design*. *Proceedings of the 8th Biennial Conference on Engineering Systems Design and Analysis*, Vol 2, 2006: p. 131-140.
49. Dhalwar, G. and T. Jadhav, *Power generation through rack & pinion in suspension system for an automobile*. *Int. J. Advance Research and Innovative Ideas in Education*, 2016. **2**(2): p. 794-796.
50. Wang, Q.-N., et al., *Structure design and parameter matching of ball-screw regenerative damper*. *Journal of Jilin University(Engineering and Technology Edition)*, 2012. **42**(5): p. 1100-1106.
51. Fang, Z., et al., *Experimental study of damping and energy regeneration characteristics of a hydraulic electromagnetic shock absorber*. *Advances in Mechanical Engineering*, 2013. **5**: p. 943528.
52. Liu, Y., L. Xu, and L. Zuo, *Design, Modeling, Lab and Field Tests of a Mechanical-motion-rectifier-based Energy Harvester Using a Ball-screw Mechanism*. *IEEE/ASME Transactions on Mechatronics*, 2017.
53. Liu, Y., X. Lin, and L. Zuo, *Design, modelling and experimental characterization of a novel regenerative shock absorber with a ball-screw-based mechanical motion rectifier*, in *MoVic RASD 2016*: Southampton.
54. Gangwar, H.K., et al., *Performance optimization of electronically controlled hydraulic fan drive (HFD) used in commercial application*. 2016, SAE Technical Paper.
55. Montazeri-Gh, M. and O. Kaviani-pour, *Investigation of the passive electromagnetic damper*. *Acta Mechanica*, 2012. **223**(12): p. 2633-2646.
56. Yang, B., et al., *Electromagnetic energy harvesting from vibrations of multiple frequencies*. *Journal of micromechanics and microengineering*, 2009. **19**(3): p. 035001.
57. Scully, B., et al., *Design and Characterization of an Electromagnetic Energy Harvester for Vehicle Suspensions*. *Imece 2009: Proceedings of the Asme International Mechanical Engineering Congress and Exposition*, Vol 10, Pts a and B, 2010: p. 1007-1016.
58. Amati, N., A. Festini, and A. Tonoli, *Design of electromagnetic shock absorbers for automotive suspensions*. *Vehicle System Dynamics*, 2011. **49**(12): p. 1913-1928.
59. Gherca, R. and R. Olaru, *Harvesting vibration energy by electromagnetic induction*. *Annals of the University of Craiova*, 2011.

60. Sato, T., K. Watanabe, and H. Igarashi, *Coupled Analysis of Electromagnetic Vibration Energy Harvester With Nonlinear Oscillation*. Ieee Transactions on Magnetics, 2014. **50**(2).
61. Suda, Y. and T. Shiiba, *A new hybrid suspension system with active control and energy regeneration*. Vehicle System Dynamics, 1996. **25**(S1): p. 641-654.
62. Karnopp, D., *Permanent magnet linear motors used as variable mechanical dampers for vehicle suspensions*. Vehicle System Dynamics, 1989. **18**(4): p. 187-200.
63. Zuo, L., et al., *Design and characterization of an electromagnetic energy harvester for vehicle suspensions*. Smart Materials & Structures, 2010. **19**(4).
64. Bao, W., *Main parameters analysis of ball screw shock absorber on suspension system performance*. 2015, SAE Technical Paper.
65. Yin, J., et al., *Investigation of equivalent unsprung mass and nonlinear features of electromagnetic actuated active suspension*. Shock and Vibration, 2015. **2015**.
66. Zou, J., et al., *Simulation research of a hydraulic interconnected suspension based on a hydraulic energy regenerative shock absorber*. 2018, SAE Technical Paper.
67. Liu, M., et al., *Design, simulation and experiment of a novel high efficiency energy harvesting paver*. Applied energy, 2018. **212**: p. 966-975.
68. Shahosseini, I. and K. Najafi. *Mechanical amplifier for translational kinetic energy harvesters*. in *Journal of Physics: Conference Series*. 2014. IOP Publishing.
69. Sabzehgar, R., A. Maravandi, and M. Moallem, *Energy regenerative suspension using an algebraic screw linkage mechanism*. IEEE/ASME Transactions on Mechatronics, 2013. **19**(4): p. 1251-1259.
70. Salman, W., et al., *A high-efficiency energy regenerative shock absorber using helical gears for powering low-wattage electrical device of electric vehicles*. Energy, 2018. **159**: p. 361-372.
71. Graves, K.E., P.G. Iovenitti, and D. Toncich, *Electromagnetic regenerative damping in vehicle suspension systems*. International Journal of Vehicle Design, 2000. **24**(2-3): p. 182-197.
72. Wang, X., *Frequency analysis of vibration energy harvesting systems*. 2016: Academic Press.
73. Suda, Y., et al. *Study on electromagnetic suspension for automobiles—simulation and experiments of performance*. in *Proceedings of the 5th International Symposium on Advanced Vehicle Control, Ann Arbor, Michigan, USA*. 2000.
74. Beno, J.H., et al., *Experimental comparison of losses for conventional passive and energy efficient active suspension systems*. 2002, SAE Technical Paper.
75. Wang, F.-C. and H.-A. Chan, *Vehicle suspensions with a mechatronic network strut*. Vehicle System Dynamics, 2011. **49**(5): p. 811-830.
76. Murty, B.V., *Electric, variable damping vehicle suspension*. 1989, Google Patents.
77. Xie, L., et al., *Damping-tunable energy-harvesting vehicle damper with multiple controlled generators: design, modeling and experiments*. Mechanical Systems and Signal Processing, 2018. **99**: p. 859-872.
78. Xie, L., et al., *Electromagnetic energy-harvesting damper with multiple independently controlled transducers: on-demand damping and optimal energy regeneration*. IEEE/ASME Transactions on Mechatronics, 2017. **22**(6): p. 2705-2713.
79. Anderson, Z.M., et al., *Active vehicle suspension system*. 2017, Google Patents.
80. Fang, Z., et al., *An optimal algorithm for energy recovery of hydraulic electromagnetic energy-regenerative shock absorber*. Applied Mathematics & Information Sciences, 2013. **7**(6): p. 2207.
81. Xu, L., et al. *Damping characteristics of a hydraulic electric rectifier shock absorber and its effect on vehicle dynamics*. in *ASME 2015 International Design Engineering Technical Conferences and Computers and Information in Engineering Conference*. 2015. American Society of Mechanical Engineers Digital Collection.
82. Li, Z., et al., *Energy-harvesting shock absorber with a mechanical motion rectifier*. Smart materials and structures, 2012. **22**(2): p. 025008.

83. Li, Z.J., et al., *Energy-harvesting shock absorber with a mechanical motion rectifier*. Smart Materials and Structures, 2013. **22**(2).
84. Liu, Y., L. Xu, and L. Zuo, *Design, modeling, lab, and field tests of a mechanical-motion-rectifier-based energy harvester using a ball-screw mechanism*. IEEE/ASME Transactions on mechatronics, 2017. **22**(5): p. 1933-1943.
85. Yu, C.-M., et al., *Experiments and analysis of the dual-overrunning clutches electro-mechanical regenerative damper prototype*. Journal of Jilin University(Engineering and Technology Edition), 2012. **42**(2): p. 292-297.
86. Smith, M.C., *Synthesis of mechanical networks: The inerter*. Ieee Transactions on Automatic Control, 2002. **47**(10): p. 1648-1662.
87. Lazar, I., S. Neild, and D. Wagg, *Using an inerter - based device for structural vibration suppression*. Earthquake Engineering & Structural Dynamics, 2014. **43**(8): p. 1129-1147.
88. Chen, M.Z., et al., *Influence of inerter on natural frequencies of vibration systems*. Journal of Sound and Vibration, 2014. **333**(7): p. 1874-1887.
89. Hu, Y.L. and M.Z.Q. Chen, *Performance evaluation for inerter-based dynamic vibration absorbers*. International Journal of Mechanical Sciences, 2015. **99**: p. 297-307.
90. Li, Y., et al., *Including Inerters in Aircraft Landing Gear Shock Strut to Improve the Touch-down Performance*. Procedia Engineering, 2017. **199**: p. 1689-1694.
91. Smith, M.C. and F.-C. Wang, *Performance benefits in passive vehicle suspensions employing inerters*. Vehicle System Dynamics, 2004. **42**(4): p. 235-257.
92. Wang, F.-C., et al. *Performance analyses of building suspension control with inerters*. in *Decision and Control, 2007 46th IEEE Conference on*. 2007. IEEE.
93. Firestone, F.A., *A new analogy between mechanical and electrical systems*. The Journal of the Acoustical Society of America, 1933. **4**(3): p. 249-267.
94. Smith, M.C., *Synthesis of mechanical networks: The inerter*. Proceedings of the 41st Ieee Conference on Decision and Control, Vols 1-4, 2002: p. 1657-1662.
95. Papageorgiou, C., N.E. Houghton, and M.C. Smith, *Experimental testing and analysis of inerter devices*. Journal of dynamic systems, measurement, and control, 2009. **131**(1): p. 011001.
96. Nie, J.-M., et al., *Research on the Inerter Structure*. Ji Xie She Ji Yu Yan Jiu(Machine Design and Research), 2012. **28**(1): p. 29-32.
97. Wang, F.C. and W.J. Su, *Inerter nonlinearities and the impact on suspension control*. 2008 American Control Conference, Vols 1-12, 2008: p. 3245-3250.
98. Papageorgiou, C., N.E. Houghton, and M.C. Smith, *Experimental Testing and Analysis of Inerter Devices*. Journal of Dynamic Systems Measurement and Control-Transactions of the Asme, 2009. **131**(1).
99. Wang, F.C., M.F. Hong, and T.C. Lin, *Designing and testing a hydraulic inerter*. Proceedings of the Institution of Mechanical Engineers Part C-Journal of Mechanical Engineering Science, 2011. **225**(C1): p. 66-72.
100. Chen, M.Z., et al., *The missing mechanical circuit element*. IEEE Circuits and Systems Magazine, 2009. **9**(1).
101. Carlin, W. and D. Soskice, *Shocks to the system: the German political economy under stress*. National Institute Economic Review, 1997. **159**(1): p. 57-76.
102. Scheibe, F. and M.C. Smith, *Analytical solutions for optimal ride comfort and tyre grip for passive vehicle suspensions*. Vehicle System Dynamics, 2009. **47**(10): p. 1229-1252.
103. Nakano, K., *Combined type self-powered active vibration control of truck cabins*. Vehicle System Dynamics, 2004. **41**(6): p. 449-473.
104. Nakamura, Y., et al., *Seismic response control using electromagnetic inertial mass dampers*. Earthquake Engineering & Structural Dynamics, 2014. **43**(4): p. 507-527.
105. Wang, F.-C. and W.-J. Su, *Impact of inerter nonlinearities on vehicle suspension control*. Vehicle system dynamics, 2008. **46**(7): p. 575-595.

106. Hartog, J.D., *LXXIII. Forced vibrations with combined viscous and coulomb damping*. The London, Edinburgh, and Dublin Philosophical Magazine and Journal of Science, 1930. **9**(59): p. 801-817.
107. Ohnishi, K., M. Shibata, and T. Murakami, *Motion control for advanced mechatronics*. IEEE/ASME Transactions On Mechatronics, 1996. **1**(1): p. 56-67.
108. Hunt, K.H. and F.R.E. Crossley, *Coefficient of restitution interpreted as damping in vibroimpact*. 1975.
109. Wang, F.C. and W.J. Su, *Impact of inerter nonlinearities on vehicle suspension control*. Vehicle System Dynamics, 2008. **46**(7): p. 575-595.
110. Webster, A.G., *Acoustical impedance and the theory of horns and of the phonograph*. Proceedings of the National Academy of Sciences of the United States of America, 1919. **5**(7): p. 275.
111. Gardonio, P. and M.J. Brennan, *On the origins and development of mobility and impedance methods in structural dynamics*. Journal of Sound and vibration, 2002. **249**(3): p. 557-573.
112. Fahy, F. and J. Walker, *Advanced applications in acoustics, noise and vibration*. 2018: CRC Press.
113. Sabanovic, A. and K. Ohnishi, *Motion control systems*. 2011: John Wiley & Sons.
114. Gatti, P.L. and V. Ferrari, *Applied mechanical and structural vibrations: theory, methods, and measuring instrumentation*. 1999: E & FN Spon.
115. Ungar, E.E. and C. Dietrich, *High-frequency vibration isolation*. Journal of sound and vibration, 1966. **4**(2): p. 224-241.
116. Gardonio, P. and M. Brennan, *Mobility and impedance methods in structural dynamics*. Vol. 9. 2004: chapter.
117. Elliott, S., et al., *Mobility analysis of active isolation systems*. Journal of Sound and Vibration, 2004. **271**(1-2): p. 297-321.
118. Busch - Vishniac, I.J., *A fundamental problem with mobility analysis of vibration isolation systems*. The Journal of the Acoustical Society of America, 1987. **81**(6): p. 1801-1804.
119. Gardonio, P., S. Elliott, and R. Pinnington, *Active isolation of structural vibration on a multiple-degree-of-freedom system, part II: effectiveness of active control strategies*. Journal of Sound and Vibration, 1997. **207**(1): p. 95-121.
120. Cuschieri, J., *Structural power - flow analysis using a mobility approach of an L - shaped plate*. The Journal of the Acoustical Society of America, 1990. **87**(3): p. 1159-1165.
121. Firestone, F., *The mobility method of computing the vibration of linear mechanical and acoustical systems: mechanical - electrical analogies*. Journal of applied Physics, 1938. **9**(6): p. 373-387.
122. Gardonio, P. and S.J. Elliott, *Active control of structure-borne and airborne sound transmission through double panel*. Journal of Aircraft, 1999. **36**(6): p. 1023-1032.
123. Gardonio, P., S. Elliott, and R. Pinnington, *Active isolation of structural vibration on a multiple-degree-of-freedom system, part I: the dynamics of the system*. Journal of sound and vibration, 1997. **207**(1): p. 61-93.
124. Xiong, Y.-P., J. Xing, and W. Price, *A power flow mode theory based on a system's damping distribution and power flow design approaches*. Proceedings of the Royal Society A: Mathematical, Physical and Engineering Sciences, 2005. **461**(2063): p. 3381-3411.
125. Xing, J.-T. and W. Price, *A power-flow analysis based on continuum dynamics*. Proceedings of the Royal Society of London. Series A: Mathematical, Physical and Engineering Sciences, 1999. **455**(1982): p. 401-436.
126. Yang, J., Y. Xiong, and J. Xing. *Investigations on a nonlinear energy harvesting system consisting of a flapping foil and an electro-magnetic generator using power flow analysis*. in *ASME 2011 International Design Engineering Technical Conferences and*

- Computers and Information in Engineering Conference*. 2011. American Society of Mechanical Engineers Digital Collection.
127. Yang, J., Y. Xiong, and J. Xing. *Power flow behaviour of the Duffing oscillator*. in *International Conference on Noise and Vibration Engineering 2012, ISMA 2012*. 2012.
 128. Yang, J., *Power flow analysis of nonlinear dynamical systems*. 2013, University of Southampton.
 129. Thomson, W., XLVII. *On a universal tendency in nature to the dissipation of mechanical energy*. The London, Edinburgh, and Dublin Philosophical Magazine and Journal of Science, 1852. **4**(25): p. 304-306.
 130. Andren, P., *Power spectral density approximations of longitudinal road profiles*. International Journal of Vehicle Design, 2006. **40**(1-3): p. 2-14.
 131. Frenzel, L.E., *Crash course in electronics technology*. 1997: Newnes.
 132. Millman, J., *Electronic Devices and Circuits [by] Jacob Millman [and] Christos C. Halkias*. 1967: McGraw-Hill.
 133. Batarseh, I. and A. Harb, *Review of switching concepts and power semiconductor devices*, in *Power Electronics*. 2018, Springer. p. 25-91.
 134. Stephen, N.G., *On energy harvesting from ambient vibration*. Journal of Sound and Vibration, 2006. **293**(1-2): p. 409-425.
 135. Cole, D. and D. Cebon, *Truck suspension design to minimize road damage*. Proceedings of the Institution of Mechanical Engineers, Part D: Journal of Automobile Engineering, 1996. **210**(2): p. 95-107.
 136. Sun, L. and X. Deng, *Predicting vertical dynamic loads caused by vehicle-pavement interaction*. Journal of transportation engineering, 1998. **124**(5): p. 470-478.
 137. Yang, J. *Force transmissibility and vibration power flow behaviour of inerter-based vibration isolators*. in *Journal of Physics: Conference Series*. 2016. IOP Publishing.
 138. Agostinacchio, M., D. Ciampa, and S. Olita, *The vibrations induced by surface irregularities in road pavements—a Matlab® approach*. European Transport Research Review, 2014. **6**(3): p. 267-275.
 139. Standardization, I.O.f., *ISO 2631-1. Mechanical Vibration and Shock- Evaluation of Human Exposure to Whole - Body Vibration. Part 1: General Requirements*. 1997.
 140. Institution, B.S., *BS 6841. Measurement and evaluation of human exposure to whole-body mechanical vibration*. 1987.
 141. Ingenieure, V.D., *Huamn exposure to mechanical vibrations whole-body vibration, VDI 2057*. 2002.
 142. Li, C., et al., *Vibration suppression using two-terminal flywheel. Part II: application to vehicle passive suspension*. Journal of Vibration and Control, 2012. **18**(9): p. 1353-1365.
 143. Žuraulis, V., L. Levulytė, and E. Sokolovskij, *The impact of road roughness on the duration of contact between a vehicle wheel and road surface*. Transport, 2014. **29**(4): p. 431-439.
 144. Zuo, L. and P.-S. Zhang, *Energy harvesting, ride comfort, and road handling of regenerative vehicle suspensions*. Journal of Vibration and Acoustics, 2013. **135**(1): p. 011002.
 145. Davis, B.R. and A. Thompson, *Power spectral density of road profiles*. Vehicle System Dynamics, 2001. **35**(6): p. 409-415.
 146. COLLINS, D. *Examining screws from three different angles*. 2016; Available from: <https://www.linearmotiontips.com/examining-screws-three-different-angles/>.
 147. Thomson Industries, I. *Why Lead Screws are the Best Fit for Many Linear Motion Applications - and How to Rightly Apply Them*. 2013, July 12; Available from: https://www.heason.com/images/datasheets/Why_Lead_Screws_Best_Fit_Linear_Motion_Applications_tae.pdf.
 148. THK. *Features of the Ball Screw*. Available from: https://tech.thk.com/en/products/pdf/en_b15_006.pdf.
 149. Erikson, K.W. and K.W. Erikson, *Long-span lead screw assembly with anti-backlash nut*. 2007, Google Patents.

150. Collins, D. *Why use a multi-start ball screw?* April 11 2018; Available from: <https://www.linearmotiontips.com/why-use-a-multi-start-ball-screw/>.
151. Hendijanizadeh, M., *Design and optimisation of constrained electromagnetic energy harvesting devices*. 2014, University of Southampton.
152. USA, G.B. *One-way sprag-clutch*. Available from: <https://www.gmnbt.com/one-way-sprag-clutch/>.
153. Colvin, F.H. and F.A. Stanley, *American Machinists' Handbook and Dictionary of Shop Terms: A Reference Book of Machine Shop and Drawing Room Data, Methods and Definitions*. 1914: McGraw-Hill Book Company, Incorporated.
154. Direct, K. *BRUSHLESS VS. BRUSHED MOTORS*. Jun 07 2017; Available from: <https://www.kdedirect.com/blogs/news/brushless-vs-brushed-motors>.
155. Hendijanizadeh, M., S.J. Elliott, and M. Ghandchi-Tehrani, *Extending the dynamic range of an energy harvester with a variable load resistance*. *Journal of Intelligent Material Systems and Structures*, 2017. **28**(20): p. 2996-3005.
156. innovation, E.p. *Permanent Magnet DC Motors Catalog*. 2017; Available from: <https://www.electrocrafter.com/files/DC05EN.pdf>.
157. Glauser, Y., *Design and study of an energy harvester system within a shock absorber in Faculty of Engineering and the Environment* Sept 2015, Southampton.

Appendix A

MATLAB Code

This section includes the following:

- i. MATALB code for velocity source (one terminal clamped)
- ii. MATALB code for force source (one terminal clamped)
- iii. MATLAB code for Pwelch analysis of measured voltage signal
- iv. MATALB code for vibration source characteristics of road vehicle
- v. MATALB code for implementing MMR in quarter car system

i) MATLAB code for velocity source system (one terminal clamped)

```

t=0:0.00001:1;%Time
l=1.1/2;%Lead screw Pitch
k=0;%spring stiffness
f=1;%frequency
c_e=10;%electrical damping
c_m=0;%mechanical damping
J=1.21;%moment of inertia of generaotr
J_2=1.21;%moment of inertia of other components
omega=2*pi*f;%rotational speed
zeta_in=abs(l/(2*pi))*omega*cos(omega*t);%Input rotationl speed
Displacement_in=(l/(2*pi))*sin(omega*t);
acceleration_in=-(l/(2*pi))*(omega^2)*sin(omega*t);
Force_in=(J+J_2)*acceleration_in+(c_e+c_m)*zeta_in;
Power_in=zeta_in.*Force_in;
Power_ele=c_e*zeta_in.^2;
T=(1/omega)*(atan(c_e/(omega*J)));%t_1
De=-c_e/J;
as=fzero(@(x)cos(omega*T)*exp(-De*T)+cos(omega*x)*exp(-De*x),0);
T_2=as;
w=0;
m=0;
o=0;
p=0;
q=0;
r=0;
for n=1:100001;
    display(n)
    if (t(n)>=T)&&(t(n)<=T_2)%Time slot between t1 and t2
        w=w+1;
        x(w)=t(n);
        zeta_disengage(w)=(l/(2*pi))*omega*cos(omega*T)*exp((De)*(x(w)-T));%Disengage rotational
        speed
        input_displacement(w)=(l/(2*pi))*sin(omega*x(w));%input displacement
        input_zeta(w)=(l/(2*pi))*omega*cos(omega*x(w));%input rotational speed
        input_acceleration(w)=-(l/(2*pi))*(omega^2)*sin(omega*x(w));%input acceleration
        force_input(w)=J_2*input_acceleration(w)+c_m*input_zeta(w)+k*input_displacement(w);%Force
        produced by the input side
        power_input(w)=force_input(w)*input_zeta(w);
        reactive_input(w)=J_2*input_acceleration(w)*input_zeta(w);
        F_gene(w)=0*input_zeta(w);
        power_dis(w)=c_e*(zeta_disengage(w).^2);

    elseif (t(n)>=T+(0.5/f))&&(t(n)<=T_2+(0.5/f)); %T1 to T2
        m=m+1;
        y(m)=t(n);
        zeta_disengaging(m)=abs((l/(2*pi))*omega*cos(omega*(T+(1/(2*f)))))*exp((De)*(y(m)-
        (T+(1/(2*f))))));
        Input_displacement(m)=(l/(2*pi))*sin(omega*y(m));%input displacement
        Input_zeta(m)=(l/(2*pi))*omega*cos(omega*y(m));%input rotational speed
        Input_acceleration(m)=-(l/(2*pi))*(omega^2)*sin(omega*y(m));%input acceleration
        Force_gene(m)=0*sin(omega*y(m));
        Force_input(m)=J_2*Input_acceleration(m)+c_m*Input_zeta(m)+k*Input_displacement(m);%For
        ce produced by the input side
        Power_input(m)=Force_input(m)*Input_zeta(m);
        Reactive_input(m)=J_2*Input_acceleration(m)*Input_zeta(m);
        Power_diss(m)=c_e*(zeta_disengaging(m).^2);
        elseif(t(n)>=T_2)&&(t(n)<=T+(0.5/f));
            o=o+1;
            z(o)=t(n);
            Zeta_engage(o)=(l/(2*pi))*omega*cos(omega*z(o));
            A_engage(o)=-(l/(2*pi))*(omega^2)*sin(omega*z(o));

```

```

Force_engage(o)=(J+J_2)*A_engage(o)+(c_e+c_m)*Zeta_engage(o);
Force_generator(o)=abs((J_2)*A_engage(o)+(c_e)*Zeta_engage(o));
Power_engage(o)=Force_engage(o)*Zeta_engage(o);
Power_di(o)=c_e*(Zeta_engage(o).^2);
Reactive_engage(o)=(J+J_2)*Zeta_engage(o)*A_engage(o);

elseif (t(n)>=0)&&(t(n)<=T);
    q=q+1;
    c(q)=t(n);
    Displacement_engage(q)=(l/(2*pi))*sin(omega*c(q));
    Velocity_engage(q)=(l/(2*pi))*omega*cos(omega*c(q));
    Acceleration_engage(q)=-(l/(2*pi))*(omega^2)*sin(omega*c(q));

Force_engaging(q)=(J+J_2)*Acceleration_engage(q)+(c_e+c_m)*Velocity_engage(q)+k*Displacement_engage(q);
Force_g(q)=abs((J_2)*Acceleration_engage(q)+(c_e)*Velocity_engage(q));
Power_engaging(q)= Force_engaging(q)*Velocity_engage(q);
Reactive_engaging(q)=(J+J_2)*Acceleration_engage(q)*Velocity_engage(q);
else
    r=r+1;
    d(r)=t(n);
    velocity_engaging(r)=(l/(2*pi))*omega*cos(omega*d(r));
    acceleration_engaging(r)=-(l/(2*pi))*(omega^2)*sin(omega*d(r));
    force_engaging(r)=(J+J_2)*acceleration_engaging(r)+(c_e+c_m)*velocity_engaging(r);
    power_engaging(r)=force_engaging(r)*velocity_engaging(r);
    power_har(r)=c_e*(velocity_engaging(r).^2);
    reactive_engaging(r)=(J+J_2)*velocity_engaging(r)*acceleration_engaging(r);
end
end
E_d=sum(power_dis);
E_e=sum(Power_di);
P_MMR=(E_e+E_d)/(length(power_dis)+length( Power_engage));
P_linear=0.5*c_e*(((l/(2*pi))*omega)^2);

figure(1)
subplot(3,1,1)
plot(t,abs(zeta_in))
hold on
plot(x,zeta_disengage)
grid on
plot(y,zeta_disengaging)
xlabel('Time(s)')
ylabel('Velocity(m/s)')
subplot(3,1,2)
plot(x,Force_input)
hold on
plot(x+0.5,Force_input)
plot(z,Force_engage)
plot(d,force_engaging)
plot(c,Force_engaging)
xlabel()
subplot(3,1,3)
plot(x,power_input)
hold on;
plot(x,reactive_input)
grid on
plot(y,Power_input)
plot(y,Reactive_input)
plot(z,Power_engage)
plot(z,Reactive_engage)

```

```

plot(c,Power_engaging)
plot(c,Reactive_engaging)
%plot(e,power_engage)
%plot(e,reactive_engage)
plot(d,power_engaging)
plot(d,reactive_engaging)
xlabel('Time(s)')
ylabel('Power(W)')

%subplot(3,1,2)
%plot(t,zeta_in)
%xlabel('Time(s)')
%ylabel('Velocity(m/s)')

figure(3)
plot(x,force_input)
hold on;
plot(Input_displacement,Force_input)
hold on;
plot(D_engage,Force_engage)
hold on;
%plot(d_engage,force_engage)
hold on;
%plot(Displacement_engage,Force_engaging)
%hold on;
%plot(displacement_engaging,force_engaging)
hold off
xlabel('Displacement(m)')
ylabel('Torque(Nm)')
figure(4)
plot(x,power_dis)
hold on
plot(y,Power_diss)
plot(z,Power_di)
%plot(e,power_ha)
plot(c,Power_engaging)
plot(d,power_har)
xlabel('Time(s)')
ylabel('Power(W)')
figure(5)

```

ii) MATLAB code for force source system (one terminal clamped)


```

F=1;%Input force
f=10;%frequency
c_m=15;%mechanical damping
c_e=10;%electrical damping
J=0.221;%moment of inertia of generaotr
J_ls=0.02;%Moment of inertia of lead screw
J_s=0.065;%Moment of inertia of small gear
J_l=0.02;%moment of inertia of large gear
J_2=J_s+J_l+J_ls;%Driving Inertia
omega=2*pi*f;%rotational speed
tspan_1=0:0.00001:0.05;%Setting up time span
y0=0;%Initial Condition
[t, y_1]=ode45(@(t,y_1)(F*sin(omega*t)-(c_e+c_m)*y_1)/(J+J_ls+J_s+J_l),tspan_1,y0);
a_1=(F*sin(omega*t)-(c_e+c_m)*y_1)/(J+J_ls+J_s+J_l);%Acceleration
F_generator=a_1*J+c_e*y_1;%Force acting on generator
a_1=a_1';
t=t';
y_1=y_1';
F_generator=F_generator';
num=find(F_generator<0&F_generator>-0.0002);
t_1=t(1,num);%Fing disengagement time instant
tspan_2=t_1:0.00001:t_1+(0.5/f);%reset time span
[ti, y_2]=ode45(@(ti,y_2)(F*sin(omega*ti)-(c_m)*y_2)/(J_ls+J_s+J_l),tspan_2,y_1(1,num));%Input during disengagement
ti=ti';
V_g=y_1(1,num)*exp(-(ti-t_1)*(c_e/J));%Generator during disengagement
V_g=V_g';
difference=V_g-abs(y_2);
num_2=find(difference<0&difference>-0.00004);%Find re_engagement
t_3=ti(1,num_2);%Find re_engagement
figure(1)
plot(t(1:num),y_1(1:num))
hold on
grid on
plot(ti(1:num_2),V_g(1:num_2))
plot(ti(1:num_2),abs(y_2(1:num_2)))
tspan_3=t_3:0.00001:t_3+(0.5/f);%reset time span
[ti_2, y_3]=ode45(@(ti_2,y_3)(F*sin(omega*ti_2)-(c_m+c_e)*y_3)/(J_ls+J_s+J_l+J),tspan_3,y_2(num_2,1));%Input during re-engagement
a_2=(F*sin(omega*ti_2)-(c_e+c_m)*y_3)/(J+J_ls+J_s+J_l);
F_generator2=c_e*y_3+a_2*J;
a_2=a_2';
ti_2=ti_2';
F_generator2=F_generator2';
num_3=find(F_generator2<0&F_generator2>-0.0002);%point of disengagement
t_4=ti_2(1,num_3);%Time disengagement
tspan_4=t_4:0.00001:t_4+(0.5/f);%reset time span
V_g2=abs(y_3(num_3,1))*exp(-(tspan_4-t_4)*(c_e/J));
V_g2=V_g2';
[ti_3, y_4]=ode45(@(ti_3,y_4)(F*sin(omega*ti_3)-(c_m)*y_4)/(J_ls+J_s+J_l),tspan_4,y_3(num_3,1));%Input during disengagement
difference2=V_g2-abs(y_4);
num_4=find(difference2<0&difference2>-0.00004);%Find re_engagement
t_5=tspan_4(1,num_4);
figure(1)
plot(ti_2(1:num_3),abs(y_3(1:num_3)))
hold on
plot(tspan_4(1:num_4),V_g2(1:num_4))
plot(ti_3(1:num_4),abs(y_4(1:num_4)))

```

iii) MATLAB code for Pwelch analysis of measured voltage signal

```
%V_dc=V-mean(V);%Remove dc part
```

```

segmentlength=20000;
%[pxx,w]=pwelch(V,segmentlength);
fs=5000;
noverlap=5000;
nfft=10000;
w=2*pi;
[pxx,f]=pwelch(V_i(:,2),segmentlength,noverlap,nfft,fs);

%frequency=w*0.5/pi;
f=f(1:160);
%f=frequency(1:160);
psd=10*log10(pxx);
PSD=psd(1:160);
plot(f,PSD)
%hold on
%V_ac_1=V_2;
%[pxx_2,w]=pwelch(V_ac_1,segmentlength);
%psd_2=10*log10(pxx_2);
%PSD_2=psd_2(1:160);
%plot(f,PSD_2,'linewidth',2)
%subplot(2,1,1)
%plot(T_i,V+0.3)
%hold on
%plot(T_i,V_2+0.6)
%grid on
%subplot(2,1,2)
%plot(f,PSD,'linewidth',2)
%hold on
%plot(f,PSD_2,'linewidth',2)
%grid on
%xlabel('Frequency:Hz')
%ylabel('Power Spectrum Density (dB/(rad/sample))')
%set(gca,'fontsize',14)

```

iv) MATLAB code for vibration source characteristics of road vehicle

```

omega=0.628:0.0628:628;
m_s=240;%Sprung mass
m_us=36;%Unsprung mass
k_s=16*(10^3);%Suspension stiffness
k_us=160*(10^3);%Tyre stiffness
c=98;%Damper
b=500;%Inertance
x_r=0.01;
for n=1:9991
    M_r(n)=(1i*omega(n))/(-(omega(n).^2)*m_s);%Receiver mobility
    Z_r(n)=1/M_r(n);%Source impedance
    Z_l(n)=(k_s-(omega(n).^2)*b+(c*1i*omega(n)))/(1i*omega(n));%Suspension mobility
    M_l(n)=1/Z_l(n);%Load impedance
    Z_s(n)=(k_us-(omega(n).^2)*m_us)/(1i*omega(n));%Source mobility
    M_s(n)=1/Z_s(n);
    t(n)=k_us/(k_us-m_us*(omega(n).^2));% Transmissibility
    %Source(n)=abs(M_s(n)/(M_l(n)+M_r(n)));
    Source(n)=abs((M_r(n)+M_l(n))/abs(M_s(n)));
    Force_source(n)=abs(1/(1+Source(n)));
    Velocity_source(n)=abs(1/(1+(1/Source(n))));
    r(n)=M_r(n)/(M_r(n)+M_l(n)+M_s(n));
    S(n)=(M_r(n)+M_l(n)+M_s(n));
    up(n)=M_r(n)+M_l(n);
    y(n)=abs(up(n)/M_s(n));
    U(n)=(M_s(n)+M_l(n))/M_r(n);
    A(n)=angle((M_s(n)+M_l(n))/M_r(n));
    Vibration(n)=abs(t(n)/(1+U(n)));
    l(n)=abs(t(n)*M_r(n));
    V_s(n)=1/(1+(1/y(n)));
    F_s(n)=1/(1+y(n));
    T(n)=abs(t(n)*r(n));
    Ratio(n)=abs(M_s(n)/M_r(n));
    %d(n)=(2*Z_s(n)+Z_r(n));
    %Max(n)=abs(k_us/d(n));
    %A(n)=abs(Z_r(n)+Z_l(n));
    %B(n)=abs(Z_r(n)*Z_s(n)+Z_l(n));
    %y(n)=A(n)/B(n);
    % T(n)=abs(M_s(n))/abs(M_l(n)+M_r(n));%Ratio between source and load
    %a(n)=1i*omega(n)*(Z_s(n)+Z_r(n)+(Z_r(n)*Z_s(n)/Z_l(n)));
    %a(n)=Z_s(n)+Z_r(n)+(Z_r(n)*Z_s(n)/Z_l(n));
    %k(n)=k_us/(1i*omega(n));
    % T(n)=abs(k(n)/a(n));
    % R(n)=abs(Z_l(n)/Z_s(n));
    %R(n)=abs(k_us/(k_us-(omega(n).^2)*m_us));
    up(n)=abs((M_s(n)*M_l(n)).^2);
    down(n)=abs((omega(n).^2)*(M_l(n)+M_r(n)+M_s(n)).^2);
    relative(n)=t(n)/(((M_r(n)+M_s(n))/M_l(n))+1);
    P_e(n)=abs((x_r^2)*(relative(n)^2)*0.5*c);
    P(n)=0.5*c*(k_us^2)*(x_r^2)*up(n)/down(n);
    Sum(n)=M_r(n)+M_l(n)+M_s(n);
    Ene(n)=abs((M_r(n)+M_l(n)+M_s(n))/(M_r(n)*M_l(n)));
    Ratio(n)=abs(Sum(n)/(M_l(n)*M_s(n)));
    %M_o(n)=M_s(n)+M_l(n)+M_r(n);
    %W(n)=Z_r(n)*Z_l(n)/Z_s(n);
    %u(n)=abs(Z_l(n)+Z_r(n)+W(n));
    %P(n)=(0.5*c*(k_us^2)*(x_r^2))/(u(n).^2);
end
%figure(1)
%subplot(3,1,1)
%loglog(0.5*omega/pi,abs(Source))
%grid on

```

```

%hold on
%xlabel('Frequency(Hz)')
%ylabel('|(Y_r+Y_i)/Y_s|')
%subplot(3,1,2)
%loglog(0.5*omega/pi,Velocity_source)
%grid on
%hold on
%xlabel('Frequency(Hz)')
%ylabel('|V_u_s/V_f_r_e_e|')
%subplot(3,1,3)
%loglog(0.5*omega/pi,Force_source)
%grid on
%hold on
%xlabel('Frequency(Hz)')
%ylabel('|F_l/F_b|')
%loglog(0.5*omega/pi,P)
%xlabel('Frequency(Hz)')
%ylabel('Power(W)')
%grid on
%hold on
figure(1)
subplot(2,1,1)
loglog(0.5*omega/pi,abs(U))
grid on
xlabel('Frequency(Hz)')
ylabel('|(Y_s+Y_l)/Y_R|')
hold on
subplot(2,1,2)
loglog(0.5*omega/pi,Vibration)
grid on
xlabel('Frequency(Hz)')
ylabel('|V_r/V_o|')
hold on
%ylabel('|(Y_r+Y_l)/Y_s|')
%figure(2)
%subplot(2,1,1)
%loglog(0.5*omega/pi,Ratio)
%hold on
%grid on
%xlabel('Frequency(Hz)')
%ylabel('P_e(W)')
%subplot(2,1,2)
%loglog(0.5*omega/pi,P)
%grid on
%xlabel('Frequency(Hz)')
%ylabel('P_e(W)')
%hold on
%subplot(3,1,1)
%loglog(omega,abs(M_r))
%hold on
%loglog(omega,abs(M_l))
%hold on
%loglog(omega,abs(M_s))
%xlabel('Angular Frequency \Omega')
%ylabel('|Mobility|')
%grid on
%subplot(3,1,2)
%loglog(omega,T)
%loglog(omega,P)
%loglog(0.5*omega/pi,T)
%xlabel('Frequency(Hz)')
%ylabel('|(Y_r+Y_l)/Y_s|')
%xlabel('Angular Frequency \omega (rad/s)')

```

```

ylabel('Transmisibility |T|')
grid on
subplot(3,1,1)

```

v) MATLAB code for implementing MMR in quarter car system

```

t=0:0.0001:10;
c_m=750;%Mechanical damper
c_e=400;%Electrical damper
m_s=1000;%Sprung mass
k=16000;%spring stiffness
Y=0.05;%Input Displacement
b_1=60;%MMR inertance
b_2=70;%Generator inertance
f=1;%Frequency
omega=2*pi*f;
F=m_s*(omega^2)*Y;% Vibration Input
syms y(t)
[V]=odeToVectorField(diff(y, 2)== (F*sin(omega*t)-(c_m+c_e)*diff(y)-k*y)/(m_s+b_1+b_2))
M = matlabFunction(V,'vars', {'t','Y'})
X_1=0;
V_1=0;
y0=[X_1 V_1];%Initial Condition
t_1=0;
t_2=10;
x=t_1:0.001:t_2;
Vel=omega*Y*cos(omega*x);
%x=linspace(t_1,t_2,10000);%Time span
sol=ode45(M,x,y0);
y=deval(sol,x);
Displacement=y(1,:);%Displacement
Velocity=y(2,:);%Velocity
Acceleration=(F*sin(omega*x)-(c_m+c_e)*Velocity-
k*Displacement)/(m_s+b_1+b_2);%Acceleration
R=Acceleration-(omega^2)*Y*sin(omega*x);
absV=Velocity+omega*Y*cos(omega*x);
absD=Y*sin(omega*x)+Displacement;
P_in=-k*Displacement.*(omega*Y*cos(omega*x))-
(c_e+c_m)*Velocity.*(omega*Y*cos(omega*x))-
(b_1+b_2)*Acceleration.*(omega*Y*cos(omega*x));%Input Power
%P_in=m_s*R.*absV+k*Displacement.*Velocity+(b_1+b_2)*Acceleration.*Velocity+(c_e+c_m)*(
Velocity.^2);
%P_in=-Vel.*(k*Displacement+(b_1+b_2)*Acceleration+(c_e+c_m)*Velocity);
P_react=m_s*R.*absV+k*Displacement.*Velocity+(b_1+b_2)*Acceleration.*Velocity;
P_react_output=b_2*Acceleration.*Velocity;
%P_react=-Vel.*(k*Displacement+(b_1+b_2)*Acceleration);
S_a=rms(R);
F_g=b_2*Acceleration+c_e*Velocity;
V_g=abs(V_1)*exp(-400*(x-t_1)/70);
P_m=c_m*(Velocity.^2);
M=sum(P_m);
P_e=c_e*(Velocity.^2);
%P_e=400*(V_g.^2);
E=sum(P_e);
P_total=P_react+P_e+P_m;
figure(1)
plot(x,abs(Velocity))
hold on
grid on
plot(x,V_g)
xlabel('Time (s)')

```

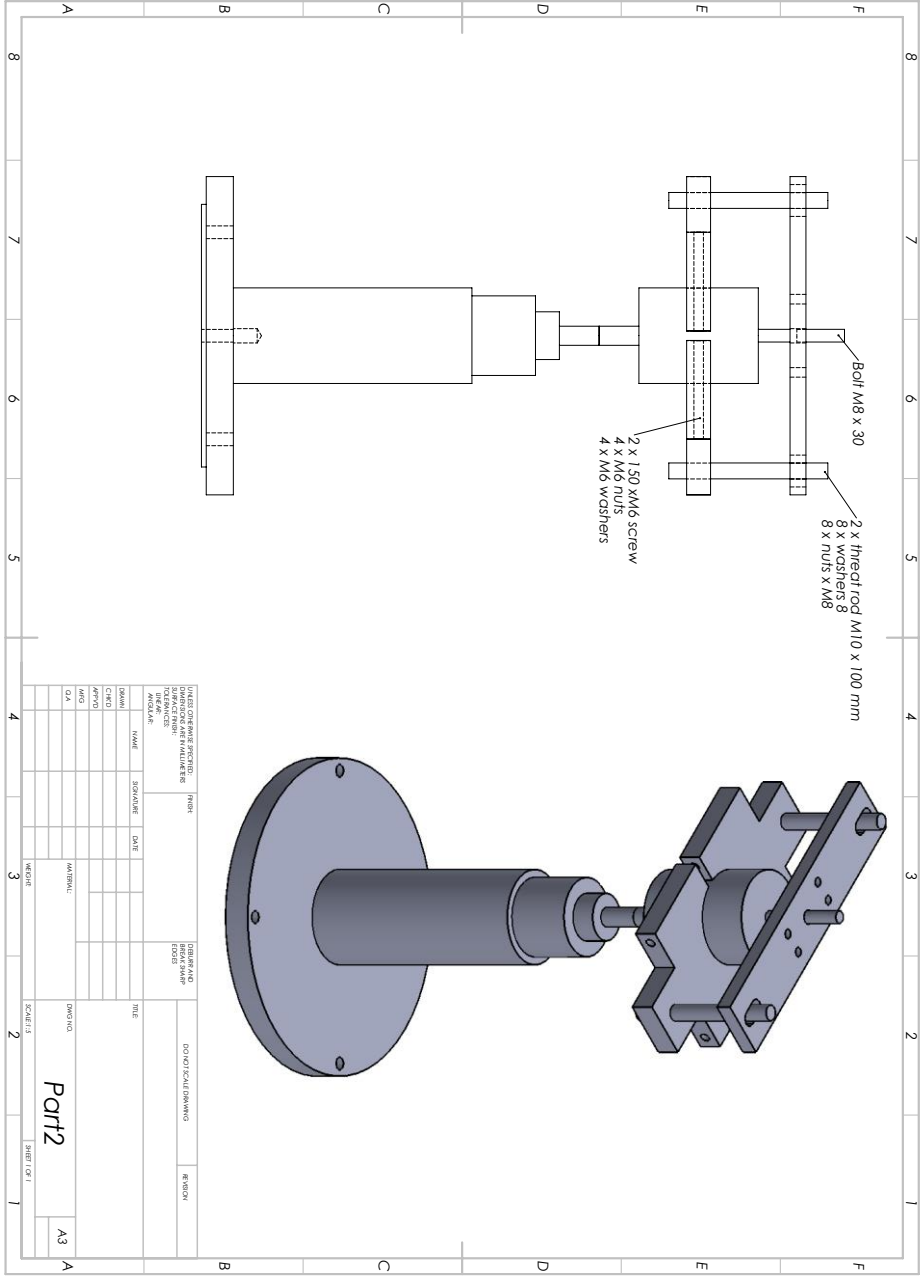
```

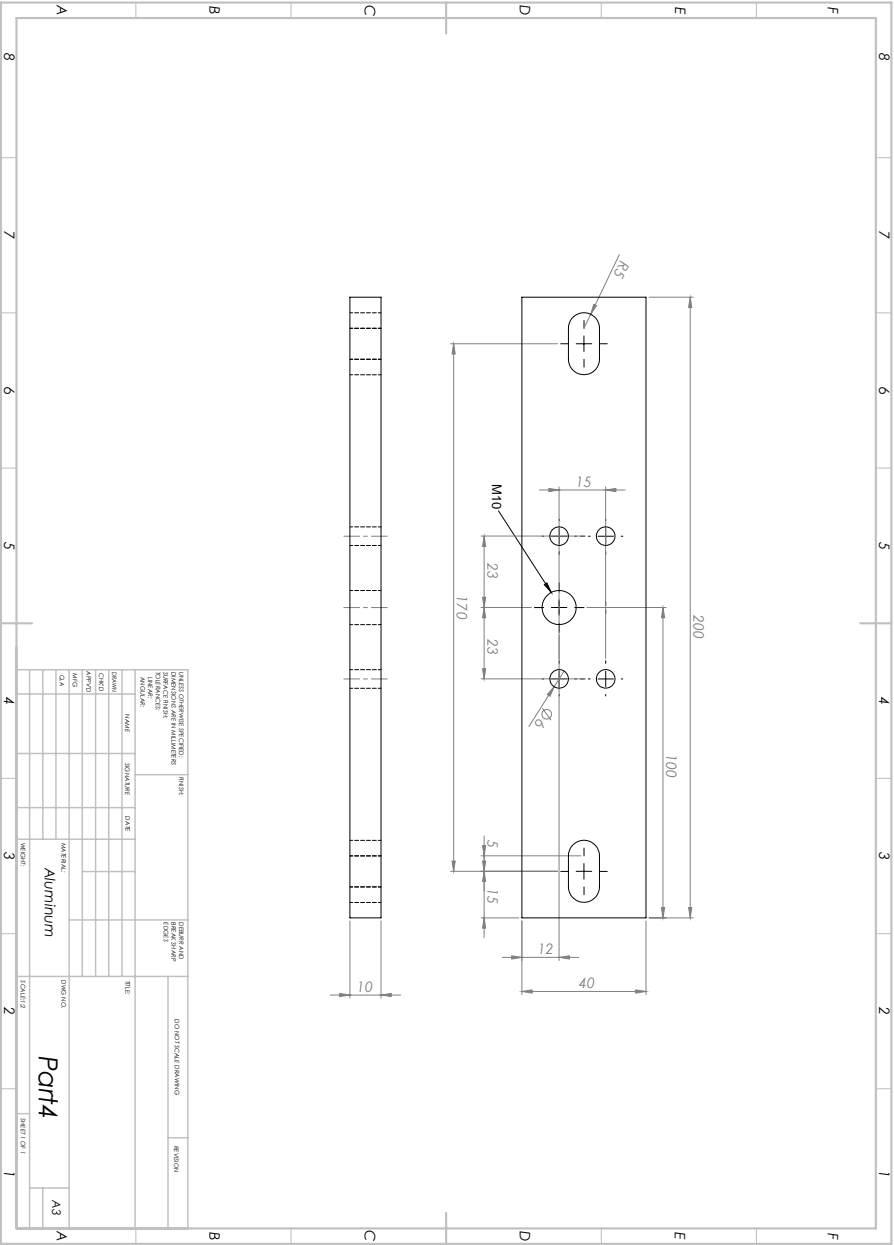
ylabel('Velocity(rad/s)')
figure(2)
plot(x,y(1,:))
hold on
grid on
xlabel('Time (s)')
ylabel('Displacement(m)')
figure(3)
plot(x,Acceleration)
hold on
grid on
xlabel('Time (s)')
ylabel('Acceleration(m/s^2)')
figure(4)
subplot(2,1,1)
plot(x,P_e)
hold on
grid on
xlabel('Time (s)')
ylabel('Power(w)')
subplot(2,1,2)
plot(x,P_m)
hold on
grid on
xlabel('Time (s)')
ylabel('Power(w)')
%figure(5)
%plot(x,R)
%hold on
%grid on
%xlabel('Time (s)')
%ylabel('Acceleration(m/s^2)')
figure(6)
plot(x,P_in)
hold on
plot(x,P_react)
plot(x,P_react_output)
grid on
xlabel('Time (s)')
ylabel('Power (w)')
figure(7)
plot(x,F_g)
xlabel('Time (s)')
ylabel('Force(N)')
%plot(x,y(1,:))%Displacement
%hold on
%plot(x,y(2,:))%Velocity
%hold on
%plot(x,Acceleration)
figure(8)
plot(x,absD)

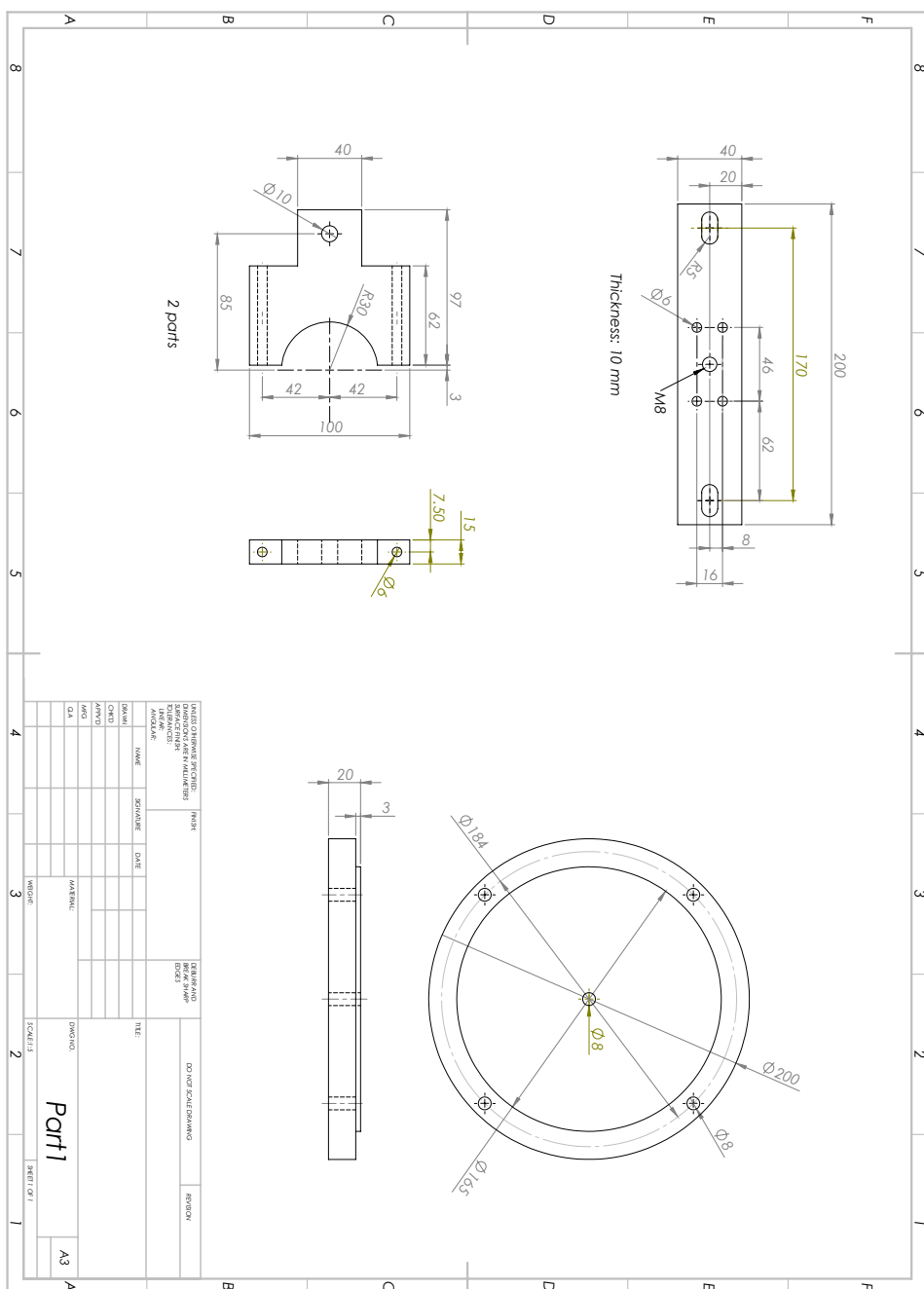
```

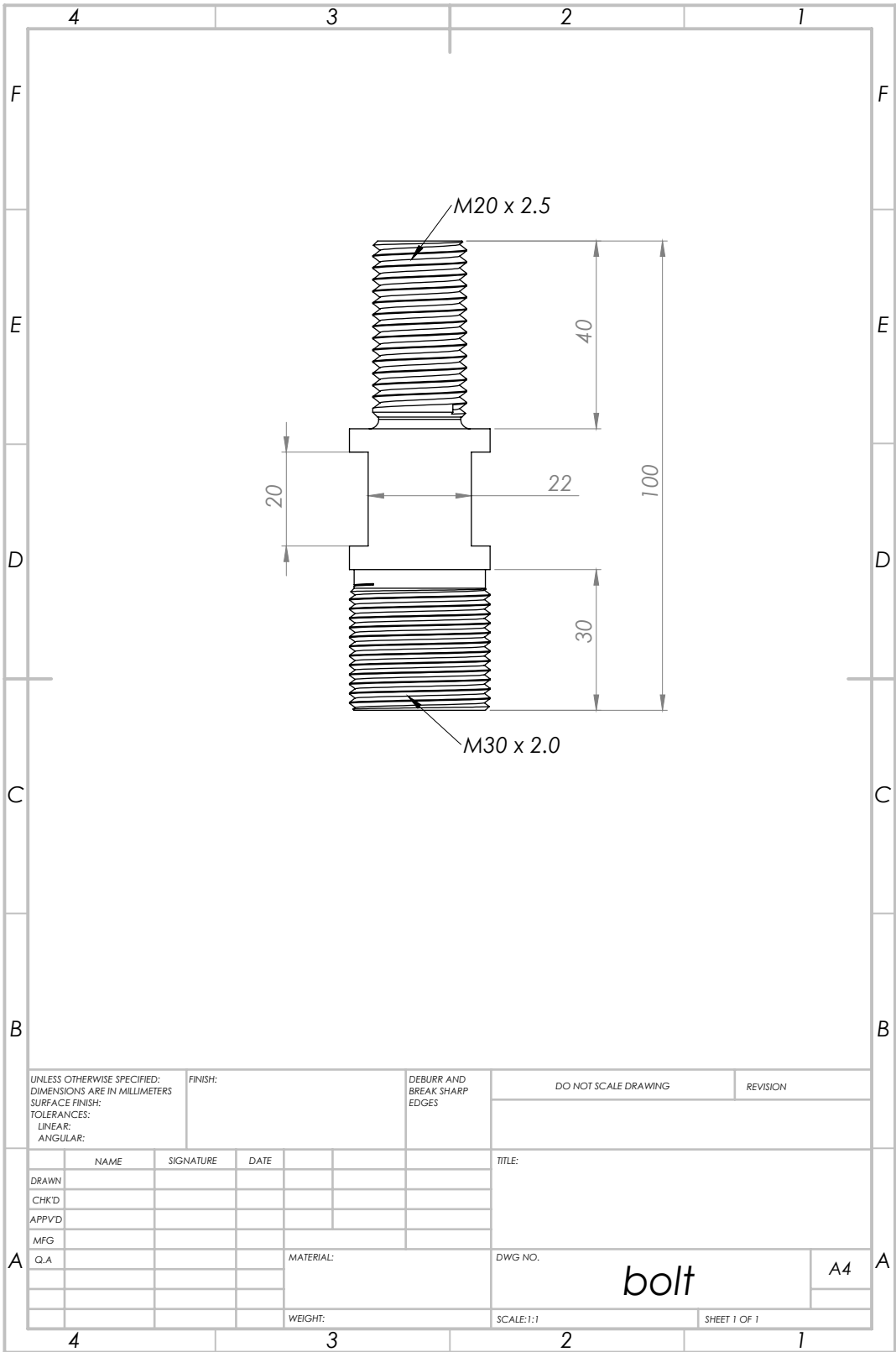
Appendix B

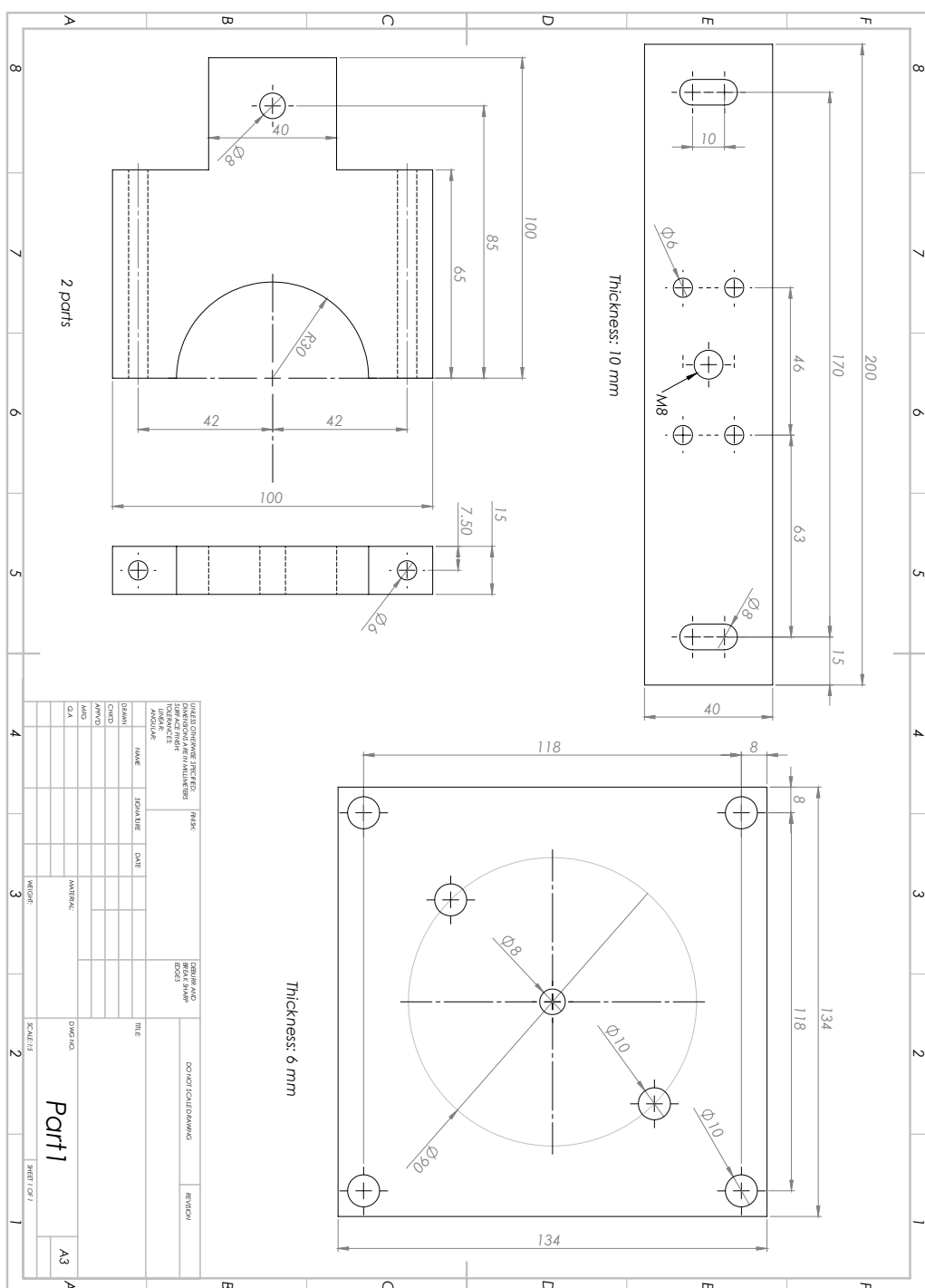
CAD Drawing of the testing rig











Appendix C

This section includes the schematic diagram of vibration source characteristics for road vehicle, where it can also be used for general case (source, isolator, receiver system)

